Department Chemie
Fachgebiet Theoretische Chemie
Technische Universität München

A Relativistic Density Functional Study of Actinide Complexation in Aqueous Solution

Florian Schlosser

Vollständiger Abdruck der von der Fakultät für Chemie der Technischen Universität München zur Erlangung des akademischen Grades eines

Doktors der Naturwissenschaften (Dr. rer. nat.)

genehmigten Dissertation.

Vorsitzender: Univ.-Prof. Dr. H. J. Neusser

Prüfer der Dissertation:

1. Univ.-Prof. Dr. N. Rösch
2. Univ.-Prof. Dr. A. Türler

Die Dissertation wurde am 17.01.2006 bei der Technischen Universität München eingereicht und durch die Fakultät für Chemie am 09.02.2006 angenommen.

Danksagung

Mein besonderer Dank gilt Herrn Prof. Dr. Notker Rösch für die Vergabe des interessanten Themas, die Bereitstellung hervorragender Rahmenbedingungen, sein großes persönliches Engagement bei der Betreuung dieser Arbeit und vor allem dafür, dass er mein Interesse für die theoretische Chemie geweckt hat.

Herrn Dr. Sven Krüger danke ich für die ausgezeichnete fachliche Betreuung, die unermüdliche Bereitschaft zu wissenschaftlichen Diskussionen und die vielen wertvollen Anregungen, die entscheidend zum Gelingen dieser Arbeit beigetragen haben.

Herrn Prof. W. Domcke und den Mitgliedern seines Arbeitskreises möchte ich ebenso wie Frau R. Mösch für das angenehme Klima am Lehrstuhl danken.

Meinen Studienkollegen Herrn Alexander Genest und Herrn Georg Eickerling sowie meinem langjährigen Zimmerkollegen Herrn Dr. André Woiterski sei hier besonders für die freundschaftliche und kollegiale Zusammenarbeit und die zahlreichen gemeinsamen Aktivitäten gedankt. Meinen Dank möchte ich ebenso allen Mitgliedern der “Aktiniden-Gruppe“ aussprechen, Frau Dr. M. García-Hernández, Frau A. Kremleva, Frau Dr. L. Moskaleva und Frau R. S. Ray. Außerdem bin ich Frau Dr. M. Fuchs-Rohr und den Herrn Dr. A. Matveev und Dr. A. Shor für die kompetente Hilfestellung bei technischen Fragen und Problemen jeglicher Art dankbar. Mein Dank gilt selbstverständlich auch allen derzeitigen und früheren Mitgliedern des Arbeitskreises für die angenehme Atmosphäre sowie interessante Diskussionen und Vorträge. An dieser Stelle seien A. Basha Mohammad, S. Bosko, P. Chuichay, Dr. C. Gehrer, Dr. C. Inntam, K. H. Lim, Dr. V. Nasluzov, Dr. K. Neyman, Dr. K. Siriwong, E. Vladimirov, Dr. A. Voityuk, M. Winkler und Dr. I. Yudanov genannt.

Nicht zuletzt gilt mein ganz besonderer Dank meiner Familie, insbesondere meiner Schwester und meinen Eltern, die mir meine Ausbildung ermöglicht haben und mich während dieser Zeit großzügig und liebevoll unterstützt haben.

Meinen Eltern

Contents

List of Abbreviations

au	atomic units
BP	Becke-Perdew (functional)
Calc.	calculated
CASPT2	complete active space with second-order perturbation theory
COSMO	conductor-like screening model
DF	density functional
DFT	density functional theory
DHF	Dirac-Hartree-Fock (method)
DK	Douglas-Kroll (procedure)
DKee	Douglas-Kroll (transformation) including electron-electron interaction
DKH	Douglas-Kroll-Hess (procedure)
DKnuc	Douglas-Kroll (transformation) restricted to nuclear potential
DKS	Dirac-Kohn-Sham (method, Hamiltonian)
DOC	dissolved organic carbon
ECP	effective core potential
EXAFS	extended x-ray absorption fine structure spectroscopy
Exp.	experimental
FC	frozen core
FF	fitting function
GGA	generalized gradient approximation (of xc functional)
HF	Hartree-Fock (method)
HOMO	highest occupied molecular orbital
IP	ionization potential
KS	Kohn-Sham (method, Hamiltonian)

LCGTO	linear combination of Gaussian-type orbitals
LDA	local density approximation (of xc functional)
LUMO	lowest unoccupied molecular orbital
MBPT2	second-order many-body perturbation theory
MO	molecular orbital
MP2	second-order Møller-Plesset perturbation theory
NMR	nuclear magnetic resonance
PBEN	Perdew-Burke-Ernzerhof (functional), modified according to Nørskov et al.
PCM	polarizable continuum model
QM	quantum mechanics
RECP	relativistic effective core potential
RI	resolution of the identity (approach)
SCF	self-consistent field (procedure)
SNSO	screened nuclear (potential) spin-orbit (method)
SO	spin-orbit (interaction, method)
SR	scalar-relativistic
UAHF	united atom – Hartree-Fock
vdW	van der Waals (radius)
VWN	Vosko-Wilk-Nusair (functional)
XANES	x-ray absorption near edge spectroscopy
XAS	x-ray absorption spectroscopy
xc	exchange-correlation (functional, potential, energy)
XRD	x-ray diffraction
ZORA	zeroth-order regular approximation

1 Introduction

1.1 Actinide compounds

Radioactivity is the “spontaneous disintegration or decay of the nucleus of an atom by emission of particles, usually accompanied by electromagnetic radiation”.[1] Starting with the discovery of the radioactivity of uranium more then hundred years ago by Becquerel (1896),[2] the interest in radioactive elements increased continuously. In the following years many natural radionuclides, i.e. mainly early members of the actinide series from actinium to uranium, have been identified. After the discovery of the neutron by Chadwick (1932) and of nuclear fission by Hahn and Strassmann (1938), a large number of artificial isotopes and also new artificial elements could be produced due to the construction of accelerators. In the early 1940s the first true transuranium elements, neptunium and plutonium, were discovered at the University of California (Berkeley).[3] In subsequent years the discovery of further transuranium elements continued successively and ended with lawrencium as the last element of the actinide series in 1961.[3]

From 1940 to 1960, research mainly focused on studies of nuclear properties of the new elements as well as on development for weapons. This work was closely accompanied by finding methods to improve the separation and isolation of actinides from fission products and lanthanides.[3–5] In the 1960s interest grew to use actinides (uranium and plutonium) for nuclear power which required efficient and safe methods to process the spent fuel and to recover the unburned actinides for further use in new fuel elements. By the late 1970s the very large amounts of high-level radioactive waste stored mainly in the United States as well as the Soviet Union and other countries using nuclear power became an increasing concern. In addition, actinides were introduced into the environment from various sources such as nuclear testing, nuclear reactor accidents, uranium mining, and nuclear weapons production during the preceding decades. Accompanied by an increased public concern this lead to studies of methods for storing nuclear waste and the cleaning of contaminated sites. Therefore, investigations of the behavior of radionuclides in the

geosphere became one of the most important fields of modern radiochemistry.[6–13]

Next to pressing environmental issues, actinides are of fundamental interest to chemists due to their unique position close to the end of the periodic table. To understand the properties and chemistry of these heavy elements relativistic effects need to be taken into account. Additionally, *f* orbital participation can lead to bonding schemes significantly different from the rest of the periodic system and even of the formally similar lanthanides.[14] The incomplete *f* and *d* subshells and the large number of stable and metastable oxidation states result in a rich chemistry and fascinating structural and electronic behavior of the actinide elements and their compounds, both in the solid state and in solution. Thus, actinides provide many challenges for chemical research.

Most information on actinides is gathered from experiments in laboratories where studies focus mainly on uranium compounds and other early actinides such as thorium, neptunium, and plutonium. Because of the radioactivity and the toxicity of the actinide compounds, special experimental procedures and security measures are required that limit investigations to few research centers. In addition, the experimental situation becomes complicated when one has to deal with actinide species in solution, e.g. under typical environmental conditions. Various factors such as pH value, concentration, and the presence of complexing ligands lead to a variety of species that can coexist in aqueous solution. Due to these complications, sometimes only limited experimental data are available.

However, an easier and safer way to obtain complementary information to experiment is already available, because nowadays the quality of theoretical chemistry calculations has reached a level that permits one to gather additional information about the chemical behavior of such compounds, their stability, solubility in water, or their tendency to complexate with available ligands.[15] Recent developments of quantum chemistry methods[16–23] rendered reliable relativistic electronic structure calculations possible even for large complexes of heavy elements and opened a computational route, complementing experimental efforts, to many properties of these complexes. Such a theoretical approach, e.g. based on density functional theory, permits one to study geometric, electronic, and energetic properties of actinides and their compounds.

In this context this thesis aims to contribute information about actinide complexation, mainly of uranium(VI), in an aqueous environment. The investigations focused on the following main topics that will be motivated in the final section of this chapter. First, solvated actinyls $[AnO_2]^{m+}$ as the initially dominant solution species of actinides in high oxidation states are discussed. The dinuclear complex $[(UO_2)_2(\mu_2\text{-}OH)_2Cl_2(H_2O)_4]$ is one

of the few polynuclear actinide hydrolysis species for which a crystal structure is known; it was investigated in its crystalline environment. Finally the bulk of this work was on actinyl complexation by important natural ligands, e.g. carbonate and carboxylate, that determine the actinide speciation under environmental conditions.

1.2 Actinides in theoretical chemistry

About 15 years ago theoretical actinide chemistry has been described as "a challenge to applied quantum chemistry."[24] Actinide elements comprise the heaviest atoms of the periodic table as far as practical chemistry is concerned. Calculations on actinide systems are demanding due to the very many electrons involved. Important correlation effects resulting from the interaction of the electrons of several open shells have to be treated adequately in the computational method applied. In addition, relativistic effects have to be taken into account for a correct description as they substantially affect the electronic structure.[25] Relativistic effects can be treated explicitly, by considering all electrons, or are included indirectly via the frozen core (FC)[26,27] approximation or the use of relativistic effective core potentials (RECP or pseudopotentials).[28–30] The latter approach is most often used as it avoids the explicit relativistic treatment of the molecular valence electronic structure that currently is not available in many quantum chemistry codes. Today, efficient scalar-relativistic methods such as the Douglas-Kroll-Hess (DKH) approach[17,31] or the zeroth-order regular approximation (ZORA)[32–34] are available. For open shell systems inclusion of spin-orbit effects can also become important.[35,36]

Species in an aqueous solution represent an important part of environmental and applied actinide chemistry. When dealing with such systems, it is essential to take solvent effects into account because they are known to significantly affect properties of molecular ions.[37] In quantum chemistry modeling these effects can be considered by explicit aqua ligands and water molecules[22,23,38–42] and/or by treating the solvent as a polarizable continuum surrounding the solute molecule (polarizable continuum model, PCM).[20,43–46] Recently, also dynamical simulations based on *ab initio* or force field molecular mechanics are used to describe the complex hydration shell(s) of actinide complexes.[47,48]

Initially methodological and hardware limitations restricted computational studies to accurate calculations on very small systems or approximate calculations on chemically more interesting systems.[16] New approaches for an approximate description of relativistic effects and the accurate treatment of electron correlation as well as algorithms for the determination of various properties opened a route to extend studies on actinide compounds.[19] At first, mainly traditional *ab initio* methods such as Hartree-Fock (HF),

second-order Møller-Plesset perturbation theory (MP2), and configuration interaction (CI) were applied.[16,49–51] More recently, methods based on density functional theory (DFT) became particularly attractive because of the inclusion of correlation in a very efficient manner.[17,18] Highly accurate multiconfigurational methods based on complete active space self consistent field (CASSCF) theory or extended by dynamic correlation effects added via second-order perturbation theory (CASPT2) are still limited to rather small systems due to high computational costs.[21] In addition, relativistic coupled cluster methods which are one of the most accurate methods for calculating electron correlation, have been applied to heavy and superheavy elements.[52,53]

Early computational studies focused on benchmark calculations targeting the structural and vibrational characterization of actinide halides or oxo cations in the gas phase.[19,49–51,54,55] Based on this experience investigations were soon extended to more specific chemical questions such as the linearity of the actinyl moiety[56–60] or the stability of different isomers and coordinating ligands.[19,54,61] With the inclusion of solvent effects studies of actinide compounds under environmental conditions became accessible. Here, computational methods can be especially useful for species that are difficult to isolate experimentally. Whereas studies of mononuclear actinide complexes are routine nowadays, investigations of polynuclear species are still scarce.[50,62–67] Next to the primary structural characterization, hydration numbers,[22,41–43,68] solvation energies,[23,43,69] hydrolysis species,[70,71] derivatives, redox behavior,[21,69] and ligand exchange mechanisms[20,40,54,72,73] are computationally investigated. Also fundamental quantities such as the heat of formation of uranyl, for which precise experimental data were missing until very recently,[74] can nowadays be determined computationally with high accuracy.[75] Though uranium is still the mostly studied element among the actinides, calculations on other light actinide elements, such as Th, Np, and Pu, are becoming more frequent in recent years.[22,41,42,54,70,71,76,77]

This brief overview of theoretical applications provided a glance at today's capabilities of computational methods and the variety of topics of current interest. Theoretical chemistry is becoming an established complementary source of information that can provide useful data to augment and enhance experimental studies. However, in addition to the aspects pointed out above, the complexity and size of real chemical systems, e.g. in the environment, limits theoretical studies to model systems. Further crucial points are the accurate evaluation of thermodynamic data and the investigation of reaction mechanisms, both of which require a high computational effort. Thus, the theoretical study of actinide complexes is still far from being a routine area of applied quantum chemistry. In fact, it represents one of the main challenges for modern computational chemistry.

1.3 Motivation and overview

For understanding the behavior of actinides in the environment, it is essential to determine the chemical species involved and to study their interaction with the surrounding media under environmental conditions.[7,78] Therefore, the chemistry of actinide elements, especially in aqueous media, is a research topic of increasing importance.[10] These studies help to gather information about processes of environmental relevance, such as actinide hydrolysis, complexation, condensation to polynuclear species, colloid formation, and interaction with the surrounding geologic media.[11] Thermodynamic and kinetic studies on the formation of actinide complexes provide data for speciation calculations. Based on these data it might be possible to predict actinide transport behavior in the environment and to design ways to retard their release and migration rates with the help of these models.

For high oxidation states (VI, V) the actinyl ions $[AnO_2]^{2+/+}$ are the initially predominant species at low pH values. Fundamental questions such as the linearity[56–59] of the actinyl moiety or the actinyl coordination[14,79–81] number have been studied. Actinyls were chosen in this thesis to investigate the importance of short-range solvent effects due to coordinated aqua ligands in the first hydration shell that turn out to be crucial for an adequate description of actinide solution species. These effects are examined for different actinides and oxidations states, i.e. U(VI), Np(VI), and Np(V). Finally, comparison to experimental data allows an evaluation of the computational method applied.

With increasing pH value and in the presence of carbon dioxide, actinide carbonate complexes become the dominating species in solution. Carbonates are important natural ligands due to their ubiquitous presence, significant concentration in many natural waters, and a strong actinide-complexing ability.[6,12,78,82] The uranyl carbonate system is by far the most extensively studied among the actinide carbonate systems. The formation of mononuclear carbonate complexes $[UO_2(CO_3)_m]^{2-2m}$ (m = 1–3) is well established. The tris(carbonato) complex $[UO_2(CO_3)_3]^{4-}$ is the dominant species over a wide pH range (pH > 7). The occurrence of polynuclear species such as the triuranyl hexa(carbonato) complex $[(UO_2)_3(CO_3)_6]^{6-}$ and the dinuclear hemicarbonate complex $[(UO_2)_2(CO_3)(OH)_3]^{-}$ has also been reported.[83,84]

Thus far, theoretical studies on uranyl carbonate species are rare and mainly limited to benchmark systems. A comprehensive study and a comparison of the different carbonate species and a systematic treatment of solvent effects is missing. Therefore, in this thesis both mono-, bi-, and trinuclear species have been studied computationally focusing on the influence of solvent effects via explicit aqua ligands from the first and second hydration shell. The most prominent species $[UO_2(CO_3)_3]^{4-}$ and $[(UO_2)_3(CO_3)_6]^{6-}$ were compared

with respect to structure and stability. While these systems are experimentally well-characterized, there is only limited information on the structure of hemicarbonate species.[84] Here a computational study can contribute valuable information to help distinguish between different suggested structural isomers.

In natural systems complexation of actinides by biological decomposition products such as humic substances plays an important role in the migration and the retardation of actinides.[7,78] Thus, understanding the interaction of actinide species with humic substances is essential. Carboxylic groups are considered as the functional groups of humic substances that are mainly responsible for the complexation of metal ions at low pH values due to their strong actinide-complexing ability.[6,78,85] Phenolic, enolic, and aliphatic OH groups, amino sites, and possibly other functional groups may also be relevant.[7,86]

Due to their complex nature and varying composition, humic substances are not well-defined substances, rather they allow only an averaged experimental characterization. On the other hand, from the computational point of view such rather large molecules are too demanding to be treated as complete model systems. Therefore it is common, as in experimental studies, to investigate their properties and interactions with the help of smaller model complexes which exhibit key features of humic substances such as the main functional groups. In this work complexes of actinyls with various carboxylic ligands – assumed to represent the main complexing sites in humic substances – such as formiate, acetate, propionate, and glycolate, were chosen as models to simulate the interaction of actinides with humic acids. The impact of chemical and structural changes in the small models employed on the actinyl complexation will be investigated to characterize variations of groups present in humic substances. In addition, the goal is to contribute to the discrimination of different coordination modes of the carboxylic ligands, i.e. monodentate, bidentate, and chelate via an adjacent hydroxo group.

Chapter 2 briefly summarizes general aspects of actinide chemistry and then focuses on actinide environmental chemistry. Experimental data on hydrolysis, actinide complexation by carbonate, carboxylate, and humic substances are presented to establish a background for the subsequent discussion. Additionally, typical experiments such as EXAFS and NMR used for identification and characterization of actinide species will be discussed with respect to the information that can be obtained from these methods.

Chapter 3 describes the computational method used in this work which relied on the parallel code PARAGAUSS. First, the basics of the applied density functional approach are presented focusing on the inclusion of relativistic effects. Then the treatment of solvent effects, essential for an adequate modeling of actinide species in aqueous solution, will be

discussed. At the end of this chapter, all computational parameters and procedures will be summarized.

Chapter 4 presents the computational results and includes a detailed discussion involving a comparison to experimental data where available. In the beginning computational data for the solvated actinyls of U(VI), Np(VI), and Np(V) are presented (Section 4.1). The second part deals with the dinuclear uranyl complex $[(UO_2)_2(\mu_2\text{-}OH)_2Cl_2(H_2O)_4]$ and describes a model of its crystalline environment (Section 4.2). Then uranyl complexation by carbonate ligands will be investigated both for mono- and polynuclear complexes (Section 4.3). In the end, results on actinide complexation by carboxylic ligands will be discussed, also with respect to implications for the complexation of actinides by humic substances (Section 4.4). A summary of the results and an outlook on future topics of interest forms the last chapter of this thesis.

2 Actinide Chemistry in Solution

2.1 General actinide chemistry

2.1.1 Oxidation states and electronic configuration

The actinide series of radioactive elements, actinium (Z = 89) through lawrencium (Z = 103), results from successive filling of the 5*f* electron shell by 14 electrons. Only the light actinides thorium, protactinium, and uranium occur naturally.[87] On the basis of natural occurrence, artificial creation, and half-lives six of the 14 elements, i.e. thorium, uranium, neptunium, plutonium, americium, and curium, are of long-term environmental concern.[88]

One of the most important properties of an actinide ion is its oxidation state. Precipitation, complexation, sorption, and colloid formation behavior differ considerably from one oxidation state to another. In contrast to the lanthanide elements that predominantly exhibit the trivalent oxidation state, the actinide elements are typically characterized by various oxidation states. Actinide ions in the trivalent (+III) and tetravalent (+IV) states occur in the form of simple hydrated ions, An^{3+} and An^{4+}. The higher oxidation states (+V, +VI) form strongly bound oxygenated species, $[AnO_2]^+$ and

Table 2.1. Oxidation states[a] of light actinide elements Ac to Cm. Most stable (bold), unstable (in parenthesis), and claimed (?) oxidation states are indicated.

Ac	Th	Pa	U	Np	Pu	Am	Cm
III	(III)	(III)	III	III	III	**III**	**III**
	IV	IV	IV	IV	**IV**	IV	IV
		V	V	**V**	V	V	V ?
			VI	VI	VI	VI	VI ?
				VII	(VII)	VII ?	

[a] Ref. 89.

Table 2.2. Valence electronic configurations[a] of light actinide atoms and ions Ac to Cm in the gas phase.[b]

	An	An^+	An^{2+}	An^{3+}	An^{4+}	An^{5+}	An^{6+}
Ac	$6d^1\,7s^2$	$7s^2$	$7s^1$	[Rn]			
Th	$6d^2\,7s^2$	$6d^1\,7s^2$	$5f^1\,6d^1$	$5f^1$	[Rn]		
Pa	$5f^2\,6d^1\,7s^2$	$5f^2\,7s^2$	$5f^2\,6d^1$	$5f^2$	$5f^1$	[Rn]	
U	$5f^3\,6d^1\,7s^2$	$5f^3\,7s^2$	$5f^3\,6d^1$?	$5f^3$	$5f^2$	$5f^1$	[Rn]
Np	$5f^4\,6d^1\,7s^2$	$5f^5\,7s^1$?	$5f^5$?	$5f^4$	$5f^3$	$5f^2$	$5f^1$
Pu	$5f^6\,7s^2$	$5f^6\,7s^1$	$5f^6$	$5f^5$	$5f^4$	$5f^3$	$5f^2$
Am	$5f^7\,7s^2$	$5f^7\,7s^1$	$5f^7$	$5f^6$	$5f^5$	$5f^4$	$5f^3$
Cm	$5f^7\,6d^1\,7s^2$	$5f^7\,7s^2$	$5f^8$	$5f^7$	$5f^6$	$5f^5$	$5f^4$

[a] [Rn] designates the closed shell noble gas electronic configuration $4f^{14}\,5d^{10}\,6s^2\,6p^6$ of radon. [b] Ref. 89.

$[AnO_2]^{2+}$, called actinyls.[89] Table 2.1 gives an overview over known oxidations states of early actinides. The dominant oxidation states rise continuously from actinium (+III) to uranium (+VI) and decrease from neptunium (+V) to plutonium (+IV) to americium (+III). The later actinides occur preferentially in oxidation state +III.

Table 2.2 gives the electronic configurations of light actinide atoms and ions that can comprise up to three open shells (5*f*, 6*d*, and 7*s*) depending on the oxidation state.[89] The elements actinium to uranium have closed-shell configurations in their most stable oxidation states (Table 2.1), whereas the later actinides exhibit open 5*f* shells.

Across the actinide series, for a given oxidation state (e.g. An^{3+} and An^{4+}), the metal atomic radius decreases as the atomic number Z increases. This actinide contraction is similar to the well-known lanthanide contraction.[90] The primary physical cause of the actinide (and lanthanide) contraction is the decreased shielding of the core positive charge across the series. Electrons added to the outermost frontier orbitals exhibit weaker screening of the charge from the additional protons in the atomic core.

2.1.2 Complexation and stereochemistry

Actinides are much more prone to complex formation than lanthanides.[14] The main reason is that the 5*f* orbitals have a wider spatial extension relative to 7*s* and 7*p* orbitals than the 4*f* orbitals have relative to the 6*s* and 6*p* orbitals.[14] Therefore the 5*f* orbitals of the actinides can be involved in covalent hybrid bonding. Additionally, the energies of the *5f*, *6d*, *7s*, and *7p* levels are comparable over a range of atoms (especially U to Am).[14] Since the orbitals also overlap spatially, bonding can involve any or even all of them.

As the actinide ions are characteristically non-polarizable and their bonding is strongly ionic they are classified as “hard” acids and consequently form strong complexes with highly ionic “hard” base ligands containing fluorine and oxygen donors, such as carbonate, hydroxide, or oxygens of water molecules.[13,89] Binding in aqueous media to softer donor atoms, such as nitrogen or sulfur, occurs in conjunction with multidentate ligands which contain both nitrogen and oxygen donors. The order of complexing ability for monoanions is $F^- > NO_3^- > Cl^- > ClO_4^-$ and for dianions $CO_3^{2-} > C_2O_4^{2-} > SO_4^{2-}$.[14] The relative tendency to form complexes decreases in the general order An(IV) > An(III) ≈ $[AnO_2]^{2+} > [AnO_2]^+$ controlled by the ionic radius and the charge.[14,89]

As the variety of ligands that form actinide complexes is huge and the number of oxidation states large, the stereochemistry found in complexes and compounds of actinides is extraordinary. The relatively large size of the actinide ions coupled with the high electrostatic attraction due to formal charges from +3 to +6 results in high coordination numbers from 6 to 9.[14]

For oxidation states III and IV octahedral coordination is most common. Coordination numbers for oxidation state V range from 6 to 9, including rare examples of cubic coordination. In oxidation state VI, actinide hexafluorides exhibit strictly octahedral coordination while coordination numbers for actinyl ions range in general from 4 to 6.[14]

2.1.3 Actinyls

Among the actinide compounds the dioxo ions $[AnO_2]^{m+}$ common for oxidation states V and VI (An = Pa–Am) are remarkably stable due to strong An-O bonds. They exhibit bond orders larger than 2 e.g. for uranyl.[90] Thus, unlike some other oxo ions the actinyls can persist through a variety of chemical changes. Actinyls exhibit characteristic bond distances of about 1.7 to 1.8 Å in solution – distinctly shorter than corresponding distances to equatorial ligands such as water (2.4 to 2.5 Å).[41]

Actinyl ions $[AnO_2]^{m+}$ are known to be linear.[91] As an exception however, the ThO_2 molecule, isoelectronic to $[UO_2]^{2+}$, is distinctly bent (122°).[90] The actinyl bonding has been studied in detail.[56–60] Mainly 6*d* and 5*f* orbitals of the actinide contribute to the An-O bonding.[59] Differences between bent ThO_2 and linear $[UO_2]^{2+}$ have been assigned to changes in relative stabilities of the atomic *d* and *f* shells.[57,59] In most actinides the *d* shell is energetically below the *f* shell and a linear conformation is preferred. However, for thorium both shells are close in energy allowing a hybridization that results in the bent structure. Besides, the influence of the 6*p* shell is under discussion. While Dirac-Hartree-Fock calculations indicated only minor importance,[57,59] studies based on an extended

Hückel approach[56] implied the relevance of the 6*p* shell. Recent DF studies in combination with x-ray absorption and emission data established that the 6*p* shell participates in the covalent uranyl bonding via a strong hybridization between $5f_\sigma$ and $6p_\sigma$ orbitals.[60]

The stereochemistry of $[AnO_2]^{m+}$ has been extensively studied and can vary considerably. The overall pattern comprises a (linear) axial O-An-O actinyl moiety that is surrounded by 4, 5, or 6 ligands in or close to its equatorial plane. This yields tetragonal, pentagonal, or hexagonal bipyramidal coordination, respectively.[14] For uranyl the pentagonal coordination is found to be preferred in general in various experimental[68,79–81] and computational studies.[23,41,43]

2.1.4 Experimental identification and characterization

Oxidation state, coordinated ligands, and experimental conditions have a significant influence on the chemical behavior of actinides. Therefore, identification and characterization of involved species is essential for understanding complex processes, e.g. under environmental conditions. While nuclear counting methods[92,93] provide a sensitive approach for determining smallest amounts of actinides, they give no information about the chemical nature of the species. In this context various experimental methods such as potentiometric titrations, infrared (IR), Raman, and nuclear magnetic resonance (NMR) spectroscopy, x-ray diffraction (XRD), and x-ray absorption spectroscopy (XAS) are applied to gain chemical and structural information.

Potentiometric studies[94] can provide information relevant to speciation, i.e. polynuclearity, number of OH ligands, and formation constants. However, the structural information gained from these data is limited because details about coordinated aqua ligands or ligand coordination types are not available.

Only x-ray crystal structure data can provide detailed information about structures based on bond lengths and bond angles, hence about the coordination modes of ligands. However, this method is limited to the availability of crystalline compounds. Naturally, x-ray diffraction does not provide explicit information about positions of hydrogen atoms. However, the discussion of hydrogen bonds is possible based on typical distances and angles determined in crystal structures. An example for such a rationalization is provided below (Section 4.2). In addition, neutron diffraction can be used to detect hydrogen centers directly.

Optical absorption and scattering spectroscopic methods are considered to be some of the most reliable techniques for detecting, discriminating, and characterizing actinide species in solution. The optical spectra show peaks due to *f-f* electron transitions. These

peaks are typically quite narrow (few nm) and the corresponding wave lengths are uniquely characteristic of the actinide element and its oxidation state.[95] Additionally, complexation, colloid formation, or sorption result in characteristic changes of the spectra which allow conclusions about the chemical state as well.[95,96]

Actinyl compounds can be characterized and identified by the symmetric (ν_s) and antisymmetric (ν_a) stretching frequencies of the actinyl moiety that can be measured by Raman scattering and infrared (IR) absorption spectroscopy, respectively.[97] A major advantage of this method is the ability to identify individual species out of a mixture of different compounds that is likely to be present in solution. It is also possible to gain basic structural information. For instance, based on Raman spectroscopic studies, a linear correlation between the symmetric stretching frequency ν_s and the number of equatorially coordinated ligands such as hydroxide or carbonate is well-established for uranyl.[83,98]

X-ray absorption spectroscopy (XAS) has become a powerful technique to study the speciation of actinides also at relatively low actinide concentration in the environment.[99] XAS is particularly useful for investigating non-crystalline and polymeric actinide compounds that can not be treated by x-ray diffraction analysis.

X-ray absorption near edge spectroscopy (XANES) can provide information about the oxidation sate, the molecular symmetry, and the local structure of an actinide compound. The absorption edge is element specific and depends on the oxidation state. For instance, L_{III} edges are found at 17168 keV for U, at 17610 keV for Np, and at 18057 keV for Pu. Variations of different oxidations states are in the order of few keV. Concentrations limits for this method are about 10^{-5} mol/L.[100]

Extended x-ray absorption fine structure spectroscopy (EXAFS) yields additional information on bond lengths to first, second, and even more distant neighbor atoms and on the corresponding coordination numbers.[101] The fine structure in absorption spectra above the L_{III} edge derives from interferences between outgoing photoelectron waves and backscattering waves from neighboring atoms. Typical parameters (estimated error bars in parenthesis) obtained from analysis of such spectra are interatomic distances R (±0.02 Å), coordination numbers (±15 to 20%), Debye-Waller factors (±0.005 $Å^2$), and the types Z of neighboring atoms (±4).[100] In EXAFS it is often not possible to differentiate between similar bond distances (within ~0.1 Å).[100] This issue is especially relevant for the discussion of An-O distances in the equatorial actinyl plane where often only an average distance can be determined. A condition for the direct interpretation of EXAFS data is that the species is present in the sample to >80%. However, under environmental conditions various complexes can coexist in solution; here EXAFS spectroscopy provides only an

average over such ensembles, in contrast to direct evidence available from e.g. vibrational spectroscopy. Concentration limits in EXAFS studies are about 5×10^{-4} mol/L.[100]

Electronic spectroscopic methods are supplemented by nuclear magnetic resonance spectroscopy (NMR), that is however restricted to the use of adequate nuclei, i.e. mainly ^{13}C and ^{17}O. NMR data provide structure and symmetry information. Besides identification of different actinides species in solution, this technique can also provide data to study equilibria of such species. Exchange reactions and exchange rates between different isomers can be investigated.[84]

2.2 Actinide environmental chemistry

The chemical behavior of actinides strongly depends on the surrounding media. Therefore understanding of actinide solution chemistry (typically aqueous solution) is essential for all environmental questions and problems. Many actinides exhibit different stable oxidation states that can result in distinctly different chemical behavior. For instance, U(IV) forms insoluble, polymeric, mixed hydroxides and carbonates in anoxic waters, but is oxidized under oxic conditions to U(VI) which, in turn, is capable of forming soluble species, allowing migration.[13] In solution hydrolysis is an essential process for most of the actinides (such as uranium and plutonium) and is strongly affected by the pH value and oxidation state. Complex formation – other than hydroxo complexes in the hydrolysis process – is controlled by the presence of complexing ligands and their concentration. The solubility of actinides depends on complex formation and colloid formation that itself is influenced by actinide concentration, presence of carrier colloids of other origin (“Fremdkolloide”), and sorption of actinides on these carrier colloids.[102] At very low actinide concentrations, e.g. in groundwaters, formation of intrinsic colloids (“Eigenkolloide”) is very improbable.[102] The diversity of these effects obviously can make experimental research quite complicated. In the next sections selected topics that are related to the actinide species investigated in this thesis will be introduced in more detail. The focus will mainly be on U and Np.

2.2.1 Oxidation states in the environment

Water has an important oxidation-reduction chemistry that limits oxidation states of actinides in solution. Therefore for most actinides the oxidation state depends on the redox potential. However, the redox potential varies strongly with the pH value that ranges from about 4 for mine waters, to pH 6 for rain and streams, to pH 8 for normal sea water and pH 10 for aerated saline residues.[10]

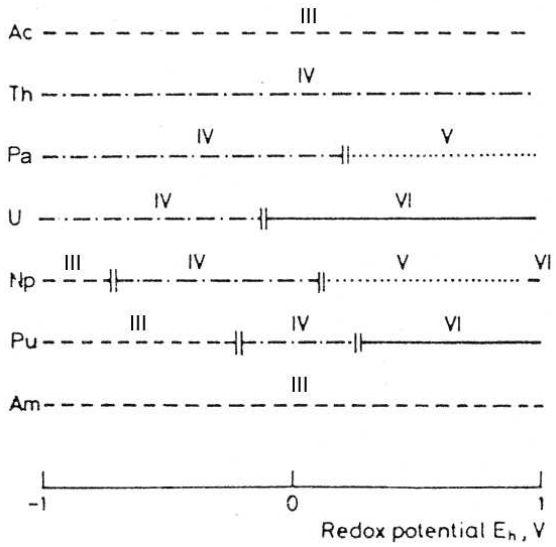

Figure 2.1. Oxidation states of early actinides (Ac to Am) at pH 7 in absence of complexing agents as a function of the redox potential E_h. Adapted from Ref. 102.

The oxidations states of early actinides (Ac to Am) in neutral aqueous media are shown in Fig. 2.1 as a function of the redox potential E_h. In general, higher values of E_h and increased pH favor higher oxidation states. Under reducing conditions (E_h < -0.1 V) only the low oxidation states III and IV are of interest for all actinides. At higher E_h values U^{4+} is oxidized to $[UO_2]^{2+}$ ($E_h \approx$ -0.1 V) and Np^{4+} is oxidized to $[NpO_2]^{+}$ ($E_h \approx$ 0.1 V). U(V) is not stable with respect to disproportionation into U(IV) and U(VI).[89] Oxidation of Pu^{4+} to $[PuO_2]^{2+}$ occurs at slightly higher redox potentials.

Therefore, in groundwaters oxidation states III and IV play the most important role except for uranium and neptunium. In oxygen-rich natural waters U(VI) and Np(V) have to be taken into account.

2.2.2 Hydrolysis

Like other metal cations actinide ions also undergo hydrolysis with increasing pH values. The hydrated actinide ions act as cationic acids and form hydroxo complexes by splitting off protons. In natural waters formation of such hydroxo complexes competes with the complexation by inorganic and organic ligands present. Substitution of the hydroxo ions can suppress hydrolysis. Under strongly basic conditions formation of precipitates of hydroxides, oxides, and basic salts or formation of colloids is possible, depending on the actinide element and its oxidation state.[10,90,94]

Hydrolysis reactions are important for all of actinides ions at pH values found in natural waters, with the exception of the pentavalent ion. Actinide(IV) ions An^{4+} have high charge-to-radius ratios and form hydrolysis products even in acidic solution, as low as pH = 0.[89] Pentavalent actinyl ions $[AnO_2]^+$ do not readily hydrolyze until pH = 9. The trivalent ions An^{3+} and the hexavalent actinyl ions $[AnO_2]^{2+}$ start to hydrolyze at about pH = 4 at room temperature. Corresponding to the formation of complexes, the tendency of hydrolysis decreases in the order An(IV) > An(III) ≈ $[AnO_2]^{2+}$ > $[AnO_2]^+$.

Uranium hydrolysis

Hydrolysis of U^{4+} has been studied in detail in acidic solutions and starts at uranium concentrations less than 0.1 mol/L, Eq. (2.1):

$$U^{4+} + n\,H_2O \rightarrow [U(OH)_n]^{4-n} + n\,H^+ \qquad (2.1)$$

Qualitatively the hydrolysis of U(IV) is similar to that of Th(IV), although conclusive identification of individual species is lacking.[103] The study of U(IV) is complicated due to the precipitation of insoluble hydroxides and oxides. There is reasonable experimental evidence for the formation of $[U(OH)]^{3+}$, in contrast to other hydrolysis products such as $[U(OH)_2]^{2+}$ and $[U(OH)_3]^+$. A substantial amount of data is consistent with the neutral species $U(OH)_4$ (or $UO_2{\cdot}2H_2O$), but it is not known whether this species is mono- or polymeric.[12,103]

The hydrolysis of uranyl(VI) has been studied extensively and begins at about pH = 3. It leads to the formation of both mono- and polynuclear hydrolysis products (*m*,*n*), i.e. $[(UO_2)_m(OH)_n]^{2m-n}$, Eq. (2.2):

$$m\,[UO_2]^{2+} + n\,H_2O \rightarrow [(UO_2)_m(OH)_n]^{2m-n} + n\,H^+ \qquad (2.2)$$

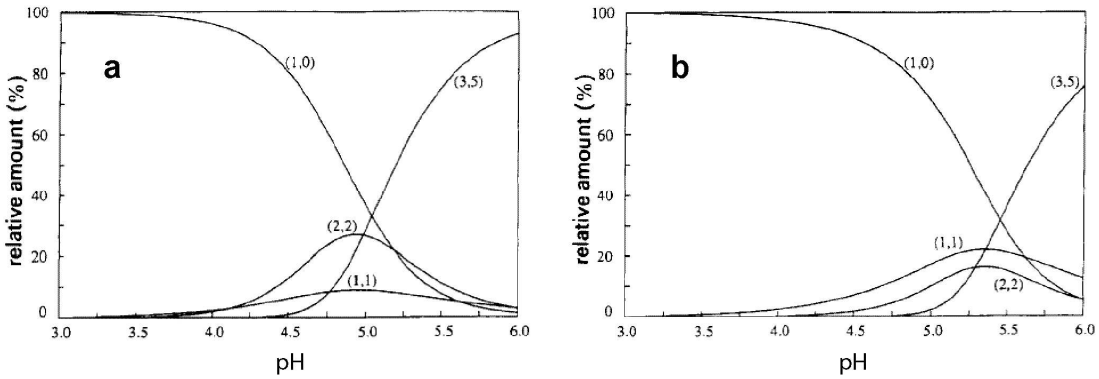

Figure 2.2. Distribution diagram (taken from Ref. 104) of uranyl(VI) hydrolysis species as a function of pH from speciation calculations for different U(VI) concentrations, 10^{-4} mol/L (a) and 10^{-5} mol/L (b). (*m*,*n*) designates corresponding uranyl hydroxo species $[(UO_2)_m(OH)_n]^{2m-n}$.

As smallest hydrolysis product $[UO_2(OH)]^+$ occurs in solutions containing less than 10^{-4} mol/L uranium.[103] At uranium concentrations above ~10^{-4} mol/L and medium pH > 4 the presence of polymeric species such as $[(UO_2)_2(OH)_2]^{2+}$, $[(UO_2)_3(OH)_4]^{2+}$, and $[(UO_2)_3(OH)_5]^+$ is well established (Fig. 2.2).[94,104] At higher pH, hydrous uranyl hydroxide precipitate is the stable species.[94] Precipitation can be prohibited by adding countercations[105] to yield monomeric hydroxide species $[UO_2(OH)_n]^{2-n}$ (n = 3, 4, 5).[106,107] The species $[UO_2(OH)_2]$, $[(UO_2)_3(OH)_7]^-$, $[(UO_2)_3(OH)_8]^{2-}$, $[(UO_2)_3(OH)_{10}]^{4-}$, and $[(UO_2)_4(OH)_7]^+$ are discussed as hydrolysis products as well.[94,108]

Although it is accepted that most hydrolysis species form, most of the scarce structural information for the polynuclear species in solution has been gained from the corresponding crystal structures;[109–112] the interpretation of solution data[113–115] is complicated by the simultaneous presence of various species. Especially the bridging mode in polynuclear species is under discussion, where next to OH bridges H_2O, O, and Cl bridges have been suggested.[110,112,116] For the dimeric species $[(UO_2)_2(OH)_2]^{2+}$ bridging by two hydroxyl groups is generally assumed and was confirmed in recent theoretical studies.[64,66]

Neptunium hydrolysis

Np(IV) is dominant under reducing conditions. The only experimentally reported hydrolysis product is $[Np(OH)]^{3+}$, other species are unknown.[117] Neptunyl(V) does not hydrolyze readily below pH = 9. At higher pH values, the hydrolysis species $NpO_2(OH)$ and $[NpO_2(OH)_2]^-$ have been observed.[118–120]

Hydrolysis of neptunyl(VI) starts at pH 3–4.[94,121] Studies indicate also polynuclear hydrolysis species similar to U(VI). The dimeric species $[(NpO_2)_2(OH)_2]^{2+}$ and the trimeric species $[(NpO_2)_3(OH)_5]^+$ have been reported.[121,122] Thus, hydrolysis of neptunium is not relevant in natural waters for low oxidation states, for Np(VI) it is very similar to U(VI).

2.2.3 Actinide complexation by carbonates

Carbonate is one of the most important natural ligands due to its ubiquitous presence in the environment. Natural waters show significant carbonate concentrations due to contact with minerals such as calcite or due to solubility of carbon dioxide (CO_2) from the air. The carbonate group acts as a bis(chelating) ligand and exhibits a strong metal-complexing ability. Thus, it is relevant for actinide complexation under environmental conditions.[12] Various stable carbonate complexes dominate actinide speciation in the presence of CO_2. In addition, such complexes play a role in industrial applications, primarily in uranium and thorium recovery from ores and nuclear fuel reprocessing.[89] For instance, in the alkali

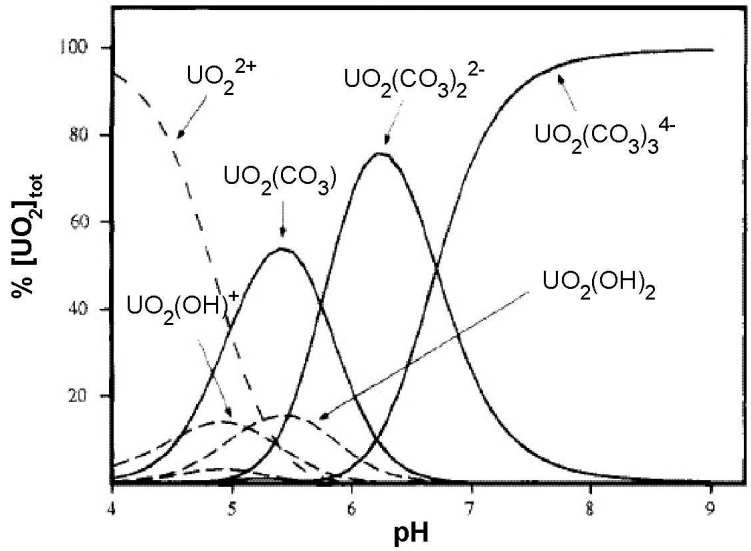

Figure 2.3. Distribution diagram (taken from Ref. 12) of uranyl(VI) species in carbonate solutions as a function of pH from speciation calculations.

leaching process for the recovery of uranium the high stability of the soluble uranyl carbonate complex is utilized as a means of selectively separating uranium from ore.[89] In the present context, the complexation of uranium(VI) by carbonates is important, to establish a chemical background for the investigation of uranyl carbonate species in Section 4.3.

Studies of actinyl(VI) carbonate systems can be quite complicated because several different ions can exist which are in rapid equilibria with one another and with the aquo ion or hydrolyzed species. The uranyl carbonate system is by far the most extensively studied among the actinide carbonate systems.[83,115,123–134] Mononuclear carbonate complexes $[UO_2(CO_3)_m]^{2-2m}$ (m = 1–3) form with increasing carbonate concentration at medium pH (Fig. 2.3).[124,127,135–137] The dominant species over a wide pH range (pH > 7) is the tris(carbonato) complex $[UO_2(CO_3)_3]^{4-}$ whose existence and composition is well established.[83,129–133]

Experimental evidence supports the existence of polynuclear solution species which form only at high metal ion concentration or high ionic strength.[103,138] At high actinide concentration and lower carbonate concentrations the polynuclear triuranyl hexa(carbonato) complex $[(UO_2)_3(CO_3)_6]^{6-}$ forms at pH 5–7.[125,128,129,134,139,140] The trimeric species is stabilized in solutions of high ionic strength and is thought to be responsible for the high solubility of UO_2CO_3(s) in carbonate solutions; thus it can influence the aquatic actinide transport.[140] The dinuclear hemicarbonate species $[(UO_2)_2(CO_3)(OH)_3]^-$ forms if the ratio between total concentrations of U(VI) and carbonate is larger than 1.[83,84]

Polynuclear complexes are not expected in natural water systems due to a low concentration of actinyl ions and low ionic strengths. However, the situation might be different in nuclear waste repositories or contaminated sites where one can expect significantly higher actinide concentrations.[12] Under typical conditions in groundwaters, monomeric actinyl carbonate complexes $[UO_2(CO_3)_m]^{2-2m}$ dominate (Fig. 2.3).

2.2.4 Actinide interaction with humic substances

Complexation of actinides by biological decomposition products such as humic substances plays an important role in the migration and the retardation of actinides in natural systems and therefore is an essential ingredient of safety analysis for radioactive waste management, including long-term storage.[6,7]

Humic materials, i.e. organic polyelectrolyte macromolecules formed by the degradation of plants and animals, occur throughout the ecosphere in soils and waters. Their concentrations are dependent on many factors such as climate, pH, substrate material, topography, and time. In soils the humic content varies from 0 to 10%.[7] In waters the dissolved organic carbon (DOC) is for instance up to 50 ppm in swamps. Samples of surface water sites exhibit DOC values from 0.1 to 8 ppm. Typical values for groundwater are 0.1 ppm and 0.5–1.2 ppm in the world's oceans.[13]

Humic substances are divided by their solubilities in humin (insoluble at all pH's), humic acid (HA, soluble at pH > 3), and fulvic acid (FA, soluble at pH < 3). In general, the structures of fulvic acids have more aliphatic and less aromatic character than humic acids. Fulvic acids are characterized by lower molecular weights 300 to 2000 amu, while 1000 to 50000 amu is typical for aquatic humic acids and 50000 to 100000 amu for soil humic acids.[7]

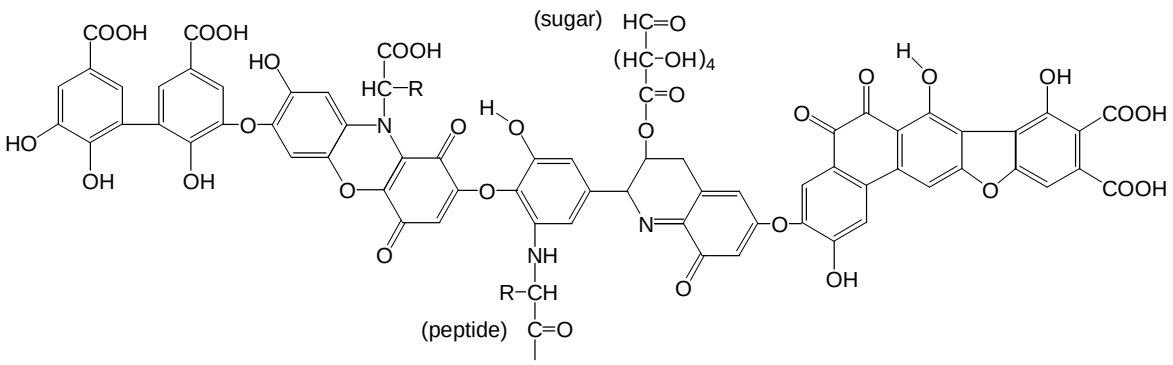

Figure 2.4. Model structure of a humic acid. Adapted from Ref. 86.

Table 2.3. Fractions of functional groups in samples of humic (HA) and fulvic (FA) acids (in percentage).[a]

	COOH	Phenolic OH	Aliphatic OH	C=O	OCH_3	Other
HA	34–50	7–14	1–8	15–30	2–4	5–29
FA	57–75	1–10	9–20	11–17	3–5	0–10

[a] Ref. 7.

As a product of organic degradation, humic materials have a non-uniform structure which varies with age, geography, and decomposition conditions. This makes characterization and weight determination difficult. Humic substances may be described by a coiled hydrocarbon backbone with several functional groups such as carboxylic, phenolic or aliphatic OH, carbonyl, and amino substituents that are discussed as complexing sites for metal ions (Fig. 2.4).[7,86] Table 2.3 lists the distribution of oxygen donor sites for samples of humic and fulvic acids.

In general, carboxylic moieties are the dominating functional groups of humic substances (Table 2.3). Their importance derives from the fact hat they are mainly responsible for the complexation of metal ions at low pH values.[6,78,85] The influence of phenolic OH groups on the complexation properties of humic acids is under investigation.[141–144] Often, the ratio of the carboxylate capacity to that of the phenolate is higher in fulvic acids than in humic acids (Table 2.3).[145] pK_a values for carboxylate groups of 3.6±0.1 and 4.8±0.2 have been found for fulvic and humic acids, respectively; pK_a values of ~9.7±0.2 have been reported for phenolic groups.[146] These data indicate that in most natural waters carboxylate groups are 80–100% ionized whereas phenolic groups remain protonated.

However, the character of humic substances depends strongly on their source which complicates the characterization of interactions of actinides and humic acids. Besides the identification of complexation sites, another major issues is to understand the complexation mechanisms in order to model or even influence the migration or the retardation of actinides.

To study interactions with carboxylic groups, actinide complexes with various carboxylate ligands have been used as model systems and have been experimentally investigated by XRD and EXAFS spectroscopy, to determine formation constants of complexes, structures, and coordination modes.[147–157] A carboxylate group can coordinate to an actinyl in bidentate (Fig 2.5a) or monodentate fashion (Fig. 2.5b); pseudobridging coordination, i.e. monodentate coordination accompanied by a strong hydrogen bond

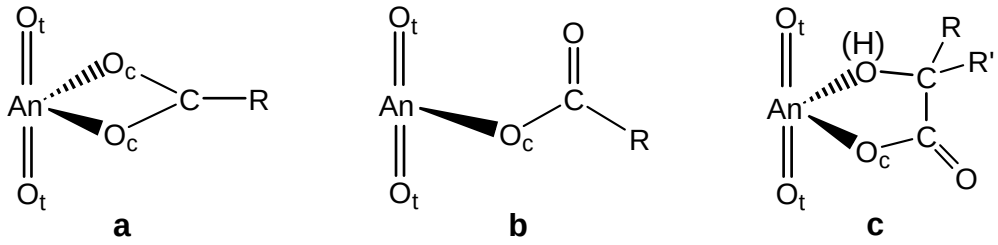

Figure 2.5. Possible coordination modes of carboxylate groups at actinyls: bidentate (a), monodentate (b), and chelate (c) coordination.

between the free carboxylate oxygen and an aqua ligand of the uranyl, has also been suggested.[97] In addition, chelate coordination via adjacent (deprotonated) hydroxo groups, e.g. in glycolate or α–hydroxyisobutyrate, is discussed (Fig. 2.5c).[155,158] Another important coordination mode, found in many crystal structures, is an arrangement where the two oxygen centers of the carboxylate form a bridge between two neighboring uranyl moieties.[147] This variety of different coordination modes overall results in linear chains, sheets, and networks.[147] Analysis of various crystal structures indicates that uranyl ions favor bidentate coordination.[159] This is reflected by the high stability of tris(carboxylato) complexes such as $M[UO_2(OOCCH_3)_3]$ (M = monovalent cation) that occur as monomers where three carboxylates act as bidentate ligands.[147] The same coordination has also been suggested for the complex $[UO_2(OOCCH_3)_3]^-$ in solution.[156]

EXAFS results both on the complexation of actinides by natural and synthetic humic acids, from solids and in solution, are interpreted as predominantly monodentate coordination.[141,150,160,161] However, it is unclear why only monodentate complexation of actinides should occur, considering the complex structure of humic substances and the predominance of carboxylic groups as complexing sites. To contribute to the discrimination of coordination types, different modes have been studied in this work, using model complexes of uranyl and neptunyl with various simple carboxylates as ligands (see Section 4.4).

The discussion of actinide migration can also be complicated by colloid formation in solution. Humic acids themselves may form colloids. In addition, the binding of metal ions to humic acids can lead to the formation of more compact, less hydrophilic structures which result in configuration changes as well as molecular aggregation and/or coagulation.[7] If such aggregates are small enough (e.g. < 45 mm) they may remain suspended in solution as colloids. Actinide ions can be incorporated as bound metal ions or the humic acid can serve as a host to the sorption of hydrolyzed actinide ions onto the colloid surface to form so called “pseudocolloids”.[82]

In addition to direct complexation, humic substance may influence the solubility and migration of actinides because of redox reactions. The reported reduction potential range of humic acids is consistent with the redox potential of hydroquinone groups that provide a source of long lived free radicals with reduction capability.[162] Photolysis of humic substances by UV light results in the production of hydrogen peroxide.[162] Thus, humic substances can induce redox reactions. Reduction will change the actinide oxidation state resulting in different species with possibly different migration properties. For instance, Pu(VI) solutions in the presence of sun light and in the absence of humic acids are quantitatively reduced within minutes to Pu(V) where the pentavalent state is stable for weeks. Upon addition of 0.1 ppm humic acids, only 40% of the plutonium was found in the pentavalent oxidation state after 48 hours due to reduction to Pu(IV) which hydrolyses as $Pu(OH)_4$.[163] Thus, knowledge about actinide speciation and the corresponding redox chemistry obviously is essential for the prediction of actinide migration.

3 Computational Method

All calculations in this thesis were carried out with the parallel code PARAGAUSS[164,165] that is based on the LCGTO-FF-DF (linear combination of Gaussian-type orbitals fitting function density functional) method.[166] Distinguishing features of PARAGAUSS are the consequent parallel implementation of all demanding tasks, an efficient relativistic treatment of heavy atoms, and various approaches for describing interactions of a system with its surrounding. These approaches include a polarizable continuum model (PCM) to simulate solvent effects,[43] a quantum mechanics/molecular mechanics method (QM/MM),[167] cluster embedding in an elastic polarizable environment (EPE),[168] and its extension to covalent substrates (covEPE).[169] Another very important feature is the full utilization of symmetry in almost all procedures, which allows a speed-up of the calculations for symmetric species or models.[170]

In the following sections, computational background information and some details are presented. As mentioned before, the treatment of actinides requires relativistic effects to be taken into account. Thus, inclusion of these effects in the density functional method applied will be briefly discussed (Section 3.1). Solvent effects are essential for actinide species under environmental conditions; they have been modeled via a PCM model (Section 3.2). Then some technical details for the calculation of vibrational frequencies will be discussed (Section 3.3). In Section 3.4, the basis sets will be described. The final section (Section 3.5) briefly summarizes computational details applied for the calculations of this thesis.

3.1 Relativistic electronic structure calculation

3.1.1 Relativistic effects

Relativistic effects in chemical terms are understood as all effects in the electron structure and derived properties of atoms or molecules which result from reducing the speed of light from an infinite to its finite value.[25] In quantum chemistry this is related to differences that are introduced if one replaces the non-relativistic Schrödinger equation by the relativistic Dirac equation.

Relativistic effects have been identified for elements starting even from a nuclear charge of about Z = 30.[25] Nevertheless, relativistic effects on the valence electrons are in general expected to be chemically important only for higher values of the nuclear charge; they become relevant for second-row transition metals ($Z \geq 39$) and are essential for a correct treatment of the actinides ($Z \geq 89$).

In chemistry three main effects are usually considered: (i) as direct effects, *s* and *p* atomic orbitals are contracted and stabilized in energy, (ii) as indirect effects, *d* and *f* atomic orbitals expand and are destabilized, and (iii) spin-orbit interaction splits atomic level with angular momentum $l > 0$ into two sub-shells with total angular momenta $j = l \pm ½$.[25,171] In Fig. 3.1, these effects are schematically illustrated for uranium valence orbitals.[171]

All three relativistic effects are of the same order of magnitude and increase roughly like Z^2 for valence shells.[25] With increasing number of Z, the relativistic component of the total energy increases proportionally to Z^n ($n > 1$). The spin-orbit splitting of valence orbitals is proportional to Z^4 and in the case of actinides several eV, i.e. comparable to chemical bond energies.[171]

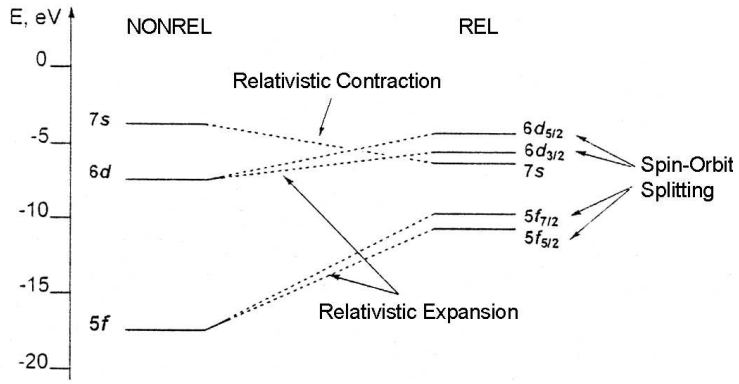

Figure 3.1. Valence levels of the uranium atom from nonrelativistic (NONREL) and relativistic (REL) Dirac-Hartree-Fock atomic calculations. Adapted from Ref. 171.

A detailed consideration of relativistic effect shows that many well-known properties of materials can only be explained within relativistic quantum mechanics.[25] For instance the unique position of gold (Z = 79) among the elements and also its spectacular color are connected to relativistic effects.[25]

3.1.2 Relativistic density functional theory

In recent years, density functional (DF) methods have become quite popular and for many applications now form the standard, having replaced the traditional wave-function based methods such as Hartree-Fock (HF), second-order Møller-Plesset perturbation theory (MP2), and configuration interaction (CI). For many chemical problems, DF methods furnish a sufficiently accurate, yet computationally efficient description of molecular structures and energetics.[172]

Within the DF approach the energy of a system is minimized with respect to variations of the electron density which forms the central quantity.[173] Hohenberg and Kohn proved that the electron density of the ground state of a system *uniquely* determines the ground state wave function and hence all properties of the ground state, even in the presence of a static external potential.[174] The corresponding variational procedure is usually carried out by solving the Kohn-Sham (KS) equations, Eq. (3.1). This leads to an effective one-electron problem governed by an effective potential v_{eff} that comprises the (external) nuclear potential v_{nuc}, the classical Coulomb or Hartree potential v_{coul}, and the exchange-correlation (xc) potential v_{xc}, Eq. (3.3).[173,175]

$$\hat{h}_{KS}\psi_i = \varepsilon_i\psi_i \tag{3.1}$$

$$\hat{h}_{KS} = -\tfrac{1}{2}\nabla^2 + v_{eff} \tag{3.2}$$

$$v_{eff} = v_{nuc} + v_{ee} = v_{nuc} + v_{coul} + v_{xc} \tag{3.3}$$

In principle, the Kohn-Sham formalism allows one to solve the Schrödinger equation exactly. However, the exact form of the exchange-correlation potential v_{xc} is unknown. It includes the electron-electron interaction beyond the classical Coulomb self-interaction of a charge density, and a part of the kinetic energy. Formally, the exchange-correlation potential is given as the functional derivative of the corresponding exchange-correlation energy E_{xc} with respect to the density ρ, Eq. (3.4).

$$v_{xc}[\rho](\vec{r}) = \frac{\delta}{\delta\rho(\vec{r})} E_{xc}[\rho] \tag{3.4}$$

Different approximations are used to describe v_{xc}.[172] The local density approximation (LDA) is derived from the homogenous electron gas and assumes that v_{xc} is a simple function of the density ρ. The generalized gradient approximation (GGA) improves this approximation by taking into account the gradient of the local electron density. Hybrid functionals mix explicitly density-dependent parts of the GGA form and the exact non-local exchange energy of the KS determinant, using a fixed ratio. In Section 3.1.3, the performance of LDA and GGA functionals will be discussed for representative actinide systems.

The relativistic analogue of the KS Hamiltonian, Eq. (3.2), is the Dirac-Kohn-Sham (DKS) Hamiltonian, Eq. (3.6). However, solving the resulting DKS equation, Eq. (3.5), requires a notably larger computational effort due to the four-component nature of the solutions that are inherently complex-valued and describe positron as well as electron degrees of freedom. If one resorts to a two-component description which explicitly treats only the electron degrees of freedom, this statement still holds, albeit to reduced extent, because spin-orbit interaction is accounted for in full.[176]

$$\hat{h}^{(4)}_{DKS}\psi^{(4)}_i = \varepsilon_i\psi^{(4)}_i \tag{3.5}$$

$$\hat{h}^{(4)}_{DKS} = c\vec{\alpha}\cdot\vec{p} + \beta c^2 + v_{eff} \tag{3.6}$$

The Douglas-Kroll approach,[177] as worked out by Hess and collaborators for molecular systems (DKH)[178] affords a two-component variational DF formalism. In most practical applications, the DKH transformation of the DKS equation, Eq. (3.7), is restricted to decoupling electron and positron degrees of freedom to second order in the effective one-electron potential of the KS theory.[17,176] This unitary transformation leads to the exact second-order DK Hamiltonian, Eq. (3.8), where E_p is the energy of a free particle of momentum p:

$$\hat{h}^{(2)}_{DK2} = U\hat{h}^{(4)}_{DK2}U^{\dagger} \tag{3.7}$$

$$\hat{h}^{(2)}_{DK2} = E_p + v^{rel}_{nuc} + v^{rel}_{coul} + v^{rel}_{xc} \qquad E_p = c\sqrt{p^2 + c^2} \tag{3.8}$$

In the DFT context, the transformation as well as its application is restricted in most practical cases to the nuclear potential v_{nuc}, i.e. one approximates $U[v_{eff}] \approx U[v_{nuc}]$, Eq. (3.9).[18,179] The electron-electron (ee) interaction, comprising the Hartree potential v_{coul} and the exchange-correlation potential v_{xc}, is added afterwards in their nonrelativistic forms.

$$\hat{h}^{(2)}_{DK2} = E_p + v^{rel}_{nuc} + v_{coul} + v_{xc} \tag{3.9}$$

This Douglas-Kroll variant will be denoted as DKnuc method. The DKH formalism generates a scalar-relativistic (SR) variant if one neglects spin-orbit (SO) interaction; otherwise, one arrives at a SO variant of the method.[180] Although the one-component SR method yields molecular structures and energetics that are often sufficiently accurate, an adequate treatment of SO interaction can be indispensable for open-shell problems. Especially effects on atomization energies can be significant because the ground state configuration can strongly be affected by SO coupling.[35,36]

The DKH transformation of the DKS equation was extended to include a self-consistent treatment of the electron-electron interaction (referred to as DKee) and implemented for the Hartree potential based on $U[\nu_{eff}] \approx U[\nu_{nuc}, \nu_{coul}]$, Eq. (3.10).[179]

$$\hat{h}_{DK2}^{(2)} = E_p + v_{nuc}^{rel} + v_{coul}^{rel} + v_{xc} \tag{3.10}$$

Screening of ν_{nuc} by ν_{coul} significantly improves the SO splitting of heavy atoms as well as g-tensor shifts in molecular systems.[179,181] The relativistic transformation of the Hartree terms was originally based on the resolution of the identity (RI) approach[179] which entails a notable computational effort because higher angular momentum functions have to be added to the basis set to ensure kinetic balance. Using analytical expressions for the matrix elements of the relativistically transformed operators, one is able to avoid the RI approach.[182] This translates to smaller basis sets and better performance as well as higher accuracy and stability of the results with respect to basis set changes.[182]

To reduce the computational effort, one may resort to a mean-field approach.[183] Boettger[184] proposed a screened nuclear potential SO (referred to as SNSO) approximation as a variant of the DKnuc method. Instead of explicit screening by electronic contributions one scales the first-order SO terms in the Kohn-Sham Hamiltonian (due to the nuclear potential) by adjustable parameters. The SNSO approximation was shown to improve the fine structure of heavy atoms.[184] Boettger's strategy was extended to a model (referred to as DKnuc SNSO) that effectively includes the second-order ee SO terms. This inclusion reduces the notable overestimation of atomic and molecular SO splittings of *p*-derived levels that is still present in the first-order SNSO approach.[184,185] The computational expense of the SNSO model, also in second order, goes hardly beyond that of the DKnuc method, yet the DKnuc SNSO results compare very well with those of the more exact DKee treatment.[185] The three described SO variants, DKnuc, DKee, and SNSO, are evaluated for actinyls of U(VI), Np(VI), and Np(V) in comparison to a standard scalar-relativistic treatment in Section 3.1.4.

3.1.3 Evaluation of exchange-correlation functionals

Three different exchange-correlation functionals were tested to determine the most adequate description of actinide systems: the LDA functional as parameterized by Vosko, Wilk, and Nusair (VWN),[186] and the GGA functionals suggested by Becke and Perdew (BP)[187,188] as well as the revised version of the Perdew-Burke-Ernzerhof functional of Nørskov et al. (PBEN).[189] LDA often yields more accurate results for molecular geometries and frequencies, whereas gradient-corrected functionals yield improved binding energies.[190,191]

To correct the overestimation of binding energies by LDA, the pertinent energetics were evaluated with the BP (GGA) functional, applied self-consistently in a "single-point fashion" at structures that previously had been optimized at the LDA (VWN) level. An additional advantage of this strategy is a reduced computational effort during the optimization due to the simpler LDA functionals. However, as the LDA minimum usually is somewhat different from the GGA minimum, the "single-point" energetic GGA evaluation is somewhat inconsistent. Thus, for a more consistent treatment one can apply GGA functionals also for the optimizations being aware of the slight overestimation of bond distances. Differences between these two strategies are usually small and may depend slightly on the systems investigated. For instance, binding energies in gold coated nickel clusters differ by at most 0.05 eV per atom compared to full GGA calculations, i.e. about 2% of the absolute binding energy.[192] Thus, a combined approximate LDA-GGA approach is justified.

Previous test calculations[55] on the actinide hexafluorides AnF_6 (An = U, Np) compared bond lengths, vibrational frequencies, and binding energies with experimental data. The results confirmed the well-known trend[190,191] that LDA distances are more accurate (±0.03 Å) and GGA tends to slightly overestimate distances (+0.04 Å), resulting in an underestimation of corresponding vibrational frequencies. However, the calculations also showed the typical overestimation of binding energies by LDA (up to ~130 kJ mol^{-1} per F in AnF_6) which renders this functional inadequate for discussions of energetics.

These general results were confirmed by calculations on uranyl dimer complexes $[(UO_2)_2(OH)_2(H_2O)_n]^{2+}$ (n = 0, 6) that produced elongated bond distances for the GGA functionals BP and PBEN.[66] The PBEN functional yields in general slightly longer bonds than the BP functional. While the strong uranyl bond is hardly affected with a GGA functional (0.01 to 0.02 Å longer compared to LDA), the equatorial U-O distances to bridging oxygen centers and to the aqua ligands are calculated distinctly longer, by 0.05 to 0.15 Å. LDA binding energies per aqua ligand in these complexes are higher by about

40 kJ/mol, i.e. 60%, compared to GGA.[66] To correct for the LDA overestimation, the GGA functionals were evaluated self-consistently in "single-point fashion" (see above). Compared to full GGA calculations, binding energies are slightly underestimated, by ~7 kJ mol^{-1} (10%).[193]

Data on actinide complexes $[AnO_2(H_2O)_5]^{2+/+}$ (see Section 4.1) and from other theoretical studies confirm the notable overestimation of bond distances in calculations which employ GGA functionals.[62,63,64] Thus, the LDA (VWN) functional was chosen for all geometry optimizations to benefit from the overall more accurate geometric parameters.

3.1.4 Evaluation of spin-orbit effects

To check the relevance of spin-orbit (SO) effects test calculations were performed for the hexa- and pentavalent actinyls $[AnO_2]^{2+/+}$ (An = U, Np) in the gas phase. Spin polarized scalar-relativistic (SR) calculations are compared to different treatments of the SO interaction: DKnuc, DKee, and SNSO (Section 3.1.2). The energy minimum was determined by fitting data points from single-point calculations to a parabola (6 to 10 data points; all fits were of high quality with $R^2 > 0.999$) because energy gradients are not available in PARAGAUSS for calculations involving SO interaction (Table 3.1).

SO effects both in VWN and BP calculations are rather small for all species, i.e. both closed-shell $[UO_2]^{2+}$ and open-shell actinyls $[UO_2]^{+}$, $[NpO_2]^{2+}$, and $[NpO_2]^{+}$. Differences to the scalar-relativistic results are smaller than 0.006 Å for the $An{=}O_t$ bond distance except for $[UO_2]^{+}$ (0.01 Å) and therefore at the edge of the numerical accuracy generally expected for the method applied. Due to these minor effects, the minima obtained from SO calculations are energetically close to those of SR calculations, i.e. energy deviations are smaller than 0.3 kJ mol^{-1}, again slightly higher for $[UO_2]^{+}$ (~0.6 kJ mol^{-1}). Thus, inclusion of SO effects on energies in a "single-point fashion" based on optimized SR structures is acceptable. Not unexpectedly, the effect on the calculated ionization potential for $[AnO_2]^{+} \rightarrow [AnO_2]^{2+}$ is more pronounced (up to 0.6 eV). This points to effects due to SO splitting which affects the energy level of the involved HOMO and thus the ionization potential. Ionization potentials calculated based on the most accurate approximation DKee show the smallest differences to those of the SR calculations, i.e. 0.01 to 0.36 eV.

Thus, spin-orbit effects both on structures and energies are considered to be rather small for all investigated actinyls. This is expected for closed-shell systems such as U(VI) and can be can be rationalized for the open-shell systems of U(V), Np(VI), and Np(V) by the strong localization of the f electrons at the actinide centers. Based on minor changes on the strong actinyl bond, effects of SO interaction on the actinyl stretching frequencies are

expected to be small. However, based on these data it is not possible to estimate SO effects on weaker bonds, e.g. to coordinated aqua ligands in the equatorial actinyl plane. In summary, spin-orbit effects will be neglected in subsequent investigations.

Table 3.1. Comparison of different relativistic methods including SO interaction (DKnuc, DKee, and SNSO) applied to hexa- and pentavalent actinyls $[AnO_2]^{2+/+}$ of U and Np in the gas phase. Also shown are results from non-relativistic (NR) and scalar-relativistic (SR) calculations. Bond distances (An=O_t, in Å), total energy differences with respect to the SR minimum (ΔE_{min}, in kJ mol^{-1}), and ionization potentials (IP, in eV) for $[AnO_2]^+ \rightarrow [AnO_2]^{2+}$ both from LDA (VWN) and GGA (BP) calculations. Deviations Δ are given with respect to the SR values.

		VWN			BP		
		An=O_t	ΔE_{min}	IP	An=O_t	ΔE_{min}	IP
$[UO_2]^{2+}$	NR	1.667					
	SR	1.702			1.719		
	Δ DKnuc	0.002	-0.015		0.002	-0.015	
	Δ DKee	-0.006	-0.261		0.001	-0.003	
	Δ SNSO	0.001	0.002		0.001	0.003	
$[UO_2]^{+}$	NR	1.682					
	SR	1.741		14.86	1.761		14.95
	Δ DKnuc	0.011	-0.600	0.62	0.010	-0.519	0.53
	Δ DKee	0.010	-0.637	0.36	0.010	-0.484	0.27
	Δ SNSO	0.010	-0.511	0.41	0.010	-0.451	0.32
$[NpO_2]^{2+}$	NR	1.667					
	SR	1.698			1.716		
	Δ DKnuc	0.001	0.005		0.001	-0.001	
	Δ DKee	-0.001	-0.006		-0.0001	-0.004	
	Δ SNSO	-0.001	0.003		-0.001	-0.003	
$[NpO_2]^{+}$	NR	1.677					
	SR	1.733		15.58	1.753		15.64
	Δ DKnuc	0.001	-0.004	0.20	0.000	-0.005	0.11
	Δ DKee	-0.001	-0.001	0.05	0.005	-0.012	-0.01
	Δ SNSO	-0.001	-0.008	0.29	-0.001	-0.010	0.26

3.2 Modeling of solvation effects

3.2.1 Solvent effects in quantum chemistry

As previously mentioned, solvent effects are crucial for the chemistry of actinide elements under environmental conditions. Solvent effects are known to affect properties of molecular ions significantly. Charged species are considerably stabilized due to solvation with respect to the gas phase and solvent effects can noticeably influence structures and energetics of such species.[37,194,195]

Major contributions to the solvent effects on molecular ions are due to the mutual polarization of the solvent and solute based on long-range Coulomb interactions.[37,194,195] Treating solvent effects is computationally rather demanding, whether done in an explicit supermolecular approach of a solvated molecule together with a sufficiently large number of solvent molecules[196] or in a perturbation treatment.[197] However, since the pioneering works of Tomasi and coworkers[198] it has become customary to represent long-range effects in quantum chemistry calculations with the help of a polarizable continuum model (PCM)[194,198] where the solute is placed in a cavity of a polarizable dielectric medium. Among many variants, the conductor-like screening model (COSMO)[199] has become very popular due to its economy.[200–202] A COSMO variant is implemented in the program PARAGAUSS employed in this thesis (see Section 3.2.2).[43]

However, for various problems it does not suffice to consider the solvent as a polarizable continuum when one aims at a more quantitative account of solvation effects. Especially short-range solvent effect due to coordinated aqua ligands or due to directed hydrogen bonds are not described by PCM models. For several actinide species in solution it has been shown that these short-range effects can be rather strong and distinctly affect molecular structures, vibrational frequencies, and solvation energies.[20,22,23,38–43,66] Therefore, a combined approach that considers both explicit coordination of aqua ligands from at least the first coordination sphere and treats the remaining solvent as a polarizable continuum is advisable.[43]

3.2.2 The conductor like screening model (COSMO)

In the COSMO approach,[199] as in all continuum models, the solute is placed in a cavity of the solvent simulated by a continuous polarizable medium with a dielectric constant ε. The solute cavity is chosen as a set of overlapping spheres centered on the atoms of the solute (Fig. 3.2). In PARAGAUSS the default radii of theses spheres are scaled by van der Waals (vdW) radii[203] (factor 1.2, except for H where the radius is not scaled). Note that PCM results are known to depend crucially on the sphere radii.[202]

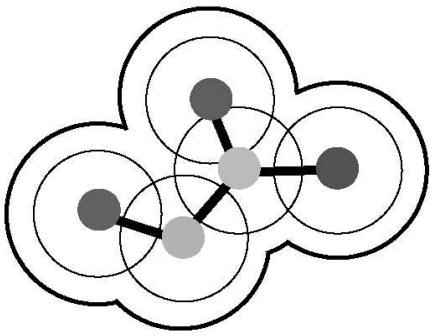

Figure 3.2. Schematic representation of the cavity constructed around the solute molecule in a polarizable continuum model (PCM).

Furthermore, the cavity shape is smoothened by introducing additional spheres according to the GEPOL algorithm to avoid cusps or narrow niches in the cavity. However, in its original implementation (GEPOL 87),[204,205] this algorithm yielded problems for certain larger systems such as the triuranyl hexa(carbonato) complex (see Section 4.3.2). In these cases, the algorithm lead to a very large number of additional spheres (up to ~100) which in turn caused problems during the tessalation of the cavity surface. Therefore, a second GEPOL variant (GEPOL 93)[206] was implemented in PARAGAUSS recently.[207] Both algorithms are compared below (see Section 3.2.3). The number of additional spheres is kept constant during a geometry optimization to avoid discontinuities of the energy during the optimization.

In the COSMO model the surface charge density due to the discontinuity of the dielectric constant at the cavity surface is determined by a conductor-like boundary condition,[199] i.e. the total Coulomb potential vanishes on the cavity surface. By partionating the cavity surface into small patches, so-called tesserae, the surface charge is approximated by a set of point charges. Point charges are placed at representative points of each tessera that can be determined in different ways.[43]

Furthermore, to allow a symmetry-adaptation of the COSMO approach, a tessalation scheme is chosen that leads to a distribution of surface grid points which complies with the symmetry of the molecule. The cavity surface is divided into polyhedra, mainly triangles, by projecting the faces of a polyhedron of a given symmetry onto a concentric sphere. The tessellation scheme is translated to each of the cavity building spheres that by construction are arranged according to the point group of the solute.

In addition to the original COSMO model, the PARAGAUSS solvent module also accounts for short-range nonbonding solvent effects via a force field.[43] It is customary to

treat dispersion and repulsion interactions by means of a pair potential approach.[208] In addition the cavitation energy, i.e. the energy required to form the cavity inside the solvent, can be estimated by a scaled particle theory,[194] which is based on the cavity of superimposed spheres which are obtained with unscaled vdW radii.[43]

Within the COSMO approach (here ε = 78.39 for water at T = 25 ºC = 298 K) solvation energies can be estimated as the difference between the COSMO total energy E_{COSMO} and the corresponding gas phase energy E_{GP}:

$$\Delta G_{sol}^{298} \approx E_{COSMO} - E_{GP} \tag{3.11}$$

In this way, solvation energies for small molecules, such as H_2O, NH_3, F^-, and OH^-, are determined in good agreement with experiment.[43] It has been shown that for compounds where water molecules of the first hydration shell act as coordinated ligands (e.g. uranyl), there is a distinct effect on the solvation energy due to ligand-metal bonding and donation of electronic charge from the ligands.[43] These short-range solvent effects are not described by the PCM model. Thus for an accurate calculation of the solvation energy, such aqua ligands have to be taken into account explicitly in the quantum chemistry models.[43]

Quantum mechanical calculations of the solute usually produce a tail of the wave function that penetrates outside the solute cavity. This results in an additional volume polarization charge density which is spread throughout the dielectric continuum outside the cavity.[209,210] Volume polarization effects have been shown to have a significant influence on free energies of solvation[211,212] and nuclear magnetic resonance shielding constants.[213] The additional charge density outside the cavity is sometimes treated by a "renormalization" of the total charge. However, these methods often are not able to reproduce the actual effects of volume polarization on free energies of solvation.[211] On the other hand, a detailed analysis[210,214] indicates that in the COSMO variant the density outside the cavity is screened to a large extent and therefore, a renormalization is usually not mandatory to achieve a proper representation of the corresponding energy contribution. This aspect has been investigated for the highly charged anionic uranyl tris(carbonato) complex $[UO_2(CO_3)_3]^{4-}$ in Section 4.3.1.

Furthermore, problems can arise from the so-called discretization error, i.e. from the representation of the charge density by discrete point charges on the tesserae.[199] This error is expected to decrease with a refinement of the size of the individual tessera. Effects on solvation energies have been shown to be rather small compared to variations caused by the choice of the cavity radii.[43]

3.2.3 GEPOL algorithms

In the following, the two GEPOL algorithms, GEPOL87 and GEPOL93, to create additional spheres in the COSMO model are compared. Corresponding sets of parameters used in these algorithms have been defined in this work to allow application of both methods with similar results. Figure 3.3 introduces the parameters used in both algorithms. For two overlapping spheres, one defines the radii r_{min} and r_{max} corresponding to the smaller and larger sphere, respectively. The angle α or the distance p are used to characterize the overlap of the two spheres (Fig. 3.3).

Before creating additional spheres, the program checks how strongly a given pair of spheres overlap. GEPOL87 uses the overlap angle $\alpha \in [0; \pi]$ (always defined with respect to the smaller sphere) as criterion. The volume inaccessible to the solvent between the two spheres decreases continuously when the overlap angle α increases (Fig. 3.3). If α is close to $\pi/2 = 90^o$ this volume becomes so small that the effect of adding more spheres becomes negligible. The alternative GEPOL93 algorithm utilizes the so-called overlap factor $f = p / 2r_{min} \in [0; 1]$ with $p = r_{min} + r_{max} - d$ (Fig. 3.3). For $\alpha = 0$ or $f = 0$ the two spheres are just touching each other and for $\alpha = \pi$ or $f = 1$ the smaller sphere is engulfed by the larger one. The overlap distance d is calculated for both approaches according to Eqs. (3.12) and (3.13), respectively. Both criteria yield the same result for $d_{max} = r_{max} + r_{min}$ ($f = 0$ or $\alpha = 0$) and $d_{min} = r_{max} - r_{min}$ ($f = 1$ or $\alpha = \pi$).

$$d = r_{min} \cos(\alpha) + \sqrt{r_{max}^2 - [r_{min} \sin(\alpha)]^2} \tag{3.12}$$

$$d = r_{max} + r_{min}(1 - 2f) \tag{3.13}$$

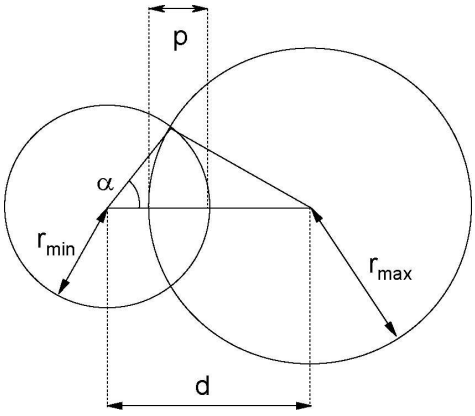

Figure 3.3. Schematic representation of two overlapping spheres and definition of parameters used in the two GEPOL variants to create additional spheres. r_{min} and r_{max} define the radii corresponding to the smaller and larger sphere, respectively. The angle α and the distance p are used to characterize the overlap of the two spheres.

Thus, the two overlap parameters α and *f* are connected via Eq. (3.14).

$$f = -\frac{1}{2}[\cos(\alpha) - 1] + \frac{1}{2}\frac{r_{max}}{r_{min}} - \frac{1}{2}\sqrt{\frac{r_{max}^2}{r_{min}^2} - [\sin(\alpha)]^2} \qquad (3.14)$$

The original GEPOL87 implementation in PARAGAUSS uses α = 2/9 π = 40º as threshold for the creation of new spheres because larger values did not affect results significantly; they only increased the computational cost.[43,204] The COSMO implementation based on this standard value was tested successfully for solvation energies of several small molecules.[43]

The default value suggested for the overlap factor *f* is 0.80.[206] However, that value has been derived for large biological systems, e.g. proteins,[206] and thus may not be adequate for the smaller actinide species investigated. In fact, preliminary calculations of several actinide complexes indicated that GEPOL93 with *f* = 0.80 yields typically larger number of additional spheres than obtained within GEPOL87 (see Table 3.2). As the number of additionally constructed spheres is known to affect solvation energies and other molecular properties, the overlap factor *f* from GEPOL93 needs to be adjusted in order to achieve an equal treatment for all investigated complexes and to allow comparison to data based on GEPOL87. Therefore, *f* was evaluated based on Eq. (3.14) for different ratios r_{max} / r_{min} keeping α = 2/9 π constant (Fig. 3.4). Based on the variations of *f* found from about 0.13 to 0.24 a new default value of *f* = 0.20 was chosen.

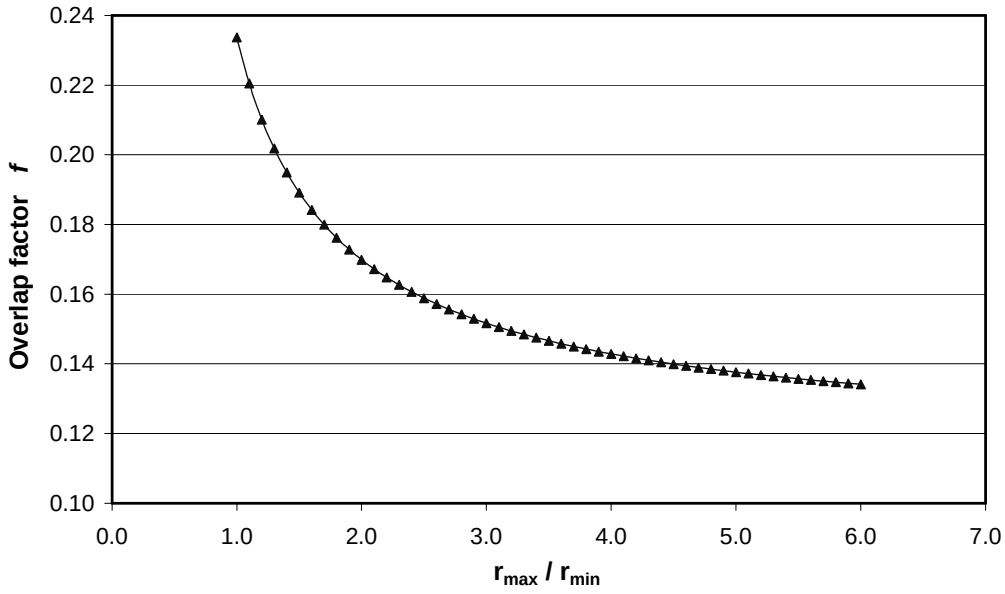

Figure 3.4. Calculated overlap factor *f* (GEPOL93) for different ratios r_{max} / r_{min} for constant α = 2/9 π (GEPOL87) according to Eq. (3.14), see text.

To evaluate differences between GEPOL87 and GEPOL93, the representative actinide complexes uranyl $[UO_2]^{2+}$ (D_{4h}), $[UO_2(H_2O)_6]^{2+}$ (D_{3d}), and bidentate uranyl monoformiate $[UO_2(OOCH)(H_2O)_3]^{+}$ (C_{2v}) are compared in Table 3.2, also with regard to the default values $\alpha = 2/9\ \pi$ and $f = 0.20$ and the originally suggested f-value of 0.80.

Table 3.2. Comparison of the GEPOL algorithms GEPOL87 and GEPOL93. Additional spheres (S) are created based on a fixed overlap angle α or overlap factor f, respectively (see Fig. 3.3 and text). Both algorithms are compared for optimizations of uranyl $[UO_2(H_2O)_n]^{2+}$ (n = 0, 6) and the bidentate uranyl monoformiate $[UO_2(OOCH)(H_2O)_3]^{+}$. Total energies E_{tot} (identical pre-decimal digits omitted), HOMO energies ε_{HOMO}, distances $U{=}O_t$ and $U{-}O_x$, and the charge of the uranium center q_U according to a Mulliken analysis for the default values of $\alpha = 2/9\ \pi$ and $f = 0.20$ in comparison to the original suggested f value of 0.80. Differences Δ between results of GEPOL93 (f = 0.20, 0.80) and GEPOL87 ($\alpha = 2/9\ \pi$) are also shown.

	S	E_{tot}, au	ε_{HOMO}, eV	$U{=}O_t$, Å	$U{-}O_x$, Å	q_U, e
$[UO_2]^{2+}$						
$\alpha = 2/9\ \pi$	0	.1129076	-11.07648	1.71795	–	2.2706
$f = 0.20$	0	.1129076	-11.07648	1.71795	–	2.2706
$f = 0.80$	0	.1129077	-11.07648	1.71795	–	2.2706
$\Delta f = 0.20$	0	$< 10^{-7}$	$< 10^{-5}$	$< 10^{-5}$	–	$< 10^{-4}$
$\Delta f = 0.80$	0	$< 10^{-7}$	$< 10^{-5}$	$< 10^{-5}$	–	$< 10^{-4}$
$[UO_2(H_2O)_6]^{2+}$						
$\alpha = 2/9\ \pi$	0	.1243777	-7.58234	1.78837	2.40554	1.2893
$f = 0.20$	0	.1243779	-7.58234	1.78837	2.40554	1.2893
$f = 0.80$	24	.1224162	-7.63724	1.78744	2.40635	1.2773
$\Delta f = 0.20$	0	$-2\cdot10^{-7}$	$< 10^{-5}$	$< 10^{-5}$	$< 10^{-5}$	$< 10^{-4}$
$\Delta f = 0.80$	24	0.0019615	-0.05490	-0.00093	0.00081	-0.0120
$[UO_2(OOCH)(H_2O)_3]^{+}$						
$\alpha = 2/9\ \pi$	4	.3385585	-7.63834	1.78281	2.39429	1.1241
$f = 0.20$	0	.3390177	-7.63354	1.78267	2.39471	1.1296
$f = 0.80$	26	.3370401	-7.67201	1.78240	2.39130	1.1176
$\Delta f = 0.20$	-4	-0.0004592	0.00481	-0.00013	0.00042	0.0055
$\Delta f = 0.80$	22	0.0015184	-0.03367	-0.00041	-0.00299	-0.0065

As expected changes between the two GEPOL algorithms increase with higher differences in the number of additional spheres (S, Table 3.2). The adjusted value $f = 0.20$ yields very similar numbers of spheres as GEPOL87 ($\alpha = 2/9\ \pi$) whereas the original value $f = 0.80$ results in more spheres, especially for larger systems (Table 3.2). Consequently, deviations between $\alpha = 2/9\ \pi$ and $f = 0.20$ are minor; for $[UO_2]^{2+}$ and $[UO_2(H_2O)_6]^{2+}$ results are almost identical due to the same number of additional spheres, deviations are slightly larger for $[UO_2(OOCH)(H_2O)_3]^{+}$, but still negligible within the considered accuracy used in the discussion of the results (Table 3.2). Differences between $\alpha = 2/9\ \pi$ and $f = 0.80$ are more pronounced, especially for $[UO_2(H_2O)_6]^{2+}$ and $[UO_2(OOCH)(H_2O)_3]^{+}$ where the number of additional spheres differs by more than 20 (Table 3.2). Total energies are affected most strongly, with changes of up to 0.002 au, i.e. about 0.05 eV. Differences of HOMO energies range from 0.03–0.05 eV. Effects on distances and charges are minor, ranging from 0.0005–0.003 Å and 0.001–0.01 e, respectively. Based on these results, the adjusted value $f = 0.20$ was chosen as default for all calculations employing GEPOL93.

3.3 Vibrational frequencies

Full frequency calculations are rather demanding for complexes of the size studied in this thesis because in the PARAGAUSS version used only first-order derivatives are available.[165] Additionally, spectroscopic measurements of actinyl complexes usually focus on the characteristic symmetric (ν_s) and antisymmetric (ν_a) actinyl stretching frequencies. Therefore, for most complexes studied, only these frequencies were determined via numeric second derivatives, by neglecting the coupling to other frequencies while the other degrees of freedom were kept frozen. This strategy generally yields reliable results for stretching frequencies; however, bending modes are known to be more affected and not easy to calculate accurately.[55] In particular, small force constants determined as finite differences of energy gradients can be susceptible to numeric inaccuracies and parameters such as the chosen displacement.

Previous gas phase (GP) and solution (PCM) calculations on uranyl and the dimeric uranyl species $[(UO_2)_2(OH)_2]^{2+}$ yielded only minor differences for ν_s, i.e. at most 0.2 and 2 cm^{-1} employing this approach compared to a full frequency calculation, respectively.[193] These differences are negligible compared to absolute experimental values of uranyl stretching frequencies that are typically in the range of 850–870 cm^{-1} for the symmetric mode ν_s and about 960 cm^{-1} for the antisymmetric mode ν_a.[97,215,216]

Additionally, test calculations in the gas phase were carried out for uranyl

$[UO_2(H_2O)_n]^{2+}$ (n = 0, 5) and bidentate (n = 0, 3) and monodentate (n = 4) uranyl monocarboxylate complexes $[UO_2(OOCR)(H_2O)_n]^+$ (R = H, CH_3, CH_2CH_3). All these complexes represent typical species investigated in the present study (Table 3.3). First, results of exact full frequency calculations are compared to those of approximate calculations where one considers only stretching modes of the uranyl moiety and omits all coupling to bending modes. Most of the studied complexes in this thesis are subjected to symmetry restrictions to reduce computational effort. Therefore also effects of such symmetry restrictions are discussed in comparison with results from unrestricted C_1 optimizations.

For all complexes investigated, results for ν_s from full and approximate frequency calculations agree very well (Δ = 0 to 4 cm^{-1}), confirming previous results.[193] Differences for the antisymmetric frequency ν_a from tests on $[UO_2(OOCR)]^+$ (R = H, CH_3, CH_2CH_3)

Table 3.3. Calculated symmetric uranyl stretching frequencies of uranyl $[UO_2(H_2O)_n]^{2+}$ (n = 0, 5) and bidentate (n = 0, 3) and monodentate (n = 4) uranyl monocarboxylate complexes $[UO_2(OOCR)(H_2O)_n]^+$ (R = H, CH_3, CH_2CH_3) in the gas phase. Results from full frequency calculations (Full) compared to approximate (Appr.) calculations where only stretching degrees of the uranyl moiety are considered.

	Full C_1	Full C_s	Appr. C_s	Exp. Sol.
$[UO_2(H_2O)_n]^{2+}$				
n = 0	1038	–	1038	
n = 5	897	904	903	870[a]
$[UO_2(OOCR)(H_2O)_n]^+$				
n = 0, R = H	948	–	946	
CH_3	940	–	936	
CH_2CH_3	933	–	933	
n = 3, R = H	889	889	886	
CH_3	876	881	880	861[b]
CH_2CH_3	868	875	879	
n = 4, R = H	874	875	874	
CH_3	860	868	869	
CH_2CH_3	861	868	869	

[a] Ref. 215. [b] Ref. 97.

are slightly higher (5–20 cm^{-1}). However, when uranyl bending modes are included, changes compared to the full frequency calculations are also reduced to about 5 cm^{-1}.[217]

Changes due to release of symmetry constraints in the optimization are as expected to be larger and correlate to changes in the uranyl bond lengths, of course. However, data for the investigated test systems indicate only minor relaxation effects for $[UO_2(H_2O)_n]^{2+}$ (n = 0, 5) and $[UO_2(OOCR)(H_2O)_n]^+$ (n = 0, 3; R = H, CH_3, CH_2CH_3), less than 0.01 Å for U=O_t. Accordingly, ν_s is hardly affected and varies by up to 9 cm^{-1}. Although relaxation from C_s to C_1 is significant for the monodentate complexes $[UO_2(OOCR)(H_2O)_4]^+$ (see Section 4.4.4), mainly the equatorial ligands are rearranged while the uranyl bond remains unaffected (Δ < 0.01 Å). Therefore changes in ν_s are also small, up to 9 cm^{-1}.

In summary, these results indicate that the symmetric uranyl stretching frequency ν_s is quite stable with respect to the applied approximations and differs by at most 10 cm^{-1}, i.e. only about 1% of its absolute value. Variations for the antisymmetric stretching frequency ν_a are slightly larger, up to 20 cm^{-1}.

3.4 Basis sets

The Kohn-Sham orbitals (see Section 3.1.2) were represented by flexible Gaussian-type basis sets, contracted in a generalized fashion using appropriate atomic eigenvectors from spin-averaged atomic calculation in I_h symmetry. The size of the basis sets and the corresponding contracted basis is given in the notation (n_0s, n_1p, n_2d, n_3f) and [N_0s, N_1p, N_2d, N_3f], respectively. n_l and N_l denote the number of orbital exponents and contracted functions, respectively, which are associated with a angular momentum l. For both U and Np, a basis set of the size (24s, 19p, 16d, 11f),[218] contracted to [10s, 7p, 7d, 4f] was used. The light atoms were described by standard basis sets:[219] (12s, 9p, 1d) → [6s, 5p, 1d] for Cl,[219a,b] (9s, 5p, 1d) → [5s, 4p, 1d] for C and O,[219c,d] and (6s, 1p) → [4s, 1p] for H.[219c,e] Exponents of all basis sets are given in Appendix A.

In the LCGTO-FF-DF method, the classical Coulomb contribution to the electron-electron interaction is evaluated via an approximate representation of the electron density, using an auxiliary basis set.[166] In this way computationally demanding four-center integrals can be efficiently avoided very at the expense of three-center integrals only. The size of the auxiliary basis sets is specified by the notation (n_0s, n_1r^2, m_1p, m_2d, m_3f). The exponents of the corresponding s- and r^2-type "fitting functions" were constructed from the s- and p-functions of the orbital basis and scaled by a factor of 2.[166] For U and Np only every other p-exponent was used due to reasons of numerical stability. In addition, five p, d, and f type

"polarization exponents" were added each as geometric series with a progression of 2.5, starting with 0.1, 0.2, and 0.3 au, respectively (see Appendix A). Thus, the auxiliary charge density basis sets were (24s, $9r^2$, 5p, 5d, 5f) for An = U, Np, (12s, $9r^2$, 5p, 5d) for Cl, (9s, $5r^2$, 5p, 5d) for C and O, (6s, $1r^2$, 5p) for H. Comparison with results of other DF calculations confirmed the accuracy of the current FF approach for actinide complexes.[55]

The actinide basis sets suggested by Minami and Matsuoka (24s, 19p, 16d, 11f)[218] together with the enlarged variation (24s, 19p, 16d, 13f, 2g) had previously been tested on the six- to four-valent actinyls $[AnO_2]^{2+}$, $[AnO_2]^{+}$, and $[AnO_2]$ and the hexahalogenides AnF_6 and $AnCl_6$ (An = U, Np).[61] With the standard basis, bond lengths were well reproduced with very small changes in distances, 0.002 to 0.009 Å (0.1–0.5%) compared to the enlarged basis. Also effects on vibrational frequencies were small, 3 to 11 cm^{-1}, i.e. less than 1% except for AcF_6 (1.5%). Notable differences arise only for binding energies, up to 0.3 eV or 4%, but they do not justify the extra cost of the larger basis sets.

In a second step, the effect of the contractions, (24s, 19p, 16d, 11f) → [10s, 7p, 7d, 4f], was checked and found to yield the same results as the uncontracted ones. For the same probe systems as before, deviations are insignificant, e.g. less than 0.25% for bond distances and less than 1% for vibrational frequencies and binding energies.[61] These results were confirmed by test calculations on the solvated uranyl ion $[UO_2(H_2O)_5]^{2+}$ and dimeric uranyl species $[(UO_2)_2(OH)_2]^{2+}$ and $[(UO_2)_2O_2]$.[193]

In addition, both more flexible, [10s, 7p, 7d, 5f], and less flexible, [9s, 7p, 6d, 4f], contraction schemes have been tested. While the smaller contraction yielded important deviations from the results of the original contraction [10s, 7p, 7d, 4f], the more flexible MO basis set showed no significant improvement.[61]

Extension of the auxiliary basis of U by a set of five g exponents, constructed according to the procedure given above, confirmed the accuracy of the selected auxiliary basis set. For instance, with additional g exponents, bond lengths of uranyl monoformiate in monodentate coordination changed by less than 0.002 Å and the total energy changed less than 4 kJ mol^{-1}. In a second test, the auxiliary basis of all atoms were extended by functions of higher angular momenta and for each angular momentum the series of exponents was increased from 5 to 7. The resulting effects were slightly larger on average, but still negligible; distances changed by less than 0.002 Å and the total energy by at most 12 kJ mol^{-1}.

Overall, these results corroborated the choice of the contracted standard basis sets (24s, 19p, 16d, 11f) → [10s, 7p, 7d, 4f] for U and Np that are employed for all calculations in this thesis.

3.5 Summary of computational details

For easy reference, the main computational parameters are summarized in this section. All calculations were carried out with the LCGTO-FF-DF (linear combination of Gaussian-type orbitals fitting function density functional) method[166] as implemented in the parallel code PARAGAUSS.[164,165] The relativistic density functional method applied is based on the second-order Douglas-Kroll-Hess (DKH) approach to the Dirac-Kohn-Sham problem (see Section 3.1.2).[17,31] Spin-orbit interaction was neglected because all uranium species examined feature U(VI) centers and a closed-shell electronic structure. In addition, comparison of scalar-relativistic and spin-orbit calculations for open-shell Np(VI) and Np(V) complexes yielded only minor effects on the parameters of interest, namely structures and energetics (see Section 3.1.4). Spin-polarized calculations were performed for the open-shell systems of Np(VI) and Np(V), whereas the closed-shell U(VI) species were treated in non-spin-polarized fashion.

Contracted Gaussian-type basis sets (Section 3.4) were used in the calculations. For the actinides U and Np a basis set of the size (24s, 19p, 16d, 11f), contracted to [10s, 7p, 7d, 4f] was used. The light atoms were described by standard basis sets: (12s, 9p, 1d) → [6s, 5p, 1d] for Cl, (9s, 5p, 1d) → [5s, 4p, 1d] for C and O, and (6s, 1p) → [4s, 1p] for H.

Throughout this work, one LDA (VWN) and two GGA (BP, PBEN) exchange-correlation functionals were employed (Section 3.1.3). Except for the purpose of evaluation, structures were optimized at the LDA level, invoking a quasi-Newton algorithm and analytical forces.[220] In view of the well-known overestimation of LDA binding energies, the GGA-BP functional was applied self-consistently to calculate binding energies in a "single-point fashion" at LDA structures. In the geometry optimizations, the total energy and elements of the density matrix were required to converge to 10^{-8} au; for the largest component of the displacement gradient vector and the update step length, the convergence criteria were set to 10^{-6} au.

The grid for the numeric integration of the exchange-correlation functional was chosen as a superposition of atom-centered spherical grids.[221] This grid construction implies a Lebedev angular integration grid of order 19 (locally accurate up to angular momentum L = ~19);[222–224] PARAGAUSS specific radial and angular grid parameters NRAD = 70 and NANG = 191 were used for all atoms.[165] For typical complexes these grids comprise about 26000, 16000, 10000, 11000, and 9000 points for An (U, Np), Cl, O, C, and H centers, respectively.

For most complexes vibrational frequencies were determined via numerical second derivatives, keeping other degrees of freedom frozen (Section 3.3).

Long-range electrostatic solvation effects were taken into account using a PCM variant, the COSMO method[199] as implemented in PARAGAUSS with the dielectric constant ε = 78.39. The solute cavities were created by vdW radii scaled by 1.2 except for H (Section 3.2.2).[43]

4 Results and Discussion

This chapter presents results of quantum chemical calculations on a variety of actinide complexes, which will be discussed in the light of experimental data. The chapter is divided in four sections.

In Section 4.1, solvated actinyl species $[AnO_2(H_2O)_n]^{2+/+}$ for An = U(VI), Np(VI), and Np(V) are considered. The discussion will include solvent effects due to coordinated aqua ligands, including a comparison between coordination numbers 4, 5, and 6. Effects of different actinides and oxidation states will be also examined. In addition, comparison to experimental solution data allows an evaluation of the computational method employed.

Section 4.2 presents results for the dinuclear complex $[(UO_2)_2(\mu_2\text{-}OH)_2Cl_2(H_2O)_4]$ that has been suggested as a hydrolysis product of uranyl. It is one of the few polynuclear uranyl species for which a crystal structure is known. Thus, this complex is used as an example to model and study the effect of a crystalline environment.

Section 4.3 focuses on uranyl complexation by carbonate ligands. Besides simple mononuclear carbonate complexes $[UO_2(CO_3)_m]^{2-2m}$ (m = 1–3), polynuclear species like the dinuclear hemicarbonate species $[(UO_2)_2(CO_3)(OH)_3]^-$ and the trinuclear triuranyl hexa(carbonato) complex $[(UO_2)_3(CO_3)_6]^{6-}$ will be presented. A central topic will be the detailed comparison of two prominent carbonate species, $[UO_2(CO_3)_4]^{4-}$ and $[(UO_2)_3(CO_3)_6]^{6-}$, with respect to structure and stability. Also, three structural isomers of the hemicarbonate species will be discussed in the light of only limited experimental data about this species in solution.

Finally, Section 4.4 shows results on actinyl complexation by carboxylate ligands. The discussion focuses on uranyl monocarboxylates $[UO_2(OOCR)]^+$ with several simple aliphatic carboxylic ligands like formiate, acetate, propionate, and glycolate. In this context, the uranyl triacetate complex $[UO_2(OOCCH_3)_3]^-$ is used as a benchmark system.

Furthermore, results for the corresponding monocarboxylate species of Np(VI) and Np(V) will be presented. The focus will be on the structural and energetic characterization as well as on the differentiation of different coordination modes of the carboxylic group (bidentate, monodentate, and chelate). The chapter concludes with a discussion of the implications of the presented results on actinide complexation by humic acids.

4.1 Solvated actinyls(VI) and actinyls(V), $[AnO_2(H_2O)_n]^{2+/+}$

Actinides in high oxidation states VI or V form dioxo cations. In aqueous solution, these actinyls acquire a ligand shell of several water molecules, $[AnO_2(H_2O)_n]^{2+/+}$. The structure of these complexes comprises an axial actinyl moiety that is surrounded by *n* aqua ligands in the equatorial plane (Fig. 4.1).

As prevailing species in solution at low pH, these complexes are of key importance for actinide solution chemistry. Therefore, actinyls – especially uranyl – have been extensively studied in solution with focus on the characterization of the coordination environment or on properties such as the actinyl solvation energy.[225,226] Both experimental[68,79–81] and theoretical[22,23,41–43,48,68] results suggest a preferred pentagonal coordination of the actinyl moieties. Theoretical studies employed a variety of methods such as HF,[42] MP2,[42] DF-LDA,[43,69] DF-GGA,[22,41] and molecular dynamics simulations,[48] but lack a systematic treatment of solvent effects. Explicit inclusion of water molecules from the first hydration shell in the theoretical models is essential.[22,43,69] However, bulk solvent effects are often omitted or taken into account only for the energy evaluation but not when optimizing the geometry. The majority of the theoretical studies deals with uranium,[22,41–43,68,69] some results are also available for neptunium[41,42] and plutonium.[22,41,42]

The following discussion of solvated actinyls $[AnO_2(H_2O)_n]^{2+/+}$ provides a systematic study of both short-range solvent effects via coordinated aqua ligands and long-range bulk solvent effects via a PCM treatment. In addition different actinyl coordination numbers N (N = *n* = 4–6) will be investigated for U(VI), Np(VI), and Np(V). For the solvated actinyls the equatorial coordination number N is identical to the number of aqua ligands *n*.

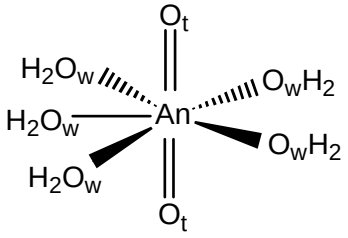

Figure 4.1. Schematic structure of solvated actinyls $[AnO_2(H_2O)_n]^{2+/+}$.

Symmetry effects

Computational studies often use symmetric model species to reduce computational costs. For the actinyl ions $[AnO_2(H_2O)_n]^{2+/+}$ it is common to assume an ideal D_{nh} symmetry based on the linear actinyl moiety and *n* aqua ligands, oriented perpendicular to the equatorial plane (Fig. 4.1). While steric repulsion effects between equatorial aqua ligands are expected to be negligible for $n = 4$, they might become relevant for higher values of *n* due to decreased distances between adjacent aqua ligands. Repulsion will result in a distortion from D_{nh} symmetry that restricts the oxygen centers of the aqua ligands to the equatorial plane. Therefore, optimizations based on D_{nh} symmetry constraints are compared to calculations with lower symmetry constraints, i.e. C_s for $n = 5$ and D_{3d} for $n = 6$; reduction of the symmetry allows aqua ligands to move outside the equatorial plane.

Table 4.1 summarizes results of PCM optimizations. These results comprise pertinent structural parameters and the symmetric actinyl stretching frequency ν_s as well as relative stabilities with respect to low symmetry structures (ΔE_{rel}). Average O-O distances between adjacent aqua ligands are used to characterize the repulsion within the ligand shell. Based on the vdW radius of oxygen, 1.42 Å,[203] one expects steric repulsion effects for O-O distances below ~2.8 Å. Deviations from the ideal D_{nh} symmetry are represented by the average absolute distance Δ_O of O centers from the equatorial plane.

Relaxation effects on distances and frequencies are minor for the pentagonal coordination ($n = 5$) of all actinyls studied. In comparison to the D_{5h} models deviations of $An{=}O_t$ distances and concomitantly the actinyl stretching frequency are small in C_s symmetry, i.e. 0.000–0.004 Å and 2–10 cm^{-1}, respectively. Changes of the average $An\text{-}O_w$ distance are a bit larger, 0.01–0.02 Å. The structural relaxation results in a slight stabilization of the complexes, which is negligible for U(VI) (3 kJ mol^{-1}), but more pronounced for Np(VI) and Np(V) (~30 kJ mol^{-1}). Although these differences are rather small, the orientation of the aqua ligands changes noticeably compared to D_{5h} (see Figs. 4.2a,b). Under D_{5h} symmetry the distance between adjacent aqua ligands (O-O: ~2.8 Å) is close to the estimated vdW distance (~2.8 Å). Steric repulsion results in notable deviations of the O centers from the equatorial plane (Δ_O: 0.3–0.4 Å). In this way, O-O distances are increased on average by 0.07 Å, 0.04 Å, and 0.02 Å for U(VI), Np(VI), and Np(V), respectively. The resulting O-O distances of 2.8–2.9 Å are insignificantly larger than the vdW distance. Thus, one expects steric repulsion effects to be small in the C_s structures.

For the U(VI) complex with five aqua ligands, also the effect of removing even the C_s symmetry constraint was investigated. Changes in the structure were minor, i.e. distances changed at most by 0.002 Å and the stretching frequency by less than 1% (see

Table 4.1. Bond distances An=O_t and An-O_w (in Å), stretching frequencies ν_s (in cm^{-1}), average distance O-O between O centers of adjacent aqua ligands (in Å), average deviation Δ_O of O centers from equatorial plane (in Å), and differences in relative energies ΔE_{rel} (in kJ mol^{-1}) for actinyls $[AnO_2(H_2O)_n]^{2+/+}$ (An = U, Np; n = 5, 6), obtained with different symmetry constraints from DF-VWN calculations including PCM treatment. Relative stabilities are calculated with reference to the complex with the lowest total energy for a given n.

	n	5	5	6	6
	sym.	D_{5h}	C_s	D_{6h}	D_{3d}
U(VI)	An=O_t	1.775	1.779	1.772	1.788
	An-O_w	2.372	2.362	2.481	2.406
	ν_s	876	869	877	832
	O-O	2.79	2.86	2.48	2.69
	Δ_O	0	0.37	0	0.70
	ΔE_{rel}	3	–	90	–
Np(VI)	An=O_t	1.754	1.758	1.751	1.765
	An-O_w	2.348	2.347	2.486	2.398
	ν_s	881	883	880	842
	O-O	2.76	2.80	2.47	2.67
	Δ_O	0	0.29	0	0.67
	ΔE_{rel}	33	–	83	–
Np(V)	An=O_t	1.814	1.814	1.810	1.826
	An-O_w	2.420	2.442	2.541	2.478
	ν_s	782	792	783	756
	O-O	2.84	2.86	2.54	2.74
	Δ_O	0	0.36	0	0.67
	ΔE_{rel}	28	–	46	–

also Section 3.3). Concomitantly, the complex is only slightly stabilized, by another ~3 kJ mol^{-1}. Based on these results, one can conclude that relaxation effects from C_s to C_1 are negligible for the subsequent discussion; C_s models seem to be adequate for treating actinyl complexes with coordination number n = 5.

As expected the larger number of equatorial ligands in the hexa-coordinated complexes $[AnO_2(H_2O)_6]^{2+/+}$ results in increased steric repulsion. Effects are smallest for Np(V) due to longer bond distances that result from the lower charge in $[NpO_2(H_2O)_6]^+$. Adjacent aqua ligands move distinctly above and below the equatorial plane (Δ_O: ~0.7 Å)

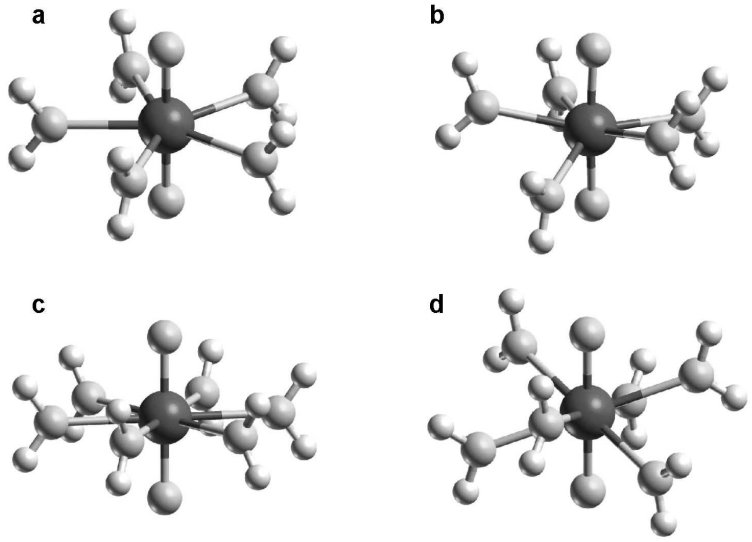

Figure 4.2. Optimized structures of $[UO_2(H_2O)_n]^{2+}$ for different symmetry constraints: n = 5 with D_{5h} (a) and C_s (b), and n = 6 with D_{6h} (c) and D_{3d} (d).

to enlarge the average O-O distance from ~2.5 Å to 2.7 Å (Figs. 4.2c,d). Differences to the ideal D_{6h} structures are larger than for coordination number n = 5. The An=O_t distances are elongated by ~0.015 Å while the An-O_w distances are distinctly shortened by 0.06–0.09 Å. These results can be rationalized by assuming a strong repulsion of the O centers due to the forced equatorial orientation under D_{6h}. This repulsion results in elongated An-O_w distances and, due to these weakened bonds, in a strengthening of the actinyl bond An=O_t, reflected by shorter An=O_t distances. Concomitantly, the actinyl stretching frequencies are noticeably larger, by 27–45 cm^{-1}. The pronounced structural relaxation from D_{6h} to D_{3d} results in a strong stabilization, by 80–90 kJ mol^{-1} for An(VI) and 46 kJ mol^{-1} for An(V) with respect to the D_{6h} complexes.

The applied D_{3d} symmetry constraint for the hexa-coordinated complexes enforces identical An-O_w bond lengths and restricts the orientation of the aqua ligands. Hay et al. investigated corresponding uranyl complexes $[UO_2(H_2O)_6]^{2+}$ without any symmetry constraints in the gas phase, based on DF-B3LYP calculations.[41] They obtained two local minima: a hexa-coordinated species with six aqua ligands in the first coordination shell and another isomer with only five ligands in the first shell and a sixth water molecule which is hydrogen-bonded to one of the other aqua ligands. The latter isomer is less stable by ~16 kJ mol^{-1}.[41] This indicates that an additional coordinative bond to an aqua ligand is stronger than a hydrogen bond in the solvation shell. The aqua ligands in the hexa-coordinated species move distinctly out of the equatorial plane, comparable to the D_{3d} structure discussed above,[41] but there is no indication of internal hydrogen bonds in the

first coordination shell. An-O_w bond lengths range from 2.52 to 2.61 Å.[41] The average An-O_w distance of 2.56 Å in the DF-B3LYP calculation is about 0.1 Å longer than in a corresponding DF-VWN calculations in the gas phase with D_{3d} symmetry (2.45 Å). This difference is typical when one compares results from GGA/hybrid and LDA exchange-correlation functionals (Table 4.3). Thus, the An-O_w bond lengths derived from D_{3d} models are expected to be in reasonable agreement with the average distance obtained from C_1 calculations. Comparison to the C_1 data indicates that the D_{3d} structures do not represent local minima, but saddle points. However, comparable average An-O_w distances, similar orientation of the aqua ligands, and the absence of internal hydrogen bonds indicate that the main relaxation effects are taken into account within the D_{3d} models. Being aware of the restrictions, these models seem justified to discuss main differences between the different coordination numbers in $[AnO_2(H_2O)_6]^{2+/+}$.

Structures and vibrational frequencies

Based on the preceding discussion, the following comparison to experimental data will be based on low symmetry models with $n = 5$ (C_s) and $n = 6$ (D_{3d}). Table 4.2 summarizes the corresponding structural parameters as well as the symmetric (ν_s) and antisymmetric (ν_a) actinyl stretching frequencies of $[AnO_2(H_2O)_n]^{2+/+}$ in comparison to the bare actinyl ($n = 0$) and to experimental data in solution.[68,79,215,216,227–232]

For all three actinides, the bare actinyl complexes ($n = 0$) exhibit the shortest An=O_t distance. Bond distances are similar for the hexavalent oxidation states of U(VI) and Np(VI), 1.72 Å and 1.71 Å, respectively. Distances are slightly shorter for Np(VI) as expected from to the actinide contraction. The An=O_t bond increases significantly to 1.74 Å for Np(V) due to the lower charge in $[NpO_2]^+$ which results in a weaker electrostatic attraction of the neptunyl oxygen centers. This general trend is also observed for all other complexes and is in agreement with experiment.

The results for bond distances are reflected in the corresponding actinyl stretching frequencies: minor differences (10 cm^{-1}) between U(VI) and Np(VI) and a significant decrease (~180 cm^{-1}) due to elongation, i.e. a weakening of the An=O_t bond for Np(V). However, in comparison to experiment, deviations of the bare actinyl complexes are significant. Concomitant with the fact that for all complexes the actinyl bond is distinctly underestimated, by 0.05–0.09 Å, one notes an overestimation of the corresponding stretching frequencies compared to experiment. This effect is more pronounced for An(VI) (140–180 cm^{-1}) than for An(V) (70–115 cm^{-1}). In accordance with previous results,[43,66] these data clearly indicate that a simple solvation model (PCM), which represents only bulk solvent effects, is not sufficient for a correct description of solvated actinyls. Rather,

Table 4.2. Bond distances (in Å) and stretching frequencies (in cm^{-1}) for actinyls $[AnO_2(H_2O)_n]^{2+/+}$ (An = U, Np; n = 0, 4, 5, 6) from PCM DF-VWN optimizations employing different symmetries (sym.) in comparison to experimental data in solution.

	n	0	4	5	6	Exp.
	sym.	D_{4h}	D_{4h}	C_s	D_{3d}	
U(VI)	An=O_t	1.717	1.771	1.779	1.788	1.76[a], 1.78[b]
	An-O_w	–	2.312	2.362	2.406	2.41[a,b]
	ν_s	998	887	869	832	870[c], 869[d]
	ν_a	1082	935	918	877	965[e], 962[f]
Np(VI)	An=O_t	1.707	1.751	1.758	1.765	1.75[f,g,h]
	An-O_w	–	2.283	2.347	2.398	2.41[h], 2.42[f,g]
	ν_s	988	889	883	842	854[i], 863[c]
	ν_a	1092	948	946	903	969[e]
Np(V)	An=O_t	1.736	1.807	1.814	1.826	1.82[h], 1.83[k], 1.85[a]
	An-O_w	–	2.361	2.442	2.478	2.49[h], 2.50[a], 2.52[k]
	ν_s	845	803	792	756	767[c,f]
	ν_a	914	824	822	779	824[e]

[a] Ref. 79. [b] Ref. 68. [c] Ref. 215. [d] Ref. 216. [e] Ref. 227. [f] Ref. 228. [g] Ref. 229. [h] Ref. 230. [i] Ref. 231. [k] Ref. 232.

these results emphasize the importance of short-range solvent effects which are caused by aqua ligands in the first coordination shell.

In fact, including 4, 5, or 6 (explicit) aqua ligands in the models results in an noticeable increase of the actinyl bond lengths by 0.04–0.09 Å compared to the bare species (n = 0). Invoking bond order conservation for the actinyl moiety, increased bonding competition at the actinide center due to additional equatorial aqua ligands is responsible for the weakening of the actinyl bond. The actinyl bond is elongated by about 0.017 Å in total when the coordination number of the actinyl increases from n = 4 to n = 6. Bond competition is also reflected within the equatorial ligand shell. The An-O_w distances increase by 0.04–0.08 Å per additional ligand. The weakening of the actinyl aqua bonds is accompanied by a lowering of the binding energies (see below). The actinyl stretching frequencies decrease distinctly in the solvated complexes (n = 4–6) compared to the bare species (n = 0), concomitant with the significant elongation of the actinyl bond (Table 4.2): for An(VI) ν_s and ν_a are reduced by 100–170 cm^{-1} and 140–200 cm^{-1}, respectively, but to a smaller extent for An(V), by 40–90 cm^{-1} and 90–130 cm^{-1}, respectively. In contrast, the smaller increase of An=O_t distances from n = 4 to n = 6 (~0.02 Å) is reflected by a

reduction of both frequencies ν_s and ν_a by ~50 cm^{-1} for An(VI) and An(V).

All complexes with n = 4, 5, and 6 agree distinctly better with experimental data than the results for the bare ions, n = 0. Both the clear underestimation of the actinyl bond as well as the corresponding overestimation of the stretching frequencies found for the bare actinyls are improved by explicitly included aqua ligands. The strong effects of the coordinated ligands on structure and frequencies indicate rather covalent than flexible or fluctuating bonds to water molecules in the first actinyl hydration shell. This conclusion is supported by the corresponding rather high binding energies (see below).

A comparison of results for the different coordination numbers with experimental data yields no clear preference for one particular value of n. For all species $[AnO_2(H_2O)_n]^{2+/+}$ independent of n or An, good agreement is found for the strong actinyl bond An=O_t with deviations up to 0.02 Å; the largest deviation (0.02 Å) is always obtained for n = 6. This would indicate a slight preference for coordination numbers n = 4 and n = 5. However, deviations for the weaker actinyl aqua bonds An-O_w are more pronounced and clearly depend on n which can be easily rationalized by the previously discussed bond competition. Although all results for An-O_w are always shorter than the experimental values, the experiment is only slightly underestimated for n = 6, by at most 0.03 Å; the calculated results for n = 5 are noticeably shorter by 0.05–0.07 Å, results for n = 4 do not reproduce the experimental values at all, with deviations of 0.10–0.15 Å. Apparently the An-O_w distance is quite sensitive to the equatorial coordination number: An-O_w values differ by 0.04–0.12 Å from n = 4 to n = 6 (Table 4.2). These short-range effects are somewhat larger than long-range solvent effects as described by the PCM model; typically the An-O_w distance is reduced by about 0.04–0.05 Å in comparison to corresponding gas phase calculations (Table 4.3). In contrast to An-O_w, the stronger actinyl bond is distinctly less affected by the coordination number (changes within 0.02 Å, Table 4.2). Corresponding long-range solvent effects are also smaller as reflected by a minor elongation of 0.01–0.02 Å (Table 4.3).

The discrepancy of the An-O_w distances to experiment merits some remarks. First, the data presented here indicates that the aqua bonds are rather flexible and react strongly to changes of their environment. This is reflected in variations for a given coordination number (0.03–0.06 Å) as well as for different coordination numbers (0.04–0.12 Å) and the distinct changes between GP and PCM data discussed above. Therefore, the interaction between the actinide center and its aqua ligands might not exhibit a pronounced energetic minimum.[43] Secondly, there may be equilibria between complexes with different numbers of aqua ligands in solution that would result in averaged values in the corresponding

EXAFS data. However, this still would not explain the observed underestimation in all results. The simultaneous presence of complexes with different coordination numbers is supported by rather small binding energies of the additional aqua ligands in $[AnO_2(H_2O)_n]^{2+/+}$ for n = 5 and n = 6 (see below). EXAFS experiments seem to indicate a clear preference of the five coordinated ligand shell (N = 4.5 to 5.3),[68,79,80,230,232] but the equatorial coordination number exhibits an uncertainty of 10–20%.[68,230]

Finally, An-O_w distances from GGA-PBEN calculations (Table 4.3) are, as is typical for GGA, notably longer than LDA-VWN results, by ~0.1 Å for n = 5 and n = 6. Thus, this crucial distance also depends on the applied exchange-correlation functional. This aspect and the dependence on the employed computational method will be discussed in more detail below. Due to these complications, the An-O_w distance is a critical parameter that has to be computed and interpreted with proper care.

Comparison of calculated actinyl stretching frequencies to experiment provides an additional opportunity to discriminate the complexes $[AnO_2(H_2O)_n]^{2+/+}$ with n = 4–6. The discussed small changes in the actinyl bond lengths for different coordination numbers n lead to noticeable changes in the corresponding frequencies, by 35–48 cm^{-1}. For n = 4 the symmetric frequency ν_s is overestimated by 17–36 cm^{-1}, while it is underestimated for n = 6 by 11–38 cm^{-1}; deviations for n = 5 are somewhat smaller, ranging from -1 to 25 cm^{-1}. The antisymmetric frequency ν_a is generally underestimated and deviations are typically larger than for ν_s. In comparison to experiment ν_a is underestimated by 0 to 28 cm^{-1}, 2 to 45 cm^{-1}, and 45 to 86 cm^{-1} for n = 4, 5, and 6, respectively (Table 4.2). The larger discrepancies for ν_a indicate that the antisymmetric frequency might be affected more strongly by coupling with adjacent equatorial ligands than the symmetric frequency ν_s (see Section 3.3). Although deviations range up to 45 cm^{-1}, i.e. up to 5% of the experimental value, best agreement for all species is found for n = 5. However, deviations for n = 4 and n = 6 are only a bit worse, ranging from 2–7 %.

In summary, based on structural and vibrational data, there is no clear indication for a specific coordination number. However, in agreement with suggestions motivated by experimental results, a slight preference for n = 5 is found when considering the distances An=O_t and the corresponding stretching frequencies. The calculated An-O_w distances point to n = 6, but are less reliable for a discrimination as discussed above.

Now, the previously discussed computational results will be compared to corresponding data of other theoretical studies.[41,42,63,233] As the majority of investigations deals with uranium with pentagonal or hexagonal coordination, other actinides and coordination numbers will not be considered in the following (Table 4.3). Some of the

presented data[41,63] are based on gas phase (GP) studies that do not consider long-range solvent effects, e.g. via a continuum model. Therefore, a direct comparison to the previously discussed LDA-VWN results including PCM from Table 4.2 is not possible. In addition, some studies[42,63] severely restrict the degrees of freedom during the optimizations, e.g. by fixing the aqua ligands to the equatorial plane.

The variety of methods based on different theoretical approaches results in a broad range of values, 1.70–1.79 Å for $U{=}O_t$ and 2.36–2.65 Å for $U\text{-}O_w$, which scatter around the experimental data, ~1.77 Å and 2.41 Å, respectively. The uranyl distance $U{=}O_t$ is usually a good parameter to judge the accuracy of the computational method because it represents a rather strong bond in contrast to the more flexible $U\text{-}O_w$ bonds (see above). In addition, it is only affected slightly by long-range solvent effects (~0.015 Å) in contrast to the $U\text{-}O_w$ distance (~0.05 Å). All methods except HF provide $U{=}O_t$ values from 1.75–1.79 Å and are in good agreement with the average experimental distance of ~1.77 Å. The distinct

Table 4.3. Bond distances (in Å) and stretching frequencies (in cm^{-1}) for solvated uranyl $[UO_2(H_2O)_n]^{2+}$ (n = 5, 6) from various theoretical gas phase (GP) and solution (SOL) studies employing different computational methods and symmetry constraints (Sym.) in comparison to data from the present work (pw) and experiment. For density functional (DF) methods also the applied exchange-correlation functional (xc) is given. For the treatment of uranium either all electrons (AE) are considered or pseudopotentials (large core RECP) are applied. Results obtained with the methods considered as standard within this thesis are highlighted.

n	Method	xc			Sym.	$U{=}O_t$	$U\text{-}O_w$	Ref.
5	HF	–	RECP	SOL	D_{5h}	1.70	2.50	42
5	MP2	–	RECP	SOL	D_{5h}	1.76	2.42	42
5	DF	B3LYP	RECP	GP	C_1	1.76	2.52	41
5	DF	B3LYP	RECP	GP	D_{5h}	1.75	2.52	63
5	DF	VWN	AE	GP	C_s	1.77	2.41	pw
5	DF	B3LYP	RECP	SOL	C_1	1.76	2.45	233
5	DF	PBEN	AE	SOL	C_s	1.79	2.46	pw
5	DF	SVWN	RECP	SOL	C_1	1.77	2.37	233
5	DF	VWN	AE	SOL	C_s	1.78	2.36	pw
6	HF	-	RECP	SOL	D_{6h}	1.70	2.64	42
6	DF	B3LYP	RECP	GP	C_1	1.76	2.56	41
6	DF	B3LYP	RECP	GP	D_{6h}	1.75	2.65	63
6	DF	PBEN	AE	SOL	D_{3d}	1.79	2.53	pw
6	DF	VWN	AE	SOL	D_{3d}	1.79	2.41	pw
	Exp.					1.76,1.78	2.41	68,79

underestimation (1.70 Å) of HF is typical for electron-rich heavy element compounds and can be rationalized by the lack of electron correlation.[234] Differences of An=O_t between n = 5 and n = 6 are minor (<0.01 Å) and thus do not provide a good criterion for differentiating between coordination numbers.

As discussed above, the determination of the distance U-O_w seems to be more critical. This conclusion is supported by the wide range of values, scattering over an interval of ~0.3 Å, as obtained from different methods. Even for the same coordination number this distance fluctuates by ~0.2 Å. Among the DF methods, results based on the same type of functional, LDA (VWN, SVWN) or GGA (B3LYP, PBEN), agree well, both for GP and PCM calculations. Results for U-O_w from solvent models (SOL) are in general significantly shorter than the corresponding gas phase data, by 0.05–0.07 Å. In addition, the well-known tendency of GGA[190,191] to yield longer metal-ligand bonds is observed: U-O_w distances are ~0.1 Å longer than in the corresponding LDA calculations. In contrast, the U=O_t bond is hardly affected (±0.02 Å). On going from n = 5 to n = 6 U-O_w increases significantly (0.05–0.15 Å); this can be rationalized by an increased bond competition at the uranium center (see above). Focusing on the PCM data, only the MP2 results for n = 5 agree well with experiment, both for U=O_t and U-O_w. Note, however, that the corresponding geometry optimization was restricted to these two degrees of freedom.[42] While DF results reproduce the U=O_t distance rather well, the U-O_w distance is slightly underestimated for LDA and overestimated for GGA (n = 5). The LDA underestimation is corrected for n = 6, while the GGA overestimation is further enhanced.

Overall, based on these data, all correlation methods, i.e. MP2 and DF, provide reasonable results, but show large variations for the An-O_w distances. As expected, the HF method is not suitable for describing these heavy-element compounds.

Energetics

The results presented so far indicate that for a differentiation between coordination numbers additional information such as results on energetics is necessary besides the structural data. First, binding energies of the aqua ligands in $[AnO_2(H_2O)_n]^{2+/+}$ will be discussed for different coordination numbers n = 4–6, Eq. (4.1). Then, the equilibria between the different species will be investigated via Eqs. (4.2) and (4.3).

$$[AnO_2]^{2+/+} + n\,H_2O \rightarrow [AnO_2(H_2O)_n]^{2+/+} \quad (4.1)$$

$$[AnO_2(H_2O)_4]^{2+/+} + H_2O \rightarrow [AnO_2(H_2O)_5]^{2+/+} \quad (4.2)$$

$$[AnO_2(H_2O)_5]^{2+/+} + H_2O \rightarrow [AnO_2(H_2O)_6]^{2+/+} \quad (4.3)$$

Table 4.4. Average binding energies (in kJ mol^{-1}) per aqua ligand in $[AnO_2(H_2O)_n]^{2+/+}$ (An = U, Np; n = 4, 5, 6) according to Eq. (4.1) and reaction energies for the addition of a further aqua ligand according to Eqs. (4.2) and (4.3), see text. Energetics are based on the GGA-BP exchange-correlation functional applied in single-point fashion at LDA-VWN optimized structures.

Eq.	n	U(VI)	Np(VI)	Np(V)
(4.1)	4	-118	-94	-59
	5	-104	-82	-56
	6	-87	-61	-35
(4.2)	$4 \rightarrow 5$	-48	-37	-45
(4.3)	$5 \rightarrow 6$	1	44	71

The corresponding binding and reaction energies are presented in Table 4.4. Binding energies per aqua ligand decrease continuously with increasing number of ligands, both for U and Np. This finding can be rationalized by the increased bonding competition at the actinide center; it corroborates the structural trends discussed above, i.e. an elongation of the bonds An=O_t and An-O_w with increasing n. The average binding energies per ligand decrease from n = 4 to n = 5 by 3–14 kJ mol^{-1} and a bit more on going from n = 5 to n = 6, by 17–21 kJ mol^{-1}. U(VI) exhibits the largest binding energies per ligand (90–120 kJ mol^{-1}); for Np(VI) they are somewhat smaller, 60–95 kJ mol^{-1}. The lower charge in the Np(V) complex results in the smallest binding energies of 35–60 kJ mol^{-1}, reflected also in the longest An-O_w distances of all complexes (Table 4.2). Especially for the hexavalent oxidation states these energies are comparable to typical moderate to strong H bonds (see also Section 4.2).[235] This is consistent with the strong structure changes for varying coordination numbers discussed above.

The complexation of an additional aqua ligand to $[AnO_2(H_2O)_4]^{2+/+}$ to yield pentagonal coordination, Eq. (4.2), is exothermic for all complexes by ~40–50 kJ mol^{-1}. Addition of a further ligand, Eq. (4.3), does not change the total energy for U(VI) (1 kJ mol^{-1}) and becomes even endothermic for Np(VI) (44 kJ mol^{-1}) and Np(V) (71 kJ mol^{-1}). Therefore, based on these data, pentagonal coordination seems to be favored energetically. However, especially for uranyl, equilibria between solvated species with varying numbers of aqua ligands are to be expected. This could provide a rationalization for the discrepancies of An-O_w values compared to experiment as discussed above. For a more thorough investigation inclusion of thermodynamic corrections will be necessary.

The reaction energies according to Eqs. (4.1) to (4.3) were also calculated on the

basis of full GGA-PBEN optimizations to validate the combined LDA-GGA approach applied in this work to evaluate energetics (see Section 3.1.3). In the latter approach the GGA-BP functional is applied in "single-point fashion" at structures that previously had been optimized at the LDA-VWN level. Binding energies per aqua ligand of $[UO_2(H_2O)_n]^{2+}$, Eq. (4.1), are calculated slightly smaller in the full PBEN calculations, by about 10 kJ mol^{-1}. The reaction energies according to Eqs. (4.2) and (4.3) differ also by at most 10 kJ mol^{-1} and show identical trends in both approaches. Thus, the combined LDA-GGA approach is justified to discuss qualitative energetic trends between the different actinyl complexes $[AnO_2(H_2O)_n]^{2+/+}$.

Effective configuration and charge distribution

To characterize differences between different actinides and different coordination numbers *n*, one may also invoke the charge distribution and the effective configurations of the actinide ions in $[AnO_2(H_2O)_n]^{2+/+}$. Table 4.5 provides the effective configuration of the actinide atom and the terminal oxygen atoms with respect to the valence configuration of uranium(VI), $7s^0\,7p^0\,6d^0\,5f^0$ and oxygen, $2s^2\,2p^4$. Table 4.6 details average Mulliken charges of atoms and total charges of the actinyl and water moieties as obtained from PCM calculations.

Table 4.5. Effective configuration of the actinide atom An and terminal oxygen atoms O_t in the actinyls $[AnO_2(H_2O)_n]^{2+/+}$ (An = U, Np; n = 0, 4, 5, 6) with respect to the valence configuration of uranium(VI), $7s^0\,7p^0\,6d^0\,5f^0$, and oxygen, $2s^2\,2p^4$. Negative values indicate reduced occupation of the corresponding lower shells. Data are based on a Mulliken analysis from PCM optimizations.

	n	An(7*s*)	An(7*p*)	An(6*d*)	An(5*f*)	2O$_t$(3*s*)	2O$_t$(2*p*)
U(VI)	0	0.02	-0.15	1.24	2.61	-0.23	8.46
	4	0.11	-0.01	1.77	2.71	-0.29	8.78
	5	0.14	-0.01	1.88	2.67	-0.29	8.80
	6	0.14	-0.01	1.83	2.74	-0.31	8.84
Np(VI)	0	0.02	-0.15	1.17	3.68	-0.22	8.47
	4	0.11	-0.03	1.73	3.84	-0.28	8.72
	5	0.14	-0.02	1.85	3.79	-0.28	8.74
	6	0.14	-0.02	1.79	3.85	-0.30	8.76
Np(V)	0	0.04	-0.04	1.14	4.11	-0.28	8.99
	4	0.13	0.00	1.64	4.17	-0.32	9.12
	5	0.16	0.02	1.75	4.16	-0.31	9.11
	6	0.16	0.02	1.75	4.11	-0.35	9.14

For U(VI), Np(VI), and Np(V), the actinyls exhibit singlet, doublet, and triplet states, respectively, independent of *n*. This result agrees with the ground states of the free actinide atomic ions: $5f^0$, $5f^1$, and $5f^2$, respectively (Table 2.2). The corresponding singlet states of the Np(V) complexes are distinctly less stable, by ~20 kJ mol^{-1} for n = 0, 4 and up to 50–80 kJ mol^{-1} for n = 5, 6. Spin-polarized calculations were carried out for both Np(V) spin states by fixing the number of unpaired electrons in the optimizations. The less stable singlet states exhibit a closed shell configuration where the HOMO is of pure Np *f* character. The corresponding triplet states result from the excitation of one electron from this HOMO to occupy the LUMO that is also of Np *f* character (see below). Spin contamination, i.e. the difference between the expectation value $\langle S^2 \rangle$ of the total spin of the Kohn-Sham determinant and the exact eigenvalue $S(S+1)$, was less than ~1% for both configurations. The following discussion will only focus on the more stable triplet states.

As expected, a comparison of U(VI), Np(VI), and Np(V) for n = 0 reveals the main change in the actinide configurations with respect to the 5*f* population. Differences for 7*s*, 7*p*, and 6*d* populations are notably smaller (<0.1 e). The extra electron in neptunyl(VI) is reflected in the increased occupation (~1.1 e) of the Np(VI) 5*f* orbitals. The additional electron occupies the HOMO which exhibits about 99% Np 5*f* character. Therefore, it is not involved in the neptunyl bond. This finding is corroborated by results from other theoretical studies[55,236] on actinyls(VI) $[AnO_2]^{2+}$ and actinide hexafluorides AnF_6 and is also in agreement with magnetic susceptibility and EPR data reported for neptunyl(VI) that provide evidence that the unpaired electron of $[NpO_2]^{2+}$ resides in a Np valence *f* orbital.[237] This analysis provides a rationalization for the rather small differences in structures and vibrational frequencies obtained for the two hexavalent actinyls (see above).

The additional *f* electron in neptunyl(V) exhibits also about 99% Np 5*f* character. However, the 5*f* population from Np(VI) to Np(V) increases overall only by ~0.3 e. The *f* character of the orbitals involved, which comprise An(5*f*) and $O_t(2p)$ contributions, is distinctly reduced in Np(V) compared to An(VI), as reflected by an increased $O_t(2p)$ population, by ~0.5 e compared to An(VI); see Table 4.5. These variations in the actinyl bonding lead to more pronounced changes in the structure of the pentavalent neptunyl compared to Np(VI), see Table 4.2.

The discussed trends between the different actinyls An(VI) and An(V) regarding the An(5*f*) and $O_t(2p)$ populations are also observed for the solvated actinyl species and independent of the number of aqua ligands *n*. Compared to the bare actinyls, the 7*s*, 7*p*, and 5*f* populations hardly increase, by ~0.1 e each. However, the 6*d* population of the actinide atoms and the 2*p* population of the terminal oxygen centers are significantly

enhanced by up to 0.6 e and 0.4 e, respectively, due to the coordinated aqua ligands. This strong short-range solvent effect is missing when only long-range solvent effects are modeled (n = 0). This effect had previously been noted.[22,43,66] It corresponds to a strong donation of electronic charge from the aqua ligands during formation of the ligand shell. The charge of the actinide ion and thus the actinyl group is notably reduced due to the coordinating aqua ligands compared to the bare actinyls (Table 4.6). The donation to the An center is a bit larger for An(VI), ~0.8–1.0 e, than for An(V), ~0.7–0.8 e. The donation to the two O_t centers is less pronounced (~0.2 e in total). Each aqua ligand is slightly positive charged, 0.2–0.3 e.

A comparison between the different coordination numbers reveals interesting trends. Because of the additional aqua ligand, the donation of electron charge to An increases by ~0.1 e on going n = 4 to n = 5. For U(VI), the effect is smaller from n = 5 to n = 6 and vanishes for Np(VI); for Np(V), it even reverses, i.e. the Np(V) charge is somewhat more positive by 0.04 e compared to n = 5. The fifth aqua ligand can provide additional electronic charge while the actinyl moiety seems saturated for n = 6 (especially for Np). This observation is corroborated by the effective configuration. In agreement with the charge donation, the actinide 6*d* population is enhanced by ~0.1 e from n = 4 to n = 5, but decreases slightly or remains unchanged on going from n = 5 to n = 6 (Table 4.5).

Table 4.6. Average Mulliken charges (in e) of selected atoms and groups of the actinyls $[AnO_2(H_2O)_n]^{2+/+}$ (An = U, Np; n = 0, 4, 5, 6).

	n	q(An)	q(O_t)	q(O_w)	q(H)	q(AnO_2)	q(H_2O)
U(VI)	0	2.27	-0.14	–	–	2.00	–
	4	1.42	-0.26	-0.62	0.45	0.89	0.28
	5	1.33	-0.27	-0.62	0.43	0.79	0.24
	6	1.29	-0.28	-0.63	0.42	0.73	0.21
Np(VI)	0	2.29	-0.14	–	–	2.00	–
	4	1.35	-0.24	-0.62	0.45	0.88	0.28
	5	1.24	-0.24	-0.62	0.43	0.75	0.25
	6	1.24	-0.24	-0.63	0.42	0.75	0.21
Np(V)	0	1.74	-0.37	–	–	1.00	–
	4	1.06	-0.41	-0.65	0.42	0.24	0.19
	5	0.92	-0.41	-0.63	0.41	0.10	0.18
	6	0.96	-0.41	-0.64	0.39	0.15	0.14

In summary, on the basis of the computational data presented both for structures and frequencies as well as energetics, one would favor pentagonal coordination for all actinyls discussed – in agreement with suggestions motivated by experimental results.[68,79–81] This conclusion is supported by effective configurations and charge distributions that indicate a saturation of the actinyl moiety for $n = 5$. Based on the strong underestimation of the An-O_w bond and energetic comparison between complexes with coordination numbers $n = 4$ and $n = 5$, the tetragonal coordination seems least likely. Hexagonal coordination can not completely be excluded as the calculated results for $n = 5$ deviate to a comparable degree from experiment and exhibit similar stability, at least for U(VI). The remaining deviations from experiment may be, at least to some extent, related to equilibria between species with different numbers of aqua ligands. The results presented are indicative for reasonably strong covalent bonds of the aqua ligands to the actinyl moiety (up to 80 kJ mol^{-1}), accompanied by a significant charge donation to the actinyl moiety and enhanced actinide 6*d* populations. The data presented for bare actinyls indicate that short-range solvent effects by explicit aqua ligands are not sufficiently represented by the PCM model alone which only accounts for long-range solvent effects. Thus, for an accurate description of solvent effects, one has to consider both short- and long-range interactions.

4.2 The dinuclear complex $[(UO_2)_2(\mu_2\text{-}OH)_2Cl_2(H_2O)_4]$ in its crystalline environment

Structural information about polynuclear actinide complexes are rare. Some data are available from EXAFS studies, which refer directly to the species in solution,[113] or from a crystal structure determination if a crystal can be grown from solution.[109–112] The dinuclear complex $[(UO_2)_2(\mu_2\text{-}OH)_2Cl_2(H_2O)_4]$ **1** (Fig. 4.3), suggested as hydrolysis product of uranyl in the presence of chlorine ions, is one of the few polynuclear uranyl species for which a crystal structure is available.[109] X-ray scattering data of a solution[113] and a crystal structure[109] were determined for **1** from hydrolyzed solutions of $UO_3{\cdot}HCl{\cdot}2H_2O$. These data suggest the presence of the dimeric unit $[(UO_2)_2(\mu_2\text{-}OH)_2]^{2+}$ which was also reported in other crystal structures.[111,238,239] This moiety seems to be a frequent structural element of dinuclear uranium species in solid state and solution.[111, 113]

The first goal is to describe the gas phase structure of complex **1,** using an appropriate all-electron scalar-relativistic DF approach.[17,66] In a second step, the aim is to model packing effects in the crystal structure of **1**. The model used can be judged by comparison with available experimental data.[109] Because **1** is neutral, long-range Coulomb interactions between the different units in the crystal should not be crucial; rather, one expects that hydrogen bonds comprise the main crystal packing effects.[109] Therefore, a model approach was chosen which neglects the Madelung field.

Crystal structure and models

The crystals of the diuranyl hydroxide dichloride complex $[(UO_2)_2(\mu_2\text{-}OH)_2Cl_2(H_2O)_4]$ **1** are monoclinic with a unit cell that contains four formula units and belongs to space group No. 14: $P2_1/n$.[109] The relative orientation of complexes **1** in the unit cell is displayed in Fig. 4.4. Complex **1** comprises two linear uranyl groups which are linked by two OH bridges. In addition to the two bridging oxygen centers O_b, each uranium center is surrounded by one chlorine as well as two further oxygen centers O_s and O_a due to coordinating aqua

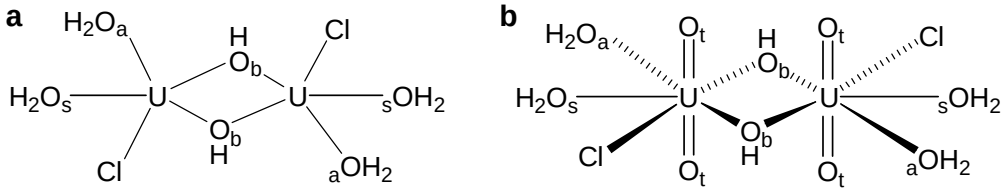

Figure 4.3. Schematic structure of the dinuclear complex $[(UO_2)_2(\mu_2\text{-}OH)_2Cl_2(H_2O)_4]$ **1**: top view (a) and side view (b). The terminal oxygen atoms of the uranyl units are not shown in the top view.

ligands (Fig. 4.3). Index *s* designates O centers of aqua ligands located *syn* relative to a Cl ligand, while index *a* refers to O centers of aqua ligands located *anti*, i.e. at the same uranium center, but on the side opposite of Cl (Fig. 4.3). The two chlorine atoms of a diuranyl complex are coordinated trans to each other.[109] Overall each U center exhibits a local coordination in the form of a pentagonal bipyramid that is typical for uranyl moieties.[14] The central moiety $[(UO_2)_2(\mu_2\text{-}OH)_2]^{2+}$ is also present in the dinuclear hydrolysis product $[(UO_2)_2(\mu_2\text{-}OH)_2(H_2O)_6]^{2+}$ where the chlorine atoms are replaced by aqua ligands.[113] Although both OH and O bridges are assumed to be possible in the diuranyl species[116] previous studies[66] confirmed the presence of OH bridges for acidic pH in the initial stage of the hydrolysis process (see Section 2.2.2). Based on the acidic experimental conditions OH bridges are also expected in complex **1**.[109,113]

The x-ray scattering data of the crystal structure do not provide explicit information about the positions of the hydrogen atoms. However, based on typical distances and angles found in the crystal structure, Åberg predicted three types of H bonds X-H···Y between adjacent complexes **1** (Fig. 4.4, 4.5).[109] The four strongest, i.e. shortest bonds (A, B), extending in *b* direction of the crystal, are assumed to exist between an oxygen center of an OH bridge and an oxygen center of an *anti* coordinated aqua ligand, $O_b\cdots H\text{-}O_a$ (A) and $O_a\text{-}H\cdots O_b$ (B) (Fig. 4.4a). Frontier groups of an adjacent complex **1** are designated in italics. Åberg predicted eight additional H bonds oriented mainly in *c* direction (Fig. 4.4b).[109] Each of the first four H bonds (C, D) involves the same water oxygen center

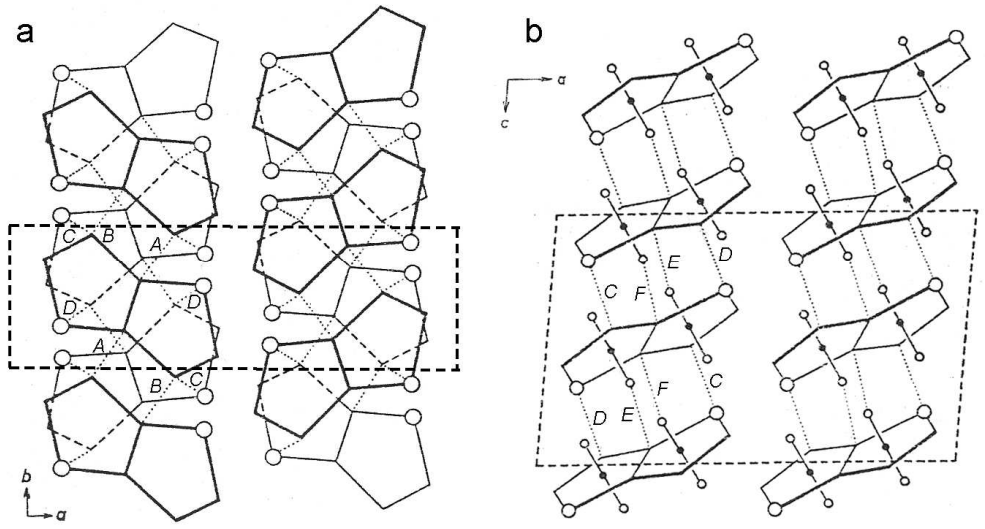

Figure 4.4. Unit cell of the crystal structure of the dinuclear complex $[(UO_2)_2(\mu_2\text{-}OH)_2Cl_2(H_2O)_4]$ **1** including the proposed H bonds A, B, C, D, E, and F: top view along *c* axis (a) and side-view along *b* axis (b). The uranyl moieties are not shown in the top view. Adapted from Ref. 109.

as H bond B and a chlorine center, O_a-H···*Cl* (C) and Cl···*H*-O_a (D); the second four H bonds (E, F) involve a bridge oxygen atom and a terminal uranyl oxygen atom, O_t···*H*-O_b (E) and O_b-H···O_t (F) (Fig. 4.5). From a comparison of the corresponding X···Y distances with typical values for H bonds[235] and the van der Waals radii of the corresponding atoms,[240] bond strengths are expected to decrease from (A, B) to (C, D) to (E, F).[109]

To determine the structure of complex **1**, two models with C_i symmetry were applied: M1 – a model of the gas phase structure, and, to account for packing effects of the crystal, M2 – a model including important features of the crystalline environment. A low symmetry model that was used to generate a starting geometry is discussed in Ref. 65.

The C_i symmetry of M1 does not constrain any degree of freedom for a geometry optimization of **1**. The experimental crystal structure shows slight deviations from C_i symmetry because the local inversion symmetry of **1** is broken by the arrangement of the neighboring complexes (Fig. 4.4): equivalent bond lengths scatter on average by 0.02 Å.[109]

To investigate the effect of the crystal hydrogen bonds on the gas phase structure of model M1, model M2 was constructed. Here, the gas phase complex obtained with model M1 is placed into a model of its crystalline environment and the relaxation of the complex due to the H bonds is investigated. Comparing the optimized structure of model M2 with the crystal structure, it is possible to check if the model environment is able to reproduce the main effects of crystal packing.

To model the effect of H bonds with neighboring complexes in the crystal, adjacent complexes **1** are represented by those frontier groups which are involved in the H bonds discussed above (Fig. 4.5). In fact, to keep model M2 neutral, H_2O and HCl molecules are

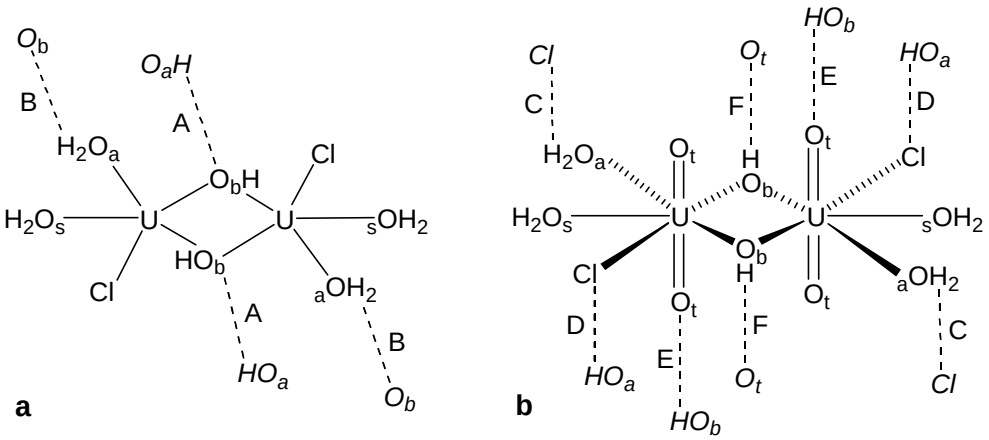

Figure 4.5. Schematic structure of the dinuclear complex $[(UO_2)_2(\mu_2\text{-}OH)_2Cl_2(H_2O)_4]$ **1** including the proposed H bonds A, B, C, D, E, and F in the crystal; see text. Top view (a) and side view (b). The terminal oxygen atoms of the uranyl units are not shown in the top view. Italics indicate frontier groups of neighbouring complexes **1** in the crystal.

chosen as the corresponding counterparts. Only the “heavy” atoms (O, Cl) of these model groups were placed at fixed positions derived from the experimental crystal structure.[109] Thus, the optimizations represent a relaxation of **1** in the fixed framework of heavy frontier atoms of surrounding species in the molecular crystal. The locations of the hydrogen centers of the model groups (hence also the orientations of the H bonds) were fully optimized, subject to the inversion symmetry constraint. The Mulliken charges of the corresponding centers O (-0.62 e) in H_2O and Cl (-0.24 e) in HCl turned out to be close to those of the corresponding atoms of **1** as calculated with reference model M1, namely -0.54 e for O_a and -0.34 e for Cl. Therefore, the chemical environment of **1** in model M2 should be sufficiently similar to that of the crystal.

At first, a model of the environment that accounted only for the strongest H bonds (A, B) was applied; as expected, this simple environment model yielded improved distances and angles of atoms directly connected to the simulated bridges (U-O_b, U-O_b', U-O_a), but the localized formation of these selected H bonds lead to major distortions in other parts of the complex (U-Cl, U-O_s). Thus, the corresponding results will not be discussed here. It was decided to include both (A, B) and (C, D) H bonds in model M2, still applying C_i symmetry. In this way, the eight strongest out of twelve H bonds assumed to be present in the crystal are modeled. Neglect of the weak bridges E and F is supported by the good agreement of the U=O_t distances with experiment in all models, indicating only small effects of these latter H bonds on the strong U=O_t bonds. Rotation of the complex **1** inside the "matrix" set up by the H bonds of the environment would result in further H bonds to the frontier groups of neighboring complexes; to prevent such artifacts, the equatorial ligand atoms of the uranyl groups were constrained in a plane, in agreement with the experimental crystal structure. To check this approximation, the relaxation of this structure was examined which lead to changes in bond lengths of **1** by less than 0.02 Å.[65]

Geometry

Table 4.7 summarizes the calculated structures of the two models studied and compares these results with experiment. First, the gas phase reference model M1 is discussed. The central dimeric unit $[(UO_2)_2(OH)_2]^{2+}$ comprises two slightly different (Δ = 0.07 Å) bonds U-O_b of the bridging hydroxyl groups between the uranyl units. The OH moieties show a longer bond U-O_b (2.39 Å) to the uranyl where H_2O is their neighboring ligand and a shorter bond U-O_b' (2.32 Å) close to a neighboring Cl ligand (Fig. 4.3a). The O_b-H bonds are bent 66.6° out of the central U-O_b-U-O_b plane. The uranyl moieties of M1 are almost linear (176.7°), very close to the linear structure of a uranyl ion $[UO_2]^{2+}$. Terminal uranium oxygen distances U=O_t are significantly longer than in corresponding gas phase

calculations of the bare uranyl ion $[UO_2]^{2+}$ (Δ = 0.08 Å) and even somewhat longer than calculated for the solvated uranyl ion $[UO_2(H_2O)_5]^{2+}$ (Δ = 0.03 Å).[43] The elongation of these bonds results from the increasing competition with other, equatorial ligands at the U center which bind stronger than water (OH, Cl). For the GP structure of the analogous dinuclear complex $[(UO_2)_2(OH)_2(H_2O)_6]^{2+}$, almost equal U=$O_t$ distances (Δ = -0.01 Å) and an increased bending of the uranyl moieties (168.0°) have been calculated.[66]

The U-O_a, U-O_s, and U-Cl bonds are bent out of the U-O_b-U-O_b plane by 15.9°, 0.9°, and 6.2°, respectively. Therefore, the typical pentagonal bipyramidal coordination of the U centers, well known from monomeric complexes,[14] is slightly distorted. The bonds to the aqua ligands U-O_a and U-O_s (2.49 Å) are somewhat longer than uranium water distances in mononuclear $[UO_2(H_2O)_5]^{2+}$ (2.42 Å) and dinuclear[66] species $[(UO_2)_2(OH)_2(H_2O)_6]^{2+}$ (2.46 Å). This elongation can be rationalized by an increasing number of stronger binding ligands. Also, the U-Cl distance (2.63 Å) indicates strong ligand bonding because it is

Table 4.7. Structure parameters (distances in Å, angles in degree) of the complex $[(UO_2)_2(\mu_2\text{-}OH)_2Cl_2(H_2O)_4]$ **1** in the gas phase (M1) and in a model of the crystalline environment (M2). Also shown are experimental values and deviations Δ M*n* (*n* = 1, 2) of calculated quantities from the crystal structure. The last column provides the types of H bonds which directly affect the corresponding distances and angles. For the designations, see Fig. 4.3 and text.

	M1	M2	Exp.[a]	Exp.[b]	Δ M1	Δ M2	H bonds
U-U	3.801	3.875	3.94(0)	3.84(1)	-0.14	-0.07	
U=O_t	1.787	1.790	1.79(2)	1.76(1)	0.00	0.00	E, F
U-O_b	2.389	2.352	2.40(2)	*2.40(1)*	-0.01	-0.05	A, B, E, F
U-O_b'	2.318	2.343	2.34(2)	*2.40(1)*	-0.02	0.00	A, B, E, F
U-O_a	2.493	2.421	2.39(2)	*2.40(1)*	0.10	0.03	A, B, C, D
U-O_s	2.486	2.497	2.50(3)	*2.40(1)*	-0.01	0.00	
U-Cl	2.626	2.661	2.75(1)	2.89(2)	-0.12	-0.09	C, D
O_t=U=O_t	176.7	174.9	178.2(9)	–	-1.5	-3.3	E, F
O_b-U-O_b	72.3	68.7	67.0(7)	–	5.3	1.7	A, B, E, F
O_a-U-O_s	65.7	68.4	68.8(9)	–	-3.1	-0.4	A, B, C, D

[a] Ref. 109, crystal structure – average values with respect to the assumed C_i symmetry; maximum scattering of 0.04 Å for distances and 1.7° for angles; reference for determining the deviations Δ = X(calc.) – X(exp.)

[b] Ref. 113, solution; *average* value for all equatorial U-O distances determined by experiment.

relatively short compared to computational results for $[UO_2Cl_4]^{2-}$ where the U-Cl distances are elongated due to the competition of four strong bonds (2.68 Å). This latter result agrees well with EXAFS data for this complex in solution (2.67 Å)[79] whereas DF GGA calculations yield longer bonds, from 2.73 to 2.81 Å.[19]

As there are no experimental data for the gas phase, the results of model M1 are compared to x-ray data in solution, to obtain first hints of solvation and crystal packing effects on the geometry. Åberg investigated solutions of hydrolyzed uranyl(VI) chloride where the U concentration was kept constant at 3 M but the OH:U ratio, i.e. the average number of OH groups per U atom, was varied form 0 to 1.11.[113] From these data sets, the ratio 1.11 is chosen for comparison in agreement with the assumed structure of **1** that exhibits two U centers linked by two OH bridges. The obtained experimental results correspond to the assumed pentagonal coordination including one U-Cl bond (n_r = 0.8(1) for U-Cl, where n_r is the number of corresponding bonds per U atom) and four equatorial U-O bonds (n_r = 4.3(2)), i.e. two bonds to bridging hydroxyl moieties and two bonds to coordinated water molecules (Fig. 4.3). The latter four uranium oxygen bonds U-O_b, U-O_b', U-O_a, and U-O_s from the first hydration sphere could not be separated by experiment[113] so that only an average distance is available (2.40 Å, Table 4.7).

The U=O_t distance of model M1 is in reasonable agreement with the data in solution (Δ = 0.03 Å) indicating that the strong U=O_t bond is slightly affected by solvation effects. The U=O_t distance found in solution (1.76 Å) is relatively short compared with other experimental data for $[UO_2]^{2+}$ in solution (1.76-1.78 Å);[68,79] in fact, one would expect a longer U=O_t bond distance in M1 because four aqua ligands of a completely solvated uranyl complex are replaced by stronger bound ligands, namely by two Cl ligands and two OH bridges. The polar U-Cl bond, on the other hand, is notably shorter than in solution (Δ = -0.26 Å) and may be elongated by screening effects and possible H bonds. The calculated average distance 2.42 Å of all equatorial U-O bonds is somewhat longer than the experimental value, by 0.02 Å. The bridging bonds U-O_b and U-O_b' are significantly shorter compared to the bonds U-O_a and U-O_s (Δ ~ -0.14 Å); this indicates increased bond strengths of the linking bridges.

Before judging the gas phase model M1 against the crystal data, the available experimental information for solution and crystal structure is briefly compared. Over all, both data are similar, with a tendency to longer bonds in the crystal except for the U-Cl distance. This may be rationalized by more flexible and dynamically changing H bonds in solution, at variance with localized H bonds in the crystal; as a result, the corresponding bonds are weakened and lengthened in a more pronounced fashion. The average U-O

distance in the crystal is 0.01 Å longer than in solution. Main deviations occur for the U-U and U-Cl distances which are noticeably different from solution, with Δ = 0.10 Å and -0.14 Å, respectively. These deviations are interpreted as indicative for a weakening of the bridging bonds due to H bonds in the crystal (A and F in Fig. 4.5). Invoking bond order conservation at the two uranyl moieties, this weakening would result in a longer U-U distance and a strengthening of the other equatorial bonds, including the U-Cl bond.

Comparison with the crystal structure reveals relatively good agreement of model M1, particularly if one considers the experimental uncertainties. Only slight deviations are found for the distances U-O_b (Δ = -0.01 Å) and U-O_b' (Δ = -0.02 Å); also, the correct order of these two distances is reproduced (U-O_b > U-O_b'). However, the U-U distance, which does not represent an actual bond (3.80 Å), is strongly underestimated (Δ = -0.14 Å) yielding a more compact complex compared to the crystal structure; this is likely due to the stronger bridging bonds. The bonds to the aqua ligands U-O_a and U-O_s are almost equal in model M1, with a somewhat longer distance U-O_a (Δ = 0.01 Å), whereas in the crystal the U-O_s bond is significantly longer, by 0.11 Å. The distance U-O_a (Δ = 0.10 Å) is too long compared to experiment whereas the length of U-O_s (Δ = -0.01 Å) agrees very well. This may be traced back to effects of the H bonds involved, i.e. A, B, C, and D for U-O_a whereas the U-O_s bond length is not affected by any of the postulated H bonds (Fig. 4.5). The underestimation of the U-Cl distance (-0.12 Å) can be rationalized with the missing weakening effects due to H bonds C and D. The linearity of the uranyl moieties is very well reproduced (Δ = -1.5°) and deviations of other characteristic angles are small, 3° to 5°.

In model M2, the H bonds A, B, C, and D were simulated to take effects of the crystalline environment into account (Fig. 4.6). Compared to model M1, this results in an elongation of most bonds. All bond distances except U-O_b are improved in comparison to model M1 (Table 4.7), with deviations Δ from experiment ranging from less than 0.01 Å up to 0.09 Å; also the U-U distance is distinctly elongated (Δ = -0.07 Å). Agreement with experimental data for U-O_a (Δ = 0.03 Å) and U-Cl (Δ = -0.09 Å) is notably improved whereas the distance U-O_s (|Δ| < 0.01 Å) is as expected hardly affected because O_s is not involved in an H bond. In contrast to model M1, the correct ordering of the lengths of the two types of aqua ligand bonds U-O_a and U-O_s is reproduced (U-O_a < U-O_s). The calculated H bond Cl···*H-O_a* (D) is notably longer than in experiment (see below) which results in a reduced effect on the corresponding U-Cl bond; this may be the reason for the relatively strong deviation from experiment calculated for the U-Cl distance (Δ = -0.09 Å). The effect of the H bonds A on the O_b atoms is significant: the distance U-O_b (Δ = -0.05 Å) changes by 0.04 Å, the bending angle of the O_b-H bond is reduced from 66.6° in model M1

to 52.9°; the distance U-O_b' is less affected and changes by 0.025 Å. Both the uranyl angle O_t=U=O_t (Δ = -3°) and the remaining angles (Δ = 1° to 5°) are in good agreement with experiment with deviations of the same order as in model M1.

Very good agreement for the strong U=O_t bonds (Δ < 0.01 Å) is also found, in fact for both models M1 and M2; thus the postulated H bonds E and F seem to affect the uranyl bonding only weakly. This corroborates the choice to neglect these weak bonds in model M2. Based on previous results for similar systems,[66] the expected accuracy of about ±0.02 Å for bond distances was not reached in model M2 for the bonds U-O_b, U-O_a, and U-Cl; however, inclusion of the most important H bonds in model M2 distinctly improved the results compared to model M1. Note that the crystal structure differs slightly from the C_i symmetry assumed for the computational models, resulting in a scattering of the experimental distances by up to ±0.04 Å; this is of the same order as experimental uncertainties (0.01 to 0.03 Å, Table 4.7). Thus, for most bonds, the remaining deviations are in the range of the experimental uncertainty, but in part they may also be caused by the applied symmetry restriction and the lack of H bonds E and F in model M2.

The crystal structure provides only limited information on H bonds, but from model M2, one can obtain the location of the hydrogen atoms involved and the angles of the simulated H bonds (Table 4.8, Fig. 4.6). The calculated H bonds A (Δ = -0.02 Å) and C (Δ = 0.04 Å) are in good agreement with the X···Y distances found in the crystal; this is noteworthy as H bonds are not described in a highly accurate fashion with a local density approximation of the exchange-correlation functional (see Δ = 0.07 Å for the H bonds B and D).[172] The Cl···O_a distance of bridge D is calculated too long which seems to indicate a

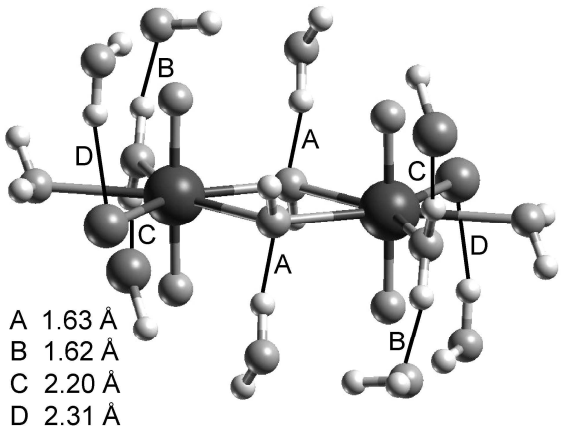

Figure 4.6. Optimized structure of the dinuclear complex [$(UO_2)_2(\mu_2$-$OH)_2Cl_2(H_2O)_4$] **1** including simulated H bonds A, B, C and D (model M2); also shown are calculated H···Y distances (Å).

weaker H bond in model M2 than expected from the crystal structure. As a consequence, the calculated U-Cl bond is less destabilized and too short (see above). The agreement of both chemical bond lengths and X···Y distances of H bonds, calculated for model M2, with the corresponding data of the crystal structure confirms that the relaxation of the gas phase structure of complex **1** (M1) is properly described in the simulated crystalline environment of model M2.

The computational results for H bonds can also be compared to typical data[235] for H···Y distances and X-H···Y angles (Table 4.8). Comparison with such data allows to classify the H bonds A and B as relatively strong, both exhibiting almost linear bonds with O_a-H···O_b angles of 173° (Table 4.8). The corresponding values for the H bonds C and D indicate typical weak to moderately strong bonds with elongated distances and O_a-H···Cl angles of 171° and 156°, respectively. Charge exchange from individual H bonds to the corresponding acceptor atoms in the complex is small; the total electronic charge donation of all eight H bonds is ~0.4 e compared to the gas phase model M1. According to a Mulliken population analysis, there is a slight charge donation to centers O_b (0.04 e) and Cl (0.03 e) from the H bonds A and D and also from H bonds B and C to both H atoms in H_2O_a (0.03 e and 0.06 e, respectively). The calculated charge donation of ~0.4 e is a deficiency of the applied model because the molecular crystal contains neutral units of **1**. A

Table 4.8. Bond distances (in Å), angles (in degree) and binding energies (BE, in kJ mol^{-1}) of modeled H bonds A, B, C, and D of model M2 in comparison with the crystal structure (in parentheses) and typical values for H bonds of various strengths. Frontier groups of adjacent complexes $[(UO_2)_2(\mu_2\text{-}OH)_2Cl_2(H_2O)_4]$ **1** are designated in italics.

			X···Y[a]	H···Y	X-H···Y	BE[c]
M2	A	*O_a-H*···O_b	2.630 (2.65)	1.632	173.2	84
	B	O_a-H···*O_b*	2.648 (2.58)	1.615	173.3	113
	C	O_a-H···*Cl*	3.177 (3.14)	2.197	171.1	14
	D	*O_a-H*···Cl	3.233 (3.16)	2.310	156.0	27
Typical values[b]		strong	2.2–2.5	1.2–1.5	175–180	60–170
		moderate	2.5–3.2	1.5–2.2	130–180	20–70
		weak	3.2–4.0	2.2–3.2	90–180	< 20

[a] Experimental values (Ref. 109) of crystal structure in parentheses.
[b] Ref. 235, typical values from various compounds.
[c] Binding energies calculated from **1** (M2) → **1** (M2 – 2X) + 2X , X = H_2O for A, B, D and X = HCl for C without geometry relaxation (see text).

net donation of electron charge should usually result in an elongation of bonds. However, compared to experiment, the deviations of calculated bond lengths in model M2 are of the same size as found for the dinuclear species $[(UO_2)_2(OH)_2(H_2O)_6]^{2+}$.[66] Thus, potential artifacts due to a net charge of complex **1** are expected to be small.

Energetics

For a comparison of the relative stabilities of the different models, the low symmetry gas phase model M1 (C_i symmetry) is chosen as reference. Model M2 is 315 kJ mol^{-1} more stable due to the simulated eight H bonds. This stabilization energy was calculated based on the reaction **1** (M1) + 6 H_2O + 2 HCl $\rightarrow$ **1**·6H_2O·2HCl (M2). With respect to the eight H bonds formed, this energy translates into an average binding energy of 39 kJ mol^{-1} per H bond. That value falls into the range of 20–70 kJ mol^{-1} which is typical for moderately strong H bonds,[235] corroborating the previously discussed structural evidence concerning their strength.

To estimate the strengths of individual H bonds, the corresponding frontier groups from model M2 were removed and the model reaction **1** (M2) $\rightarrow$ **1** (M2 – 2X) + 2X where X = H_2O for the H bonds A, B, and D and X = HCl for H bond C considered. No structure relaxation was allowed. The energies of the H bonds A, B, C, and D, estimated in this way, are 84, 113, 14, and 27 kJ mol^{-1}, respectively (Table 4.8). Interestingly, the strength of the H bonds for both pairs (A, B) and (C, D) is not increasing as one would expect for shorter X···Y distances (Table 4.8). The calculated energies confirm the previous classification of the H bonds based on the structural evidence: H bonds A and B, with average binding energies of about 99 kJ mol^{-1}, represent typical strong H bonds (60–170 kJ mol^{-1})[235] whereas H bonds C and D are significantly weaker, with average binding energies of about 21 kJ mol^{-1}. Together with the good overall agreement of the detailed geometry of model M2 with the crystal structure, these energy results corroborate that the simulated H bonds represent the main crystal packing effects.

In summary, H bonds in the crystal environment were described via model H_2O and HCl moieties mimicking the effect of frontier groups of neighboring complexes **1**. In this model, the calculated structure is significantly improved. Average deviations from experiment are reduced from 0.04 Å to 0.03 Å for bond distances (maximum deviation 0.09 Å for U-Cl) and from 3.5° to 2.6° for angles (maximum deviation 5°). Based on this model, lengths and angles of the hydrogen bonds were determined, indicating moderate and strong H bonds with an average binding energy of 39 kJ mol^{-1}. These computational results corroborate earlier suggestions based on experimental results[109] concerning the location and strength of H bonds.

4.3 Uranyl complexation by carbonate ligands

Under environmental conditions in the presence of carbon dioxide (CO_2) actinide carbonate complexes become one of the dominating species in aqueous solution.[12] This section focuses on the uranyl carbonate system which is the most extensively studied among the actinide carbonate systems.[12] First, mononuclear carbonate complexes $[UO_2(CO_3)_m]^{2-2m}$ (m = 1–3) will be investigated including a discussion of short-range (via explicit water molecules in the models) as well as long-range solvation effects (Section 4.3.1). Secondly, the well-studied tris(carbonato) complex $[UO_2(CO_3)_3]^{4-}$ and the polynuclear triuranyl hexa(carbonato) complex $[(UO_2)_3(CO_3)_6]^{6-}$ will be compared to data from EXAFS studies (Section 4.3.2). Finally, different isomers of the dinuclear hemicarbonate species $[(UO_2)_2(CO_3)(OH)_3]^-$ will be presented and discussed with respect to available experimental data (Section 4.3.3).[83,84]

Previous theoretical studies on uranyl carbonate species are rare and mainly limited to benchmark systems. A comprehensive investigation and comparison of the different carbonate species and a systematic treatment of solvent effects is missing so far. One investigation dealt with the mono(carbonato) complex[44] $[UO_2(CO_3)]$, both in the gas phase and in aqueous solution, while several studies are available for the tris(carbonato) complex $[UO_2(CO_3)_3]^{4-}$.[39,64,67,241,242] A very recent study presented first data on the trimeric complex $[(UO_2)_3(CO_3)_6]^{6-}$ in the gas phase.[67] Two further theoretical studies focused also on neptunium(V)[76] and plutonium(IV)[77] carbonate complexes.

4.3.1 Monomeric uranyl carbonates, $[UO_2(CO_3)_m]^{2-2m}$

To reduce the computational effort, high symmetry was assumed for the models of mononuclear carbonate complexes $[UO_2(CO_3)_m]^{2-2m}$, i.e. C_{2v} (m = 1), D_{2h} (m = 2), and D_{3h} symmetry (m = 3), in line with the experimental crystal structure of the $[UO_2(CO_3)_4]^{4-}$ moiety.[12] In all these compounds, the carbonate ligands exhibit bis(chelating) coordination and are located in the equatorial plane which is perpendicular to the uranyl moiety (Fig. 4.7). Characteristic distances in these complexes are U=O_t, U-O_{C1}, U-O_{C2}, and U-C; O_{C1} designate oxygen centers of the carbonate ligands that bind to the uranium center and O_{C2} is used for the terminal oxygen centers, respectively (Fig. 4.7).

To account for short-range solvation effects, the models were extended by considering explicit water molecules (keeping the symmetry of the models). Additional aqua ligands (n) from the first hydration shell are included in models (m,n), i.e. $[UO_2(CO_3)_m(H_2O)_n]^{2-2m}$, to saturate the equatorial uranyl coordination sites (Fig. 4.8). Three aqua ligands were chosen for the mono(carbonato) complex (Fig. 4.8a), i.e. model

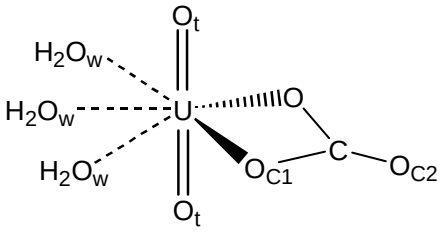

Figure 4.7. Schematic structure of the uranyl carbonate complex $[UO_2(CO_3)(H_2O)_3]$ with bis(chelating) coordination of the carbonate ligand. Structures are characterized by distances U=O_t, U-O_{C1}, U-O_{C2}, U-O_w, and U-C.

(1,3), resulting in the typical pentagonal coordination of the uranium center[14] that is also found for the solvated uranyl ion $[UO_2(H_2O)_5]^{2+}$.[79–81] For the bis(carbonato) complex, hexagonal coordination with two additional aqua ligands, i.e. model (2,2), was considered (Fig. 4.8b). Steric repulsion between the ligands in the equatorial uranyl plane – discussed for hexa-coordinated $[UO_2(H_2O)_6]^{2+}$ (see Section 4.1) – is reduced due to the smaller O_{C1}-U-O_{C1} angles (~55°) of the two carbonates. Thus, enough space is expected to be available for two additional aqua ligands. A hexagonal coordination is also well-known from crystal structures[130] for the tris(carbonato) complex (Fig. 4.8c) whose first hydration shell is saturated by the three carbonate ligands. Thus, the corresponding model (3,0) does not include further aqua ligands. The employed models are in agreement with coordination numbers of corresponding Np(V) carbonates $[NpO_2(CO_3)_m]^{1-2m}$ suggested by EXAFS[243] and theoretical[76] data. Neptunyl(V) complexes are usually larger and show longer bonds than the corresponding actinyl(VI) compounds due to the reduced charge (see Section 4.1). The larger size provides space for additional ligands, but the weaker bonds suggest a reduced binding capacity. Thus, a similar coordination number is expected for actinyl(V) and actinyl(VI) complexes. This is confirmed by the suggested identical pentagonal coordination for the corresponding solvated actinyls $[AnO_2(H_2O)_5]^{2+/+}$ (Section 4.1).

Structures of uranyl carbonate complexes $[UO_2(CO_3)_m]^{2-2m}$

Gas phase (GP) and solvation (PCM) results for the mononuclear uranyl carbonate complexes (*m*,*n*) are summarized in Table 4.9. The optimized structures of models (1,3), (2,2), and (3,0) are displayed in Figs. 4.8a–c, respectively.

As expected, the increase of the number of carbonate ligands leads to a weakening of the strong terminal uranyl bond due to the enhanced bonding competition at the uranium center. In the GP models the U=O_t distance is successively elongated from 1.78 Å in model (1,0) to 1.84 Å in model (3,0) which is also reflected in the continuously decreasing symmetric uranyl stretching frequency ν_s, 876 cm^{-1} for (1,0) and 742 cm^{-1} for (3,0).

Table 4.9. Calculated structural parameters (distances in Å) and symmetric uranyl stretching frequency (ν_s, in cm^{-1}) of uranyl carbonate complexes (*m*,*n*), i.e. $[UO_2(CO_3)_m(H_2O)_n]^{2-2m}$ (*m* = 1–3). Additional water molecules (*n*) from the first hydration shell are included to saturate the equatorial uranyl coordination sites (Fig. 4.8). Results from gas phase (GP) and solvation (PCM) calculations are compared with data from another theoretical study (GP, calc., see text for details). For the designations of the atoms, see Fig. 4.7.

	(*m*,*n*)	U=O_t	U-O_{C1}	U-O_{C2}	U-C	C-O_{C1}	C-O_{C2}	ν_s
GP	(1,0)	1.779	2.143	3.856	2.660	1.352	1.196	876
	(1,3)	1.801	2.249	3.968	2.762	1.340	1.206	837
	(2,0)	1.818	2.301	3.996	2.761	1.325	1.235	791
	(2,2)	1.828	2.371	4.092	2.849	1.316	1.243	770
	(3,0)	1.839	2.465	4.198	2.924	1.304	1.274	742
Calc.[a]	(1,0)	1.776	2.136	3.851	2.652	1.355	1.199	880
	(2,0)	1.814	2.295	3.990	2.755	1.326	1.235	805
	(3,0)	1.835	2.462	4.196	2.916	1.304	1.280	760
PCM	(1,0)	1.774	2.203	3.908	2.692	1.329	1.216	870
	(1,3)	1.802	2.293	3.998	2.769	1.320	1.230	822
	(2,0)	1.814	2.299	3.990	2.756	1.319	1.234	783
	(2,2)	1.824	2.379	4.095	2.851	1.308	1.244	742
	(3,0)	1.843	2.396	4.107	2.856	1.307	1.250	737

[a] Ref. 67.

Concomitantly, all distances to the carbonate ligands U-O_{C1}, U-O_{C2}, and U-C are distinctly elongated from (1,0) to (3,0) by about 0.32 Å, 0.34 Å, and 0.26 Å, respectively. The weakening of the U-O_{C1} bonds results in a strengthening of the neighboring C-O_{C1} bonds which shorten by 0.05 Å in total. Concomitantly, the terminal C-O_{C2} bond elongates by 0.08 Å (Table 4.9).

A recent theoretical study by Dixon et al. presented data for models (1,0), (2,0), and (3,0) in the gas phase, see Table 4.9.[67] They applied a similar computational approach, using a DF method with a LDA-VWN exchange-correlation functional, but employed a small core RECP for uranium in contrast to the all-electron method used here. The results obtained are in very good agreement with the data of this work (Table 4.9). Deviations range from 0.001 to 0.008 Å for distances and are a bit more pronounced for the uranyl stretching frequency 4 to 18 cm^{-1}.

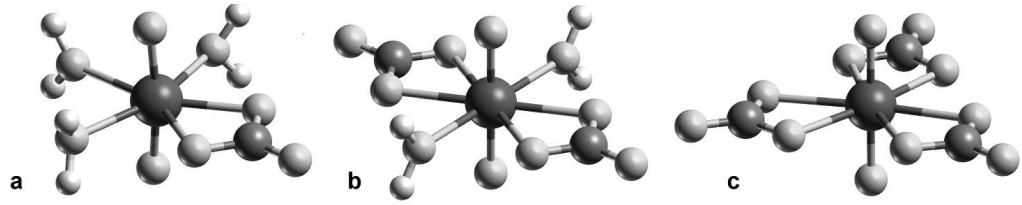

Figure 4.8. Optimized structures from PCM calculations of uranyl carbonate complexes (*m*,*n*), i.e. $[UO_2(CO_3)_m(H_2O)_n]^{2-2m}$: (1,3) (a), (2,2) (b), and (3,0) (c). Additional water molecules (*n*) from the first hydration shell are included to saturate the equatorial uranyl coordination sites.

Including additional aqua ligands for m = 1 and m = 2 via models (1,3) and (2,2) results in a further reduction of the uranium binding capacity. Consequently, the distances U=O_t and U-O_{C1} in (1,3) are elongated by about 0.02 Å and 0.11 Å compared to (1,0). The effect of two additional aqua ligands in model (2,2) is slightly smaller in comparison to (2,0), reflected by the elongation of U=O_t by 0.01 Å and U-O_{C1} by 0.07 Å. Overall, these findings indicate notable effects of additional aqua ligands on the structure of the complexes. However, these variations due to additional aqua ligands are smaller than structural changes arising from the coordination of further carbonate ligands (Table 4.9). This can be rationalized by the fact that binding energies of H_2O ligands are calculated lower than those of carbonate ligands (see below, Table 4.10). The inclusion of long-range solvent effects (PCM) has no effect on the overall trends, i.e. on the weakening of all U-O bonds when going from (1,0) to (3,0) (Table 4.9). The sizes of the complexes obtained from PCM calculations are more similar to each other than in the GP calculations, as reflected by the range of equatorial distances. Comparing models (1,0) to (3,0) U-O_{C1}, U-O_{C2}, and U-C distances range from 2.20–2.40 Å, 3.91–4.11 Å, and 2.69–2.86 Å, respectively. These intervals are distinctly broader for complexes in the gas phase: 2.14–2.47 Å, 3.86–4.20 Å, and 2.66–2.92 Å, respectively. On the other hand, PCM effects on the strong axial U=O_t bond are rather small with changes less than ±0.01 Å (Table 4.9). Therefore the uranyl stretching frequency is somewhat lower in PCM calculations (Table 4.9). Surprisingly, PCM effects on the polar U-O bonds do not strictly follow the increasing charge of the complexes. As expected, the strongest changes are obtained for the highly charged (3,0) complex, but they are comparable to those calculated for the smallest, neutral (1,0) species (Table 4.9). The strong effects in model (1,0) might be rationalized by the fact that U=O_t and U-O_{C1} bonds are more polar than in the other complexes. This interpretation is supported by an analysis of the corresponding Mulliken charges in the GP complexes. Charges of O_t and O_{C1} centers are comparable for all species

(differences < 0.1 e), but complex (1,0) shows the highest uranium charge (differences > 0.3 e) due to missing electron donation from further ligands. The uranyl bond (1.80 Å) and the bonds to the aqua ligands (~2.40 Å) of the PCM model (1,3) are slightly elongated compared to corresponding bonds of the complex $[UO_2(H_2O)_5]^{2+}$ (1.78 Å and 2.36 Å, see Section 4.1, Table 4.2). This is concomitant to the fact that the uranyl-carbonate bonds are stronger than the uranyl-aqua bonds.

Energetics

In the further discussion binding energies of the carbonate and aqua ligands will be investigated according to Eqs. (4.4) and (4.5):

$$[UO_2(CO_3)_m(H_2O)_n]^{2-2m} \rightarrow [UO_2(H_2O)_n]^{2+} + m\,[CO_3]^{2-} \quad (4.4)$$

$$[UO_2(CO_3)_m(H_2O)_n]^{2-2m} \rightarrow [UO_2(CO_3)_m]^{2-2m} + n\,H_2O \quad (4.5)$$

The strong uranyl-carbonate bond is reflected in the distinctly higher binding energies of the carbonate ligands compared to the aqua ligands (Table 4.10). Average carbonate binding energies in the GP models are 2758, 1791, and 973 kJ mol^{-1} for the complexes (1,0), (2,0), and (3,0), respectively, and decrease significantly, by ~900 kJ mol^{-1}, for each additional ligand. The high values result from the strong electrostatic attraction between the positive uranyl $[UO_2]^{2+}$ and the negative carbonates $[CO_3]^{2-}$. The neutral aqua ligands exhibit distinctly smaller average binding energies of 92 kJ mol^{-1} in model (1,3); this value is reduced compared to the solvated uranyl $[UO_2(H_2O)_5]^{2+}$ (221 kJ mol^{-1}), indicating that the carbonate ligands saturate a major part of the uranyl binding capacity. However, the

Table 4.10. Binding energies (in kJ mol^{-1}) per carbonate or aqua ligand of uranyl carbonates (*m*,*n*), i.e. $[UO_2(CO_3)_m(H_2O)_n]^{2-2m}$, from gas phase (GP) and solvation (PCM) calculations according to Eqs. (4.4) and (4.5), see text. Energetics are based on the GGA-BP exchange-correlation functional applied in single-point calculations at LDA-VWN optimized structures.

(*m*,*n*)	GP		PCM	
	CO_3^{2-}	H_2O	CO_3^{2-}	H_2O
(0,5)	–	-221	–	-104
(1,0)	-2758	–	-587	–
(1,3)	-2222	-92	-393	-66
(2,0)	-1791	–	-466	–
(2,2)	-1484	20	-337	-8
(3,0)	-973	–	-374	–

relatively strong aqua bonds lead to noticeable changes in the structure discussed above. The carbonate bond is weakened due to additional aqua ligands by about 500 and 300 kJ mol^{-1} in models (1,3) and (2,2), respectively. The positive value for the aqua ligand binding energy (20 kJ mol^{-1}) in model (2,2) indicates that in the gas phase the second additional aqua ligand is unbound.

The binding energies of carbonate ligands in the PCM model are noticeably smaller due to screening effects: 587, 466, and 374 kJ mol^{-1} for the complexes (1,0), (2,0), and (3,0), respectively (Table 4.10). The average binding energy is reduced by about 100 kJ mol^{-1} per additional carbonate ligand. The energies of the neutral aqua ligands are less affected by screening and are therefore only somewhat reduced to 66 kJ mol^{-1} in model (1,3); this value is about half of that calculated for $[UO_2(H_2O)_5]^{2+}$ (104 kJ mol^{-1}). The rather high aqua binding energy in model (1,3) seems to indicate a propensity for coordinating an additional aqua ligand. The corresponding hexagonal uranyl coordination might be stable; recall the similar stability of pentagonal and hexagonal coordination in $[UO_2(H_2O)_n]^{2+}$ (see Section 4.1). Here, the hexagonal coordination might be even more favored because the steric hindrance in the equatorial plane is reduced as a result of the small O_{C1}-U-O_{C1} angle (~55°) of the carbonate ligand. In contrast to the GP results, the hexagonal coordination, i.e. binding of two aqua ligands, is stable for the PCM model (2,2). However, the small average binding energy of only 8 kJ mol^{-1} indicates that the bond to the second aqua ligand is rather weak.

Finally, the successive bonding of an additional carbonate ligand is discussed for the reaction: (1,0) → (2,0) → (3,0). Both for GP and PCM models the formation of the (2,0) complex is distinctly exothermic by 824 and 345 kJ mol^{-1} due to the formation of strong carbonate bonds. The addition of the third carbonate ligand is also exothermic for PCM, by 190 kJ mol^{-1}. The third carbonate ligand is weaker bound, as reflected in the decreased average carbonate binding energy on going from (2,0) to (3,0); this trend is a consequence of the fact that the third carbonate ligand has to compete with the other two strongly bound ligands. In contrast to the PCM model, the third carbonate is not bound in the gas phase (+663 kJ mol^{-1}) because of the electrostatic repulsion between the two negatively charged species $[UO_2(CO_3)_2]^{2-}$ and $[CO_3]^{2-}$.

If one considers additional aqua ligands in the series of reactions (1,3) → (2,2) → (3,0), then the trends discussed above do not change. However, the reaction energy for the first step is distinctly decreased, to 509 kJ mol^{-1} for the GP model and to 162 kJ mol^{-1} for PCM model. Forming an additional carbonate bond is associated with the breaking of three rather strong bonds to aqua ligands (see Table 4.10). The reaction energies of the second

step are less affected when aqua ligands are accounted for in the model (2,2), concomitant with the fact that aqua ligands are weakly bound in complex (2,2) (see Table 4.10). In the PCM model, addition of the third ligand yields a higher reaction energy than addition of the second carbonate (174 kJ mol^{-1}). This may point to higher stability of the tris(carbonato) complex, inline with the experimentally suggested dominance of the latter complex over a wide range of pH values.

Solvation effects for the uranyl carbonate complexes are modeled by explicit aqua ligands and a PCM treatment. If one compares results for models with and without explicitly aqua ligands, i.e. (1,3) vs. (1,0) and (2,2) vs. (2,0), structural changes due to the coordinated H_2O ligands are distinctly larger than effects which result from applying the PCM approach (Table 4.9). This confirms results for solvated actinyls (Section 4.1) and of previous studies,[43,66] where it had been found that the PCM model alone can not describe with sufficient accuracy short-range solvent effects in the first hydration sphere of uranyl. Rather, it is necessary to explicitly include aqua ligands for an adequate description of such complexes.

Uranyl tris(carbonato) complex $[UO_2(CO_3)_3]^{4-}$

As experimental data are missing for the mono- and bis(carbonato) uranyl complexes in solution, one is left with an evaluation of the theoretical results for the tris(carbonato) complex $[UO_2(CO_3)_3]^{4-}$. This complex has been extensively studied both experimentally[83,126,129–133] and theoretically.[39,64,241,242] The present results for the gas phase (GP) and for aqueous solution (PCM) are summarized in Table 4.11.

Compared to EXAFS data from solution[131,132] both GP and PCM results for the bare complex distinctly overestimate the uranyl bond U=O_t, 1.84 Å compared to the experimental value of 1.80(2) Å. This discrepancy is rather large compared to those obtained in previous studies[43,55,66] that indicated an accuracy of the applied computational method of about ±0.02 Å for the uranyl bonds. As a consequence of the fact that the uranyl bonds are described too weak, the experimental stretching frequency (812 cm^{-1})[129,133] is significantly underestimated in the calculations, by about 72 cm^{-1}. In the GP model the equatorial bonds U-O_{C1} are calculated somewhat longer, by 0.02–0.03 Å, than the experimental values from solution (2.43–2.44 Å); on the other hand, the PCM results are too short by 0.03–0.04 Å. This trend is also reflected in the other equatorial distances U-O_{C2} and U-C (Table 4.11).

However, the overall rather large deviations both for distances and frequencies indicate missing effects in the models, probably due to the screening of the carbonate ligands by the solvent which will be discussed below.

Table 4.11. Calculated structural parameters (distances in Å) and symmetric uranyl stretching frequency (ν_s, in cm^{-1}) of the uranyl tris(carbonato) complex $[UO_2(CO_3)_3]^{4-}\cdot(H_2O)_{n'}$. Additional water molecules (n') from the second coordination shell are included to simulate hydrogen bonds to the carbonate ligands (Fig. 4.9b). Results from calculations on gas phase (GP) and solvation (PCM) models are compared with experimental EXAFS data for aqueous solution and results from various other calculations (Calc., see text for details). For the designations of atoms, see Fig. 4.7.

	n'	U=O_t	U-O_{C1}	U-O_{C2}	U-C	ν_s
GP	0	1.839	2.465	4.198	2.924	742
	6	1.810	2.462	4.176	2.888	796
	12	1.795	2.464	4.176	2.878	827
PCM	0	1.843	2.396	4.107	2.856	737
	6	1.819	2.405	4.118	2.856	777
Exp. Sol.[a]		1.80	2.44	4.20	2.89	812[c]
Sol.[b]		1.80(2)	2.43(2)	4.13(4)	2.89(4)	809[d]
Calc.						
DF-SVWN, GP [e]	0	1.835	2.462	4.197	2.916	760
DF-SVWN, GP [f]	0	1.815	2.430	4.166	2.902	783
DF-PBE96, GP [e]	0	1.825	2.527	4.271	2.994	778
DF-B3LYP, GP [g]	0	1.80–1.84	2.54–2.60	–	–	–
DF-B3LYP, GP [h]	0	1.848	2.576	–	–	–
DF-PW91, GP [i]	0	1.85	2.56	4.39	3.01	–
DF-PW91, PCM [i]	0	1.85–1.86	2.46–2.48	4.16–4.21	2.90–2.93	–
MBPT2, GP [k]	0	1.894	2.426	4.790	2.893	–
MBPT2, PCM [k]	0	1.881	2.407	4.111	2.841	–
MP2, GP [g]	0	1.83–1.84	2.50–2.54	–	–	–
HF, GP [g]	0	1.73–1.74	2.56–2.58	–	–	–

[a] Ref. 132. [b] Ref. 131. [c] Ref. 133. [d] Ref. 83. [e] Ref. 67. [f] Ref. 67, more diffuse basis set. [g] Ref. 241, intervals due to different RECPs and basis sets. [h] Ref. 39. [i] Ref. 64, intervals due to different basis sets. [k] Ref. 242.

To address possible methodological influences, the present results are compared with other theoretical data available for $[UO_2(CO_3)_3]^{4-}$ (n' = 0, Table 4.11). Dixon et al. applied a DF method with a local exchange-correlation functional (LDA-SVWN) and employed a small core Stuttgart RECP for uranium, but they did not account for solvation effects in their calculations.[67] The default uranium orbital basis set used was extended by diffuse s-,

p-, d-, and f-exponents of 0.005. Differences between the results from the two basis sets are noteworthy. All distances become somewhat shorter with the extended basis set, by 0.01 to 0.03 Å (Table 4.11). The SVWN data from the calculation with the default U basis set agree well with results from this work; deviations of distances range from 0.001 to 0.008 Å (Table 4.11). The influence of diffuse functions was checked by adding one s-, p-, d-, and f-exponent each to the U basis in the present work (see Section 3.4). These exponents were obtained by dividing the most diffuse s-, p-, d-, and f-exponents by a factor of three (see Appendix A for exponents). Results for $[UO_2(CO_3)_3]^{4-}$ show deviations of distances up to 0.01 Å for GP and up to 0.005 Å for PCM models. These changes point to the importance of diffuse functions when dealing with highly charged anionic systems such as $[UO_2(CO_3)_3]^{4-}$. However, one should note that such effects can not be expected to fully compensate for the deviations to experiment found for the PCM model (about 0.03–0.04 Å, Table 4.11).

Dixon et al. also applied a gradient-corrected exchange-correlation functional (GGA-PBE96) which is known to yield longer distances than LDA functionals (see also Section 3.1.3).[190,191] This propensity is reflected in the significantly elongated equatorial distances U-O_{C1}, U-O_{C2}, and U-C in the PBE96 calculations, by ~0.07 Å, compared to those of the corresponding SVWN calculation (Table 4.11). Thus, the results obtained with the PBE96 functional overestimate the experimental values by up to 0.1 Å.

Vázquez et al.[64] applied a ZORA[32–34] scalar-relativistic DF method to both GP and PCM models. The chosen gradient-corrected exchange-correlation functional GGA-PW91 shows a comparable overestimation of distances as discussed above for the GGA-PBE96 functional. Equatorial distances U-O_{C1} and U-O_{C2} from the GP model fail to reproduce the experimental data with deviations from 0.1 to 0.2 Å (Table 4.11). The uranyl bonds U=O_t (1.85–1.86 Å) are slightly longer than for LDA (1.84 Å) and therefore overestimate the experimental value, 1.80(2) Å, even more.[131] The PCM model yields results in distinctly better agreement; however, distances are slightly too long, i.e. 2.46–2.48 Å for U-O_{C1} (exp. 2.43–2.44 Å) and 2.90-2.93 Å for U-C (exp. 2.89(4) Å). Note that the equatorial distances are still somewhat too long although the weakened axial uranyl bonds would suggest shorter equatorial bonds due to a higher binding capacity at the uranium center.

Gagliardi et al. reported *ab initio* calculations based on second-order many-body perturbation theory (MBPT2) where the aqueous environment was treated by a reaction field Hamiltonian using a spherical cavity.[242] Similar to the previously discussed DF-GGA results, this method distinctly overestimates the uranyl bonds U=O_t (1.88–1.89 Å); U–O_{C1} distances are underestimated to some extent (2.41–2.43 Å). A multiconfigurational

treatment (CASPT2) leads to shorter, but still rather long U=O_t distances (1.85 Å).[242] On the other hand, CASPT2 results for U-O_{C1} (2.41 Å) and U-C (2.84 Å), obtained with a solvation model, agree satisfactorily with experimental values which are underestimated by about 0.02 Å and 0.05 Å, respectively.

Tsushima et al. applied several methods such as HF, MP2, and DF-B3LYP, employing relativistic effective large core potentials (RECP) for uranium, but they did not include solvation effects in their calculations.[241] HF data indicate a distinct underestimation (1.73–1.74 Å) of the uranyl bond (1.80 Å), accompanied by an overestimation of the U-O_{C1} distance by more than 0.1 Å. Such an underestimation of U=O_t is typical for HF which lacks a treatment of electron correlation that is particularly important for heavy element compounds. Similar results have also been found for $[UO_2(H_2O)_5]^{2+}$ (see Section 4.2, Table 4.3). On the other hand, MP2 and DF-B3LYP results slightly overestimate the uranyl bonds U=O_t, i.e. with 1.83–1.84 Å and 1.80–1.84 Å, respectively. The ranges of the computational results reflect the effects of different basis sets, with and without inclusion of polarization and diffuse functions. However, the corresponding equatorial distances U-O_{C1}, 2.48–2.52 Å for MP2 and 2.50–2.53 Å for DF-B3LYP, are calculated significantly too long, by more than 0.1 Å. Schreckenbach et al. had previously noted that large-core ECP DF-B3LYP calculations generally give reliable axial U=O_t distances, but somewhat overestimate equatorial U-O distances.[244] Gas phase DF-B3LYP results from Hemmingsen et al., yielding 1.85 Å for U=O_t and 2.58 for Å U-O_{C1}, show the same trends and agree with data of Tsushima.[39]

This comparison of theoretical results for the bare tris(carbonato) complex $[UO_2(CO_3)_3]^{4-}$ indicates an overestimation of the axial uranyl bonds independent of the theoretical method applied. Gas phase results from gradient-corrected DF methods like PW91 and B3LYP fail to reproduce the equatorial distances U-O_{C1} (deviations >0.1 Å), while DF-LDA and MBPT2 methods perform better for GP models, but still show rather large deviations from experimental values. Including solvation effects via a PCM approach based on a spherical cavity does not significantly improve the results. This finding indicates that bulk solvent effects alone are not sufficient to describe these complexes adequately. Tsushima et al. suggested to consider explicitly counterions and/or water molecules when treating the aqueous tris(carbonato) complex.[241] However, the inclusion of counterions like Ca^{2+} and Ba^{2+} lead to a distinctly asymmetric distribution of U-O_{C1} and U-C distances (up to 0.3 Å).[241] If realistic, it should be possible to resolve such discrepancies in the EXAFS experiments, but there are no such reports to date. On the other hand, accounting explicitly for water molecules yielded slightly improved distances that nevertheless were still too long.[241] However, this overestimation may be due to the

applied DF-B3LYP functional and the missing PCM treatment.

Inspired by these results, water molecules from the second hydration shell (*n*') were explicitly included in the extended models $[UO_2(CO_3)_3]^{4-}\cdot(H_2O)_{n'}$ to account for hydrogen bonds to the carbonate ligands. For *n*' = 6 (Fig. 4.9b) two additional water molecules are located next to each carbonate ligand inside the equatorial plane; for *n*' = 12, four water molecules are placed symmetrically near each carbonate ligand, two above and two below the equatorial plane. Thus, both models also exhibit D_{3h} symmetry. Note that these water molecules do not represent the real structure of the second solvation shell, but are introduced to qualitatively model the solvation effects. The corresponding GP and PCM results are also summarized in Table 4.11.

GP results for the model with six additional water molecules (*n*' = 6) agree noticeably better with experiment than the results discussed previously for the bare complex (*n*' = 0). The uranyl bond $U{=}O_t$ (1.81 Å) is 0.02 Å shorter and now in very good agreement with the experimental value, 1.80(2) Å.[131] Concomitantly, the deviation of the uranyl stretching frequency (796 cm^{-1}) decreased to 16 cm^{-1}. In addition, all equatorial distances $U\text{-}O_{C1}$ (2.46 Å), $U\text{-}O_{C2}$ (4.18 Å) and U-C (2.89 Å) are slightly shorter, by 0.01 Å, 0.02 Å, and 0.03 Å, respectively. Therefore, these bond distances fall almost within the experimental uncertainty range: $U\text{-}O_{C1}$ 2.43(2) Å, $U\text{-}O_{C2}$ 4.13(4) Å, and U-C 2.89(4) Å.

In the model with *n*' = 6, one can distinguish between two sets of hydrogen bonds from the two water molecules to each carbonate ligand (Fig. 4.9b, Table 4.12), namely $O_{C1}\cdots H\text{-}O_w$ and $O_{C2}\cdots H\text{-}O_w$ (see Fig. 4.7 for the designations). These hydrogen bonds are characterized by $O_{C2}\cdots H$ and $O_{C1}\cdots H$ distances of 1.64 Å and 2.03 Å; the corresponding angles $O_C\cdots H\text{-}O$ are 159° and 133°, respectively. Compared to characteristic values from various compounds, these data indicate hydrogen bonds of moderate strength which typically are 1.5 Å to 2.2 Å long and exhibit angles from 130° to 180°.[235] The calculated

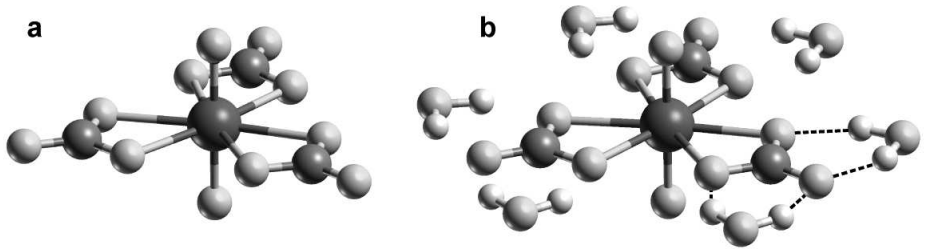

Figure 4.9. Optimized structures from PCM calculations on the uranyl tris(carbonato) complex $[UO_2(CO_3)_3]^{4-}\cdot(H_2O)_{n'}$: bare complex (*n*' = 0) (a) and model with *n*' = 6 additional water molecules from the second coordination shell (b) to simulate hydrogen bonds bridges (dashed lines) to the carbonate ligands.

average binding energy of 142 kJ mol^{-1} in the gas phase is, as expected, lower than for uranium water bonds in the first hydration sphere of $[UO_2(H_2O)_5]^{2+}$ (221 kJ mol^{-1}), but larger than in $[UO_2CO_3(H_2O)_3]$ (92 kJ mol^{-1}). This binding energy indicates a strong bond as also reflected in the distinct changes of the structure. The hydrogen bonds lead to a weakening of the terminal C-O_{C2} bond of the carbonate ligands, by ~0.01 Å, and consequently result in a slight shortening of the C-O_{C1} bond, by about 0.01 Å. This causes a minor contraction of the whole complex as reflected indirectly in the U-C distance which becomes 0.03 Å shorter. The weakening effect on the carbonate ligand is transferred via the equatorial U-O_{C1} bond to the uranyl bond U=O_t that is strengthened (0.02 Å shorter) while the distance U-O_{C1} itself is hardly affected.

The second GP model with 12 aqua ligands (n' = 12) leads to a small reduction of the uranyl bond U=O_t (1.80 Å) by 0.01 Å and, concomitantly, to a further increased stretching frequency (827 cm^{-1}) that is somewhat larger than the experimental value, by 15 cm^{-1}. Changes in the equatorial distances are minor (less than 0.01 Å); apparently, the binding capacity for hydrogen bonds is already saturated by two additional water molecules per carbonate ligand (n' = 6). The geometry of the hydrogen bonds for n' = 12 is comparable to that of the model with n' = 6 (Table 4.12); it exhibits slightly increased distances $O_{C2}\cdots H$ of 1.80 Å and $O_{C1}\cdots H$ of 2.13 Å; the corresponding angles $O_C\cdots H$-O are 160° and 134°. The elongated distances indicate weaker hydrogen bonds compared to the complex with

Table 4.12. Bond distances (in Å), angles (in degree), and average binding energies per aqua ligand (BE, in kJ mol^{-1}) of hydrogen bonds in models $[UO_2(CO_3)_3]^{4-}\cdot(H_2O)_{n'}$ (n' = 6, 12) from gas phase (GP) and solvation (PCM) calculations in comparison to typical values for hydrogen bonds of various strengths. For the designations of atoms, see Fig. 4.7 and the text.

		GP			PCM		
n'		X···H	X···H-Y	BE	X···H	X···H-Y	BE
6	$O_{C2}\cdots H$-O_w	1.64	159	142	1.77	147	24
	$O_{C1}\cdots H$-O_w	2.03	133		1.77	144	
12	$O_{C2}\cdots H$-O_w	1.80	155	111	–	–	–
	$O_{C1}\cdots H$-O_w	2.13	131		–	–	
Exp.[a]	strong	1.2–1.5	175–180	–	1.2–1.5	175–180	60–170
	moderate	1.5–2.2	130–180	–	1.5–2.2	130–180	20–70
	weak	2.2–3.2	90–180	–	2.2–3.2	90–180	< 20

[a] Ref. 235, typical values of hydrogen bonds from various compounds.

n' = 6 due to the competition of twelve, instead of six water molecules. This analysis is corroborated by the lower average ligand binding energy of 111 kJ mol^{-1}. Overall, both models, with n' = 6 and n' = 12, agree distinctly better with the experimental data, both for axial and equatorial distances with deviations of less than 0.03 Å for bond distances and about 2%, i.e. 16 cm^{-1}, for the uranyl stretching frequency.

In a next modeling step, long-range solvent effects are described in addition, for the model n' = 6 via the PCM approach. As a result, the uranyl bond U=O_t (1.82 Å) is 0.02 Å shorter than for the complex with n' = 0; it comes closer to the experimental value, 1.80(2) Å,[131] but is still somewhat larger. Accordingly, the uranyl stretching frequency (777 cm^{-1}) is also improved, but calculated too small by 36 cm^{-1}. The stronger uranyl bonds are accompanied by weaker equatorial bonds as reflected by elongated distances U-O_{C1} (2.41 Å), U-O_{C2} (4.12 Å); these bonds are 0.02 Å and 0.01 Å, respectively, longer than in the model with n' = 0. The U-C distance is not affected (2.86 Å).

The two sets of hydrogen bonds are more similar to each other than in the GP models; this can be seen from the fact that the O_{C2}···H and O_{C1}···H distances are comparable (both 1.77 Å) and the corresponding angles O_C···H-O are very similar, 147 and 144°, respectively (Table 4.12). According to a Mulliken population analysis, the screening has rendered the charges of the two carbonate oxygen centers O_{C2} and O_{C1} quite similar in solution (-0.50 e and -0.48 e, respectively), in contrast to the GP results, -0.46 e and -0.56 e, respectively. In agreement with an average binding energy of 24 kJ mol^{-1}, these data indicate typical moderate hydrogen bonds also in solution.[235] As expected, this binding energy is significantly smaller than that of direct uranium aqua bonds from the first hydration shell in $[UO_2(H_2O)_5]^{2+}$ (104 kJ mol^{-1}) and in $[UO_2CO_3(H_2O)_3]$ (66 kJ mol^{-1}).

Overall, agreement to experiment is improved compared to n' = 0 but with deviations of up to 0.04 Å for distances and about 4%, i.e. 36 cm^{-1}, for the stretching frequency slightly worse than in the corresponding GP calculations for n' = 6 and n' = 12.

Comparison of GP and PCM results may indicate an overestimation of bulk solvent effects in the PCM model when one has to deal with highly charged anionic species like $[UO_2(CO_3)_3]^{4-}$ (see also $[(UO_2)_3(CO_3)_6]^{6-}$ below). This is reflected in the distinct reduction of all equatorial distances by 0.03 to 0.09 Å compared to GP data when the PCM approach is applied to complexes with either n' = 0 and n' = 6. PCM effects are distinctly smaller for neutral or less strongly charged species like $[UO_2(CO_3)]$ and $[UO_2(CO_3)_2]^{2-}$ where bond distance change by 0.01 to 0.05 Å (Table 4.9).

One reason for this overestimation could be related to electronic density outside the cavity that is neglected in the COSMO model. However, as discussed above (Section

3.2.2), the density outside the cavity is screened to a large extent in the COSMO approach. [210,214] In contrast to other PCM variants, volume polarization affects the free energies of solvation only to a minor extent when the COSMO approach is applied.[210, 214] Thus, one expects also only small effects on structures. To investigate this aspect in more detail, the cavity around the solute was expanded to account for more diffuse electronic charge by increasing the radii of the atomic spheres. For this purpose, the default scaling factor (*s*) of the van der Waals radii (1.2, see Section 3.2.2) was increased to 1.3 (~10%) and 1.5 (25%). Table 4.13 compares results for $[UO_2(CO_3)_3]^{4-}\cdot(H_2O)_{n'}$ (n' = 0, 6).

As expected for the COSMO method, differences between calculations for the various scaling factors are minor both for n' = 0 and n' = 6 (Table 4.13). For s = 1.5 changes in bond distances range from 0.002 to 0.008 Å with respect to the default value s = 1.2. The equatorial distances U-O_{C1}, U-O_{C2}, and U-C elongate concomitantly with the increasing scaling factor; this brings the computational results closer to the experimental data. However, the rather small changes (< 0.01 Å) can not significantly reduce the absolute deviations from experiment that range from about 0.03–0.05 Å for n' = 0 and 0.02–0.03 Å for n' = 6. Therefore, the electronic charge density outside the cavity does not seem to be the main reason for the overestimation of long-range solvent effects. This problem for highly charged anionic species, also diagnosed below for $[(UO_2)_3(CO_3)_6]^{6-}$, warrants further study.

Table 4.13. Calculated structural parameters (distances in Å) of the uranyl tris(carbonato) complex $[UO_2(CO_3)_3]^{4-}\cdot(H_2O)_{n'}$. Additional water molecules (n') from the second coordination shell are included to simulate hydrogen bonds to the carbonate ligands (Fig. 4.9b). Results from solvation (PCM) calculations with different scaling factors (s) for the atomic van der Waals radii are compared with experimental EXAFS data for aqueous solution. For the designations of atoms, see Fig. 4.7.

n'	s	U=O_t	U-O_{C1}	U-O_{C2}	U-C	C-O_{C1}	C-O_{C2}
0	1.2	1.843	2.396	4.107	2.856	1.307	1.250
	1.3	1.845	2.399	4.112	2.858	1.307	1.253
	1.5	1.845	2.404	4.120	2.864	1.306	1.256
6	1.2	1.819	2.405	4.118	2.856	1.302	1.262
	1.3	1.817	2.409	4.124	2.860	1.301	1.264
	1.5	1.816	2.412	4.127	2.861	1.300	1.266
Exp.	Sol.[a]	1.80	2.44	4.20	2.89	–	–
	Sol.[b]	1.80(2)	2.43(2)	4.13(4)	2.89(4)	–	–

[a] Ref. 132. [b] Ref. 131.

In summary, the mononuclear complexes $[UO_2(CO_3)_m]^{2-2m}$ (m = 1–3) are characterized by the strong bis(chelating) coordination of carbonate ligands. Additional aqua ligands in the first hydration shell act as relatively strong ligands. Agreement with experimental data for aqueous solution is distinctly improved for $[UO_2(CO_3)_3]^{4-}$ if one includes additional water molecules from the second coordination in the model. Based on structural and energetic arguments, the corresponding hydrogen bonds can be characterized as moderately strong. Comparison of GP and PCM results reveals that long-range solvent effects are overestimated in the PCM model when one deals with highly charged anionic species. This conclusion is based on distinct reductions of all equatorial distances when the PCM approach is applied. Therefore, best agreement with experiment is obtained for GP models with additional water molecules. For $[UO_2(CO_3)_3]^{4-}$ the deviation for the uranyl bond U=O_t is less than 0.01 Å, the uranyl stretching frequency deviates by about 2%, i.e. 16 cm^{-1}. Equatorial bond distances are calculated slightly too short by 0.01 Å to 0.03 Å, but almost within the experimental error bars.

4.3.2 The triuranyl hexa(carbonato) complex, $[(UO_2)_3(CO_3)_6]^{6-}$

Next to the tris(carbonato) complex $[UO_2(CO_3)_3]^{4-}$ the most prominent carbonate species of this type is the triuranyl hexa(carbonato) complex $[(UO_2)_3(CO_3)_6]^{6-}$. This anion represents a challenge to the computational method applied due to its size and number of electrons.

To reduce the computational effort, the trimeric complex $[(UO_2)_3(CO_3)_6]^{6-}$ was calculated in D_{3h} symmetry, in line with the experimental crystal structure.[12] It comprises three bis(chelating) carbonates which occupy terminal positions while the remaining three ligands in central positions belong to a rare type of μ_3-bridging carbonates (Fig. 4.10a).[129,134] As before, additional water molecules (n') from the second coordination shell were considered to account for hydrogen bonds to the carbonate ligands in the extended models $[UO_2)_3(CO_3)_6]^{6-}\cdot(H_2O)_{n'}$ (n' = 6, 9; Fig. 4.10bc).

Structure of the triuranyl hexa(carbonato) complex $[(UO_2)_3(CO_3)_6]^{6-}$

Averaged GP and PCM results for the bare complex (n' = 0) are given in Table 4.14, the optimized structure is displayed in Fig. 4.10a. Compared to EXAFS data from solution[129] both GP and PCM results for n' = 0 overestimate the experimental value, 1.79 Å, of the uranyl bond U=O_t, calculated at 1.81 Å and 1.82 Å, respectively.[129] This trend is similar but less pronounced than the one found for $[UO_2(CO_3)_3]^{4-}$. The experimental uranyl stretching frequency is underestimated by 38 cm^{-1} and 44 cm^{-1}, respectively.

Table 4.14. Calculated averaged structural parameters (distances in Å) and symmetric uranyl stretching frequency (ν_s, in cm^{-1}) of the triuranyl hexa(carbonato) complex $[(UO_2)_3(CO_3)_6]^{6-}\cdot(H_2O)_{n'}$. Additional water molecules (n') from the second coordination shell are included to simulate hydrogen bonds to the carbonate ligands (Figs. 4.10 b,c). Results from calculations on gas phase (GP) and solvation (PCM) models are compared with experimental EXAFS data for aqueous solution and results from another study of GP models (Calc., see text for details). For the designations of atoms, see Fig. 4.7.

	n'	U=O_t	U-O_{C1}	U-O_{C2}	U-C	U-U	ν_s
GP	0	1.813	2.476	4.173	2.906	5.094	794
	6	1.802	2.470	4.181	2.888	4.993	818
	9	1.797	2.471	4.159	2.875	5.030	827
Calc.[a]	0	1.811	2.475	4.155	2.904	5.104	798
Calc.[b]	0	1.796	2.454	4.125	2.894	4.937	832
PCM	0	1.818	2.415	4.087	2.847	4.930	788
	6	1.808	2.418	4.103	2.841	4.895	804
	9	1.804	2.422	4.083	2.824	4.925	811
Exp. Sol.[c]		1.79	2.46	4.17	2.90	4.92	831.6

[a] Ref. 67. [b] Ref. 67, more diffuse basis set. [c] Ref. 129.

One should note that only average equatorial distances could be determined for U-O_{C1} and U-C from the EXAFS data. In the GP model the individual U-O_{C1} and U-C distances to the bridging and terminal carbonates differ by up to 0.1 Å and 0.04 Å, respectively (see Fig. 4.12). These differences are discussed in more detail in a comparison between the triuranyl hexa(carbonato) and the uranyl tris(carbonato) complex below. The average equatorial distances U-O_{C1}, U-O_{C2}, and U-C agree well with experimental data; the largest deviation is found for U-O_{C1}, 0.016 Å. The distance U-U (5.09 Å) is distinctly longer, by 0.17 Å, than the EXAFS result for complexes in solution, indicating strong electrostatic repulsion between the three uranyl moieties. Applying the PCM model has a distinct effect on all equatorial distances and leads to a shortening of U-O_{C1}, U-O_{C2}, and U-C by 0.06 Å, 0.08 Å, and 0.06 Å, respectively. Therefore experimental values are distinctly underestimated by 0.05 to 0.08 Å. Note that the shorter distance U-U (4.93 Å) matches the experimental result (4.92 Å) very well. This shortening of the equatorial distances can be rationalized by a weakened repulsion between the uranyl units due to screening effects in the PCM model.

The DF-SWVN study by Dixon et al. discussed for $[UO_2(CO_3)_3]^{4-}$ provided also results on GP models for $[(UO_2)_3(CO_3)_6]^{6-}$ (Table 4.14).[67] Results obtained with their default U basis set (see above) agree well with those of this work, bonding distances differ by 0.001–0.002 Å, non-bonding distances by 0.002–0.018 Å, and the uranyl stretching frequency by 4 cm^{-1}. The results of Ref. 67 show significant effects on the structures due to inclusion of diffuse functions in the U basis (Table 4.14). Differences between calculations with the default and the more diffuse U basis set range from 0.01–0.02 Å for bond distances U=O_t and C-O and become more pronounced for individual U-O_{C1} distances and the non-bonding distances U-O_{C2} and U-C with 0.05 to 0.08 Å. The U-U distance is distinctly reduced by 0.17 Å. In the light of these results, the influence of diffuse function was also examined in the present work on the GP model of $[(UO_2)_3(CO_3)_6]^{6-}$ by applying a more diffuse U basis set (see discussion of $[UO_2(CO_3)_3]^{4-}$ for details). Differences to calculations with the standard U basis set, 0.001–0.008 Å for all distances, are smaller than those obtained by Dixon et al. (see above). The pronounced effects on the complex structure because of the inclusion of diffuse functions found by Dixon et al. are not reproduced with the basis sets applied here. A further extension of the uranium basis sets is needed to investigate this aspect in more detail.

The more diffuse basis functions lead to a shortening of all equatorial distances in the GP models (Table 4.14). Thus, the underestimation of these distances with respect to the EXAFS data (by 0.05–0.08 Å) found in the PCM models might become even larger when employing a more diffuse basis. Overall, the results of the present work clearly indicate the importance of diffuse basis functions for describing the electronic charge density of highly anionic uranyl species such as $[UO_2(CO_3)_3]^{4-}$ and $[(UO_2)_3(CO_3)_6]^{6-}$.

Following the insight gained from the preceding discussion of $[UO_2(CO_3)_3]^{4-}$, additional water molecules from the second coordination shell are considered to form extended models $[UO_2)_3(CO_3)_6]^{6-}\cdot(H_2O)_{n'}$. The six water molecules of the model with n' = 6 are located next to the three terminal carbonate ligands in the equatorial plane, in analogy to the model $[UO_2(CO_3)_3]^{4-}\cdot(H_2O)_6$ (Fig. 4.10b). The resulting sets of hydrogen bonds are designated by $O_{C1}\cdots$H-O_w and $O_{C2}\cdots$H-O_w (see Fig. 4.7 for designations). For n' = 9, three water molecules are placed in addition next to the three bridging carbonate ligands, resulting in a third set of hydrogen bonds designated by $O_{C3}\cdots$H-O_w (Fig. 4.10c). The corresponding GP and PCM results are given in Table 4.14; the optimized structures for n' = 6 and n' = 9 are displayed in Figs. 4.10 b and c, respectively.

GP results for n' = 6 and n' = 9 are noticeably improved compared to results for the bare complex (n' = 0). The uranyl bond U=O_t (1.80 Å) is shortened by 0.01 Å and now is in good agreement with the experimental value (1.79 Å).[129] Accordingly, the deviation of

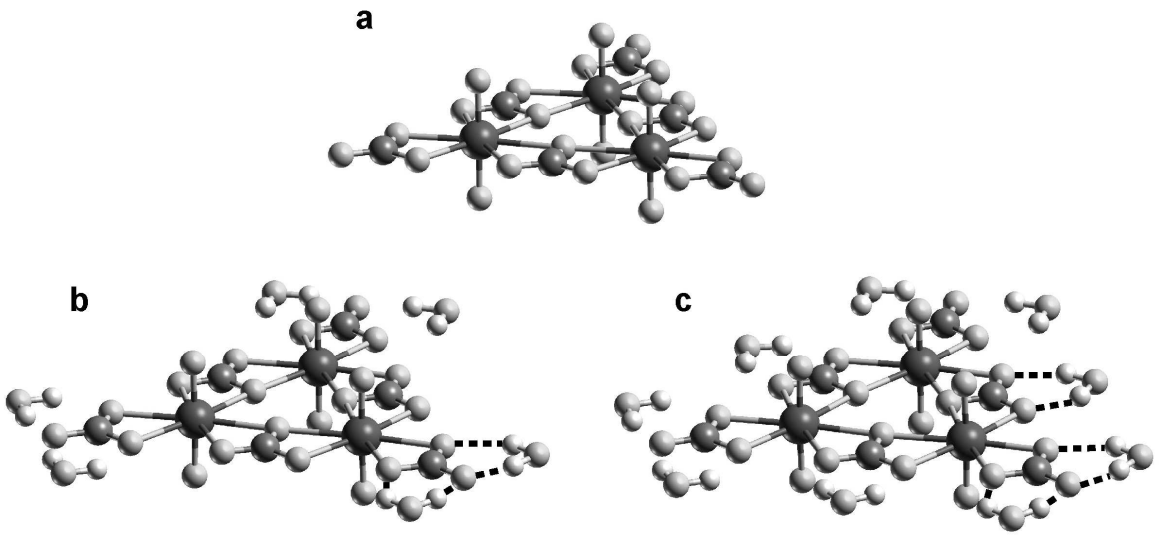

Figure 4.10. Optimized structures from PCM calculations of the triuranyl hexa(carbonato) complex $[UO_2)_3(CO_3)_6]^{6-}\cdot(H_2O)_{n'}$: bare ($n'$ = 0) complex (a) and models with n' = 6 (b) and n' = 9 (c) additional water molecules from the second coordination shell to simulate hydrogen bonds (dashed lines) to the carbonate ligands.

the uranyl stretching frequency (exp. 818 cm^{-1}) is decreased to 14 cm^{-1} (n' = 6) and 5 cm^{-1} (n' = 9), respectively. Equatorial distances are only slightly changed, by at most 0.01 Å, and now agree very well with experiment; deviations are less than ±0.01 Å both for n' = 6 and n' = 9. The distance U-U, 4.99 Å for n' = 6 and 5.03 Å for n' = 9, is reduced compared to the complex with n' = 0, but still larger than the experimental value (4.92 Å). The differences between models with n' = 6 and n' = 9 (bond distances differ less than 0.02 Å, stretching frequency differs by 9 cm^{-1}) indicate small but notable effects due to the three additional hydrogen bonds at the bridging carbonates.

The geometries of the hydrogen bonds from the water molecules to each terminal carbonate ligand (see Figs. 4.10 b,c; Table 4.15) are comparable to those of the previously discussed tris(carbonato) complex (Table 4.12). These hydrogen bonds are characterized by distances $O_{C2}\cdots H$ and $O_{C1}\cdots H$ of 1.63/1.64 Å and 2.03/2.11 Å for n' = 6/9; the corresponding angles $O_C\cdots H\text{-}O_w$ are 160°/161° and 134°/131°. The third set of hydrogen bonds to the bridging carbonate ligands in the model with n' = 9 exhibits distances $O_{C3}\cdots H$ of 1.86 Å and angles of 145°, falling in between the results obtained for the other two sets. Overall, these data indicate moderately strong hydrogen bonds,[235] as found previously for $[UO_2(CO_3)_3]^{4-}$. The calculated average binding energies in the gas phase models, 138/123 kJ mol^{-1} for n' = 6/9, are only slightly smaller than the results for the corresponding tris(carbonato) complex (142 kJ mol^{-1}, n' = 6). As expected, the hydrogen bonds elongate

Table 4.15. Bond distances (in Å), angles (in degree), and average binding energies per aqua ligand (BE, in kJ mol^{-1}) of hydrogen bonds in models $[(UO_2)_3(CO_3)_6]^{6-}\cdot(H_2O)_{n'}$ (n' = 6, 9) from gas phase (GP) and solvation (PCM) calculations; also shown are typical values for hydrogen bonds of various strengths. For the designations of atoms, see Fig. 4.7 and text.

		GP			PCM		
n'		X···H	X···H-Y	BE	X···H	X···H-Y	BE
6	$O_{C2}\cdots H\text{-}O_w$	1.63	160	138	1.69	156	19
	$O_{C1}\cdots H\text{-}O_w$	2.03	134		1.95	133	
9	$O_{C2}\cdots H\text{-}O_w$	1.64	161	123	1.68	157	15
	$O_{C1}\cdots H\text{-}O_w$	2.11	131		2.00	130	
	$O_{C3}\cdots H\text{-}O_w$	1.86	145		1.84	143	
Exp.[a]	strong	1.2–1.5	175–180	–	1.2–1.5	175–180	60–170
	moderate	1.5–2.2	130–180	–	1.5–2.2	130–180	20–70
	weak	2.2–3.2	90–180	–	2.2–3.2	90–180	< 20

[a] Ref. 235, typical values of hydrogen bonds from various compounds.

the $C\text{-}O_{C2}$ distances of the terminal carbonate ligands, by ~0.02 Å, and shorten the second $C\text{-}O_{C1}$ bond, by ~0.02 Å. Thus, the $U\text{-}O_{C1}$ bonds, elongated by ~0.05 Å, are notable weakened and the uranyl bonds $U{=}O_t$, ~0.01 Å shorter, are somewhat stronger.

Employing the PCM model for n' = 6 and n' = 9 also improves results with respect to experiment compared to the calculations on the bare complex (n' = 0, Table 4.14). The shortened uranyl bond $U{=}O_t$ (1.81/1.80 Å for n' = 6 and 9, respectively) is in reasonable agreement with the experimental value (1.79 Å), the stretching frequency (804/811 cm^{-1}) is too small by 28/21 cm^{-1}. As the uranyl bonds become stronger, the equatorial distances $U\text{-}O_{C1}$ (2.42/2.42 Å) and $U\text{-}O_{C2}$ (4.10/4.08 Å) elongate. However, this effect only slightly reduces the distinct underestimation obtained for n' = 0, to ~0.04–0.09 Å. The elongation of the $U\text{-}O_C$ distances is reflected in shorter U-U distances (4.90/4.93 Å) that agree well with the experimental value (4.92 Å).

In contrast to the tris(carbonato) complex, hydrogen bonds in the PCM model are similar to those of the GP model with distances $O_{C2}\cdots H$ of 1.69/1.68 Å and $O_{C1}\cdots H$ of 1.95/2.00 Å for n' = 6/9; the corresponding angles $O_C\cdots H\text{-}O_w$ are 156°/157° and 133°/130°, respectively (Table 4.15). Data for the third set of hydrogen bonds $O_{C3}\cdots H\text{-}O_w$ in the model with n' = 9 also fall in between the values of the other two sets, with distances $O_{C2}\cdots H$ of 1.84 Å and angles of 143°. The binding energies, 19/15 kJ mol^{-1}, are somewhat

smaller than in the corresponding tris(carbonato) complex (24 kJ mol^{-1}, n' = 6). Based on these distances, angles, and binding energies, the hydrogen bonds in solution can also be classified as moderately strong.[235]

Overall, agreement with experiment is improved when additional water molecules are included both in GP and PCM models. As for $[UO_2(CO_3)_3]^{4-}$ best agreement with experimental data is found for the extended GP model (n' = 9); deviations are less than 0.01 Å for all distances (except U-U: 0.1 Å) and 5 cm^{-1}, i.e. less than 1%, for the uranyl stretching frequency. The corresponding PCM calculation (n' = 9) yields satisfactory results for the uranyl bond length (too long by 0.01 Å) and the corresponding symmetric stretching frequency (21 cm^{-1}), but distinctly underestimates the equatorial distances, by 0.04 to 0.09 Å. Therefore, as already discussed for the tris(carbonato) complex, these results also indicate an overestimation of long-range solvent effects in the PCM model as one has to deal with a highly charged anionic species (charge here: –6 e). This strong effect is noticeable in the distinct reduction of 0.05–0.09 Å compared to the GP model for all equatorial distances when the PCM approach is applied to the model complexes with n' = 0, 6, and 9.

Comparison of the uranyl tris(carbonato) and the triuranyl hexa(carbonato) complexes

The existence of the trimeric species $[(UO_2)_3(CO_3)_6]^{6-}$ is confirmed by crystal structures and has also been reported in solutions of high ionic strength.[125,134,139,140] The predominant presence of the trimer has been suggested for the pH range from ~4–6.5 provided that the ratio between the total U(VI) and total carbonate concentrations is significantly smaller than 1 (see Fig. 4.11).[134] However, some studies indicate that at lower ionic strength this species does not form and the tris(carbonato) species $[UO_2(CO_3)_3]^{4-}$ is the dominant species over a wide pH range (pH > 7).[136,137] To address this question, the following discussion will focus on a detailed comparison between the two species, involving also energy aspects.

The trimeric complex can be considered as a "superposition" of three $[UO_2(CO_3)_3]^{4-}$ moieties. The three central carbonate ligands are shared between the three uranyl units while the remaining three carbonate ligands exhibit the same terminal coordination as in the tris(carbonato) complex (Fig. 4.12).

For the structural comparison the focus will be on GP and PCM results as calculated for the bare complexes, without considering additional water ligands (n' = 0, Fig. 4.12). Effects of hydrogen bonds are discussed above and do not change the observed trends essentially. The structures of the two kinds of carbonates in the trimeric complex differ noticeably. In the GP structures the terminal carbonates of $[(UO_2)_3(CO_3)_6]^{6-}$ are similar to

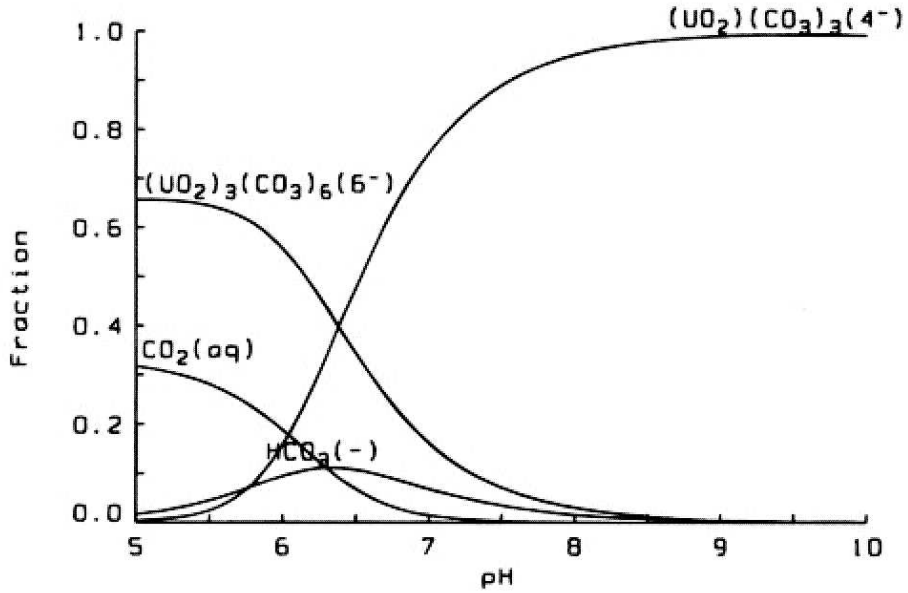

Figure 4.11. Speciation diagram (taken from Ref. 134) for the U(VI)-carbonate system as a function of pH; $[UO_2^{2+}]_{tot}$ = 100.00 mM, $[CO_3^{2-}]_{tot}$ = 300.00 mM.

the ligands of $[UO_2(CO_3)_3]^{4-}$. The C-O_{C2} bond is as expected shorter than the C-O_{C1} distances, by 0.03 Å. In contrast to the terminal ligands, the bridging carbonate groups exhibit no free O_{C2} center, but a μ_3-coordinated bridging O_{C1} center between two uranyl moieties (Fig. 4.12). The corresponding C-O_{C1} distance is slightly longer, by 0.02 Å, than the other two C-O_{C1} distances to regular μ_2-coordinated O_{C1} centers. The μ_3-coordination is also reflected in the distinctly longer distance U-O_{C1} (2.55 Å) to the central bridging carbonates (Fig. 4.12). The second U-O_{C1} distance (2.46 Å) is similar to the one in the complex $[UO_2(CO_3)_3]^{4-}$. Overall, these points to a weaker bonding of the bridging carbonates. This conclusion is corroborated by shorter, i.e. stronger, U-O_{C1} bonds (2.42 Å) to the terminal carbonate groups in $[(UO_2)_3(CO_3)_6]^{6-}$.

The structural trends discussed for the gas phase are also found in the corresponding PCM models (Fig. 4.12). The distances C-O_{C2} and C-O_{C1} of terminal carbonates differ by about 0.06 Å; this difference is more pronounced than in the GP model (0.03 Å). All U-O_{C1} bonds of the PCM model are significantly shorter, by 0.03–0.08 Å. The terminal carbonates of $[(UO_2)_3(CO_3)_6]^{6-}$ are also stronger bound than the bridging ones, as indicated by U-O_{C1} distances of 2.34 Å (terminal) as well as 2.44 Å and 2.47 Å (μ_3).

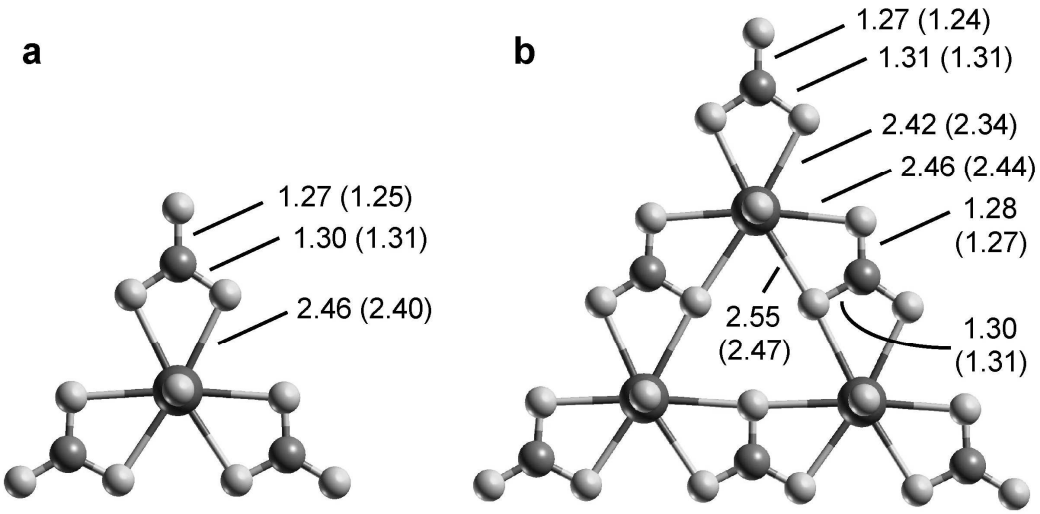

Figure 4.12. Comparison of uranyl carbonate complexes $[UO_2(CO_3)_3]^{4-}$ (a) and $[(UO_2)_3(CO_3)_6]^{6-}$ (b). Characteristic distances (in Å) from gas phase (GP) and solvation calculations (PCM, in parenthesis).

The longer U-O_{C1} bonds to the bridging carbonates, found both in GP and PCM models, can be interpreted as an effectively lower coordination of the uranyl moieties in the trimeric complex compared to $[UO_2(CO_3)_3]^{4-}$. In line with the shorter U=O_t distances, this finding points to a lower stability of the trimer. To examine this aspect, the stability of the trimer is considered according to the following model reactions:

$$3\,[UO_2(CO_3)_3]^{4-} \rightarrow [(UO_2)_3(CO_3)_6]^{6-} + 3\,[CO_3]^{2-} \quad (4.6)$$

$$3\,[UO_2(CO_3)_3]^{4-} + 3\,[H_3O]^{+} \rightarrow [(UO_2)_3(CO_3)_6]^{6-} + 3\,[HCO_3]^{-} + 3\,H_2O \quad (4.7)$$

According to speciation calculations,[134] the tris(carbonato) complex $[UO_2(CO_3)_3]^{4-}$ is dominant at basic pH > 7, while the trimeric complex $[(UO_2)_3(CO_3)_6]^{6-}$ occurs at slightly acidic pH < 6.5 (see Fig. 4.12). The transition between both complexes appears at almost neutral pH 6–7 (see Fig. 4.12). Thus, model reactions were chosen for basic and acidic pH regimes. Both reactions model the formation of the trimer complex from three $[UO_2(CO_3)_3]^{4-}$ moieties. Eq. (4.6) is most appropriate for a strongly basic pH environment Carbonate ions are the dominant species in the carbon dioxide equilibrium, $CO_2/H_2CO_3 \leftrightharpoons [HCO_3]^- \leftrightharpoons [CO_3]^{2-}$, under such conditions (pH > 10.5). In contrast, Eq. (4.7) models acidic to neutral pH conditions. Here, one expects the presence of $[H_3O]^+$ and $[HCO_3]^-$ rather than $[CO_3]^{2-}$.

Before entering into a detailed discussion of the formation reactions, Eqs. (4.6) and (4.7), one should briefly address the accuracy of the PCM approach for small molecules such as H_2O, $[H_3O]^+$, $[HCO_3]^-$, and $[CO_3]^{2-}$ involved in the model reactions. The availability of experimental solvation free energies and pK_a values allows one to evaluate computational models that are used to simulate solvent effects. As an error of only 5.7 kJ mol^{-1} in the value of the free solvation energy produces an error of 1 pK_a unit, the corresponding theoretical calculations need to be performed at a high level of theory. Previous work mainly focused on the calculation of neutral species or singly charged ions. Solvation energies of H_2O, $[H_3O]^+$, NH_3, or $[OH]^-$ can be determined in good agreement with experiment based on DF calculations employing a PCM approach (see Section 3.2.2).[43] pK_a calculations based on Complete Basis Set Methods[245] combined with PCM continuum models have reached almost chemical accuracy for small simple organic compounds such as carboxylic acids or substituted phenols.[246–248] These studies indicate that solvated phase optimized structures of the anions are essential for obtaining such an accuracy.[247] The inclusion of water molecules to simulate hydrogen-bonds to the anions improves the results.[248] For small highly charged anions the effect of long-range electrostatic interactions is significant. A recent study suggested that for systems such as $[CO_3]^{2-}$, $[HCO_3]^-$, or acetate Monte Carlo simulations combined with QM/MM potentials give reliable pK_a values while PCM based methods yield satisfactory results only in individual cases.[249] The subsequent discussion does not aim at the calculation of solvation energies, but intends to provide qualitative energetic trends between $[UO_2(CO_3)_3]^{4-}$ and $[(UO_2)_3(CO_3)_6]^{6-}$ based on the model reactions suggested. Thus, one may expect that the accuracy of the DF-PCM method applied is sufficient for that purpose.

Under basic conditions, the trimeric species is stable as reflected by a slightly negative reaction energy of -45 kJ mol^{-1} obtained from Eq. (4.6) when applied to the GP model. This small reaction energy indicates that the reaction is electrostatically rather well balanced. The exothermicity might result from a more pronounced charge distribution over four instead of three species at the right-hand side of Eq. (4.6). However, the formation of the trimer becomes endothermic, by 338 kJ mol^{-1}, when the PCM model is applied. On the one hand, screening of the charges reduces the electrostatic repulsion, on the other hand, in solution the three educts $[UO_2(CO_3)_3]^{4-}$ are slightly more stabilized [3x(-2622) = 7866 kJ mol^{-1}] than the four products $[(UO_2)_3(CO_3)_6]^{6-}$ and $[CO_3]^{2-}$ [-4306 + 3x(-1059) = 7483 kJ mol^{-1}], see Table 4.16. Thus, the educt side of Eq. (4.6) is favored by 383 kJ mol^{-1} which results in an overall endothermic reaction energy. The size of the stabilization energies (Table 4.16) follows the charge of the species.

Table 4.16. Stabilization energies E_s (in kJ mol^{-1}) for uranyl(VI) carbonate complexes and molecules considered in Eqs. (4.6) to (4.10) calculated as the difference between total energies from GP and PCM calculations. *n*' represents the number of water molecules out of the hydration shell that are explicitly accounted for in the model complexes.

	n'	E_s
$[UO_2(CO_3)_3]^{4-}$	0	-2622
	6	-2086
$[(UO_2)_3(CO_3)_6]^{6-}$	0	-4306
	9	-3584
$[CO_3]^{2-}$	0	-1059
	3	-776
$[HCO_3]^-$	0	-281
	3	-219
$[H_3O]^+$	0	-386
	1	-303
H_2O	0	-29
	1	-48

Based on Eq. (4.7), the formation of the trimer is strongly exothermic under acidic to neutral conditions. The large reaction energy in the gas phase, -4263 kJ mol^{-1}, results from changed pH conditions. At acidic pH one expects the formation of $[HCO_3]^-$ according to

$$[CO_3]^{2-} + [H_3O]^+ \rightarrow [HCO_3]^- + H_2O \qquad (4.8)$$

This reaction is strongly exothermic in the gas phase (-1406 kJ mol^{-1}) because differently charged educts are combined. This reactions energy is reduced to -270 kJ mol^{-1} due to the stabilization of the ions in the PCM approach (Table 4.16), especially the reactants $[CO_3]^{2-}$ (-1059 kJ mol^{-1}) and $[H_3O]^+$ (-386 kJ mol^{-1}). This stabilization also compensates the endothermic reaction energy of Eq. (4.6). Thus, in contrast to basic pH conditions, Eq. (4.6), the formation of the trimer complex becomes exothermic when the PCM model is employed, by -473 kJ mol^{-1} based on Eq. (4.7).

From the previous structural discussion it is obvious that short-range solvation effects due to water molecules from the second solvation shell might be important for the stability of uranyl carbonate complexes. To improve the model reactions, such short-range effects are included by taking into account hydrogen bonds via explicit water molecules

based on the extended models $[UO_2(CO_3)_3]^{4-}\cdot(H_2O)_6$ and $[(UO_2)_3(CO_3)_6]^{6-}\cdot(H_2O)_9$. For a more balanced description, hydrogen bonds to oxygen centers of all species involved in the model reactions are considered, i.e. three additional water molecules for $[CO_3]^{2-}$ and $[HCO_3]^-$ and one for $[H_3O]^+$ and H_2O, respectively.

$$3\,[UO_2(CO_3)_3]^{4-}\cdot(H_2O)_6 \rightarrow [(UO_2)_3(CO_3)_6]^{6-}\cdot(H_2O)_9 + 3\,[CO_3]^{2-}\cdot(H_2O)_3 \quad (4.9)$$

$$3\,[UO_2(CO_3)_3]^{4-}\cdot(H_2O)_6 + 3\,[H_3O]^+\cdot(H_2O) \rightarrow [(UO_2)_3(CO_3)_6]^{6-}\cdot(H_2O)_9 + 3\,[HCO_3]^-\cdot(H_2O)_3 + 3\,H_2O\cdot(H_2O) \quad (4.10)$$

The discussed trends of the model reactions without additional water molecules, Eqs. (4.6) and (4.7), are not changed, for neither the GP nor the PCM model. The formation reactions according to Eq. (4.9), -189 kJ mol^{-1}, as well as Eq. (4.10), -2919 kJ mol^{-1} are exothermic in the gas phase. Application of the PCM model results in an endothermic reaction (157 kJ mol^{-1}) under basic conditions, Eq. (4.9), and an exothermic reaction (-139 kJ mol^{-1}) in an acidic to neutral environment, Eq. (4.10).

The difference in stabilization energies (Table 4.16) between complexes with coordinated water molecules and the corresponding bare complexes is significant for the large uranyl carbonate species, 536 kJ mol^{-1} for the complex $[UO_2(CO_3)_3]^{4-}\cdot(H_2O)_6$ and 722 kJ mol^{-1} for the higher charged complex $[(UO_2)_3(CO_3)_6]^{6-}\cdot(H_2O)_9$. As expected from the smaller size this difference is less pronounced for $[CO_3]^{2-}$ (283 kJ mol^{-1}), $[HCO_3]^-$ (62 kJ mol^{-1}), $[H_3O]^+$ (83 kJ mol^{-1}), and H_2O (19 kJ mol^{-1}).

In summary, a comparison between structural data for the tris(carbonato) complex and the triuranyl hexa(carbonato) indicates an effectively lower uranyl coordination of the uranyl moieties in $[(UO_2)_3(CO_3)_6]^{6-}$, where one relies on the rather long bridging U-O_C distances compared to those of $[UO_2(CO_3)_3]^{4-}$. Overall, the results of the model reactions agree with experimental findings, i.e. formation of the triuranyl hexa(carbonato) $[(UO_2)_3(CO_3)_6]^{6-}$ is preferred at acidic to neutral pH, whereas the tris(carbonato) complex $[UO_2(CO_3)_3]^{4-}$ is stable at basic pH. However, effects such as different ionic strengths or different concentrations of uranyl or carbonate can not be discussed based on simple model reactions, but may significantly affect the speciation equilibria as indicated by various experimental results.[125,134,139,140]

4.3.3 The dimeric uranyl hemicarbonate complex, $[(UO_2)_2(CO_3)(OH)_3]^-$

The previously discussed triuranyl hexa(carbonato) complex $[(UO_2)_3(CO_3)_6]^{6-}$ is structurally well characterized by x-ray diffraction and EXAFS data.[131] However, for other polynuclear species there are only limited experimental data available, e.g. for the dinuclear hemicarbonate species $[(UO_2)_2(CO_3)(OH)_3]^-$ that has been suggested in several studies.[83,84] The ternary hemicarbonate species is predominant in aqueous solution over a broad pH range (pH > 6), provided that the ratio between the total U(VI) and total carbonate concentrations is larger than 1 (see Fig. 4.13).[84] This corresponds either to aqueous solutions with a high uranium or with a rather low carbonate content.

The experimental characterization of these species is complicated by ligand exchange reactions which lead to equilibria of several isomers. The occurrence and distribution of different isomers were examined by EXAFS, ^{13}C and ^{17}O NMR spectroscopy.[84] NMR data provide structure and symmetry information as well as information about the rate of ligand exchange reactions. EXAFS gives superimposed structural information for the ensemble of different isomers present in solution.

From the stoichiometry of the complex and the known coordination geometry of the uranyl ion[40] it has been suggested[84] that the two uranyl moieties in $[(UO_2)_2(CO_3)(OH)_3]^-$ are linked by bridging carbonate and/or hydroxide groups and that the complex contains coordinated aqua ligands. Based on these assumptions Szabo et al. proposed four possible main isomers A to D (Fig. 4.14).[84] Isomer A is characterized by a central bridging

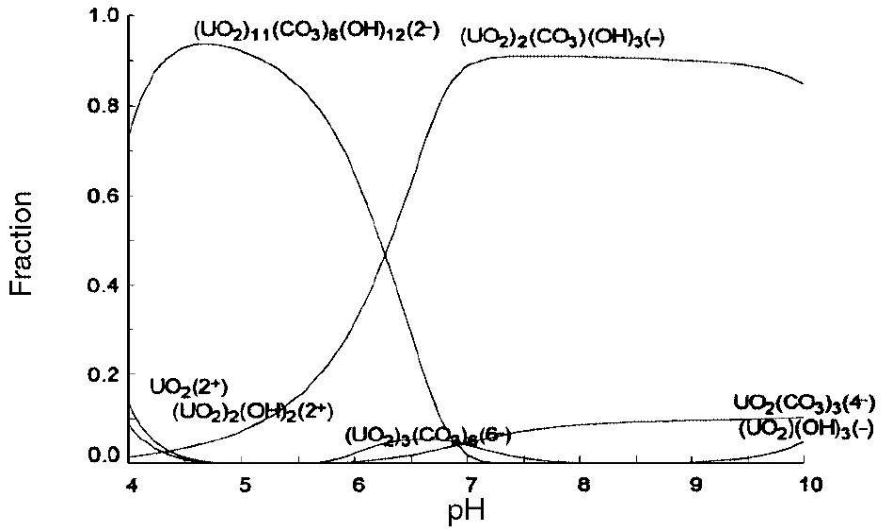

Figure 4.13. Speciation diagram (taken from Ref. 84) for the U(VI)-carbonate system as a function of pH; $[UO_2^{2+}]_{tot}$ = 20.00 mM, $[CO_3^{2-}]_{tot}$ = 15.00 mM.

carbonate group similar to those in the triuranyl hexa(carbonato) complex $[(UO_2)_3(CO_3)_6]^{6-}$ (see Section 4.3.2, Fig. 4.10a). One carbonate oxygen center connects the two uranyl moieties as a μ_3-bridge while the other two oxygen centers each show a typical μ_2-coordination to one of the uranyl units (Fig. 4.14). The remaining coordination sites of the uranyls are saturated by three η-coordinated hydroxo groups and three aqua ligands. Besides the structure of isomer A given in Fig. 4.14, additional isomers are possible due to a different arrangement of the non-bridging ligands, i.e. OH and H_2O. The model isomers chosen in Fig. 4.14 are those where the interaction between negative oxygen centers of the hydroxide and carbonate groups in the complex is minimized by shielding via adjacent aqua ligands. In contrast to isomer A, the carbonate group is not involved in the bridging of isomer B, but it acts as a typical bis(chelating) ligand as discussed for uranyl monocarbonates $[UO_2(CO_3)_m]^{2-2m}$ (see Section 4.3.1). Two μ_2-bridging OH groups link the two uranyl moieties. The central dimeric unit $[(UO_2)(\mu_2\text{-}OH_2)_2]^{2+}$ (Fig. 4.14) is well-known from dinuclear uranyl hydrolysis complexes such as $[(UO_2)_2(OH_2)_2(H_2O)_6]^{2+}$ or $[(UO_2)_2(OH_2)_2Cl_2(H_2O)_4]$ (see Sections 2.2.2 and 4.2). The pentagonal uranyl coordination is achieved by one additional η-coordinated OH and three aqua ligands. In isomer C both the carbonate and one hydroxo group are involved in the bridging. The OH group forms a μ_2-bridge as in isomer B, while one oxygen center of the carbonate group acts as a μ_3-bridge between the two uranyl moieties (Fig. 4.14). Two η-coordinated OH and three aqua ligands occupy further uranyl coordination sites. Finally, isomer D is the only species that exhibits only a single bridge between the two uranyl units via the terminal oxygen center

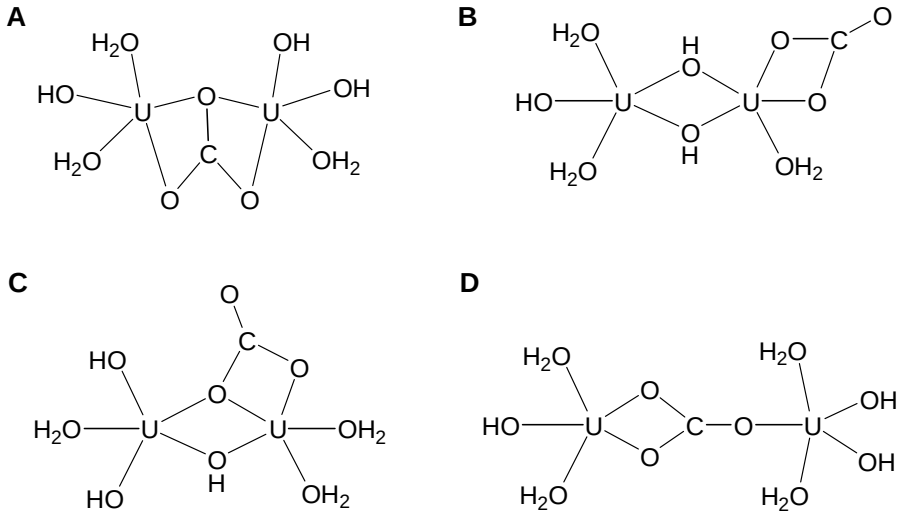

Figure 4.14. Suggested isomers A–D for the hemicarbonate complex $[(UO_2)_2(CO_3)(OH)_3]^-$. The axial uranyl oxygen centers are not shown in this top view. Adapted from Ref. 84.

of a bis(chelating) carbonate group (Fig. 4.14). Because of the single bridge one additional coordination site is available at the uranyls in isomer D. Thus, four instead of three aqua ligands are included in the model structure (Fig. 4.14). All three OH groups are η-coordinated.

X-ray diffraction and EXAFS data from complexes with comparable structural elements indicate that the isomers suggested should differ in their U-U distances. The U-U distance in isomer A should be comparable to ~4.9 Å reported[129] for $[(UO_2)_3(CO_3)_6]^{6-}$. A shorter U-U distance of ~3.9 Å has been determined experimentally[114,115] for dimeric complexes comprising the moiety $[(UO_2)(OH_2)_2]^{2+}$ and thus is expected for isomers B and C. The U-U distance for isomer D is estimated to be much larger, ~6.6 Å, based on the summation of distances from $[UO_2(CO_3)_3]^{4-}$ (U-C: ~2.9 Å; C-O: ~1.3 Å)[131,132] and $[UO_2(H_2O)_5]^{2+}$ (U-O_w: ~2.4 Å).[68,79]

The EXAFS data of $[(UO_2)_2(CO_3)(OH)_3]^-$ show an U-U distance of 3.90 Å.[84] However, a distinct U-U peak is absent that is typically observed in EXAFS spectra of solutions containing a single polynuclear species such as $[(UO_2)_3(CO_3)_6]^{6-}$, $[(UO_2)_2(OH)_2]^{2+}$, or $[(UO_2)_3(OH)_5]^+$. Thus, at least two isomers with slightly different U-U distances should be present in solution.[84] Based on the estimated U-U distance of ~6.6 Å, isomer D is ruled out to be present in the investigated solutions in significant concentration. In addition, the less efficient use of the carbonate binding capacity (see Fig. 4.14) makes isomer D energetically unfavorable. The EXAFS data yield pentagonal uranyl coordination based on equatorial coordination numbers, one terminal hydroxide group per uranium and additional aqua ligands. This leaves isomer C as most consistent with the EXAFS data.

The corresponding NMR data provide evidence that the isomers must be present in comparable amounts, i.e. their relative stability cannot differ much.[84] In addition, one expects that differences in the relative stabilities are larger for isomers with different kinds of bridges, i.e. A vs. B and C. Ligand interchange is mainly expected to result from the exchange of non-bridging ligands. Based on the NMR data, a distribution has been suggested comprising 80% of isomer C, 15% of isomer B, and 5% for isomer A.[84]

Models

The computational models for isomers A, B, and C were chosen according to the three main structures discussed above (Fig. 4.14), while isomer D was left out for reasons previously given. As discussed in Section 4.1, the explicit inclusion of aqua ligands is important for an accurate description of solvated uranyl species.[22,43,69] Therefore, three aqua ligands were added to saturate the equatorial uranyl coordination sites, yielding the

typical pentagonal uranyl coordination in line with the EXAFS data (Fig. 4.14).[84]

In a first pre-optimization step the three isomers A, B, and C were modeled applying C_s symmetry constraints, i.e. restricting O and C centers of the carbonate and aqua ligands to the equatorial uranyl plane (Fig. 4.14). In addition, the imposed C_s symmetry prevents out-of-plane bending of the OH groups. However, previous studies[65] on the dinuclear complex $[(UO_2)_2(OH)_2Cl_2(H_2O)_4]$ indicated a noticeable stabilization due to bending of the OH groups that becomes relevant for an energetic comparison of the three isomers. Thus, these restrictions were released employing C_1 models without any constraints.

Structures

Table 4.17 summarizes averaged structural parameters for the three isomers A–C based on DF-VWN optimizations for the C_s and C_1 models. Bulk solvent-effects were taken into account via a PCM approach. Optimized structures for the C_1 models are displayed in Fig. 4.15, while Fig. 4.16 shows selected distances of the three isomers. The uranium oxygen distances discussed are differentiated by the corresponding terminal (O_t), hydroxo (O_h), water (O_w), and carbonate (O_c) oxygen centers (Fig. 4.14). Oxygen centers that act as direct bridges between the two uranium centers are designated as O_b, both for bridging hydroxo and carbonate groups (Fig. 4.14). In addition, the average distance U-O_{eq} of all equatorial uranium oxygen distances is also given.

First, the two different symmetry constraints applied will be briefly addressed. Comparison of the results for C_s and C_1 models indicates rather small changes on averaged

Table 4.17. Averaged distances (in Å) for isomers A, B, and C (Fig. 4.14) of the dinuclear uranyl hemicarbonate complex $[(UO_2)_2(CO_3)(OH)_3]^-$ from PCM calculations obtained with different symmetry constraints (C_s, C_1) compared to EXAFS data from solution.

	Sym.	U=O_t	U-O_h	U-O_b	U-O_w	U-O_c	U-O_{eq}	U-C	U-U
A	C_s	1.819	2.148	2.413	2.441	2.488	2.36	2.874	4.796
B	C_s	1.820	2.113	2.317	2.454	2.329	2.34	2.792	3.877
C	C_s	1.822	2.171	2.337	2.415	2.439	2.32	2.857	3.984
A	C_1	1.815	2.170	2.407	2.441	2.499	2.36	2.880	4.779
B	C_1	1.817	2.156	2.323	2.473	2.325	2.35	2.787	3.781
C	C_1	1.822	2.167	2.337	2.425	2.461	2.32	2.875	4.010
Exp.[a]	Fit 1	1.80	2.26	2.47	2.47	2.47	2.43	2.89	–
	Fit 2	1.81	2.26	2.47	2.47	2.47	2.43	2.89	3.90

[a] Ref. 84.

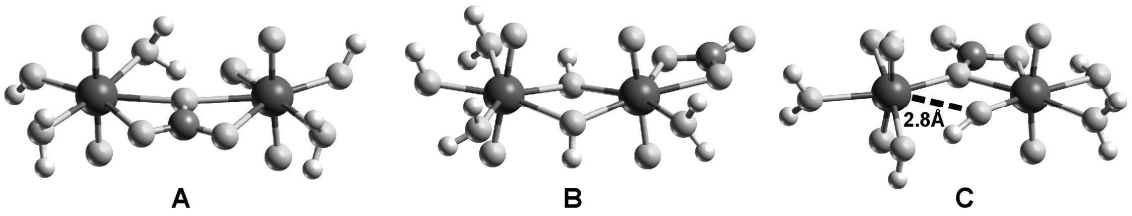

Figure 4.15. Optimized structures for isomers A, B, and C (C_1 models) of the dinuclear uranyl hemicarbonate complex $[(UO_2)_2(CO_3)(OH)_3]^-$ from PCM calculations.

distances (Table 4.17), i.e. less than 0.02 Å for all bond distances except U-O_h (up to 0.04 Å). The strong effect on the U-O_h distance can be rationalized by the bending of the OH groups in the C_1 models. The OH groups are mainly bent out of the equatorial plane (Fig. 4.15) with U-O-H angles ranging from 110° to 130°. In addition, the other ligands relax slightly out of the equatorial plane in the C_1 models. This is especially pronounced for isomer B where the central U-O_b-U-O_b moiety is noticeably twisted (dihedral angle of 15°) which results in a tilting of both actinyl units relative to each other (Fig. 4.15). The relaxations stabilize isomers A, B, and C by 26, 23, and 23 kJ mol^{-1}, respectively, with respect to total energies of the corresponding C_s structures. The subsequent discussion will focus on the more stable C_1 models.

Now characteristic features and differences of isomers A–C will be examined. Comparison of the computational data of the isomers yields similar results for isomers B and C (Table 4.17), in line with their similar composition (Fig. 4.14). Changes to isomer A, on the other hand, are more pronounced for the distances U-O_b, U-O_c, and U-U. This can be rationalized by the different type of bridging compared to isomers B and C.

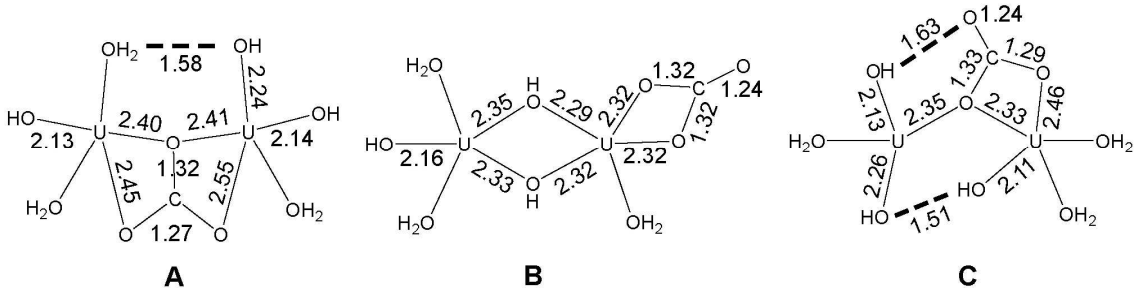

Figure 4.16. Selected distances (in Å) for isomers A, B, and C (C_1 models) of the dinuclear uranyl hemicarbonate complex $[(UO_2)_2(CO_3)(OH)_3]^-$ from PCM calculations. Dashed lines indicate internal hydrogen bonds. The terminal oxygen atoms of the uranyl units are not shown for clarity.

The nature of the bridging of isomer A is comparable to that of the trinuclear species $[(UO_2)_3(CO_3)_6]^{6-}$ (see Section 4.3.2). This is reflected in the rather long U-U distance of 4.8 Å which is similar to ~4.9 Å calculated for $[(UO_2)_3(CO_3)_6]^{6-}$ (see Section 4.3.2, Table 4.14). The bridging carbonate unit exhibits also C-O distances which are close (within 0.01 Å) to those of $[(UO_2)_3(CO_3)_6]^{6-}$ (Fig. 4.12). The two U-O_b bridges (~2.41 Å) are 0.06 Å shorter which indicates that the bridging between the uranyl moieties is stronger in $[(UO_2)_2(CO_3)(OH)_3]^-$. This conclusion is corroborated by the U-U distance which is ~0.1 Å shorter than in $[(UO_2)_3(CO_3)_6]^{6-}$ (see Table 4.14). This shortening reflects the absence of a third coordinating uranyl unit which causes steric strain in $[(UO_2)_3(CO_3)_6]^{6-}$. In addition, the two U-O_c distances, 2.45 and 2.55 Å (Fig. 4.16), are elongated compared to those of $[(UO_2)_3(CO_3)_6]^{6-}$ (2.44 Å). The relatively long distance of 2.55 Å can be rationalized by the competition with the two strong hydroxo ligands at the same uranium center (Fig. 4.16). Isomer A exhibits three η-OH ligands with rather short U-O_h distances of 2.13 Å, 2.14 Å, and 2.24 Å. The distance of 2.24 Å results from a weakening of the U-O_h bond due to the formation of an internal hydrogen bond to an adjacent aqua ligand of the other uranyl (Fig. 4.16). This hydrogen bond can be classified as moderately strong based on the O···H distance of 1.58 Å and the corresponding O···H-O_w angle of 144°.[235]

The calculated U-U distance of isomer B (3.8 Å) is significantly shorter than the value obtained for isomer A (~4.8 Å) and agrees well with the value of ~3.9 Å, calculated for the comparable dimeric uranyl complex $[(UO_2)(OH_2)_2(H_2O)_6]^{2+}$.[66] The four bridging bonds U-O_b of isomer B, ~2.32 Å on average, are 0.03 Å longer than those of $[(UO_2)(OH_2)_2(H_2O)_6]^{2+}$. This weakening of the bridging bonds can be rationalized by the presence of hydroxo and carbonate ligands in the hemicarbonate complex which are stronger bound than the aqua ligands of $[(UO_2)(OH_2)_2(H_2O)_6]^{2+}$. The bis(chelating) carbonate group of isomer B exhibits the same coordination as in the uranyl monocarbonates (see Section 4.3.1). The C-O distances of isomer B are almost identical (within 0.01 Å) to those of $[UO_2CO_3(H_2O)_3]$ (Table 4.9), while the U-O_c distances, 2.32 Å (Fig. 4.16), are slightly longer, by 0.03 Å, in the hemicarbonate complex. The latter elongation indicates that the bridging U-O_b bonds (~2.32 Å) are stronger than the U-O_w bonds (~2.40 Å) of $[UO_2CO_3(H_2O)_3]$. The shortest U-O distance of isomer B, 2.16 Å, is that to the single η-OH ligand (Fig. 4.16).

The U-U distance of isomer C (4.0 Å) is close to the one obtained for isomer B (3.8 Å) as expected from the structural similarity. Isomer C is suggested to exhibit bridging by one OH and one carbonate group (Fig. 4.14). However, the optimized structure shows one bridging U-O distance of 2.81 Å (Fig. 4.15) that is significantly longer than typical

U-O bonds (Table 4.17). Thus, in contrast to the assumed OH bridge between the two uranyls (Fig. 4.14) the actual structure is better described by a single U-O_h bond to the "right-hand" uranyl moiety (Fig. 4.16). This analysis is corroborated by the corresponding U-O_h distance of 2.11 Å which is in the typical range of η-OH bond lengths. This "opening" of the bridge might result from a weakening of the bridging bonds due to the competition with two strongly bound OH ligands at the "left-hand" uranyl moiety (Fig. 4.16). This conclusion is supported by the uranyl bonds which are longer (by 0.1 Å), hence weaker, in the uranyl moiety at the "left-hand" side. In addition, the single U-O_h bond at the uranyl on the "right-hand" side is part of an internal hydrogen bond between the H center of the OH group and the O center of an adjacent OH ligand of the uranyl at the "left-hand" side (Fig. 4.16). The corresponding H···O distance of 1.51 Å and O-H···O angle of 153° indicate a moderately strong bond.[235] Due to this hydrogen bond the corresponding U-O_h bond of the uranyl at the "left-hand" side (2.26 Å) is noticeably longer than the bonds to the other two η-OH ligands (~2.12 Å, Fig. 4.16) of isomer C. Thus, isomer C exhibits three η-OH ligands like isomer A. A second internal hydrogen bond forms between the free terminal oxygen center of the carbonate ligand and the OH group at the neighboring uranyl (Fig. 4.16). The H···O distance of 1.69 Å and O-H···O angle of 161° are similar to the first hydrogen bond and point also to a moderate strength.[235] These two hydrogen bonds might cause isomer C to be more stable than the other two isomers (see below). The structure of the bridging carbonate differs from that in isomers A and B. One carbonate oxygen center is involved in the bridging, the corresponding U-O distance of 2.33 Å (Fig. 4.16) is similar to values of U-O_b bridges of isomer B (~2.32 Å). The second non-bridging U-O distance, 2.46 Å (Fig. 4.16), is noticeably longer and compares better to the U-O_c distance of isomer A (~2.50 Å) than to that of isomer B (~2.33 Å). The difference of the two U-O distances is also reflected in the corresponding C-O bonds: the longer (1.33 Å) and shorter (1.29 Å) CO bonds refer to the shorter and longer U-O distances, respectively (Fig. 4.16).

Throughout this discussion the argument of a constant uranyl binding capacity and corresponding bond order conservation of ligands in the equatorial plane was used frequently. Based on this argumentation, one would expect a rather constant average U-O_{eq} distance for complexes which exhibit a similar uranyl coordination environment and the same number of equatorial ligands. The comparison of the three isomers indicates similar values of U-O_{eq} for isomers A (2.35 Å) and B (2.36 Å), whereas isomer C is characterized by a slightly shorter value, 2.32 Å (Table 4.17). This difference can be rationalized by the previously discussed long non-bonding U-O distance (~2.8 Å) that leads to an effective

under-coordination of one uranyl moiety of isomer C which features only four ligands in contrast to the pentagonal coordination of all other uranyl moieties of the three isomers (Fig. 4.15). As expected, the average U-O_{eq} distance, ~2.29 Å, of this under-coordinated uranyl moiety of isomer C is distinctly shorter than the one of the neighboring pentagonal coordinated uranyl moiety, ~2.35 Å. Thus, the average U-O_{eq} value of isomer C is smaller.

The presented data for the three isomers suggest an average U-O_{eq} distance of 2.35–2.36 Å for dimeric uranyl complexes that exhibit a pentagonal uranyl coordination. This value agrees very well with data from previous calculations on OH- and O-bridged uranyl dimers, $[(UO_2)(OH_2)_2(H_2O)_6]^{2+}$ and $[(UO_2)O_2(H_2O)_6]$, which both yielded U-O_{eq} distances of 2.36 Å.[66] These results clearly point to the importance of the uranyl coordination number for the determination of U-O_{eq}. Structural differences such as the different kinds of bridges in isomers A–C have minor effects only. This conclusion is corroborated by a detailed discussion of data obtained for uranyl monocarboxylates in Section 4.4.4 which suggested average U-O_{eq} values for monomeric penta-coordinated uranyl complexes of 2.36–2.38 Å. These values agree well with U-O_{eq} distances obtained for the uranyl dimeric species, 2.35–2.36 Å. The U-O_{eq} values of the dimers are slightly shorter because the bridging atoms benefit from the binding capacities of two uranyl moieties.

Comparison to experimental data

Finally, the computational results of the C_1 models of the three isomers will be compared to experimental EXAFS data in solution (Table 4.17).[84] This comparison is complicated by the fact that the obtained EXAFS data represent a superposition of structures of the different isomers which are expected to be present simultaneously in solution. In addition, further difficulties are connected to the problematic resolution of similar equatorial U-O distances in EXAFS studies. Considering these limitations one can not expect the same agreement of computational and experimental data as obtained for other systems where well-defined actinide species were discussed (see Sections 4.3.1, 4.3.2, and 4.4.1).

The EXAFS spectra were interpreted based on two different fits (Table 4.17). The second fit allowed an identification of the U-U distance at 3.90 Å.[84] Both fits yield identical results for all other distances, but somewhat different coordination numbers. The EXAFS data allowed a differentiation of the equatorial distances into two components: ~1.5(±0.3) short U-O distances of 2.26 Å per U center, assigned to η-OH groups,[68,106] and ~3.7(±0.6) longer U-O distances of 2.47 Å, assigned to bridging hydroxide,[109] coordinated carbonate,[129] and aqua[68,79] ligands (Table 4.17). These assignments were based on a comparison to data of corresponding uranyl compounds. A further resolution of the second

group of U-O distances was not possible.

The calculated U-U distance of isomer A (4.8 Å) agrees well with the EXAFS data (~4.9 Å) of the trinuclear species $[(UO_2)_3(CO_3)_6]^{6-}$ which exhibits a similar bridging structure as discussed here.[129] In agreement with experiment, the calculated U-U distances of isomers B (3.8 Å) and C (4.0 Å) are distinctly shorter and agree well with the experimental value of ~3.9 Å, determined for corresponding dinuclear complexes featuring $[(UO_2)(OH_2)_2]^{2+}$ moieties.[114,115] Thus, the experimental U-U distance of 3.9 Å obtained for the hemicarbonate complex clearly points to a predominating presence of isomers B or C.

A differentiation of the isomers by other structural parameters is difficult. The terminal uranyl distances are similar for all three isomers (1.82 Å, Table 4.17) and agree well with the experimental values, 1.80–1.81 Å.[84] The average equatorial distance U-O_{eq} (2.32–2.36 Å) is shorter than the averaged experimental data (2.43 Å). As discussed above, U-O_{eq} depends strongly on the uranyl coordination number (see also Section 4.4.4). The rather long experimental value may point to a higher average coordination of the uranyls. The three isomers exhibit some O-U-O angles of 84–96° between adjacent OH and H_2O ligands which are a consequence of the small uranyl carbonate angles O_c-U-O_c (~55°). Such rather large angles indicate that in the equatorial plane there is space for coordinating additional aqua ligands; cf. the calculated O_w-U-O_w angles of ~75° in $[UO_2(H_2O)_5]^{2+}$ and 68° in $[UO_2(H_2O)_6]^{2+}$ (see Section 4.1). Thus, because the coordination number may change dynamically,[84] hexagonal coordination of uranyl in some systems seems possible.

For a better comparison, the equatorial U-O distances can be differentiated into two groups in line with the experimental suggestion. The shortest U-O distances (2.16–2.17 Å) are calculated for the strong U-O_h bonds. The other U-O bonds – U-O_b, U-O_c, and U-O_w – range from 2.3 to 2.5 Å (Table 4.17), confirming the experimental difficulties of a further resolution. However, the experimentally suggested short value of U-O_h (2.26 Å) is significantly underestimated, by ~0.1 Å, in all calculated isomers. The averaged longer U-O distances for isomers B (2.37 Å) and C (2.40 Å) also underestimate the experimental value (2.47 Å), while the value for isomer A (2.44 Å) agrees better due to the longest individual U-O distances (Table 4.17). However, equatorial U-O distances of the solvated uranyl $[UO_2(H_2O)_n]^{2+}$ were also somewhat underestimated (see Section 4.1), even in a more pronounced fashion in the case of uranyl monocarboxylates (see Section 4.4.2).

A definitive rationalization of these deviations is difficult. The general underestimation of equatorial bond distances might point to systematic errors in the DF-LDA method applied, but one hast to keep in mind that this method yields overall good agreement with experimental data for structurally well-characterized actinyl species such

as $[UO_2(CO_3)_3]^{4-}$, $[(UO_2)_3(CO_3)_6]^{6-}$, or $[UO_2(OOCCH_3)_3]^{-}$. DF methods employung GGA or hybrid exchange-correlation functionals typically overestimate distances in these compounds (see for instance Sections 4.1 and 4.4.1). The larger discrepancies discussed above are typically found for systems where the first coordination shell of uranyl is not well-defined, i.e. when the number of aqua ligands required to saturate free uranyl coordination sites or the coordination mode of ligands are not exactly known as in the hemicarbonate complex or the uranyl monocarboxylates (see Section 4.4.2). In these cases comparison to EXAFS data is complicated because the samples studied experimentally likely contain a mixture of complexes which leads to a superimposition of different structures. Discrepancies between theoretical and EXAFS data will be discussed in more detail in Section 4.4.4; that discussion points to the importance of the equatorial coordination number. Thus, the underestimations found may partially be explained by a higher coordination number of the actual complexes in solution than assumed in the computational models.

Finally, the U-C distance, which does not represent an actual bond, is in good agreement with experiment (2.89 Å) for isomers A and C (2.88 Å), but distinctly shorter in isomer B, by ~0.1 Å. The latter short value of isomer B can be rationalized by a stronger bound carbonate group because it is not involved in the bridging. This conclusion is reflected by the shortest U-O_c and U-C distances of all isomers (Table 4.17).

In summary, none of the isomers shows overall good agreement with the experimental data, especially with respect to the too short equatorial U-O distances. Because U=O_t and equatorial U-O distances of the three isomers are comparable, there is no preference for a specific isomer on the basis of the experimental data. The rather similar structural parameters obtained indicate that a differentiation of the isomers by EXAFS is indeed difficult. Still, based on the calculated U-U distance, one would clearly favor isomers B and C in agreement with the experimental suggestion.

Energetics

The structural discussion did not furnish clear evidence for the dominant presence of one particular isomer. Computational data allows to compare relative stabilities of the three isomers to determine the most stable isomer (Table 4.18). Differences between the three isomers are small. The order of stabilities is identical for C_s and C_1 models, deviations result from the slightly more pronounced relaxation of isomer A (see above). Isomer C was determined to be most stable, whereas isomers B and A are slightly less stable, by 5 and 11 kJ mol^{-1}, respectively, for the C_1 models. Using these relative stabilities, a Boltzmann distribution of the three isomers was calculated at the experimental temperature of

T = 298 K (Table 4.18). The distribution indicates isomer C as predominant species (86%), followed by isomers B (13%) and A (1%). These results are in very good agreement with the experimental suggestion, also favoring isomer C (80%, Table 4.18).[84]

However, the underlying small energy differences of a few kJ mol^{-1} between the three isomers have to be interpreted carefully because they are at the edge of the accuracy that can be expected from the computational method applied. For a quantitative evaluation, thermodynamic corrections need to be taken into account. For the three isomers contributions to the internal energy and entropy due to rotational and vibrational motion need to be considered (see Appendix B). One expects noticeable changes of the vibrational frequencies, especially of the carbonate and hydroxo moieties, due to the different kind of bridging in the isomers. The analysis of thermodynamic data for the uranyl monocarboxylates (see Section 4.4.4) indicates changes of Gibbs free energies in the order of 5–10 kJ mol^{-1} due to variations of frequencies by few hundreds of cm^{-1}. Even if one assumes comparable frequencies for isomers B and C on the basis of their structural similarity, an estimation of effects on the relative stabilities is difficult because of the small energetic differences. Furthermore, one has to consider that each of the isomers A–C can be varied further by interchanging the positions of the non-bridging ligands leading to further isomers that might exhibit similar stabilities.

In addition, formation of external hydrogen bonds to oxygen centers of carbonate ligands (see Section 4.3.1) or to bridging OH groups (see Section 4.2) is known to affect structures and thus also energetic stabilities. In the three isomers A–C, oxygen centers of

Table 4.18. Relative stabilities (ΔE_{rel}, in kJ mol^{-1}) for isomers A, B, and C (Fig. 4.14) of the uranyl hemicarbonate complex $[(UO_2)_2(CO_3)(OH)_3]^-$ with respect to the isomer with lowest total energy based on models with different symmetry constraints (C_s, C_1). Given are also the corresponding probabilities according to a Boltzmann distribution ($D_{Boltzmann}$, in %, T = 298 K) and the experimentally determined distribution in solution (D_{Exp}, in %).

	Sym.	A	B	C
ΔE_{rel}	C_s	14	5	–
	C_1	11	5	–
$D_{Boltzmann}$	C_s	0.3	11	89
	C_1	1	13	86
D_{Exp} [a]		5	15	80

[a] Ref. 84.

the carbonate ligands, of the η-OH ligands as well as of the bridging OH groups provide most probable coordination sites for hydrogen bonds (Fig 4.16). The isomers can be differentiated by the number of terminal carbonate oxygen centers (*a*) and η-OH ligands (*b*) which are expected to be the main targets for stronger hydrogen bonds, based on the lower oxygen coordination numbers of these groups. Such a differentiation indicates the highest capability for hydrogen bonds of isomer C ($a = 1$, $b = 3$) as compared to isomers A ($b = 3$) and B ($a = 1$, $b = 1$). However, one has to take into account that some of the available coordination sites are already occupied by internal hydrogen bonds as discussed above for isomers A and C. Modeling of such effects is complicated and beyond the scope of this investigation.

In summary, based on the computational data presented, a preference for isomers B and C over isomer A is indicated by the geometric as well as energetic results. Although the energetic estimates clearly are in favor of isomer C, in line with the experimental suggestion, this result has to be taken with due caution as a definite differentiation between the two isomers is difficult due to similar structural parameters and relative stabilities.

4.4 Actinyl complexation by carboxylate ligands

Carboxylic groups exhibit a strong propensity to complexate actinyl units, comparable to the previously discussed carbonate groups. They are able to coordinate to an actinyl ion in a bidentate or a monodentate fashion. In the following sections results on actinyl complexation by carboxylate ligands will be presented for different actinides and oxidations states. Short-range solvent effects are explicitly accounted for via aqua ligands of the first hydration shell and long-range electrostatic interactions are described via a polarizable continuum model.

In the first part (Section 4.4.1), uranyl triacetate $[UO_2(OOCCH_3)_3]^-$ is discussed in detail as a benchmark system and compared to experimental data and theoretical results from other studies. Then the focus is on uranyl monocarboxylates $[UO_2(OOCR)]^+$ with several simple aliphatic carboxylic ligands (Section 4.4.2). The main interest lies on the structural and energetic characterization of different carboxylate coordination modes as well as on their differentiation (bidentate, monodentate, chelate via an adjacent hydroxo group). In Section 4.4.3, the study of uranyl(VI) is extended to the corresponding neptunyl(VI) and neptunyl(V) carboxylates $[NpO_2(OOCR)]^{+/0}$. Both for uranium and neptunium the actinyl carboxylate distances show rather large discrepancies to experimental EXAFS and x-ray diffraction data. To rationalize these deviations, a detailed discussion in Section 4.4.4 will address several model aspects as well as experimental uncertainties. Based on the results from this discussion, implications for the complexation of actinides by humic substances are outlined in the final section (Section 4.4.5).

4.4.1 Uranyl(VI) triacetate, $[UO_2(OOCCH_3)_3]^-$

To assess the accuracy of the applied computational approach, uranyl triacetate, $[UO_2(OOCCH_3)_3]^-$, has been studied as a benchmark system. Bidentate coordination of all three ligands and C_{3v} symmetry is assumed (Fig. 4.17). This complex is suited as a test case because, on the one hand, experimental data confirming the chosen structural model are available for comparison;[97,147–151,156] on the other hand, the uranium coordination sphere of $[UO_2(OOCCH_3)_3]^-$ is saturated by three acetate ligands and thus there are no short-range solvent effects via aqua ligands which are directly coordinated to the metal center. To investigate the influence of aqua ligands in the second hydration shell, also the solvated model species $[UO_2(OOCCH_3)_3]^-\cdot(H_2O)_3$ was examined where three water molecules were added in the equatorial uranyl plane to model the effect of hydrogen bonds to the carboxyl groups (see Fig. 4.18b).

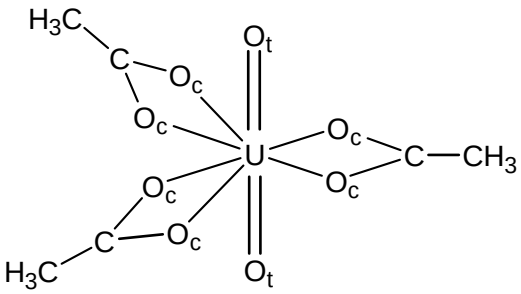

Figure 4.17. Schematic structure of the uranyl triacetate complex $[UO_2(OOCCH_3)_3]^-$ with bidentate coordination of the acetate ligands. The structure is characterized by the distances $U{=}O_t$, $U\text{-}O_c$, U-C, and $U\text{-}CH_3$.

In Table 4.19, computational results on uranyl triacetate both from gas phase (GP) and solvation (PCM) calculations are presented; Fig. 4.18a displays the optimized structure from the PCM calculation. Both sets of results are quite similar. The main difference corresponds to the $U\text{-}O_c$ distance that is slightly shorter in the PCM model, by 0.025 Å; other pertinent bond distances differ at most by 0.02 Å (Table 4.19). The elongation of the $U{=}O_t$ bond (0.01 Å) in the PCM calculation is reflected in a slightly reduced uranyl stretching frequency, which is calculated 26 cm^{-1} lower than for the corresponding complex in the gas phase. Models with three explicit water molecules in the second coordination shell yield slightly longer equatorial bond distances. Both for GP and PCM models, the equatorial distances increase by about the same amount ($U\text{-}O_c$ by 0.01 Å, U-C by 0.03, and $U\text{-}CH_3$ by 0.02 Å) when aqua ligands were added in the second hydration shell (Table 4.19). As expected, the formation of hydrogen bonds between the aqua ligands and the O_c centers of the carboxylate groups weakens the uranium carboxylate bonds $U\text{-}O_c$. Concomitantly with this weakening of the equatorial $U\text{-}O_c$ bonds, the terminal $U{=}O_t$ bonds become stronger, as reflected in a shorter bond length, by 0.01 Å, and a larger symmetric stretching frequency, 20 cm^{-1} (Table 4.19).

The most elaborate model $[UO_2(OOCCH_3)_3]^-\cdot(H_2O)_3$ (Table 4.19, Fig. 4.18b), includes solvation effects via three explicit aqua ligands in the second coordination shell and a PCM treatment. Of all models, its structure agrees best with EXAFS data for solution.[156] Deviations are less than 0.01 Å for the bonds $U{=}O_t$ and $U\text{-}O_c$, less than 0.02 Å for the $U\text{-}CH_3$ distance, and only 8 cm^{-1} for the symmetric uranyl stretching frequency. These results illustrate the accuracy of the computational models; their quality is rather typical for actinide complexes.[55,64,69]

To address possible methodological influences, the present results are compared with other electronic structure calculations on $[UO_2(OOCCH_3)_3]^-$ (Calc., Table 4.19). Dixon et

Table 4.19. Calculated structural parameters (distances in Å) and symmetric uranyl stretching frequency (ν_s, in cm^{-1}) of uranium triacetate $[UO_2(OOCCH_3)_3]^-\cdot(H_2O)_{n'}$ for bidentate coordination compared to experimental data from solution (Sol.) and crystals (Cryst.) as well as other calculated results (Calc.). Given are results from gas phase (GP) and solvation (PCM) calculations of the bare complex (n' = 0), as well as results including three water molecules to simulate hydrogen bonding to the carboxylate ligands (n' = 3). xc designates the exchange-correlation functionals employed in the DF calculations (see text for details). For the designations of atoms, see Fig. 4.17.

	n'	xc	U=O_t	U-O_c	U-C	U-CH_3	ν_s
GP	0	VWN	1.792	2.449	2.816	4.315	837
GP	3	VWN	1.783	2.459	2.848	4.337	857
PCM	0	VWN	1.803	2.424	2.817	4.299	811
PCM	3	VWN	1.792	2.438	2.849	4.323	831
Exp.							
Sol.[a]			1.78(2)	2.44(2)	–	4.34	823
Cryst.[b]			1.78(1)	2.48(2)	2.88(3)	–	–
Calc.							
GP [c]	0	VWN	1.79	2.44	2.81	4.31	850
GP [d]	0	PW91	1.81	2.51	–	4.38	–
GP [e]	0	BP	1.81	2.52	2.89	4.41	810
GP [e]	3	BP	1.80	2.53	2.92	4.43	825
PCM [d]	0	PW91	1.81	2.50	–	4.38	–
PCM [e]	0	BP	1.82	2.49	2.89	4.39	785
PCM [e]	3	BP	1.81	2.50	2.91	4.41	799

[a] Refs. 98, 156. [b] Average from Refs. 147–151. [c] Ref. 67. [d] Ref. 64.
[e] present work.

al. also applied a DF method with a local exchange-correlation functional (LDA-VWN) and employed a small core Stuttgart RECP for uranium.[67] As expected, the results for a GP model agree well with the corresponding results of the present work; deviations of distances are smaller than 0.01 Å, the uranyl stretching frequency differs by 13 cm^{-1} (Table 4.19).

Results from DF calculations are known to depend on the exchange-correlation functional, e.g. LDA vs. GGA (see Section 3.1.3). Thus, for $[UO_2(OOCCH_3)_3]^-\cdot(H_2O)_{n'}$ (n' = 0, 3) the GGA-BP functional was applied in addition to the LDA-VWN functional (Table 4.19). For GP and PCM models all distances are longer than the corresponding

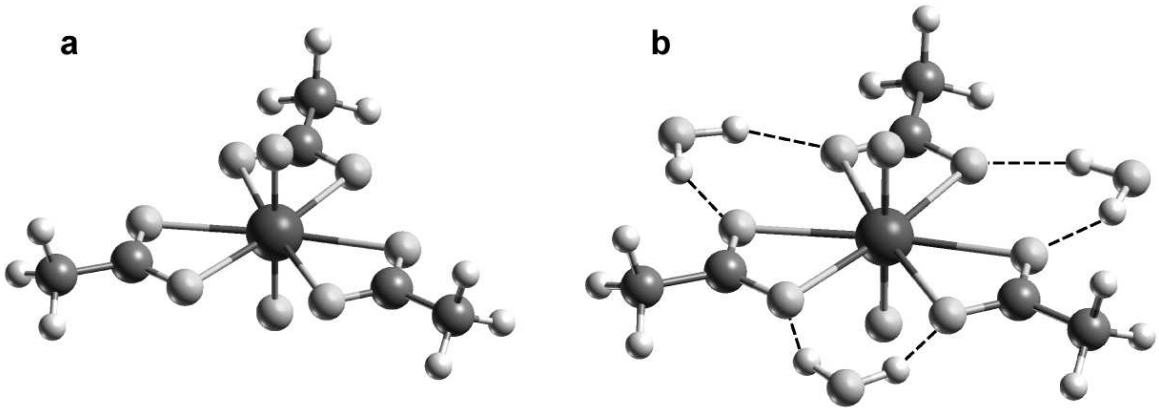

Figure 4.18. Optimized structures of uranyl triacetate complexes $[UO_2(OOCCH_3)_3]^-$ without (a) and with three additional water molecules (b) to simulate hydrogen bonding of the solvent to the carboxylate ligands (dashed lines).

LDA results. This trend – also observed for solvated actinyl complexes (see Section 4.1) and uranyl carbonates (see Section 4.3.1) – is typical for gradient-corrected exchange-correlation functionals.[190,191] The strong axial uranyl bonds U=O_t are slightly elongated, by 0.02 Å, while the equatorial distances are affected significantly stronger: U-O_c is longer by ~0.07 Å, U-C by 0.07 Å, and U-CH_3 by 0.09 Å. Concomitantly with the weaker uranyl bond, the uranyl stretching frequency is calculated smaller than in the LDA calculations, by 26–32 cm^{-1}. However, compared to experimental data in solution, all GGA distances are too long, for each model investigated: U=O_t by 0.02–0.04 Å, U-O_c and U-CH_3 by 0.05–0.09 Å. Differences between GP and PCM calculations are minor. Slightly longer U=O_t (by 0.01 Å) and shortened U-O_c bonds (by 0.03 Å) are obtained for the PCM models.

Vázquez et al. employed a similar computational approach, using a ZORA scalar-relativistic DF method with a GGA-PW91 functional and a PCM model for long-range solvent effects.[64] Results are almost identical for GP and PCM models; interatomic distances differ at most by 0.01 Å (Table 4.19). Compared to experimental data in solution, all pertinent distances are too long: U=O_t by 0.03 Å, U-O_c by 0.06–0.07 Å, and U-CH_3 by 0.04 Å.[64] The GGA-PW91 results are very similar to the corresponding GGA-BP data discussed above; differences are only 0.01 Å for U=O_t and U-O_c and somewhat larger for U-CH_3, 0.01–0.03 Å (Table 4.19).

In summary, the presented results show only minor differences between GP and PCM structures of the uranyl triacetate complex; distances differ by ~0.02 Å. Inclusion of water molecules from the second hydration shell induces changes of similar size for the bond distances U=O_t and U-O_c (~0.01 Å). As expected, the exchange-correlation

functional employed has a more pronounced effect on distances. The GGA calculations yield significantly longer equatorial distances than the LDA calculations, 0.06–0.08 Å for U-O_c and U-C, and up to 0.1 Å for U-CH_3. The stronger uranyl bonds U=O_t are also noticeably elongated, by 0.02 Å in comparison with the LDA results.

The LDA results slightly overestimate the U=O_t distance of experimental EXAFS data from solution (by 0.01–0.02 Å) and agree well for U-O_c (± 0.02 Å). However, all GGA bond distances are distinctly longer than the experimental values, on average 0.03 Å for U=O_t and 0.07 Å for U-O_c. This analysis confirms the choice of the local density approximation for the determination of geometries.[190,191]

4.4.2 Uranyl(VI) monocarboxylates, $[UO_2(OOCR)]^+$

In the natural environment, complexation of actinides by humic substances plays an important role in the migration and the retardation of actinides.[7,78] Thus, understanding the interaction of actinide species with humic substances becomes essential. Carboxylic groups are considered as the functional groups of humic substances which are mainly responsible for the complexation of metal ions (see Section 2.2.4).[6,78] As humic substances are structurally multifarious and not well defined and, in addition, due to their size too demanding to be treated as a whole with an accurate quantum chemical method, model complexes of actinyls with various small carboxylic ligands are chosen to characterize their properties. The focus is on uranyl monocarboxylate complexes $[UO_2(OOCR)]^+$ that are suggested at low pH (see Section 2.2.4).

Model aspects

To characterize possible variations in humic substances the impact of structural and chemical changes in the carboxylic groups on the actinyl complexation will first be investigated. One goal is to clarify the influence of the size of the aliphatic residue R of the carboxylate ligand, in particular till which distance a specific organic environment will affect the carboxylic group and its complexation properties. Chemical variations of R also have to be examined. Effects on the uranyl complexation will be discussed based on characteristic parameters of the complexes, namely the uranyl distance U=O_t, the angle O_t=U=O_t, and the uranyl stretching frequency ν_s as well as the distances U-O_c and U-C to centers of the carboxylic ligand (see Fig. 4.19a). The two carboxylate oxygen centers can be differentiated by *syn* ($O_{c,s}$) and *anti* ($O_{c,a}$) orientation with respect to H centers of the neighboring C_α center (Fig. 4.19b). Bidentate coordination is assumed in these preliminary models, additional equatorial ligands (like H_2O) as well as long-range solvent effects via PCM have been omitted in these model studies.

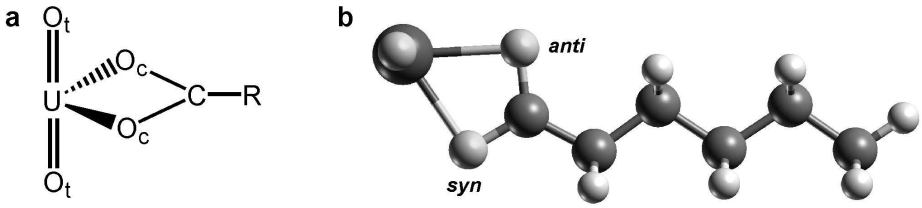

Figure 4.19. Schematic structure (a) of a uranyl monocarboxylate $[UO_2(OOCR)]^+$, R = C_nH_{2n+1}, with bidentate coordination and (b) optimized GP structure for n = 5 applying C_s symmetry constraints. The two carboxylate O_c centers are differentiated by *syn* ($O_{c,s}$) and *anti* ($O_{c,a}$) orientation with respect to H centers of the neighboring C_α center.

Results for uranyl monocarboxylates $[UO_2(OOCR)]^+$, R = C_nH_{2n+1}, with aliphatic ligands ranging from formiate (n = 0) to hexanoate (n = 5) are given in Table 4.20. In all models C_s symmetry constraints were applied with respect to the equatorial uranyl plane. Fig. 4.19b shows a representative structure for n = 5.

Surprisingly, changes for all considered parameters are rather small for complexes from n = 0 to n = 5 (Table 4.20). Differences between the various complexes are minor for the distances U=O_t (up to 0.007 Å), U-$O_{c,a}$ (up to 0.018 Å), and U-C (up to 0.012 Å). The U-$O_{c,s}$ distance overall shows larger variations among the various systems, up to 0.04 Å; this finding can be rationalized by the dissimilar environment of the two O_c centers with respect to the aliphatic residue R where H atoms from the adjacent C_α center are closer to $O_{c,s}$ (Fig. 4.19b). Thus, one obtains two U-O_c distances that differ by up to 0.03 Å for complexes with n > 1. Lack of further equatorial ligands yields an asymmetric equatorial environment of the uranyl moiety and leads to a slightly bent uranyl structure with O_t=U=O_t ≈ 172°. The small changes of U=O_t are reflected in similar O_t=U=O_t angles (within 0.8°) and uranyl stretching frequencies (within 20 cm^{-1}) of complexes with different n. The positive inductive effect of the aliphatic residue results in a donation of electron density to the uranyl moiety and a reduction of the uranyl charge q(UO_2) with increasing n (Table 4.20). The electron donation reduces the electrostatic attraction between U and O_t centers as corroborated by the weakening of the uranyl bonds and the reduction of the uranyl stretching frequency.

Overall, convergence of all parameters is reached for the uranyl butanoate complex (n = 3, Table 4.20). Thus, the chain lengths is expected to have only a minor influence on the local actinyl complexation. Models comprising chains up to the C_γ atom of the residue R should be rather accurate for simulating complexation by longer organic molecules. Effects, especially steric, of side chains in R close to the uranyl moiety are expected to be more relevant than the length of the chain.

Table 4.20. Calculated interatomic distances (in Å), Mulliken charge q of the uranyl moiety (in e), and symmetric uranyl stretching frequency ν_s (in cm^{-1}) of bidentate uranyl monocarboxylate model complexes $[UO_2(OOCR)]^+$, R = C_nH_{2n+1}, for n = 0 to 5 in the gas phase. For the designations of atoms, see Fig. 4.19. Convergence of the results for different chain lengths is essentially reached for n = 3 (highlighted).

n	U=O_t	O_t=U=O_t	U-$O_{c,s}$	U-$O_{c,a}$	U-C	q(UO_2)	ν_s
0	1.745	172.6	2.242	2.242	2.628	0.96	946
1	1.749	172.0	2.224	2.224	2.640	0.91	936
2	1.750	171.8	2.213	2.227	2.635	0.90	933
3	1.751	171.8	2.205	2.234	2.635	0.89	932
4	1.751	171.8	2.206	2.234	2.635	0.88	930
5	1.752	171.8	2.206	2.236	2.634	0.87	927

The chemical variation of R is investigated by comparing complexes with saturated aliphatic ligands (R = H, CH_3, CH_2CH_3) to those with unsaturated (R = $CH{=}CH_2$) and α–substituted ligands (R = CH_2–OH, CH_2–NH_2). Results are summarized in Table 4.21 and compared to average experimental data of bidentate uranyl carboxylate complexes in solution. In all computational models C_s symmetry constraints were applied with respect to the equatorial uranyl plane. A PCM treatment is omitted.

As anticipated, chemical variations in the local environment of the complexation site cause larger effects than variations in the chain length discussed before (Table 4.20). However, overall changes are also minor, only 0.01 Å for U=O_t and up to 0.05 Å for U-O_c and U-C. The uranyl moieties are slightly bent with small variations of the O_t=U=O_t angle (up to 2°). The uranyl stretching frequency is sensitive to small changes of the U=O_t distance and varies by up to 26 cm^{-1} (~3%). All ligands show comparable uranyl charges (within 0.1 e) indicating similar charge donation capabilities despite the different substituents R.

Calculated features of the acrylate complex (R = $CH{=}CH_2$) are very similar to complexes with aliphatic residues (R = CH_3 and CH_2CH_3). This can be seen for distances, the uranyl charge, and the uranyl stretching frequency (Table 4.21). Data for the complexes with glycolate (R = CH_2–OH) and formiate substituents (R = H) are comparable. The similar uranyl charge in both complexes is slightly higher than for complexes with longer aliphatic residues (R = CH_3 and CH_2CH_3). Therefore, the positive inductive effect seen for R = CH_3 is to some extent compensated by the negative inductive effect of the OH group for R = CH_2–OH. On the other hand, the amino group in R = CH_2–NH_2 acts as electron

Table 4.21. Calculated interatomic distances (in Å), Mulliken charge q of the uranyl moiety (in e), and symmetric uranyl stretching frequency ν_s (in cm^{-1}) of bidentate uranyl monocarboxylate model complexes $[UO_2(OOCR)]^+$ for various residues R in the gas phase. Average experimental distances are also shown. For the designations of atoms, see Fig. 4.19.

R	U=O_t	O_t=U=O_t	U-$O_{c,s}$	U-$O_{c,a}$	U-C	q(UO_2)	ν_s
H	1.745	173	2.242	2.242	2.628	0.96	946
CH_3	1.749	172	2.224	2.224	2.640	0.91	936
CH_2CH_3	1.750	172	2.213	2.227	2.635	0.90	933
$CH{=}CH_2$	1.751	171	2.216	2.220	2.635	0.89	932
$CH_2{-}OH$	1.748	172	2.226	2.253	2.635	0.94	936
$CH_2{-}NH_2$	1.755	173	2.252	2.277	2.651	0.85	920
Exp.[a]	1.78(1)	–	2.46(4)	2.46(4)	2.87(4)	–	–

[a] Average values from bidentate carboxylate species in solution from Refs. 79, 151, 155.

donor via the nitrogen lone pair. Thus, the uranyl charge is noticeably smaller than in the other complexes. Concomitantly, this complex exhibits the longest uranyl distance and the lowest uranyl stretching frequency of all complexes (Table 4.21).

In comparison to the average experimental values all distances are too short (Table 4.21). Whereas the uranyl bond is only 0.02–0.03 Å shorter than in experiment, the equatorial distances U-O_c and U-C are distinctly underestimated by more than 0.2 Å. On the one hand, these deviations can be explained by the fact that long-range solvent effect are not represented in these GP models; taking them into account should result in an elongation of the polar U-O bonds due to screening. As there are no further equatorial ligands in these model complexes, the uranyl moiety, typically exhibiting a pentagonal coordination, is severely under-coordinated.[68,79–81] Coordinated aqua ligands in solution are known to have a distinct effect on the structure of a complex, as previously discussed for solvated actinyl complexes (Section 4.1) and uranyl carbonates (Section 4.3.1).[43,66] An increased binding competition at the uranium center will increase the equatorial distances. Therefore, both short- and long-range solvent effects will be included in models of the subsequent sections.

In summary, chain length and chemical variation affect the uranyl complexation by a bidentate carboxylate group only to a minor extent and result in rather small changes of characteristic parameters, such as the uranyl distance and the uranyl charge. The uranyl stretching frequency reacts somewhat more sensitive to small changes of the uranyl bonds.

These results suggest that modeling of variations of the carboxylate ligand, e.g. in humic substances, should be feasible in a combined QM/MM approach. One can treat the short-range environment of the uranyl moiety explicitly with a QM method and the long-range effects beyond the C_γ center of the residue R to good accuracy via a MM approach.

Aliphatic monocarboxylates $[UO_2(OOCR)(H_2O)_n]^+$

In the following sections structure and energetics of uranyl monocarboxylate model complexes $[UO_2(OOCR)(H_2O)_n]^+$ will be examined in detail for various types of coordination of the carboxylate ligands. In addition, short- as well as long-range solvation effects will be studied. These complexes are known to exist in solution at appropriate conditions;[97,98,151,250] furthermore, they may serve as simple models of complexing sites of humic substances as discussed above. Results will be compared to structural information from EXAFS experiments. Previous efforts in clarifying structural aspects of complex heavy-element systems, like heterogeneous catalysts,[251] demonstrated that it is very useful to supplement EXAFS derived information by accurate quantum chemistry modeling.

Experimental background and models

The choice of structural models for uranyl monocarboxylate complexes in aqueous solution has been guided by pertinent x-ray crystal structure data and EXAFS results. For that reason and to provide a basis for the subsequent discussion of the results obtained, first the experimental background is summarized focusing on structural characteristics that are commonly invoked to distinguish between bidentate, monodentate, and chelate coordination of a carboxylate group to a uranyl moiety (Fig. 4.20).

Only x-ray crystal structures provide definite information on the coordination type of carboxylate ligands. The analysis of various crystal structures indicates that uranyl ions favor bidentate coordination.[159] This is reflected by the high stability of tris(carboxylato) complexes, e.g. $M[UO_2(OOCCH_3)_3]$ (M = monovalent cation) that occur as monomers in

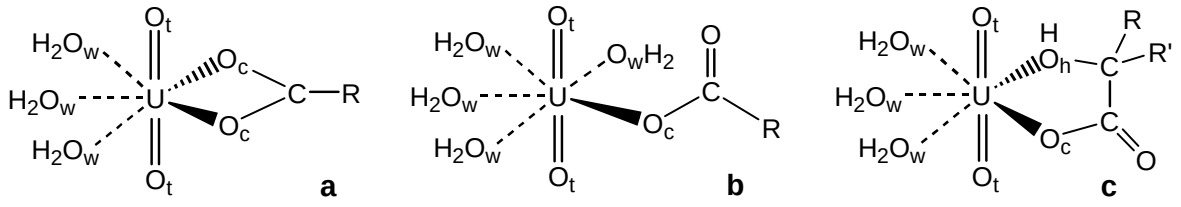

Figure 4.20. Schematic structures of uranyl monocarboxylate complexes $[UO_2(OOCR)(H_2O)_n]^+$. The carboxylate ligands can be coordinated in bidentate (a), monodentate (b), or chelate (c) fashion to the uranyl ion. Additional aqua ligands are coordinated in the equatorial plane to yield pentagonal coordination of the uranium center.

which three carboxylates act as bidentate ligands.[147] The same coordination has also been suggested for the uranyl triacetate complex $[UO_2(OOCCH_3)_3]^-$ in solution (Section 4.4.1). According to an overview[160] of several crystalline uranyl carboxylate complexes, bidentate coordination is generally characterized by two U-O_c distances of 2.48±0.05 Å, associated with one U-C distance of 2.86±0.05 Å per carboxylate ligand (Fig. 4.20a); the U-C distance does not represent a direct bond, of course. On the other hand, distinctly shorter U-O_c distances, 2.39±0.05 Å, were found for monodentate coordination (Fig. 4.20b);[160] the corresponding U-C distance of 3.5±0.1 Å is clearly elongated.[149,152] Distances U-O_w to oxygen centers of the first hydration shell, 2.42±0.06 Å, are similar to U-O_c distances in the monodentate case.[160] Carboxylates that comprise an α–hydroxy group, e.g. as in glycolate or α–hydroxyisobutyrate, can also exhibit a chelate coordination to uranyl via that OH group (Fig. 4.20c). The corresponding U-O_c distance of ~2.37 Å is comparable to that of monodentate coordination, whereas the chelating bond to the hydroxo group U-O_h is significantly longer, ~2.50 Å.[157] The U-C distance of ~3.3 Å falls between the values for bidentate and monodentate coordintaion.[157] All three coordination modes yield similar distances U=O_t to terminal oxygen centers of uranyl, 1.76±0.03 Å.[157,160]

The interpretation of the corresponding EXAFS data is normally based on a comparison with the typical distances derived from crystal structures as presented above. However, in the EXAFS spectra, it is often not possible to differentiate various types of equatorial U-O distances, because U-O_w distances are comparable to U-O_c distances of monodentate, chelate and sometimes even bidentate carboxylate ligands. Therefore, in most cases only an average equatorial distance U-O_{eq} can be derived.

A number of EXAFS data in solution has been obtained on uranyl complexation by carboxylic ligands such as acetate and glycolate.[151,155] Accordingly, bidentate coordination is characterized by U-O_c distances of 2.43–2.50 Å associated with U-C distances of 2.84–2.91 Å; these results are similar to previously discussed data in crystalline systems. For bidentate coordination, equatorial oxygen distances U-O_{eq} are 2.42±0.04 Å on average.[79,151,155] Definitive EXAFS data for monodentate coordination in solution are rare; average U-O_{eq} values are ~2.38±0.04 Å.[151,155] When U-C distances of ~2.9 Å (indicative of bidentate coordination) are absent, then these U-O_{eq} distances are generally assigned to monodentate carboxylate ligands.[149,150] As for monodentate coordination, resolution of different equatorial U-O distances by EXAFS is usually not possible for chelate coordination. The corresponding average U-O_{eq} distance of 2.37±0.01 Å is comparable to the value of monodentate coordination.[155] However, chelate coordination can be identified by the presence of an additional U-C distance at 3.25±0.03 Å.[155] Typical uranyl-water

distances U-O_w distances in solution of 2.38±0.02 Å and 2.41±0.01 Å have been reported for $[UO_2(OOCCH_3)(H_2O)_n]^+$ and $[UO_2(H_2O)_5]^{2+}$, respectively; they indeed are similar to reported U-O_{eq} values. [68,79,151]

EXAFS data on the complexation of actinides by natural and synthetic humic acids are interpreted as predominantly monodentate coordination, based on average U-O_{eq} distances of 2.37–2.39 Å and missing U-C distances near ~2.9 Å or ~3.3 Å that would be indicative for bidentate or chelate coordination, respectively.[141,150,160,161] However, it is unclear why only monodentate complexation of actinides should occur, considering the complex structure of humic substances and the predominance of carboxylic groups as complexing sites that typically prefer a bidentate coordination.[159] A detailed discussion of complexation of actinyls by humic substances is provided in Section 4.4.5.

To contribute to the discrimination of mono-, bidentate, and chelate complexes, these different coordination modes were studied in model complexes $[UO_2(OOCR)(H_2O)_n]^+$ of uranyl with formiate (R = H), acetate (R = CH_3), propionate (R = CH_2CH_3), and glycolate (R = CH_2OH) ligands. Chelate coordination via the α–OH group was assumed for the glycolate ligand. Short-range solvent effects were accounted for by adding explicit aqua ligands (*n*) in the first hydration sphere, three for bidentate and chelate and four for monodentate coordination (Fig. 4.20). In this way, the typical pentagonal coordination of an uranyl moiety was achieved.[14,152,155] Note that hexagonal coordination has also been suggested for some uranyl carboxylate complexes.[151]

To reduce the computational effort, C_s symmetry constraints were applied in all models, except for the bidentate coordination mode with R = H (C_{2v}). In the monodentate and chelate systems the equatorial uranyl plane, spanned by O centers of the carboxylate ligand (O_c) and the aqua ligands (O_w), was chosen as symmetry plane (Figs. 4.20b,c). For the bidentate systems, the equatorial plane as well as a plane perpendicular to it which includes the uranyl moiety were considered (Fig. 4.20a). In the following, only results from the energetically more stable conformers which feature the equatorial plane as mirror plane are discussed. In general, differences between the two bidentate models are small, i.e. distances, differ at most by 0.02 Å, angles at most by 2°, and total energies at most 10 kJ mol^{-1}.

Geometry of bidentate uranyl carboxylate complexes

Table 4.22 summarizes the results for bidentate complexation of the uranyl complexes $[UO_2(OOCR)(H_2O)_3]^+$ with R = H, CH_3, CH_2CH_3, and CH_2OH (Fig. 4.21). As stated before, solvation effects were taken into account by three explicit aqua ligands of the first hydration sphere, supplemented by a PCM treatment.

Table 4.22. Calculated structural parameters (distances in Å) and symmetric uranyl stretching frequency ν_s (in cm^{-1}) of uranyl(VI) monocarboxylates $[UO_2(OOCR)(H_2O)_n]^+$ exhibiting bidentate (bi, n = 3), monodentate (mono, n = 4), and chelate (chel, n = 3) carboxylate coordination compared to experimental data for aqueous solution (sol.) and from crystal structures (cryst.). Solvent effects were included via n explicit aqua ligands and a PCM treatment. Also given are average changes ΔH_2O due to addition of the aqua ligands to the corresponding bare complexes $[UO_2(OOCR)]^+$ in the gas phase, and ΔPCM due to embedding of the complexes $[UO_2(OOCR)(H_2O)_n]^+$ in a PCM environment. Average changes Δbi and Δmono are calculated with respect to the corresponding bidentate and monodentate complexes. For the designations of the atoms, see Fig. 4.20.

	R	U=O_t	U-O_c	U-O_h	U-C	U-O_w	U-O_{eq}	ν_s
bi	H	1.783	2.394		2.770	2.356	2.371	860
	CH_3	1.787	2.371		2.769	2.360	2.364	858
	CH_2CH_3	1.786	2.369		2.768	2.369	2.369	853
	CH_2OH	1.783	2.393		2.771	2.353	2.369	862
	ΔH_2O avg.	0.03	0.11		0.10	–	0.16	-56
	ΔPCM avg.	0.01	0.04		0.03	-0.06	-0.02	-23
Exp.	CH_3 sol.[a]	1.78(1)	2.50(2)		2.91(2)	2.38(2)	2.43(2)	861
	sol.[b]	1.78(1)	2.46(4)		2.87(4)	2.40(4)	2.42(4)	–
	cryst.[c]	1.76(3)	2.48(5)		2.86(5)	2.36(4)	2.42(6)	–
mono	H	1.788	2.221		3.400	2.415	2.376	850
	CH_3	1.790	2.201		3.401	2.421	2.377	846
	CH_2CH_3	1.790	2.201		3.401	2.421	2.377	849
	CH_2OH	1.786	2.247		3.400	2.408	2.375	852
	ΔH_2O avg.	0.03	0.14		0.00	–	0.37	-54
	ΔPCM avg.	0.01	0.04		0.03	-0.04	-0.02	-22
	Δbi avg.	0.00	0.16		-0.63	-0.06	-0.01	9
Exp.	sol.[b]	1.78(1)	–		–	–	2.38(4)	–
	cryst.[c]	1.76(3)	2.39(5)		3.5(1)	2.42(6)	2.36(2)	–
chel	CH_2OH	1.790	2.229	2.423	3.272	2.380	2.359	846
	ΔH_2O avg.	0.03	0.09	0.06	0.06	–	0.16	-50
	ΔPCM avg.	0.01	0.08	-0.03	0.02	-0.07	-0.03	-18
	Δbi avg.	0.01	-0.16	–	0.50	0.03	-0.01	-17
	Δmono avg.	0.00	-0.02	–	-0.13	-0.03	-0.02	-6
Exp.	sol.[d]	1.79(1)	–	–	3.25(3)	–	2.37(1)	–
	cryst.[e]	1.75(1)	2.37	2.50	3.3	–	2.36(2)	–

[a] Refs. 97, 98, and 151. [b] Average values from Refs. 79, 151, and 155. [c] Average values from Refs. 150, 151, and 160. [d] Average values from Ref. 155. [e] Ref. 157.

The calculated structural parameters of these complexes vary only slightly for the various residues R. These small changes are in line with results from the test systems where effects of model size and type had been probed (see above). Formiate and glycolate as well as acetate and propionate complexes form two pairs with very similar structural parameters; distances differ at most by 0.01 Å (Table 4.22). In the first pair of complexes, R = H and R = CH_2OH, the U-O_c bond is 0.02 Å longer than in the complexes with R = CH_3 and R = CH_2CH_3. This points toward a weaker bonding of the carboxylate group in the former two cases. These trends, albeit faint, are confirmed by energetic considerations and are also obtained for monodentate carboxylate coordination (see below). Concomitantly, one finds shorter uranyl bonds U=O_t and stronger uranyl symmetric stretching frequencies than in the second pair of complexes (Table 4.22). Furthermore, the aqua ligands are a little closer to the uranium center, by ~0.01 Å, for complexes with R = H and R = CH_2OH.

For a detailed investigation of solvation, short-range and long-range effects were simulated in two consecutive steps. First, changes ΔH_2O (Table 4.22) due to the addition of three explicit aqua ligands to a bare uranyl carboxylate complex $[UO_2(OOCR)]^+$ were calculated for a GP model; then, that aqua complex $[UO_2(OOCR)(H_2O)_3]^+$ was embedded in a PCM environment, to give changes ΔPCM. All differences Δ listed in Table 4.22 represent average values of all four types of carboxylate complexes; deviations from these averages are less then 0.01 Å for distances and 5 cm^{-1} for the uranyl stretching frequency.

Explicit consideration of aqua ligands leads to a distinct elongation of the uranium carboxylate distances U-O_c by 0.11 Å and U-C by 0.10 Å (ΔH_2O, Table 4.22). The U=O_t distance is elongated by 0.03 Å, whereas the O_t=U=O_t angle is hardly affected; it decreases from 172° to 171°. These bond elongations result from increased bonding competition with the aqua ligands at the uranium center. The weaker uranyl bonds are reflected in a reduction of the uranyl stretching frequency, by 56 cm^{-1} on average. These strong effects

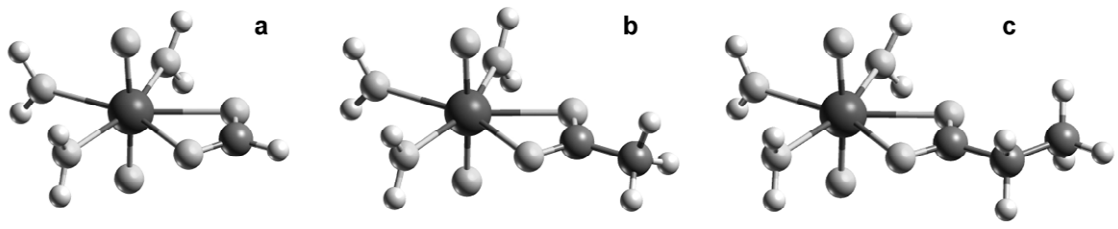

Figure 4.21. Optimized structures of uranyl monocarboxylate complexes $[UO_2(OOCR)(H_2O)_3]^+$, R = H (a), CH_3 (b), and CH_2CH_3 (c), with bidentate coordination of the carboxylate group.

due to the coordination of aqua ligands confirm previous findings,[43,69] namely that aqua ligands of the first hydration shell interact rather strongly with the uranium center (see also Sections 4.1 and 4.3.1).

Long-range solvent effects (modeled via PCM) further elongate the distances U-O_c, U-C, and U=O_t, by 0.04 Å, 0.03 Å and 0.01 Å, respectively (ΔPCM, Table 4.22). These elongations result from a screening of the polar bonds U=O_t and U-O_c. The weakening of the uranyl bond is reflected in a further reduction of the uranyl stretching frequency by ~23 cm^{-1}. In contrast to the other U-O bonds, uranium-water distances decrease significantly, by ~0.06 Å, due to the PCM treatment. This reduction is also observed for U-O_w distances of solvated actinyl complexes (see Section 4.1) and uranyl carbonates (see Section 4.3.1). In summary, the solvent effects described by the PCM model are noticeably smaller than changes due to aqua ligands of the first solvation shell.

Because only few experimental structure data are available for systems assigned as monocarboxylate species, results are also compared to averaged data of complexes with different carboxylate ligands as well as compounds that comprise more than one carboxylate ligand (Table 4.22). EXAFS data from solution give superimposed structural information if different species are present in the solution under investigation.[155] For the monocarboxylate systems studied here, solution data from EXAFS[151] and Raman[97] studies are only available for the uranyl monoacetate complex (R = CH_3, Table 4.22) that has been suggested to exhibit a bidentate carboxylate ligand.

The uranyl moieties are calculated to feature terminal uranium-oxygen distances U=O_t of 1.78–1.79 Å and slightly bent O_t=U=O_t moieties with angles of 174–177°. The calculated U=O_t distances are typical for small uranyl complexes and agree very well with experimental data for uranyl acetate, 1.78(1) Å,[151] and average data for bidentate complexes in solution, 1.78(1) Å.[151,155] Concomitant with the accurate results for U=O_t, the calculated symmetric uranyl stretching frequencies ν_s of 853–860 cm^{-1} also match the experimental value of 861 cm^{-1} for R = CH_3.[97] Average uranium-aqua distances U-O_w of 2.36 Å are in satisfactory agreement with experimental data for acetate, 2.38(2) Å[151] as well as averages of experimental data, ~2.40(4) Å.[79,151] The values obtained for distances and uranyl frequency are quite similar to results calculated for the solvated uranyl ion $[UO_2(H_2O)_5]^{2+}$ (see Section 4.1, Table 4.2): 1.78 Å for U=O_t, ~2.36 Å for U-O_w, and 869 cm^{-1} for ν_s. Thus, a bidentate carboxylate group affects the uranyl moiety in a similar way as two aqua ligands.

The uranium carboxylate bond in the bidentate model complexes is characterized by distances U-O_c of 2.37–2.39 Å and U-C of 2.77 Å (Table 4.22). However, these distances

are distinctly shorter, more than 0.1 Å, than the corresponding EXAFS data for R = CH_3, namely 2.50(2) Å for U-O_c and 2.91(2) Å for U-C.[151] Only slightly smaller differences occur compared to averaged solution data for bidentate coordination, where average values of 2.46(4) Å and 2.87(4) Å have been obtained for U-O_c and U-C, respectively.[151] Concomitantly, also the average distance U-O_{eq} from uranyl to neighboring oxygen atoms is underestimated, by ~0.05 Å. These discrepancies are significantly larger than those found for the uranyl triacetate benchmark system (see Section 4.4.1) and for other uranyl complexes based on DF calculations;[61,64,69] thus, they may point to an underestimation of the uranium carboxylate bond distances in the employed models. On the other hand, the rather long experimental interatomic distances between U and the carboxylate group obtained for uranyl monoacetate (2.50 Å, Table 4.22)[151] in comparison to averaged data for complexes with two or three bidentate carboxylate ligands (2.46(4) Å, Table 4.22) are hard to rationalize. One would expect longer uranium carboxylate distances for complexes that comprise more carboxylate ligands if one considers bonding competition at the uranium center and the fact that carboxylate ligands bind stronger than aqua ligands (see below). In line with this expectation, both distances U-O_c and U-C of the uranyl monoacetate complex have been calculated 0.05 Å shorter (see Table 4.19) than for the triacetate complex. However, the U-O_c value of 2.50 Å suggested for uranyl monoacetate in Ref. 151 exceeds the experimental results for triacetate (2.44–2.48 Å, Table 4.19) and thus seems somewhat too large. Nevertheless, differences between the calculated structures of uranyl monocarboxylate complexes and EXAFS data remain rather large with respect to the underestimation of the uranyl carboxylate bonds. Further possible reasons for those discrepancies will be addressed in more detail in Section 4.4.4.

Geometry of monodentate uranyl carboxylate complexes

Now results from the corresponding calculations on complexes with monodentate coordination will be presented, namely for $[UO_2(OOCR)(H_2O)_4]^+$ with R = H, CH_3, CH_2CH_3, and CH_2OH (Table 4.22, Fig. 4.22). Solvation effects were taken into account as before; however, to reach pentagonal coordination of the uranyl moiety, four explicit aqua ligands were added to the complexes. Besides a general discussion, results will be compared to those for the corresponding bidentate complexes (Δbi in Table 4.22).

Again, all complexes feature similar optimized structural parameters. Terminal uranium-oxygen distances U=O_t, 1.79 Å, are calculated a little longer, by 0.004 Å on average, than for complexes with bidentate coordination. With O_t=U=O_t angles of ~172°, the uranyl moieties are bent slightly more and the uranyl stretching frequencies, 846–852 cm^{-1}, are somewhat smaller, by 9 cm^{-1} on average, than in the corresponding bidentate carboxylate complexes. The pairs of complexes with formiate and chelate substituents as

well as acetate and propionate substituents exhibit comparable features, as found for the corresponding bidentate complexes: the U-O_c bond is ~0.03 Å longer for the first pair, while the aqua ligands are a little closer than in the second pair. The longer U-O_c distances indicate weaker carboxylate bonds in the first pair of complexes. This weaker bonding is also corroborated by shorter U=O_t distances and larger uranyl stretching frequencies than in the second pair of complexes (Table 4.22). In agreement with qualitative conclusions from the analysis of experimental data,[160] the U-O_c distances are calculated notably shorter (2.22 Å) and the U-C distances significantly longer (3.40 Å) than the corresponding parameters of bidentate complexes: U-O_c = 2.38 Å and U-C = 2.77 Å. Uranium aqua distances, 2.42 Å, are determined longer than in the bidentate complexes (Δbi = -0.06 Å, Table 4.22). This finding can be rationalized by bonding competition with four, instead of three aqua ligands.

As before, solvent effects were analyzed by a stepwise build-up of the models. Comparing explicit coordination of aqua ligands and bare complexes without PCM treatment (ΔH_2O, Table 4.22), one notes significantly longer distances U-O_c (0.14 Å) and U=O_t (0.03 Å) due to bonding competition with the four equatorial aqua ligands. As discussed for bidentate coordination, incorporation of aqua ligands reduces the uranyl stretching frequency, here by ~54 cm^{-1} (Table 4.22). However, U-C distances are hardly affected by the inclusion of aqua ligands in the first coordination shell (ΔH_2O < 0.005 Å on average), despite the distinct elongation of the U-O_c bonds. This surprising finding results from the reduction of the U-O_c-C angle from ~160° in the bare complex to ~147° in the complex with aqua ligands. This change of the bond angle can be rationalized by an attractive interaction between the "free" negatively charged O_c center of the carboxylic group and the positively charged H centers of adjacent aqua ligands (Fig. 4.22). Subsequent embedding in a PCM environment yields smaller corrections (ΔPCM, Table 4.22), comparable to those calculated for the bidentate complexes. Because of screening

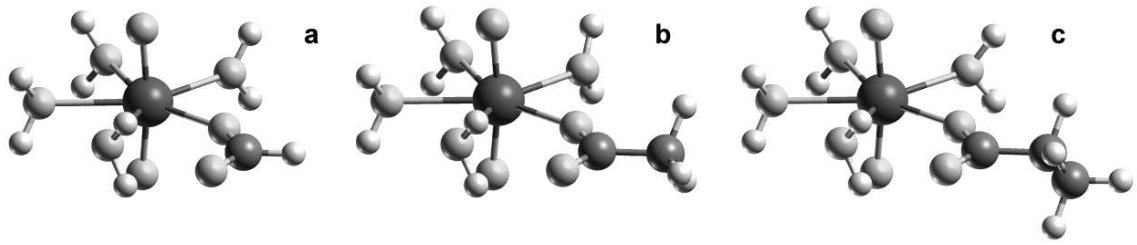

Figure 4.22. Optimized structures of uranyl monocarboxylate complexes $[UO_2(OOCR)(H_2O)_4]^+$, R = H (a), CH_3 (b), and CH_2CH_3 (c), with monodentate coordination of the carboxylate group and C_s symmetry constraints.

effects, the distances U-O_c, U-C, and U=O_t are longer by 0.04 Å, 0.03 Å and 0.01 Å, respectively. The angle U-O_c-C increases slightly to ~150° in the PCM treatment. The U-O_w distance decreases by 0.04 Å and the uranyl stretching frequency is ~22 cm^{-1} smaller, concomitant with the slightly elongated uranyl bonds (Table 4.22).

Comparison with available experimental data reveals that terminal uranium-oxygen distances U=O_t, 1.79 Å, agree well with the corresponding average experimental value, 1.78(1) Å.[151,155] Also bond lengths of aqua ligands, 2.42 Å, are in line with typical experimental values, 2.40(4) Å.[79,151] The characteristic parameters of the carboxylate bond, U-O_c (2.22 Å) and U-C (3.40 Å), are found to be considerably shorter than experimental results derived from crystals,[151,152,161] by ~0.2 Å and 0.1 Å, respectively. Although these differences may be somewhat smaller for complexes in solution, a clear underestimation is expected, as in the case of bidentate coordination (see above). Furthermore, the calculated average of U-O bond lengths in the equatorial plane, U-O_{eq} = 2.38 Å, agree well with available experimental data for solution, 2.38 Å (Table 4.22).[151,155] However, as the present calculations show, the distance U-O_{eq} is of limited value as indicator of the coordination mode because it averages over the quantities U-O_c and U-O_w that differ widely – by up to 0.2 Å (Table 4.22). In favorable cases, EXAFS measurements may be able to resolve two such bond distances when a carboxylate ligand is coordinated in monodentate fashion.

The U-C distances of monodentate ligands are calculated 0.63 Å longer than those of bidentate ligands. Despite the large deviations of the absolute values, the corresponding trend of the experimental estimate, 0.6(1) Å for solvated complexes (Table 4.22), is very well reproduced. It is difficult to assess the calculated difference of the U-O_c distances (0.17 Å longer for bidentate coordination) because experimental values are restricted to crystal data from which one estimates that difference at 0.1 Å (Table 4.22). In agreement with experiment, the bonds from U to the aqua ligands are calculated slightly shorter in the bidentate case. These calculated results yield a similar average value U-O_{eq} for mono- and bidentate complexes (within 0.01 Å) – at variance with the experimental trend that suggests ~0.04 Å longer U-O_{eq} distances for bidentate coordination. Note, however, that the intervals of the experimental results for both coordination modes overlap (Table 4.22).

Geometry of chelate uranyl carboxylate complexes

Glycolate is the only ligand investigated that can exhibit a chelate coordination via the α-OH group besides bidentate and monodentate coordination. Under acidic conditions (pH < 4), glycolate complexes $[UO_2(OOCCH_2OH)_m]^{2-m}$ (m = 1–3) have been suggested to form.[155,158] The experimental data indicates that only the carboxylate end of the glycolate group is coordinated to the uranyl moiety at these pH values.[155,158] The OH group is

expected to remain protonated in contrast to the more acidic carboxylate group. Above pH ~5, it has been reported that the proton of the α–OH group dissociates and simultaneously a chelate coordination forms in solution, e.g. the bis(glycolato) complex $[UO_2(OOCCH_2O)_2]^{2-}$ or the dimeric complex $[(UO_2)_2(OOCCH_2O)_2]$.[158]

Structural data on chelate coordination of carboxylates are rare. The crystal structure[157] of uranyl glycolate $[UO_2(OOCCH_2OH)_2]$ exhibits a pentagonal coordination of the uranyl moiety. One glycolate ion chelates the uranium atom as discussed above and is linked via the second carboxylate oxygen center to a neighboring uranium center. The second glycolate ion bridges between two adjacent uranyl moieties with one carboxylate oxygen bound to each uranyl. Thus, all carboxylate groups bind to two uranyl moieties. Uranyl complexation by glycolic and α–hydroxyisobutyric acid was investigated in solution at different pH values and uranyl : carboxylate ratios.[155] The corresponding EXAFS results at low pH values (pH 4–5) have been interpreted to represent a monodentate coordination of the glycolic ligand and bidentate coordination of the α-hydroxyisobutyric ligand. For higher pH values (pH 7–8) chelate coordination has been suggested in both cases, based on characteristic U-C distances of ~3.25 Å.[155] Speciation calculations indicate bis(carboxylato) complexes as dominant species under these conditions. For both pH regimes, similar $U\text{-}O_{eq}$ distances of 2.36–2.37 Å have been obtained with glycolic as well as α–hydroxyisobutyric acid. The corresponding coordination numbers suggest pentagonal coordination of the uranyl unit.[155]

In the following, chelate coordination will be discussed for the monoglycolate complex $[UO_2(OOCCH_2OH)(H_2O)_3]^+$. This complex allows a direct comparison between the three main coordination modes for complexes with the same substituent $R = CH_2OH$ of the carboxyl group $OOCR^-$ (Table 4.22). Deprotonation of the OH group will not be considered for the monocarboxylate complexes that are expected to be present at low pH; however, as discussed above, it might be relevant in chelate complexes at higher pH values. The corresponding computational results are presented in Table 4.22, the chelating bond to the OH group is designated by $U\text{-}O_h$ (Fig. 4.20c). To reach pentagonal coordination of the uranyl moiety, three explicit aqua ligands were added to the complex. Results are compared to those for the corresponding bidentate and monodentate glycolate complexes (Δbi and Δmono in Table 4.22). The corresponding optimized structures of all glycolate coordination modes are displayed in Fig. 4.23.

Solvent effects have been analyzed by explicit consideration of aqua ligands in the models (ΔH_2O), followed by a PCM treatment (ΔPCM). Coordination of aqua ligands distinctly elongates the distances $U\text{-}O_c$ (0.09 Å), $U\text{-}O_h$ (0.06 Å), and $U{=}O_t$ (0.03 Å) due to

bonding competition at the uranium center and leads to a reduced uranyl stretching frequency (by 50 cm^{-1}). These ΔH_2O increments are similar to previously discussed data obtained for bidentate and monodentate coordination (Table 4.22). Subsequent embedding in a PCM environment results in smaller corrections (ΔPCM, Table 4.22), except for the distinctly longer U-O_c bonds, by 0.08 Å. Long-range solvent effects result in an elongation of the distances U-O_c by 0.08 Å, U-C by 0.02 Å, and U=O_t by 0.01 Å. The uranyl stretching frequency is reduced by 18 cm^{-1}, concomitant with the slightly elongated uranyl bonds (Table 4.22). Distances U-O_w decreased by 0.07 Å and U-O_h by 0.03 Å.

The terminal uranium-oxygen distances U=O_t, 1.79 Å, agree well with the corresponding average experimental value, 1.79(1) Å.[155] The characteristic U-C distance (3.27 Å) matches the experimental value from solution (~3.25 Å). Discussion of the equatorial U-O distances is complicated: as for the monodentate complexes, only an average U-O_{eq} value is available. Although the U-O_{eq} value of 2.36 Å agrees well with experiment (~2.38 Å), comparison with the crystal structure data suggests the same distinct underestimation of individual equatorial U-O bonds (U-O_c by ~0.14 Å and U-O_h by 0.08 Å) that was observed for bidentate and monodentate complexes. Note that the reference crystal structure of $[UO_2(OOCCH_2OH)_2]$ exhibits two glycolate ligands which both act as bridges between adjacent uranyl moieties (see above).[157] Based on the higher coordination of the glycolates and the competition of two glycolate ligands at the uranium center, one expects longer U-O_c and U-O_h bonds in the crystal than in the monoglycolate complex. This may at least partially rationalize why the distances U-O_c and U-O_h are calculated shorter than these experimental values. Experimental data for bond lengths of aqua ligands are not available for chelate complexes. The calculated value of 2.38 Å is slightly shorter than the corresponding data from bidentate complexes (~2.40 Å).

Finally, results for the chelate coordination of the glycolate ligand will be compared with the other two coordination modes (Δbi and Δmono in Table 4.22). The order of U-O_c

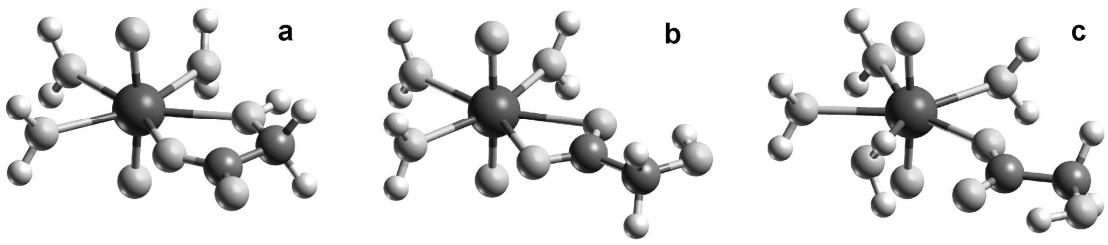

Figure 4.23. Optimized structures of uranyl monoglycolate complexes $[UO_2(OOCCH_2OH)(H_2O)_n]^+$ with chelate (a), bidentate (b), and monodentate (c) coordination of the carboxylate group and C_s symmetry constraints.

and U-C distances agrees qualitatively with experimental data from crystal structures (Table 4.22); as already discussed, it is not possible to directly compare to EXAFS data from solution because the resolution of different equatorial U-O distances is problematic. The U-O_c distances follow the order bidentate >> monodentate > chelate. The calculated bidentate glycolate complex yields by far the longest U-O_c bond, ~0.15 Å longer than determined for the corresponding monodentate and chelate structures. This can be rationalized by the fact that in the bidentate complex the carboxylate group coordinates via two competing U-O_c bonds. Thus, the U-O_c bonds are calculated longer than the strong single U-O_c bond in the monodentate and chelate complexes (Fig. 4.23). The latter complexes show comparable U-O_c values, but in the monodentate the distance is 0.02 Å longer. The corresponding U-C distances exhibit the ordering bidentate << chelate < monodentate. The coordination via both carboxylate oxygen centers of the bidentate complex brings the carbon center of the glycolate group closer to the uranyl moiety than for the other two coordination modes (Fig. 4.23). Thus, the corresponding U-C distance is the shortest of all complexes (Table 4.22). On the other hand, the single U-O_c bond in the monodentate complex allows more freedom for the orientation of the carboxylate carbon center and leads to a longer U-C distance (Fig. 4.23). In contrast to the monodentate complex, the orientation of the glycolate ligand in the chelate complex is restricted by the formation of the chelating U-O_h bond (Fig. 4.23).

The shortening (hence strengthening) of the U-O_c bonds when going from chelate to monodentate to bidentate coordination results in a weakening of the corresponding U=O_t bonds (longer by 0.01 Å in total) and thus in a larger uranyl stretching frequency, by 17 cm^{-1} in total (Table 4.22). The uranyl bonds of all complexes (1.78–1.79 Å) agree well with experiment, but do not provide a suitable criterion for distinguishing between the various coordination modes (Table 4.22). The average U-O_{eq} distance of 2.36 Å is calculated somewhat shorter for the chelate complex than for the monodentate complex (by 0.016 Å), in line with the experimental difference (~0.01 Å). However, the significantly longer U-O_{eq} distance suggested by experiment for bidentate coordination (2.42 Å) is not reproduced by the calculations (2.37 Å). In fact, the bidentate U-O_{eq} value is comparable to those of chelate and monodentate complexes.

Comparison of calculated structures of the uranyl monocarboxylates and EXAFS data reveals significant differences, in particular the underestimation of the actinyl carboxylate bonds for all three coordination modes investigated. In addition, the obtained average U-O_{eq} distances do not allow a differentiation between the different coordination modes, at variance with experimental suggestions. In Section 4.4.4 these discrepancies to the experimental data will be critically examined.

Energetics

Supplementing the structural discussion, energetic aspects of uranyl monocarboxylate species of the three different coordination modes will now be considered. Bidentate (bi, with n = 3 aqua ligands), monodentate (mono, n = 4), and chelate (chel, n = 3) complexes will be compared, preserving the equatorial coordination number of uranyl at five. This comparison will be based on energy changes during formal reactions that will permit one to estimate the strength of metal-ligand bonds. The primary goal is a qualitative differentiation between the different coordination modes as a quantitative energetic discussion is rather difficult and demanding for various reasons, e.g. due to the difficulty to describe the extended hydration spheres of all species involved. As before, long-range solvation effects were modeled via PCM and the aqua ligands of the uranyl moiety were treated explicitly, because they are moderately strongly bound; weaker hydrogen bonds were neglected.

As a rough measure of metal-ligand bonding in uranyl monocarboxylate complexes, the ligand abstraction energies ΔE_{carb} of the carboxylate ligand, Eq. (4.11), and ΔE_{aqua} of the aqua ligands, Eq. (4.12), have been calculated (Table 4.23).

$$[UO_2(OOCR)(H_2O)_n]^+ \rightarrow [UO_2(H_2O)_n]^{2+} + [RCOO]^- \quad (4.11)$$

$$[UO_2(OOCR)(H_2O)_n]^+ \rightarrow [UO_2(OOCR)]^+ + n\,H_2O \quad (4.12)$$

Table 4.23. Ligand abstraction energies ΔE_{carb}, Eq. (4.11), and ΔE_{aqua}, Eq. (4.12), (in kJ mol^{-1}) of complexes $[UO_2(OOCR)(H_2O)_n]^+$ for bidentate (bi, n = 3), monodentate (mono, n = 4), and chelate (chel, n = 3) coordination. Results are given for systems in the gas phase (GP) and for PCM solvation models, applying the GGA-BP exchange-correlation functional in single-point fashion at the LDA-VWN optimized structures.

	R	ΔE_{carb}		ΔE_{aqua}	
		GP	PCM	GP	PCM
bi	H	1128	203	414	249
	CH_3	1157	225	395	241
	CH_2CH_3	1151	223	390	238
	CH_2OH	1074	186	404	249
mono	H	975	130	527	302
	CH_3	994	144	513	296
	CH_2CH_3	990	143	509	296
	CH_2OH	923	117	523	310
chel	CH_2OH	1057	192	384	237

For the gas phase (GP) as well as in solution (PCM), the carboxyl abstraction energies ΔE_{carb} confirm that formiate and glycolate bind weaker than acetate and propionate as inferred from the longer U-O_c distances (Table 4.22). This finding is related to the fact that electron donation is stronger by alkyl substituents than by H. The electron donation from the glycolate ligand to the uranyl moiety is weaker because of the OH group which exhibits a negative inductive effect. Thus, glycolate complexes feature the lowest ligand abstraction energies in the series. The unfavorable charge separation in the gas phase, Eq. (4.11), results in high ΔE_{carb} values for bidentate, ~1150 kJ mol^{-1}, and monodentate carboxyl ligands, ~1000 kJ mol^{-1}. In bidentate and monodentate coordination, the glycolate ligand is less strongly bound (by ~75 kJ mol^{-1}) than the corresponding aliphatic ligands; chelate coordination (1057 kJ mol^{-1}) is comparable to bidentate coordination (1074 kJ mol^{-1}). When including a PCM treatment the abstraction energies are distinctly reduced, ΔE_{carb} for monodentate aliphatic carboxylates is estimated at ~140 kJ mol^{-1} and noticeably higher for bidentate complexes, ~220 kJ mol^{-1}. Thus, differences of ΔE_{carb} between bidentate and monodentate coordination are considerably smaller in aqueous solution (70–80 kJ mol^{-1}). In comparison to the aliphatic ligands the glycolate ligand is bound weaker by about 25 kJ mol^{-1} both for mono- and bidentate complexes. In solution the chelate coordination shows the highest ligand abstraction energy (192 kJ mol^{-1}) within the three glycolate coordination modes at variance to the gas phase where the bidentate coordination is favored (Table 4.23).

Solvation effects also reduce the abstraction energy of the aqua ligands. One estimates the average binding energy per such ligand at 80 kJ mol^{-1} for bidentate and chelate and at 75 kJ mol^{-1} for monodentate carboxyl coordination (ΔE_{aqua}, Table 4.23). The presented data suggest that complexes which exhibit different coordination modes are expected to be comparable in energy. Assuming the same coordination number (five) for all models, then the energy gain of ~70–80 kJ mol^{-1} in case of bidentate and chelate carboxylate coordination is essentially compensated by the loss of one aqua ligand bond (~80 kJ mol^{-1}) in these complexes compared to the monodentate complexes.

To further examine the stability of the different coordination modes, the fragmentation (ΔE_{frag}) of the solvated complexes into uranyl, carboxylate, and aqua ligands is investigated according to the following transformation (Table 4.24):

$$[UO_2(OOCR)(H_2O)_n]^+ \rightarrow [UO_2]^{2+} + [RCOO]^- + n\,H_2O \qquad (4.13)$$

All complexes are stable with respect to fragmentation both in the gas phase and in aqueous solution. In the gas phase, due to the unfavorable charge separation, Eq. (4.13), fragmentation energies are very large: ~1960 kJ mol^{-1} for bidentate aliphatic complexes

Table 4.24. Fragmentation energies ΔE_{frag}, Eq. (4.13), and ligand substitution energies ΔE_{sub}, Eq. (4.14), (in kJ mol^{-1}) of complexes $[UO_2(OOCR)(H_2O)_n]^+$ for bidentate (bi, n = 3), monodentate (mono, n = 4), and chelate (chel, n = 3) coordination. Results are given for calculations in the gas phase (GP) and with PCM solvation models, applying the GGA-BP exchange-correlation functional in single-point fashion at the LDA-VWN optimized structures.

	R	ΔE_{frag}		ΔE_{sub}	
		GP	PCM	GP	PCM
bi	H	1940	595	-835	-75
	CH_3	1970	617	-864	-97
	CH_2CH_3	1964	615	-858	-95
	CH_2OH	1886	579	-781	-58
mono	H	1970	602	-865	-82
	CH_3	1989	616	-883	-96
	CH_2CH_3	1985	615	-879	-95
	CH_2OH	1918	590	-812	-69
chel	CH_2OH	1869	585	-764	-64

and ~1980 kJ mol^{-1} for the corresponding monodentate complexes. These energies are reduced by about 70 kJ mol^{-1} for glycolate due to the lower ligand binding energies discussed previously (Table 4.23). Again, the formiate complex is calculated slightly less stable than the complexes with larger carboxyl substituents. In solution (PCM treatment), the fragmentation energies drop to about one third of the GP values: ~610 kJ mol^{-1} for bi- and monodentate aliphatic complexes. This reduction can be rationalized by the large solvation energy of the small, charged uranyl moiety (-1245 kJ mol^{-1}) which stabilizes the fragmentation products. Solvation of the carboxylate ion (~ -270 kJ mol^{-1}) contributes to a smaller extent. The rather weak preference of monodentate coordination obtained in the gas phase vanishes for the aliphatic complexes if solvation is taken into account. The three coordination modes of glycolate exhibit also very similar fragmentation energies that differ only within ~10 kJ mol^{-1} (Table 4.24). Thus, one is lead to conclude that, irrespective of the coordination mode, the uranyl binding capacity is comparable if one assumes the same coordination number. This finding corroborates the preceding analysis of ligand abstraction energies.

Finally, the competition between aqua and carboxylate ligands is examined via the formal substitution of aqua ligands of the solvated uranyl ion $[UO_2(H_2O)_5]^{2+}$ by a carboxylate ligand:

$$[UO_2(H_2O)_5]^{2+} + [RCOO]^- \rightarrow [UO_2(OOCR)(H_2O)_n]^+ + (5–n)\ H_2O \qquad (4.14)$$

The corresponding reaction energies ΔE_{sub} are also listed in Table 4.24. For all complexes considered, the formation of monocarboxylate species via substitution of aqua by carboxylate ligands is favored, in agreement with the known complexing propensity of carboxylate ligands in aqueous solution.[78] In the gas phase, substitution energies ΔE_{sub} are much larger (by absolute value), about -845 kJ mol^{-1} for bidentate aliphatic complexes and about -875 kJ mol^{-1} for the corresponding monodentate complexes; the glycolate complexes again yield somewhat reduced substitution energies, by ~65 kJ mol^{-1}. Substitution is strongly exothermic because oppositely charged moieties are combined. In aqueous solution, the reactants are strongly stabilized, hence the reaction energies are significantly smaller (by absolute value), 80–90 kJ mol^{-1} for bi- and monodentate aliphatic and about 60–70 kJ mol^{-1} for glycolate complexes. Once again, the slight preference for monodentate coordination, calculated for the gas phase, vanishes in solution. The ligand substitution energies of the three glycolate coordination modes agree within ~10 kJ mol^{-1}.

Note the rather similar values of the substitution energy for complexes with different carboxylate coordination modes (Table 4.24), despite the fact that an additional aqua ligand is released for bidentate and chelate complexes. Therefore, in aqueous solution, there is no clear energetic preference for any of the three coordination modes when solvation effects are taken into account. This conclusion holds under the assumption that pentagonal coordination of uranyl prevails for all complexes. One expects a slight thermodynamic preference for bidentate and chelate coordination when zero point energies and entropy effects are taken into account (see Section 4.4.4).

4.4.3 Neptunyl(VI) and neptunyl(V) monocarboxylates, $[NpO_2(OOCR)]^{+/0}$

In this section the investigation of actinyl monocarboxylates will be extended to Np(VI) and Np(V). The same models as for the corresponding uranyl(VI) complexes in Section 4.4.2 have been used. Also solvent effects have been accounted for in the same fashion, by adding explicit aqua ligands with subsequent PCM treatment. Results for mono- and bidentate carboxylate coordination will be compared to U(VI) data and experimental data if available.

Structures of neptunyl(VI) monocarboxylates

In Table 4.25 the computational results of the neptunyl(VI) monocarboxylates $[NpO_2(OOCR)(H_2O)_n]^+$, R = H, CH_3, and CH_2CH_3, are given for bidentate (n = 3) and monodentate (n = 4) coordination. Structural parameters of the neptunyl(VI) complexes differ only slightly among the various residues R, for either coordination type (Table 4.25): differences are minor for Np=O_t (up to 0.004 Å) as well as for Np-C, Np-O_w, and Np-O_{eq} (up to 0.01 Å); the largest changes are obtained for Np-O_c (up to 0.025 Å). This is in line with trends observed for the corresponding uranyl(VI) complexes (see Section 4.4.2). Among the three residues, formiate complexes again are somewhat peculiar, with the shortest Np=O_t and the longest Np-O_c bonds of the series. This indicates a weaker bonding of the carboxylate group for R = H, confirmed by an energy analysis (see below).

Characteristic differences between the two coordination modes are identical to those found for U(VI) monocarboxylates. The monodentate complexes feature a short Np-O_c bond (~2.18 Å) and a longer Np-C distance (~3.38 Å). As expected, the carboxylate ligand in the bidentate case exhibits an elongated Np-O_c bond (~2.36 Å) and a reduced Np-C distance (~2.77 Å). The neptunyl bond Np=O_t (~1.77 Å) and the Np-O_{eq} distance (2.35–2.36 Å) do not differ much between the two coordination modes.

Overall, results are very similar to the previously discussed uranyl(VI) complexes. For both coordination modes all pertinent distances are slightly shorter, by ~0.02 Å, than those of the corresponding uranyl(VI) complexes (ΔU(VI) in Table 4.25). This trend is expected from the actinide contraction (see Section 2.1.1) and agrees very well with the experimentally found reduction of the actinyl bond An=O_t, by 0.02 Å, for solvated actinyls from U(VI) to Np(VI) (see Section 4.1, Table 4.2).[68,79,229–231] In line with the weaker neptunyl bonds the neptunyl stretching frequency is increased in the bidentate case by ~30 cm^{-1}, whereas the effect in the monodentate case is quite weak (2 cm^{-1}). The similarities between Np(VI) and U(VI) point to a fairly similar bonding of both hexavalent actinides. This is rationalized by the fact that the additional *f* electron in Np(VI) is very localized in an Np 5*f* orbital and is not involved in the neptunyl bond. This analysis is corroborated by the results for solvated actinyl(VI) complexes (see Section 4.1) and previous theoretical studies on bare actinyls(VI) $[AnO_2]^{2+}$ and actinide hexafluorides AnF_6.[54,236]

Structural experimental data of neptunyl(VI) carboxylate complexes are not available. The dominant oxidation state of neptunium is V (see Section 2.1.1). To allow some evaluation of the calculated data, the comparison is based on experimental data for U(VI) carboxylates which are expected to exhibit comparable features as the

Table 4.25. Calculated interatomic distances (in Å) and symmetric neptunyl stretching frequency ν_s (in cm^{-1}) of neptunyl(VI) monocarboxylates $[NpO_2(OOCR)(H_2O)_n]^+$ exhibiting bidentate (bi, n = 3) and monodentate (mono, n = 4) carboxylate coordination Experimental data for U(VI) are also shown as well as averaged (avg.) results for Np(VI) and U(VI) monocarboxylates for all residues R. Differences ΔU(VI) are given with respect to U(VI) data from Table 4.22. For the designations of atoms, see Fig. 4.20a.

	R	Np=O_t	Np-O_c	Np-C	Np-O_w	Np-O_{eq}	ν_s
bi	H	1.763	2.376	2.751	2.333	2.350	873
	CH_3	1.766	2.351	2.752	2.340	2.345	899
	CH_2CH_3	1.767	2.353	2.752	2.337	2.346	892
Exp.	U(VI) sol.[a]	1.78(1)	2.46(4)	2.87(4)	2.40(4)	2.42(4)	–
	U(VI) cryst.[b]	1.76(3)	2.48(5)	2.86(5)	2.36(4)	2.42(6)	–
	Np(VI) avg.	1.77	2.36	2.75	2.34	2.35	888
	U(VI) avg.	1.79	2.38	2.77	2.36	2.37	857
	ΔU(VI)	-0.02	-0.02	-0.02	-0.02	-0.02	31
mono	H	1.765	2.194	3.373	2.398	2.357	856
	CH_3	1.768	2.174	3.380	2.401	2.356	848
	CH_2CH_3	1.768	2.172	3.381	2.402	2.356	847
Exp.	U(VI) sol.[a]	1.78(1)	–	–	–	2.38(4)	–
	U(VI) cryst.[b]	1.76(3)	2.39(5)	3.5(1)	2.42(6)	2.36(2)	–
	Np(VI) avg.	1.77	2.18	3.38	2.40	2.36	850
	U(VI) avg.	1.79	2.21	3.40	2.42	2.38	848
	ΔU(VI)	-0.02	-0.03	-0.02	-0.02	-0.02	2

[a] Average values from Refs. 79, 151, 155. [b] Average values from Refs. 150, 151, 160.

corresponding Np(VI) species. This conclusion is corroborated by theoretical and experimental data on solvated actinyl(VI) complexes $[An(H_2O)_n]^{2+}$ (Section 4.1, Table 4.2).

Due to the minor differences between results calculated for Np(VI) and U(VI) species (Table 4.25), the main deviations to experiment remain the same as discussed for uranyl(VI) carboxylates (see Section 4.4.2). These deviations relate to the neptunyl carboxylate bond Np-O_c which is distinctly underestimated, by about 0.1 Å for bidentate and 0.2 Å for monodentate coordination compared to the experimental U(VI) data; the corresponding Np-C distance is also too short by about 0.1 Å. In addition, the calculations do not reproduce that the equatorial Np-O_{eq} distance is longer for bidentate than for monodentate coordination, as suggested by experiment.

Structures of neptunyl(V) monocarboxylates

Now the study will be extended to the corresponding monocarboxylates $[NpO_2(OOCR)(H_2O)_n]$, R = H, CH_3, and CH_2CH_3, of neptunyl(V). Np(V) systems can exhibit a triplet or singlet ground state configuration. Spin-polarized calculations were carried out for both spin states by fixing the number of unpaired electrons in the optimizations. Spin contamination was less than ~1% for both configurations. The singlet states of the Np(V) complexes are less stable by about 43 kJ mol^{-1} for bidentate and 23 kJ mol^{-1} for monodentate complexes. The singlet states exhibit a closed shell configuration where the HOMO is of pure Np *f* character. The corresponding triplet states result from the excitation of one electron from this HOMO to occupy the LUMO that is also of Np *f* character. This analysis agrees with results found for solvated neptunyl(V) complexes in Section 4.1. The following discussion will only focus on the more stable triplet states.

The general trends observed for the corresponding U(VI) and Np(VI) complexes remain. Structures of the neptunyl(V) complexes vary slightly for the different residues R (Table 4.26). Differences of bond distances are somewhat more pronounced for bidentate (0.01–0.03 Å) than for monodentate coordination (0.01–0.02 Å). As before, the formiate complex exhibits the shortest Np=O_t and longest Np-O_c bonds of the series. The expected weaker bonding for R = H is confirmed by the energetic evaluations (see below).

However, in contrast to the minor differences between U(VI) and Np(VI) complexes, changes in the structures between Np(V) and Np(VI) monocarboxylates are much more pronounced. This can be rationalized by the reduced charge and the changes of the neptunyl bonding between $[NpO_2]^{2+}$ and $[NpO_2]^{+}$ as discussed in Section 4.1 for solvated neptunyls $[NpO_2(H_2O)_n]^{2+/+}$. The Np(V) monocarboxylates show longer distances than the corresponding Np(VI) complexes. For both coordination modes, the strong neptunyl bonds Np=O_t increase by 0.05 Å, the carboxylate distances Np-O_c by ~0.1 Å and the distance Np-C by ~0.08 Å; the distances Np-O_w and Np-O_{eq} are also longer, by about 0.10 Å for bidentate and 0.07 Å for monodentate coordination. These significant differences are in line with changes observed between crystal structures of uranyl(VI) and neptunyl(V) carboxylates (Tables 4.25, 4.26) as well as with EXAFS data of neptunyl(VI) and neptunyl(V) in solution (see Section 4.1, Table 4.2). The weakening of the neptunyl bond is accompanied by a strong reduction of the neptunyl stretching frequency, by about 110 cm^{-1} for bidentate and 80 cm^{-1} for monodentate coordination.

Experimental data for neptunyl(V) carboxylate complexes are scarce. Formation of neptunyl monocarboxylate complexes in solution is confirmed for acetate and oxalate.[252,253] Structural data are limited to some crystal structures. Based on a summary of

Table 4.26. Calculated interatomic distances (in Å) and symmetric neptunyl stretching frequency ν_s (in cm^{-1}) of neptunyl(V) monocarboxylates $[NpO_2(OOCR)(H_2O)_n]$ exhibiting bidentate (bi, n = 3) and monodentate (mono, n = 4) carboxylate coordination. Also shown are experimental data for Np(V) as well as averaged (avg.) results for Np(V) and Np(VI) monocarboxylates for all residues R. Differences ΔNp(VI) are given with respect to the data for Np(VI) from Table 4.25. For the designations of atoms, see Fig. 4.20a.

	R	Np=O_t	Np-O_c	Np-C	Np-O_w	Np-O_{eq}	ν_s
bi	H	1.818	2.470	2.822	2.408	2.433	771
	CH_3	1.821	2.445	2.819	2.417	2.428	770
	CH_2CH_3	1.830	2.441	2.815	2.449	2.446	778
Exp.	Np(V) cryst.[a]	1.85(3)	2.59(8)	2.94(4)	2.47(7)	2.55(2)	–
	Np(V) avg.	1.82	2.45	2.82	2.42	2.42	773
	Np(VI) avg.	1.77	2.36	2.75	2.34	2.35	888
	ΔNp(VI)	0.05	0.09	0.07	0.08	0.07	-115
mono	H	1.820	2.328	3.442	2.454	2.429	773
	CH_3	1.822	2.310	3.446	2.457	2.428	769
	CH_2CH_3	1.822	2.316	3.451	2.459	2.430	769
Exp.	Np(V) cryst.[a]	1.84(2)	2.45(2)	–	2.47(7)	2.47(2)	–
	Np(V) avg.	1.82	2.32	3.45	2.46	2.43	770
	Np(VI) avg.	1.77	2.18	3.38	2.40	2.36	850
	ΔNp(VI)	0.05	0.14	0.07	0.06	0.07	-80

[a] Ref. 143.

data from several neptunyl(V) carboxylate crystal structures in Ref. 143, average distances for bidentate and monodentate coordination modes are given in Table 4.26. One has to consider, that most of the crystals exhibit a mixture of bidentate, monodentate, and bridging carboxylates. In addition, a direct comparison of these data to the computational results in solution is problematic due to packing effects that occur only in the crystals.

Comparison to averaged crystal structure data indicates that the two main differences to experiment are of the same size as those found for U(VI) and Np(VI) monocarboxylates. The neptunyl carboxylate distances Np-O_c and Np-C are distinctly underestimated by more than 0.1 Å for both coordination modes. Furthermore, the elongated Np-O_{eq} distance suggested for bidentate complexes from experiment (~0.08 Å) is calculated only slightly longer than in the monodentate complexes (by ~0.02 Å). The subsequent Section 4.4.4 will address these rather pronounced deviations from the experimental data.

Energetics

The calculated ligand substitution energies ΔE_{sub}, Eq. (4.14) are chosen to compare energetic trends for U(VI), Np(VI), and Np(V) monocarboxylates (Table 4.27). The structural resemblance between Np(VI) and U(VI), discussed above, is reflected in very similar substitution energies of all corresponding U(VI) and Np(VI) complexes; they differ at most by 6 kJ mol^{-1} (Table 4.27). As already seen for U(VI) monocarboxylates, both carboxylate coordination modes are also energetically comparable in the Np(VI) complexes. The replacement of aqua ligands by carboxylates requires ~89 kJ mol^{-1} for bidentate and ~93 kJ mol^{-1} for monodentate coordination. As indicated during the discussion of the structures, the formiate complexes (R = H) exhibit the smallest ligand replacement energies in the series (Table 4.27).

Substitution energies are significantly lower for Np(V) complexes, by ~54 kJ mol^{-1} for bidentate and ~63 kJ mol^{-1} for monodentate complexes. This can be rationalized by the reduced charge of neptunyl(V) monocarboxylates. The formiate complexes again show the smallest ΔE_{sub} values of all species.

Table 4.27. Ligand substitution energies ΔE_{sub} (in kJ mol^{-1}), Eq. 4.14, of actinyl(VI) and actinyl(V) monocarboxylates $[AnO_2(OOCR)(H_2O)_n]^{+/0}$ for bidentate (bi, n = 3) and monodentate (mono, n = 4) coordination. Results are given for calculations with PCM solvation models, applying the GGA-BP exchange-correlation functional in single-point fashion at the LDA-VWN optimized structures. Also given are differences ΔU(VI) and ΔNp(VI) with respect to corresponding U(VI) and Np(VI) results, respectively.

		ΔE_{sub}	
An	R	bi	mono
U(VI)	H	-75	-82
	CH3	-97	-96
	CH2CH3	-95	-95
Np(VI)	H	-74	-88
	CH3	-95	-94
	CH2CH3	-98	-95
	ΔU(VI) avg.	0	-2
Np(V)	H	-27	-25
	CH3	-40	-30
	CH2CH3	-39	-36
	ΔNp(VI) avg.	54	63

In summary, the hexavalent neptunyl(VI) and uranyl(VI) monocarboxylates exhibit very similar structural and energetical features, whereas the pentavalent Np(V) complexes are characterized by significantly longer distances and reduced ligand substitution energies. Structural parameters do not vary much for different residues R.

The main difference between bidentate and monodentate coordination is related to the actinyl carboxylate distances An-O_c and An-C, where the trends of calculated quantities qualitatively agree with the corresponding experimental data. Both coordination modes exhibit a similar stability independent of the actinide and oxidation state. Comparison to experiment reveals significant discrepancies due to an underestimation of the actinyl carboxylate bonds for all three investigated actinides U(VI), Np(VI), and Np(V). In the next section these deviations will be critically discussed.

4.4.4 Discussion of discrepancies to experimental data

The discrepancies between calculated structures of uranyl monocarboxylate complexes and EXAFS data, as just described, are rather large and noteworthy if one recalls the overall good agreement of density functional results for other uranyl complexes with experimental structure data,[19,43,55] including the benchmark system uranyl triacetate (see Section 4.4.1). The following discussion presents a summary how calculated results for uranyl monocarboxylates differ from experimental data for uranyl carboxylates. The critical discussion examines on the one hand limitations of the computational model approach employed. More advanced example calculations are used to shed light on various model aspects. On the other hand, the experimental situation also has to be discussed regarding accuracy and uncertainties. The discussion will focus on the two main types of carboxylate complexation, bidentate and monodentate coordination. Chelate coordination is excluded because experimental data are limited; however, many aspects of the discussion also apply to this coordination mode.

The main deviation from experimentally based information is related to the uranyl carboxylate U-O_c distances. These distances are calculated too short by about 0.2 Å for monodentate and 0.1 Å for bidentate complexes (see Table 4.22). Note, however, that the experimental value for the monodentate case refers to a crystalline system where uranyl is coordinated by more than one carboxylate ligand. Moreover, separation of equatorial U-O distances into different shells is not easy by EXAFS spectroscopy if bond distances are very similar.[250] Calculated and experimentally derived U-C distances differ by up to 0.1 Å for either coordination mode; the calculations again yield shorter values. On the other hand, uranyl bonds U=O_t as well as uranyl-aqua distances U-O_w agree well with

experiment. Yet, the averaged value U-O_{eq} satisfactorily matches experiment only for monodentate complexes. For bidentate complexes, the calculations underestimate this quantity by ~0.05 Å. Thus, the longer distance U-O_{eq}, suggested by experiment for bidentate coordination, is not reproduced by the calculations. This latter discrepancy is somewhat larger than the experimental error bars. The more pronounced differences calculated for the uranyl-carboxylate distances U-O_c and U-C are obviously outside experimental uncertainties.

Symmetry restrictions

Probably the most important approximation of this study is the use of C_s-symmetric models that restrict the free orientation of the aqua ligands and might hinder the formation of hydrogen bonds within the ligand shell. Thus, the role of these symmetry restrictions was examined by optimizations without symmetry constraints. The corresponding results for the uranyl monocarboxylate complexes $[UO_2(OOCR)(H_2O)_n]^+$, R = H, CH_3, and CH_2CH_3, are given in Table 4.28.

Re-optimization of the *bidentate* coordinated species resulted in minor changes only compared to results of previous calculations with C_s-symmetric models (ΔC_s in Table 4.28). Average deviations of bond lengths for all complexes are less than 0.01 Å. The orientation of the aqua ligands does not change and thus no hydrogen bonds, "internal" to the ligand sphere, are formed (Figs. 4.24a,c). The rather small structural relaxations are

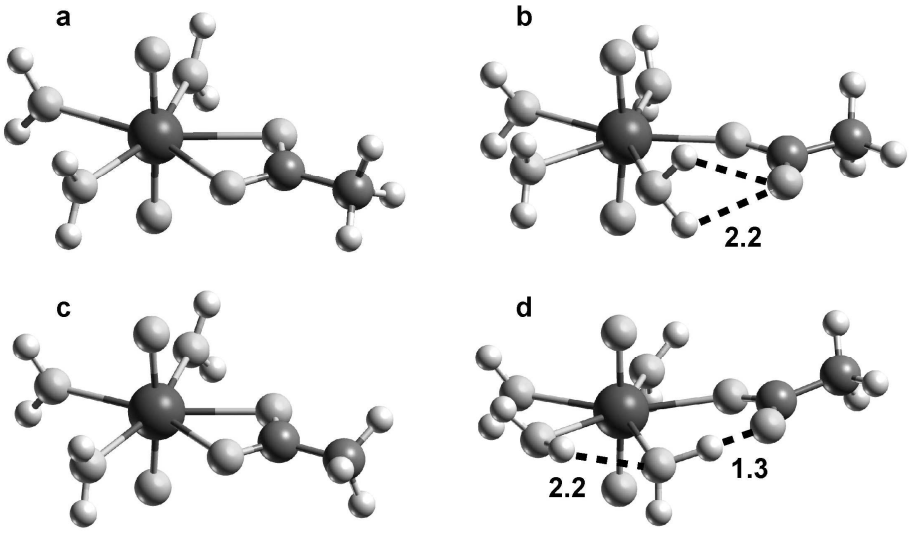

Figure 4.24. Optimized structures of uranyl monoacetate $[UO_2(OOCCH_3)(H_2O)_n]^+$ exhibiting bidentate (bi, n = 3) and monodentate (mono, n = 4) carboxylate coordination for different symmetries: (a) C_s, bi; (b) C_s, mono; (c) C_1, bi; (d) C_1, mono. Also shown are calculated O···H distances (Å) of hydrogen bonds that are formed within the ligand sphere.

also reflected in the negligible stabilization of the complexes, about 2 kJ mol^{-1}. Thus, the use of C_s models is perfectly justified for bidentate coordination.

As expected, stronger effects are found for the *monodentate* case, but they neither deteriorate nor improve the overall agreement with experiment in a significant fashion. The changes are due to a rotation of the aqua ligand adjacent to the uncoordinated carboxylate oxygen $O_{c'}$ (Figs. 4.24b,d). A pseudobridging coordination results which shows a hydrogen bond to the $O_{c'}$ center (Fig. 4.24d). This new "internal" H bond is expected to be of moderate strength based on the H···$O_{c'}$ distance of ~1.3 Å, the O_w-H···$O_{c'}$ angle of ~170°,

Table 4.28. Calculated interatomic distances (in Å) and symmetric uranyl stretching frequency ν_s (in cm^{-1}) of uranyl(VI) monocarboxylates $[UO_2(OOCR)(H_2O)_n]^+$ exhibiting bidentate (bi, n = 3) and monodentate (mono, n = 4) carboxylate coordination without symmetry constraints, compared to experimental data for aqueous solution (sol.) and crystals (cryst.). Solvent effects are included via n explicit aqua ligands and a PCM treatment. Relative stabilities (ΔE) are given with respect to total energies of C_s-symmetric models as reference. Also presented are average differences (ΔC_s) with respect to the corresponding data of models with C_s symmetry (Table 4.22). For the designations of atoms, see Fig. 4.20.

	R	U=O_t	U-O_c	U-C	U-O_w	U-O_{eq}	ΔE
bi	H	1.783	2.393	2.767	2.354	2.369	0
	CH_3	1.786	2.371	2.772	2.365	2.367	-3
	CH_2CH_3	1.787	2.371	2.769	2.366	2.368	-1
	ΔC_s	<0.01	<0.01	<0.01	<0.01	<0.01	-2
Exp.	CH_3 sol.[a]	1.78(1)	2.50(2)	2.91(2)	2.38(2)	2.43(2)	
	sol.[b]	1.78(1)	2.46(4)	2.87(4)	2.40(4)	2.42(4)	
	cryst.[c]	1.76(3)	2.48(5)	2.86(5)	2.36(4)	2.42(6)	
mono	H	1.786	2.290	3.341	2.394	2.373	-31
	CH_3	1.789	2.291	3.352	2.382	2.364	-28
	CH_2CH_3	1.790	2.287	3.333	2.383	2.364	-30
	ΔC_s	<0.01	0.08	-0.06	-0.03	-0.01	-30
Exp.	sol.[b]	1.78(1)	–	–	–	2.38(4)	
	cryst.[c]	1.76(3)	2.39(5)	3.5(1)	2.42(6)	2.36(2)	

[a] Refs. 97, 98, 151. [b] Average values from Refs. 79, 151, 155. [c] Average values from Refs. 150, 151, 160.

and the stabilization of the monodentate complexes by about 30 kJ mol^{-1}.[235] Concomitantly, the U-O_c bond elongates significantly by ~0.08 Å and the U-C as well as U-O_w distances decrease by ~0.06 Å and 0.03 Å, respectively. These changes decrease the underestimation of the U-O_c bond for monodentate coordination from 0.2 Å (Table 4.22) to about 0.1 Å, but also slightly worsen the agreement for U-C. The average distance U-O_{eq} decreases by 0.01 Å only; the resulting value of 2.36 Å still agrees well with the experimental value of 2.38 Å (Table 4.28), but it is only slightly shorter than the value of the corresponding bidentate complex (2.37 Å). Thus, also without symmetry constraints the main deviations to experiment with respect to U-O_c and U-O_{eq} remain.

Gibbs free energies

The previously presented energetical data (see Section 4.4.2) need to be reevaluated because of the significant stabilization of monodentate in contrast to bidentate complexes. The substitution reaction from Eq. (4.14), in which aqua ligands of the solvated uranyl ion $[UO_2(H_2O)_5]^{2+}$ are replaced by carboxylate ligands, is chosen as criterion to study various relaxation effects. In addition, thermodynamic corrections to the ligand substitution energies ΔE_{sub} are included in Table 4.29. The equations to calculate the corresponding enthalpies ΔH_{sub} and Gibbs free energies ΔG_{sub} are summarized in Appendix B. Based on Eq. (4.14), zero-point energy contributions were calculated using the normal modes of all species after re-optimization without symmetry constraints. The normal mode analyses confirmed the obtained minima in all cases. To avoid the demanding frequency calculation

Table 4.29. Ligand substitution energies ΔE_{sub}, enthalpies ΔH_{sub}, and Gibbs free energies ΔG_{sub} (in kJ mol^{-1}) of complexes $[UO_2(OOCR)(H_2O)_n]^+$ calculated according to Eq. (4.14) for bidentate (bi, n = 3) and monodentate (mono, n = 4) coordination for models without symmetry constraints. Results are given for calculations in the gas phase (GP) and with PCM solvation models, applying the GGA-BP exchange-correlation functional in single-point fashion at the LDA-VWN optimized structures.

	R	ΔE_{sub}		ΔH_{sub}		ΔG_{sub}	
		GP	PCM	GP	PCM	GP	PCM
bi	H	-832	-72	-839	-79	-867	-107
	CH_3	-861	-91	-868	-98	-902	-132
	CH_2CH_3	-859	-91	-861	-93	-901	-133
mono	H	-901	-110	-905	-114	-896	-104
	CH_3	-926	-121	-930	-125	-916	-111
	CH_2CH_3	-921	-122	-921	-123	-910	-112

for the PCM models, frequencies calculated for corresponding GP models were used as approximations instead. This approximation is justified as the changes of frequencies expected between the GP and PCM models are rather small. For instance, full frequency calculations for GP and PCM models of $[UO_2(H_2O)_5]^{2+}$ show differences between corrsponding frequencies of about 40 cm^{-1} on average. These differences are comparable to those obtained for the uranyl stretching frequency of uranyl monocarboxylates (18–23 cm^{-1}, Table 4.22). Analysis of thermodynamic data for $[UO_2(H_2O)_5]^{2+}$ indicates that the enthalpy changes by 1–2 kJ mol^{-1} and the Gibbs free energy by up to 5 kJ mol^{-1} when the evaluation is based on PCM instead of GP frequencies. Thus, the trends of the energies discussed below should not be affected, especially if the calculation of substitution energies, Eq. (4.14), benefits from some error cancellation.

Comparing ligand substitution energies ΔE_{sub} with previous calculations (Table 4.24) one notices only minor changes for bidentate coordination both for GP and PCM models, up to 6 kJ mol^{-1}. This is in line with the negligible relaxation effects. However, the monodentate complexes are distinctly stabilized due to the formation of the internal hydrogen bonds, by ~40 kJ mol^{-1} for GP and ~27 kJ mol^{-1} for PCM models. Thus, in contrast to the previous results for models with symmetry constraints, the monodentate coordination is favored both for GP (~65 kJ mol^{-1}) and PCM models (~33 kJ mol^{-1}) based on total energies; this preference is most pronounced for the uranyl formiate complex (R = H, Table 4.29).

Inclusion of zero-point energies and thermal corrections to determine the corresponding substitution enthalpies ΔH_{sub} slightly stabilizes both bidentate and monodentate complexes compared to ΔE_{sub} (up to 7 kJ mol^{-1}, Table 4.29). The stabilization is a little larger in the bidentate case and therefore reduces the preference to the monodentate coordination.

Finally, entropy effects were considered for the evaluation of the Gibbs free energies ΔG_{sub}. They lead to a significant stabilization of the bidentate coordination by ~30 kJ mol^{-1} for R = H and R = CH_3 and ~40 kJ mol^{-1} for R = CH_2CH_3. In contrast, the monodentate complexes are somewhat destabilized, by ~10–15 kJ mol^{-1}. These different effects can be rationalized by considering Eq. (4.14). In the bidentate case (n = 3) the carboxylate ligand occupies two equatorial coordination sites of the uranyl ion; thus, two aqua ligands are released in the substitution reaction. However, in the monodentate case (n = 4) only one aqua ligand is split off. Thus the number of reactants remains unchanged in the monodentate case, whereas the second aqua ligand, released in the bidentate case, leads to a favorable entropy contribution due to an increased disorder. Concomitantly, the

preference of the monodentate coordination is reduced. In the GP models, monodentate coordination is still favored for R = H (29 kJ mol^{-1}), but only to a minor extent for R = CH_3 (14 kJ mol^{-1}) and R = CH_2CH_3 (9 kJ mol^{-1}). In the PCM models, bidentate coordination is now preferred, noticeably for R = CH_3 and R = CH_2CH_3 by ~20 kJ mol^{-1} and rather weakly for R = H (3 kJ mol^{-1}). These results agree with the chemical expectation that a bidentate carboxylate should be more strongly bound.

In summary, both coordination modes exhibit comparable stabilities, a tendency to bidentate coordination is found when thermodynamic corrections are accounted for. Note, however, that these evaluations are based on the assumption of a pentagonal coordination in all uranyl complexes involved. The occurrence of other coordination numbers, i.e. different numbers of aqua ligands, would affect the results obtained due to entropy effects as discussed above. The probability, that complexes of different coordination numbers N are simultaneously present, and the consequences of changes in N will be addressed next.

Experimental situation

As the structural discussion so far did not furnish a coherent rationalization for the discrepancies between calculated and experimental findings, the experimental situation will now be addressed in more detail. Complications arise from the fact that the number of carboxylate ligands and their coordination mode strongly depend on pH and the relative concentration with respect to that of uranyl. In addition, different uranyl carboxylate complexes can coexist.[98,155,250] While EXAFS spectroscopy provides an average over such ensembles, vibrational spectroscopy yields direct evidence.[97,98] A recent EXAFS study suggested that the prevailing coordination mode in a sample changes on the time scale of months,[250] based on the observation of a slight increase of U-O_{eq} and the equatorial uranyl coordination number (N). Despite all these complications, rather small changes in geometric parameters and coordination number, as provided by fits of EXAFS data, are frequently ascribed to changes of the predominant coordination mode and the number of carboxyl ligands.[155,160,250]

In agreement with experimental indications that the coordination mode apparently changes with slight modifications of the pH, concentration, ligand type etc.,[151,155,250] the present calculations suggest that mono- and bidentate coordination exhibit rather similar stability. However, calculated structure differences exceed the uncertainties of EXAFS determinations discussed above. These discrepancies can, at least partially, be ascribed to the fact that in experiment it is not easy to exclude the presence of complexes with more than a single carboxyl ligand. This is in line with the geometric differences calculated for mono- (N = 5) and triacetate (N = 6) complexes in solution (see Section 4.4.1 and 4.4.2).

For instance, the calculated distances U-O_c and U-O_{eq} increase by more than 0.05 Å on going from uranyl mono- to triacetate (Tables 4.19 and 4.22). Thus, the longer U-O_{eq} distance of bidentate triacetate complexes in solution found experimentally (0.06 Å relative to monodentate complexes), can be mainly attributed to an increase of the coordination number from 5 to 6. Because EXAFS studies yield the coordination number N corresponding to U-O_{eq} with an uncertainty of 15–25%,[151,155,156] such a change cannot be excluded. Also, the experiments may have been carried out for an ensemble of monodentate (or pseudobridging) and bidentate complexes.

Based on these uncertainties on the value of the equatorial coordination number N, changes due to different values of N will be discussed in more detail. The computational models employed are based on pentagonal coordination of uranyl (N = 5) because it was found to be preferred in general in various experimental[68,79] and computational studies.[23,41] Previous computational work[43,69] as well as a recent review[254] confirmed this conclusion for uranyl complexes in aqueous solution of low pH. However, other structures of the first coordination shell with 4 or 6 equatorial ligands have also been discussed.[68,151,250] Additional aqua ligands would increase the bonding competition at the uranium center, hence result in longer equatorial U-O bonds. In fact, calculations for $[UO_2(H_2O)_n]^{2+}$ in aqueous solution yield elongated U-O_w distances, from 2.31 Å to 2.36 Å and 2.41 Å, for N = *n* = 4, 5, and 6, respectively (see Table 4.2, Section 4.1). Also uranyl carboxylate crystal structures demonstrate that U-O_{eq} distances vary with the coordination number in a characteristic fashion. From the data base assembled in Ref. 160 one derives average U-O_{eq} values of 2.39±0.02 Å for N = 5 and 2.48±0.02 Å for N = 6. From EXAFS data on uranyl(VI) complexes in solution one determines a smaller difference for U-O_{eq} between pentagonal and hexagonal coordination, namely 2.39±0.02 Å for N ≈ 5 and 2.43±0.02 Å for N ≈ 6.[151,155,156] These latter values have to be taken with due caution because of the error bars of N (see above). All these data corroborate the conclusion that the average U-O_{eq} distance is noticeably elongated when the coordination number N increases.

To investigate this aspect in a calculation on uranyl monocarboxylate complexes, uranyl(VI) monoacetate $[UO_2(OOCCH_3)(H_2O)_n]^+$ was chosen as a representative system to study hexagonal uranyl coordination (Table 4.30). One additional aqua ligand was added to the previously discussed penta-coordinated monoacetates to achieve a coordination number of N = 6.

As expected, one notices significant changes in the equatorial coordination shell for both bidentate and monodentate coordination. Surprisingly, the axial uranyl distances are not affected by these changes (Table 4.30). This indicates that the uranyl binding capacity

Table 4.30. Calculated interatomic distances (in Å) and symmetric uranyl stretching frequency ν_s (in cm^{-1}) of uranyl(VI) monoacetate $[UO_2(OOCCH_3)(H_2O)_n]^+$ exhibiting bidentate (bi) and monodentate (mono) carboxylate coordination for different equatorial coordination numbers N (N = 5, 6) compared to experimental data for aqueous solution (sol.) and crystals (cryst.). Solvent effects are included via *n* explicit aqua ligands and a PCM treatment. For the designations of atoms, see Fig. 4.20.

	n	N		$U=O_t$	$U-O_c$	U-C	$U-O_w$	$U-O_{eq}$	ν_s
bi	3	5		1.787	2.371	2.772	2.365	2.367	854
	4	6		1.787	2.400	2.783	2.462	2.441	846
	Exp.	CH_3 sol.[a]		1.78(1)	2.50(2)	2.91(2)	2.38(2)	2.43(2)	861
		sol.[b]		1.78(1)	2.46(4)	2.87(4)	2.40(4)	2.42(4)	–
		cryst.[c]		1.76(3)	2.48(5)	2.86(5)	2.36(4)	2.42(6)	–
mono	4	5		1.789	2.291	3.401	2.382	2.364	824
	5	6		1.790	2.363	3.389	2.465	2.448	838
	Exp.	sol.[b]		1.78(1)	–	–	–	2.38(4)	–
		cryst.[c]		1.76(3)	2.39(5)	3.5(1)	2.42(6)	2.36(2)	–

[a] Refs. 97, 98, 151. [b] Average values from Refs. 79, 151, 155. [c] Average values from Refs. 150, 151, 160.

is essentially saturated with 5 equatorial coordination sites. Concomitantly, the uranyl stretching frequencies change only in minor way, by 8–14 cm^{-1}. At variance with those small effects, the aqua ligands move significantly out of the equatorial plane to minimize steric repulsion (Fig. 4.25). This results in a distinct increase of the average $U-O_w$ distance both for bidentate (by 0.10 Å) and monodentate (by 0.08 Å) coordination. These elongations indicate a weakening of the uranyl aqua bonds, on average. The steric effects are compensated to some extent by the formation of hydrogen bonds between adjacent aqua ligands as well as between the carboxylate O centers and H centers of neighboring aqua ligands (Figs. 4.25c,d). The corresponding O···H distances, from 1.8 Å to 2.2 Å (Fig. 4.25), are characteristic for moderate hydrogen bonds (typically 1.5–2.2 Å),[235] whereas the shorter O···H distance of 1.3 Å to the "free" carboxylate oxygen center in the monodentate complexes indicates a rather strong H bond (typically 1.2–1.5 Å).[235] Because of these stabilizations, the addition of one aqua ligand becomes slightly exothermic both for bidentate (24 kJ mol^{-1}) and monodentate (18 kJ mol^{-1}) complexes. However, comparison to average binding energies of aqua ligands in the corresponding penta-coordinated

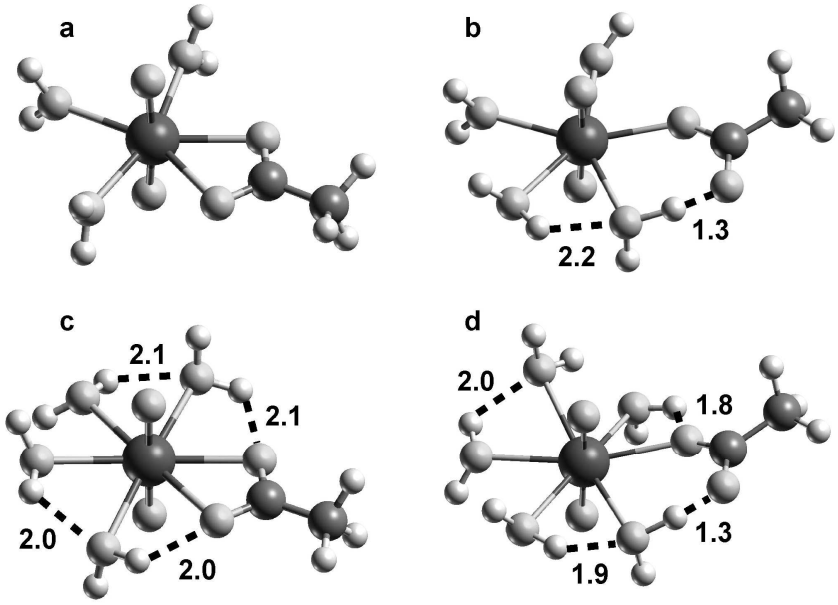

Figure 4.25. Optimized structures of uranyl monoacetate $[UO_2(OOCCH_3)(H_2O)_n]^+$ exhibiting bidentate (bi) and monodentate (mono) carboxylate coordination for different equatorial coordination numbers N: (a) N = 5, bi; (b) N = 5, mono; (c) N = 6, bi; (d) N = 6, mono. Also shown are calculated O···H distances (Å) of hydrogen bonds that are formed within the ligand sphere.

monocarboxylate complexes (75–80 kJ mol^{-1}, Table 4.23) indicates rather weak bonds to the aqua ligands, in line with the long U-O_w distances.

The increased bonding competition at the uranyl center and the formation of hydrogen bonds to the carboxylate oxygen centers (Fig. 4.25) results in longer U-O_c bonds. This weakening of bonds is more pronounced for monodentate (0.07 Å) than bidentate (0.03 Å) coordination. It can be rationalized by stronger hydrogen bonds in the monodentate complex, indicated by two shorter O···H distances of 1.3 Å and 1.8 Å – compared to ~2.0 Å in the bidentate complex (Figs. 4.25c,d). The corresponding U-C distances are hardly affected (±0.01 Å). Because of the longer U-O_w and U-O_c distances the average U-O_{eq} values for N = 6 are distinctly longer than those for N = 5, by about 0.08 Å (Table 4.30).

The changes resulting from the higher coordination number only partially improve the agreement with experimental data. The underestimation of the U-O_c distance is reduced from ~0.1 Å for N = 5 (Table 4.28) to 0.06 Å for bidentate and to 0.03 Å for monodentate complexes. However, the underestimation of U-C remains at ~0.1 Å (Table 4.30). The U-O_w distances are overestimated compared to the experimental values, by 0.05–0.06 Å. As found for the corresponding penta-coordinated complexes (Table 4.30), similar U-O_{eq}

distances of 2.44–2.45 Å are obtained for both coordination modes in the hexa-coordinated complexes. These U-O_{eq} values agree well with the experimental one suggested for bidentate coordination (~2.42 Å), but are notably longer than the one expected for monodentate coordination (~2.38 Å). A coordination comparison to experiment just based on U-O_{eq} would indicate that hexagonal coordination is favored for bidentate complexes (2.44 Å, Table 4.30) and pentagonal coordination is preferred for monodentate structures (2.36 Å, Table 4.28). In agreement with this analysis, hexagonal coordination has been suggested for uranyl monoacetate.[151] This conclusion is supported by larger O_w-U-O_w angles between the aqua ligands of the bidentate complexes that result from the rather small O_c-U-O_c angle of ~55° (Fig. 4.25). Thus, more space and less steric repulsion favors the coordination of an additional aqua ligand in the bidentate complexes. The experimentally observed change of U-O_{eq} on going from mono- to bidentate complexes is more likely due to an accompanying alteration of the average coordination number than a rearrangement of the first coordination shell at fixed coordination number. However, noticeable deviations to experimental data remain for the individual distances U-O_c and U-C, irrespective of the different coordination numbers.

Hydrolysis

With increasing pH, uranyl is known to form various hydrolysis species which might lead to significantly changed structure parameters (see Section 2.2.2).[104,108,255] The presence of carboxylate ions suppresses the formation of hydroxo complexes in solution; speciation calculations did not yield any evidence for larger amounts of these species together with carboxylates.[151,155] On the other hand, also a small fraction of pure hydroxo complexes or mixed complexes with carboxylates could affect ensemble averages of structure parameters if the geometric parameters of these alternative complexes would considerably deviate from those of pure carboxylate complexes.

To study this aspect, complexation of the first uranyl hydrolysis species $[UO_2(OH)]^+$ by formiate, acetate, and propionate will be discussed for bidentate coordination. Pentagonal coordination of the uranyl moiety was achieved by adding two additional aqua ligands in the models $[UO_2(OH)(OOCR)(H_2O)_2]$, R = H, CH_3, and CH_2CH_3. Long-range solvent effects were included via a PCM treatment. The OH ligand is located *anti* to the carboxylate ligand (Fig. 4.26). C_s symmetry constraints were applied in all models to reduce the computational effort; the symmetry plane includes the uranyl moiety and the OH ligand (Fig. 4.26). Results are summarized in Table 4.31.

The hydrolysis complexes are characterized by a strong bond of the hydroxo group, designated by U-OH. This bond (2.12 Å) is significantly shorter than all other equatorial

Table 4.31. Calculated structural parameters (distances in Å) and symmetric uranyl stretching frequency (ν_s, in cm^{-1}) of uranyl(VI) hydroxide monocarboxylates $[UO_2(OH)(OOCR)(H_2O)_2]$ exhibiting bidentate carboxylate coordination compared to experimental data of uranyl(VI) monocarboxylates from aqueous solution (sol.). Average changes ΔOH are calculated with respect to corresponding bidentate uranyl(VI) monocarboxylates $[UO_2(OOCR)(H_2O)_3]^+$ (Table 4.22).

R	U=O_t	U-O_c	U-C	U-O_w	U-OH	U-O_{eq}	ν_s
H	1.804	2.467	2.837	2.435	2.115	2.384	819
CH_3	1.806	2.443	2.841	2.439	2.121	2.377	813
CH_2CH_3	1.806	2.440	2.832	2.442	2.120	2.377	814
ΔOH avg.	0.02	0.07	0.07	0.08	–	0.01	-42
Exp. CH_3 sol.[a]	1.78(1)	2.50(2)	2.91(2)	2.38(2)	–	2.43(2)	861
sol.[b]	1.78(1)	2.46(4)	2.87(4)	2.40(4)	–	2.42(4)	–

[a] Refs. 97, 98, and 151. [b] Average values from Refs. 79, 151, and 155.

U-O distances (Table 4.31). Under favorable conditions EXAFS experiments should be able to resolve this distance (see Section 2.1.4). The increased bonding competition due to the U-OH bond causes distinctly longer equatorial distances U-O_c (by 0.07 Å), U-C (by 0.07 Å), and U-O_w (by 0.08 Å) than determined for uranyl(VI) monocarboxylates (ΔOH in Table 4.31). These elongations might also partially result from the reduced charge of $[UO_2(OH)(OOCR)(H_2O)_2]$ compared to $[UO_2(OOCR)(H_2O)_3]^+$. The terminal uranyl bonds are slightly elongated, by 0.02 Å, which is reflected in a smaller uranyl stretching frequency, by ~42 cm^{-1}.

Surprisingly, despite the significant changes of equatorial U-O distances compared to those of uranyl(VI) monocarboxylates, the U-O_{eq} distances change by only 0.01 Å (see Table 4.22). The formation of the short U-OH bond (2.12 Å) is compensated by an elongation of the distances U-O_c (~2.45 Å) and U-O_w (2.44 Å). Thus, the average U-O_{eq} value of 2.38 Å is very similar to results of bidentate (2.37 Å) and monodentate (2.38 Å) uranyl(VI) monocarboxylates (Table 4.22) as well as of the solvated uranyl complex $[UO_2(H_2O)_5]^{2+}$ (2.36 Å, see Section 4.1, Table 4.2). The unifying feature of all these species is the same pentagonal uranyl coordination. Thus, variations of ligand types and coordination modes do not seem to affect the (average) distance U-O_{eq} if the total coordination number is kept constant (here: N = 5). This observation is corroborated by

computational results for different types of uranyl(VI) complexes, all exhibiting pentagonal coordination. For instance, uranyl complexes $[UO_2(OR)(H_2O)_4]^+$ with several small alcoholates, such as ethanolate or phenolate, and the corresponding uranyl alcohol complexes $[UO_2(OHR)(H_2O)_4]$, show identical U-O_{eq} values of ~2.38 Å.[256]

U-O_{eq} values of hexa-coordinated uranyl complexes with different kinds of ligands are also quite similar and show noticeably longer U-O_{eq} values as determined for penta-coordinated complexes. The hexa-coordinated uranyl monocarboxylates discussed above exhibit U-O_{eq} distances of 2.44 Å for bidentate and 2.45 Å for monodentate coordination (Table 4.30). Comparable results were obtained for the solvated actinyl complex $[UO_2(H_2O)_6]^{2+}$ (2.41 Å, see Section 4.1, Table 4.2) and uranyl triacetate (2.42 Å, see Section 4.4.1, Table 4.19). Obviously, the coordination of an additional O donor ligand – independent of the ligand type – increases U-O_{eq} from ~2.37 Å (N = 5) to ~2.43 Å (N = 6). These corroborates previous findings that U-O_{eq} mainly depends on the coordination number N and confirms the applied concept of bond order conservation.

In the following, the results calculated for the uranyl(VI) hydroxide monocarboxylates are compared to experimental data suggested for bidentate uranyl carboxylates in solution. The distinct underestimation of U-O_c and U-C distances (~0.1 Å, Table 4.22) in $[UO_2(OOCR)(H_2O)_3]^+$ is noticeably reduced in $[UO_2(OH)(OOCR)(H_2O)_2]$ to about 0.01 Å for U-O_c and 0.03 Å for U-C. U-O_w distances are slightly longer than expected from experiment, by ~0.04 Å. The U-O_{eq} distance of 2.38 Å remains shorter than expected for bidentate coordination (~2.42 Å) as found also for the uranyl carboxylates (2.37 Å, Table 4.22). However, this difference between bidentate and monodentate coordination suggested by experiment (~0.04 Å, Table 4.22) might be rather attributed to changes in the coordination number N from 5 to 6 (~0.06 Å, see above) as discussed in the preceding paragraph. In addition, the uranyl bond is somewhat too long, by 0.02 Å,

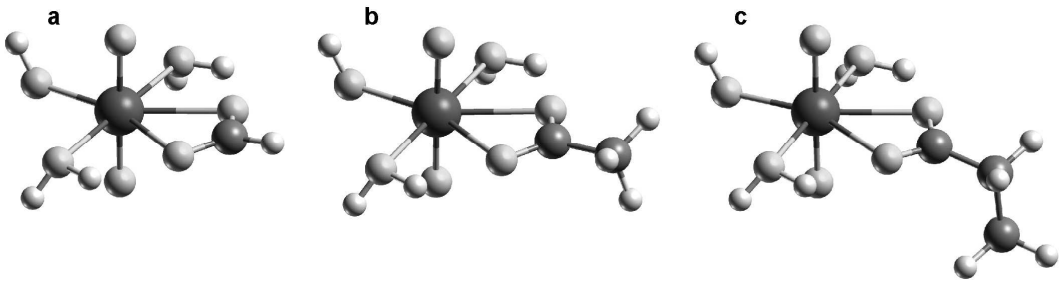

Figure 4.26. Optimized structures of uranyl hydroxide monocarboxylates $[UO_2(OH)(OOCR)(H_2O)_2]$, R = H (a), CH_3 (b), and CH_2CH_3 (c), with bidentate carboxylate coordination and C_s symmetry constraints.

concomitant with an underestimation of the uranyl stretching frequency by 46 cm^{-1}. Interatomic distances of the hydroxo complexes, especially between uranyl and the carboxylate ligand, overall agree much better with experimental data than the results calculated for the uranyl monocarboxylate complexes. However, one does not expect that these hydrolysis species dominate because of the low pH values in the experiments and corresponding speciation calculations.[151,155]

Hydrogen bonds

Another way to improve the realism of the computational models is by inclusion of water molecules of the second hydration shell to simulate hydrogen bonds to the negative oxygen centers of the carboxylate groups. Such hydrogen bonds are expected to reduce the uranium-carboxylate interaction, resulting in longer U-O_c bonds. However, three further water molecules in the model of uranyl triacetate (see Section 4.4.1) increased the U-O_c distance by 0.01 Å only. Thus, changes due to the inclusion of such hydrogen bonds are not expected to reduce significantly the discrepancies of uranyl monocarboxylates with experimental data.

Summary

To clarify the open questions raised above, further experimental efforts to discriminate different equatorial U-O contacts are desirable, although this is known to be a difficult task.[250] From the discussion of various sources of discrepancies between EXAFS results and the calculated structures, a straightforward interpretations of EXAFS data of complexes in solution by reference to structures from crystals seems to be questionable for uranyl carboxylate complexes. Uncertainties are related to the number and type of species simultaneously present in solution and to the geometric details of their coordination.

Based on the results for penta-coordinated uranyl monocarboxylates, the average U-O_{eq} distances are expected to be similar at constant uranyl coordination number, irrespective of the coordination mode (Section 4.4.2). This conclusion is corroborated by evidence from calculations on uranyl compounds that exhibit different coordination numbers, such as the solvated uranyl ion (Section 4.1), uranyl triacetate (Section 4.4.1), as well as selected uranyl monoacetates (Section 4.4.4). As expected from the increased bonding competition at the uranyl center, U-O_{eq} distances increase with the coordination number, on going from tetragonal to pentagonal and hexagonal coordination. Thus, variations of average U-O_{eq} distances derived in EXAFS investigations are more likely due to changes of the coordination number than due to frequently invoked variations of the coordination mode. This holds independent of results for U-C which more clearly indicate the coordination mode, but such data are not available from experiment in many cases.

4.4.5 Implications on actinyl complexation by humic acids

Carboxylic groups are the dominant functional groups of humic substances and are considered as the main complexation sites for actinides (see Section 2.2.4).[6,7] Therefore, conclusions drawn from the discussion of actinyl complexation by monocarboxylates (Section 4.4.4) provide a basis for the investigation of the actinyl complexation by humic substances. This section summarizes the experimental data[85,143,144,149,160] available on complexation by humic acids and also discusses implications from the present computational studies on actinyl monocarboxylates.

EXAFS studies were performed to investigate the complexation of uranyl(VI)[149,160] and neptunyl(V)[143] by natural and synthetic humic acids (Table 4.32). Unfortunately, the EXAFS data obtained did not allow the resolution of different equatorial An-O distances. Thus, a differentiation between the carboxylate and other equatorial ligands is not possible and only a single An-O_{eq} value, averaged over all equatorial An-O distances, could be determined. Definite information on An-O_c can only be obtained from crystal structure data. The actinyl distances An=O_t are too similar to allow a conclusive differentiation (see Table 4.32).

The An-O_c values given in Table 4.32 have been calculated as averaged values from several crystal structures of actinyl carboxylates with bidentate and monodentate coordination.[143,160] These data suggest noticeably longer An-O_c distances for bidentate coordination. The average An-O_{eq} values obtained from EXAFS studies on actinyl complexation by humic substances are usually compared to these reference An-O_c values (Table 4.32). Based on this comparison, the rather short An-O_{eq} distances determined for actinyl humates are interpreted as an indication for predominantly monodentate coordination, both for U(VI) and Np(V) (Table 4.32).[143,160]

However, it is unclear why only monodentate complexation of actinides should occur in humic substances, considering their complex structure and the presence of various functional groups. Taking into account the predominance of carboxylic groups in humic substances, that generally favor a bidentate coordination,[159] one would expect to find mainly this type of coordination. The preference of bidentate over monodentate coordination is supported by computed Gibbs free energies for uranyl monocarboxylates (see Table 4.29). In contrast to monodentate coordination, it is usually possible to identify characteristic U-C distances in the EXAFS spectra of bidentate (~2.9 Å) or chelate (~3.3 Å) uranyl carboxylate complexes (see Section 4.4.2).[151,155] However, no such U-C distances are found in the EXAFS spectra of U(VI) humates. Thus, the absence of these distances has been interpreted as an indirect evidence for monodentate coordination.[143,160]

Table 4.32. EXAFS data (distances in Å) for the complexation of uranyl(VI) and neptunyl(V) with natural and synthetic humic acids (HA) in comparison to averaged data form crystal structures of several actinyl carboxylate complexes. The crystal structure data provide distances An-O_{eq} averaged over complexes with a given equatorial coordination number N (N = 5 or 6) as well as distances An-O_c for a given coordination mode of the carboxylate ligand (monodentate and bidentate). For the designations of atoms, see Fig. 4.20.

		An=O_t	An-O_{eq}	An-O_c
U(VI)-HA[a]		1.77–1.78	2.37–2.39	–
Cryst.[b]	N = 5	1.76±0.03	2.39±0.02	
	N = 6	1.74±0.04	2.48±0.02	
	mono	1.76±0.03		2.39±0.05
	bi	1.76±0.03		2.48±0.05
Np(V)-HA[c]		1.84–1.85	2.48–2.49	–
Cryst.[d]	N = 5	1.85±0.03	2.45±0.03	
	N = 6	1.85±0.03	2.55±0.03	
	mono	1.85±0.03		2.46±0.04
	bi	1.85±0.03		2.59±0.08

[a] EXAFS data from solution, Refs. 149, 160. [b] Averaged values from crystal structures, Ref. 160. [c] EXAFS data from solution, Ref. 143. [d] Averaged values from crystal structures, Ref. 143.

In the light of the previous discussion about the accuracy and the uncertainties of EXAFS data for uranyl carboxylate complexes (Section 4.4.4), a straightforward interpretation of the coordination mode based on An-O_{eq} alone seems questionable. Rather, it seems advisable to discuss the original conclusions why monodentate coordination should be favored.

First, it does not seem permissible to compare the An-O_c bonds to the carboxylate group directly to the average An-O_{eq} values that relate to all equatorial ligands. From the crystal structures, it is not possible to obtain specific An-O_{eq} values for bidentate or monodentate coordination because in most crystals the carboxylate ligands around a specific An center do not exhibit one specific coordination mode, but are coordinated in bidentate, monodentate, and/or bridging fashion at the same time.[143,160] Also, additional ligating groups other than carboxylates are present in the crystals,[143,160] e.g. OH, OR, NO_3, or H_2O. Thus, the corresponding An-O_{eq} values provide an average over different ligand

types and coordination modes. On the other hand, An-O_c values derived from crystal structures for carboxyl groups that exhibit a specific coordination mode show strong variations. This can be rationalized by bonding competition at the actinyl center between the carboxylates and other equatorial ligands such as OH or H_2O that can exhibit rather different bond strengths. For instance, the An-O_c bonds in crystal structures of U(VI) carboxylates vary significantly, 2.32–2.44 Å for monodentate and 2.38–2.58 Å for bidentate coordination.[160] Thus, An-O_c values can not be considered as a reliable reference. In addition, note that these values are obtained from crystal structures and are used for the interpretation of EXAFS data in solution. However, packing effects, not present in solution, might affect the actinyl coordination in crystals.

A differentiation of the complexes according to the equatorial coordination number is usually not considered in the interpretation of experimental findings. However, the preceding analysis showed this quantity to be of significant influence on the value of An-O_{eq} (see Section 4.4.4). Therefore, for the present discussion, the crystal structure data[143,160] were re-evaluated with respect to the equatorial coordination number, N = 5 or 6 for U(VI) and Np(V) (Table 4.32). For a given value of N, the resulting An-O_{eq} values are rather similar, irrespective of the underlying coordination mode or additional ligands present in the ligand sphere. For instance, U-O_{eq} distances obtained from crystal structures of U(VI) carboxylates range from 2.36 to 2.43 Å for N = 5 and from 2.46 to 2.51 Å for N = 6.[160] These intervals are distinctly narrower, hence more characteristic, than the corresponding intervals of An-O_c derived from the same crystal structure data for carboxylates at bidentate and monodentate coordination (see previous paragraph). The An-O_{eq} distances determined for uranyl carboxylate crystals with N = 6 are distinctly elongated compared to those with N = 5. This is in agreement with computational results obtained for uranyl monoacetate (see Section 4.4.4). For U(VI) humates, EXAFS results suggested an equatorial coordination number of 5.[149,160] The corresponding U-O_{eq} distances of 2.37–2.39 Å agree well with average experimental data from crystal structures for N = 5 (2.39±0.02 Å, Table 4.32) and the present computational results for penta-coordinated actinyl monocarboxylates, both for bidentate (2.37 Å, Table 4.28) and monodentate coordination (2.36 Å, Table 4.28). In contrast, U-O_{eq} values derived from crystal structures for hexagonal uranyl coordination are noticeably longer (2.48±0.02 Å, Table 4.32).

The equatorial coordination number, derived from EXAFS data[143] for Np(V) humates, is ~3 which appears to be too low. Based on crystal structures, the most likely coordination number of Np(V) complexes is 5.[143] The experimental Np-O_{eq} distances of Np(V) humates, 2.48–2.49 Å, are somewhat longer than average values for Np(V) crystal structures for N = 5 (2.45±0.03 Å, Table 4.32) and the present computational data of penta-

coordinated Np(V) monocarboxylates (2.43–2.45 Å, Table 4.26). However, these values are noticeably shorter than Np-O_{eq} values determined experimentally for N = 6 (2.55±0.03 Å, Table 4.32). Overall, this comparison points to a pentagonal coordination in the actinyl humate complexes, both for U(VI) and Np(V), as one expects An-O_{eq} distances to be significantly longer for a hexagonal coordination (Table 4.32).

The preceding discussion of actinyl humate complexation employs results and conclusions which were obtained for small actinyl carboxylate complexes. At this point the applicability of results based on such model systems needs to be discussed. As shown at the beginning of Section 4.4.2, chain length as well as chemical variations of the carboxylate residue only slightly affect the uranyl complexation by carboxylate groups. As a result, characteristic parameters, such as uranyl distances and the uranyl stretching frequency, hardly change. In addition, complexation by aromatic carboxylates, which might occur more frequently in humic acids rather than complexation by aliphatic carboxylates,[86] has been investigated by quantum chemistry modeling.[257] The corresponding results indicate only minimal structural changes; bond lengths differ less than 0.01 Å from corresponding values calculated for aliphatic carboxylates. Therefore, the present model strategy is justified because structural and chemical variations only slightly affect the structure of the complexes.

However, when considering actinyl complexation by humic substances, one has to take into account in addition that complexing sites other than carboxyl groups may be relevant and thus can affect the EXAFS spectra (see Section 2.2.4). Most probable candidates are sites offering chelate-type complexation, e.g. via neighboring phenolic OH groups. The influence of phenolic OH groups on the complexation process was experimentally investigated for synthetic humic acids.[85,143,144] After chemical blocking of the OH groups by permethylation, the loading capacity, a measure of the maximum number of available complexing sites of the humic acids, is significantly reduced.[85,143,144] The impact of phenolic OH groups increased with increasing pH, as expected because of the higher degree of deprotonation.[143] However, the corresponding EXAFS data indicate that mean structural parameters of actinyl humate complexes, e.g. An=O_t and An-O_{eq} bond distances, are not changed after OH groups have been blocked.[85,143] In this context, one has to recall that EXAFS results represent average values over all interactions between humic acid and the actinyl. If phenolate groups show equatorial coordination parameters comparable to those of carboxylate groups, a differentiation by EXAFS may not be feasible. In fact, EXAFS studies of uranyl(VI) complexes with catechol (2–hydroxyphenol) and pyrogallol (3,4–dihydroxybenzol), which both feature phenolic OH groups, yield average U-O_{eq} values of 2.39–2.40 Å at pH ~5.[258] These values are close to U-O_{eq} values

obtained for U(VI) humates (2.37–2.39 Å, Table 4.32).

On the basis of this discussion, the participation of phenolic groups in the complexation process can not be excluded. The reduced loading capacity after chemical blocking of phenolic OH groups clearly indicates an influence on the complexation behavior of humic acids. On the one hand, steric effects, i.e. steric hindrances due to the permethylated OH groups, may affect the complexation properties of carboxylic centers close to blocked OH groups. Besides, a phenolic group adjacent to a carboxylate group can coordinate to an actinyl by forming either five- or six-membered chelate rings. In EXAFS studies it may not be possible to differentiate between actinyl complexation by carboxylic or phenolic groups because, as indicated above, U-O_{eq} distances are probably quite similar. It is desirable to carry out further experimental and theoretical studies of uranyl complexes with small and well-defined organic complexes that comprise phenolic OH and/or carboxylic groups.

In summary, the interpretation of EXAFS results on the basis of An-O_{eq} as indication for monodentate complexation of actinyls by humic acids remains questionable. The present computational results indicate, in line with data from crystal structures, that variations of An-O_{eq} distances result more probably from changes of the coordination number than from alterations of the carboxylate coordination mode. The frequently invoked assumption that bidentate complexes generally exhibit noticeably longer An-O_{eq} distances than monodentate complexes is not reproduced by the calculations. Thus, the exclusion of bidentate or other coordination modes solely on the basis of “short” An-O_{eq} values does not seem justified.

A comparison of calculated U-O_{eq} values of uranyl monocarboxylates to EXAFS data indicates that uranyl in the humate complexes is penta-coordinated, in agreement with experimental suggestions. However, the structural EXAFS data available for uranyl humates can not be assigned to a specific carboxylate coordination mode because similar U=O_t and U-O_{eq} distances are calculated for different coordination modes of carboxylate ligands in penta-coordinated uranyl complexes. Besides, one also has to consider that ligands other than carboxylates may exhibit similar equatorial parameters. An energy analysis of the computed results suggests, that various carboxylate coordination modes imply similar stability, and indicates a slight preference for bidentate coordination when thermodynamic corrections are accounted for. The fact that U-C distances, which are characteristic for carboxylates with bidentate or chelate coordination, are lacking in the EXAFS results indirectly points to monodentate coordination.

Overall, the present calculations indicate that the structural information available from EXAFS studies is not sufficient to clarify definitely the complexation mode of actinyls by humic substances, especially if one takes into account that EXAFS can only provide superimposed structural information for ensembles of different species that are likely present in solution. In particular, the average An-O_{eq} distance is not suitable for differentiating between coordination sites and modes. Further experimental efforts to discriminate different equatorial An-O contacts are desirable to allow a better characterization of the equatorial ligand shell. The application of other experimental methods such as vibrational spectroscopy and further theoretical studies are necessary for a more comprehensive understanding of the complex actinyl humate system.

5 Summary and Outlook

The behavior of actinides in the geosphere has become one of the most important research fields of actinide chemistry. This interest is based on current environmental issues, such as the management of nuclear waste and the cleaning of contaminated sites. Data from experimental and theoretical studies are used to predict the transport of actinides in the environment and to design ways to retard their release. Actinides also are of fundamental interest because their large number of oxidation states results in a rich chemistry and a fascinating structural diversity. Furthermore, actinide complexes show bonding schemes which differ significantly from those of other elements, even from those of the formally similar lanthanides, because actinide *f* orbitals can participate in the bonding.

In this work, the complexation of actinides in aqueous solution was studied computationally, within the framework of density functional (DF) theory. Such a quantum chemical approach represents an alternative way to obtain information about actinide compounds besides experimental investigations; the latter are complicated because of the radioactivity and the toxicity of the actinides as well as the simultaneous presence of a variety of species in solution. This thesis concentrated mainly on uranium in its most stable oxidation state VI. Available experimental data for this oxidation state allow one to validate the computational approach chosen. For comparison, corresponding neptunium(VI) and neptunium(V) complexes have also been studied.

At first solvated actinyls $[AnO_2(H_2O)_n]^{m+}$ of U(VI), Np(VI), and Np(V) were discussed considering different numbers of aqua ligands in the computational models (Section 4.1). Results for the dinuclear uranyl complex $[(UO_2)_2(\mu_2\text{-}OH)_2Cl_2(H_2O)_4]$, suggested as hydrolysis product of uranyl, were compared to detailed structural information, available for this molecular crystal (Section 4.2). The investigations were extended to mono- and polynuclear uranyl carbonate complexes which determine the environmental actinide speciation in the presence of carbon dioxide (Section 4.3). Finally,

the focus was on actinyl carboxylate complexes (Section 4.4). The latter systems may also serve as simple models of complexing sites of biological decomposition products, such as humic substances, that are expected to play an important role for the migration of actinides under natural conditions. After some remarks on the computational method applied, the results obtained for these various actinyl complexes will be summarized below.

Calculations on actinide systems are challenging because relativistic effects as well as electron correlation have to be accounted for in an accurate fashion. All actinide complexes in this thesis were calculated with an all-electron scalar-relativistic DF method based on the Douglas-Kroll approach as implemented in the program PARAGAUSS, developed in the research group of Prof. Rösch. Geometry optimizations were carried out at the LDA level while energetic parameters were determined with a GGA functional. When dealing with actinide complexes in solution an accurate modeling of solvation effects is essential. Short-range solvent effects were considered explicitly via coordinated aqua ligands of the first hydration shell and long-range electrostatic interactions were described by treating the remaining solvent as a polarizable continuum (PCM).

In the absence of further complexing ligands, solvated actinyl ions $[AnO_2(H_2O)_n]^{m+}$ represent the dominant uranium and neptunium species in aqueous solution at low pH values. Coordination of the actinyl moiety by 4 to 6 aqua ligands in the equatorial plane was investigated for U(VI), Np(VI), and Np(V). The computational results obtained for structures, vibrational frequencies as well as energetics favor a coordination by 5 aqua ligands, in agreement with experimental suggestions. This finding is supported by an analysis of the effective electronic configuration of the actinyl; also the charge distribution in the complexes indicates a saturation of the actinyl binding capacity for the penta-coordinated complexes. Coordination by four aqua ligands seems least plausible, but hexa-coordination can not be completely excluded, especially for U(VI). The slight underestimation of calculated actinyl-aqua distances compared to EXAFS data may be related to the simultaneous presence of species with five *and* six aqua ligands in solution.

The results obtained for solvated actinyls indicate rather strong bonds of the aqua ligands. Their average binding energies were calculated at ~90 kJ mol^{-1} for An(VI) and ~60 kJ mol^{-1} for An(V). The formation of the actinyl-aqua bonds is accompanied by a significant charge donation to the actinyl moiety and an enhancement of the actinide 6*d* population. A comparison to bare actinyls shows, as expected, that a solvation treatment solely based on the PCM model can not account for these short-range solvent effects. Rather, for an adequate description of such complexes, it is necessary to include aqua ligands explicitly in the quantum mechanical models.

Comparison of U(VI), Np(VI), and Np(V) complexes reveals that both hexavalent actinyls show very similar structural and energetic properties. This finding is attributed to the fact that the extra electron of neptunyl(VI) is localized in an *f* orbital at the actinide center and does not participate in the actinyl bond. For neptunyl(V) the lower charge and changes in the actinyl bonding result in a distinct elongation of bond distances, in line with experimental data, and a reduction of the binding energy of the aqua ligands.

At higher pH values (pH > 4) uranyl is known to form polynuclear species in solution. The dinuclear uranyl chloride complex $[(UO_2)_2(\mu_2\text{-}OH)_2Cl_2(H_2O)_4]$ has been suggested in the presence of chlorine ions. It is one of the few polynuclear uranyl species for which a crystal structure is known. This complex was studied modeling the gas phase structure as well as the molecular crystal. Hydrogen bonds from and to the crystal environment were described via model H_2O and HCl moieties mimicking the effect of frontier groups of neighboring complexes in the crystal. The calculated gas phase structure is similar to the experimental crystal geometry. Major deviations can be traced to the effect of hydrogen bonds present in the crystal. When the eight strongest hydrogen bonds were included in a model of the crystalline environment of the complex, the calculated structure improved significantly. Lengths and angles of the hydrogen bonds, determined with this model, indicate that these hydrogen bonds are moderate or strong, with an average binding energy of 39 kJ mol^{-1}. These computational results corroborate experimental suggestions concerning the location and strength of the hydrogen bonds in the crystal structure.

In the presence of carbon dioxide actinide carbonate complexes become one of the dominating species in solution. In this work mono-, bi-, and trinuclear uranyl carbonates were investigated. The mononuclear complexes $[UO_2(CO_3)_m]^{2-2m}$ (m = 1–3) exhibit a ligand arrangement with strong bis(chelating) carbonate bonds. Additional aqua ligands from the first hydration shell act as relatively strong ligands. The agreement of the calculated geometry with experimental EXAFS data from solution is improved for the tris(carbonato) complex $[UO_2(CO_3)_3]^{4-}$ when water molecules of the second coordination shell were included in the model to simulate hydrogen bonds to carbonate oxygen centers. These hydrogen bonds can be characterized as moderately strong. A comparison of gas phase (GP) and PCM results to experimental data indicates an overestimation of long-range solvent effects in the PCM model, likely because of the large negative charge of the species. Best agreement with experiment was found for GP models with additional water molecules. The same trend was seen for the polynuclear triuranyl complex $[(UO_2)_3(CO_3)_6]^{6-}$. This anion represents a challenge to the computational method applied, because of its size and the number of electrons to be treated. An extended GP model with nine water molecules matches the experimental data for $[(UO_2)_3(CO_3)_6]^{6-}$ very well. A

comparison between structural data for the tris(carbonato) and the triuranyl hexa(carbonato) complex points to an effectively lower coordination of the uranyl moieties in $[(UO_2)_3(CO_3)_6]^{6-}$ where the bridging U-O distances are rather long compared to those of $[UO_2(CO_3)_3]^{4-}$. Energetic results from model reactions correspond with the experimental finding that $[(UO_2)_3(CO_3)_6]^{6-}$ is present at acidic to neutral pH, whereas the formation of $[UO_2(CO_3)_3]^{4-}$ is favored at basic pH.

In contrast to the well-studied complexes $[UO_2(CO_3)_3]^{4-}$ and $[(UO_2)_3(CO_3)_6]^{6-}$ there is only limited experimental information on the structure of the hemicarbonate species $[(UO_2)_2(CO_3)(OH)_3]^{-}$. This complex has been suggested to be predominant over a broad pH range (pH > 6) at appropriate conditions. Experimental studies indicate the presence of different isomers in solution due to ligand exchange reactions. Three isomers A–C with different bridging geometries were studied. The two uranyl moieties can be linked by a carbonate group (A), two hydroxo groups (B), or one hydroxo and one carbonate group (C). A differentiation of the isomers by structural parameters is difficult because calculated characteristic U-O bond distances are comparable for the three isomers. However, compared with EXAFS results for species in solution, the computed U-U distances clearly point to the presence of isomers B and C rather than isomer A. The relative stabilities of the isomers favor isomer C, in line with the experimental suggestion; the corresponding calculated Boltzmann distribution agrees very well with findings from NMR spectroscopy.

Finally, complexation of actinides by carboxylic groups was examined. Carboxylic groups are considered as the main complexing sites of humic substances because of their strong actinide-complexing ability. The monocarboxylate complexes $[AnO_2(OOCR)]^{m+}$ of U(VI), Np(VI), and Np(V) with the small ligands formiate, acetate, propionate, and glycolate were studied in this work. The investigations focused on a comparison and characterization of different coordination modes of the carboxylic group (bidentate, monodentate, or chelate via an adjacent hydroxo group). Aqua ligands were included in the models to yield the typical five-fold coordination of the actinyl moiety.

Calculated uranyl bond distances agree well with the experimental data but do not allow a differentiation of the coordination modes because they are very similar for all complexes. The uranyl carboxylate distances qualitatively reflect the experimentally suggested order between the three coordination modes. However, these distances are calculated distinctly shorter, by ~0.1 Å, than the corresponding data from crystal structures. These discrepancies are rather large compared to the generally good agreement of density functional results for other uranyl complexes with experimental structure data (within ~0.02 Å), including the benchmark system uranyl triacetate. Besides, experimental

data suggest that the average equatorial distance U-O_{eq} is significantly longer for bidentate than for monodentate coordination. However, the computed U-O_{eq} distances are comparable for bidentate, monodentate, and chelate coordination if one assumes penta-coordination of the uranyl in all complexes. Evaluation of energies of model reactions suggests a comparable stability of the various coordination modes. If one takes thermodynamic effects into account, then bidentate coordination is slightly preferred over monodentate coordination, by about 20 kJ mol^{-1}, mainly as an effect of entropy.

Overall, comparison with experiment revealed significant discrepancies for uranyl monocarboxylates: bond distances to the carboxylate ligand are significantly underestimated in the calculations and the average equatorial distance U-O_{eq} does not allow a differentiation of coordination modes, at variance with the current interpretation of EXAFS experiments. A definitive rationalization of these deviations is difficult. When symmetry restrictions, applied in the theoretical models, were released, structures relaxed, especially in the monodentate complexes, but the agreement with the experimental data did not improve. The underestimation of equatorial bond distances may point to a systematic error in the DF-LDA method applied, but one has to keep in mind that this method yields overall good agreement with experimental data for structurally well-characterized uranyl species such as $[UO_2(CO_3)_3]^{4-}$, $[(UO_2)_3(CO_3)_6]^{6-}$, or $[UO_2(OOCCH_3)_3]^-$. DF methods employing GGA or hybrid exchange-correlation functionals typically overestimate distances in these compounds. The larger discrepancies discussed here are typically found for systems where the first coordination shell of uranyl is not well-defined, i.e. when the number of aqua ligands, required to saturate free uranyl coordination sites, or the coordination mode of ligands are not exactly known. This is the case for solvated actinyls, the hemicarbonate complex, or the actinyl monocarboxylates. For these complexes, comparison with EXAFS data is complicated because the samples studied experimentally likely contain a mixture of various species which leads to a superimposition of different structures in the experimental data.

Furthermore, a straightforward interpretation of EXAFS data of complexes in solution by reference to structures from crystals seems questionable in the case of carboxylates. As a result of this comparison, variations of average U-O_{eq} distances observed in EXAFS are currently interpreted as a change of the coordination mode. On the basis of evidence from calculations on uranyl monocarboxylates, uranyl triacetate, as well as the solvated uranyl ion, it seems more likely that the differences of U-O_{eq} values are caused by changes of the uranyl coordination number. Thus, the underestimation of equatorial distances in computational models with a five-fold coordination of the uranyl moiety may partially be rationalized by an average uranyl coordination number of the

actual complexes in solution larger than 5.

Results for model actinyl carboxylate complexes may also be used to investigate the more complicated case of actinyl complexation by humic acids. The interpretation of EXAFS results taking An-O_{eq} as indication for monodentate complexation of actinyls by humic acids needs to be re-evaluated in the light of the computational results obtained for actinyl monocarboxylates. A comparison of calculated An-O_{eq} values of uranyl(VI) and neptunyl(V) monocarboxylates to EXAFS data indicates that the actinyl moiety in the humate complexes is penta-coordinated, in agreement with experimental suggestions. However, the structural EXAFS data available for actinyl humates can not be assigned to a specific carboxylate coordination mode because similar An-O_{eq} distances are calculated for different carboxylate coordination modes in penta-coordinated actinyl complexes. Thus, the frequently invoked assumption that bidentate complexes exhibit noticeably longer An-O_{eq} distances than monodentate complexes is questionable. The exclusion of bidentate or other coordination modes solely on the basis of "short" An-O_{eq} values does not seem justified. Actinide-carbon distances, which are characteristic for carboxylates with bidentate or chelate coordination, are lacking in the EXAFS results; this fact has been interpreted as indirect evidence for monodentate coordination.

Besides these considerations one also has to take into account that ligands other than carboxylate groups may exhibit similar equatorial parameters. Most probable candidates would be sites offering chelate-type complexation such as phenolic hydroxo groups. Further experimental efforts to discriminate different equatorial An-O contacts are desirable to allow a better characterization of the equatorial ligand shell in actinyl humate complexes.

Overall, this thesis demonstrated that scalar-relativistic density functional methods in combination with a careful treatment of solvent effects provide an adequate approach for studying mono- and polynuclear actinyl complexes in aqueous solution. The present work collects some fundamental and systematic findings on the complexation of actinyls with different ligands expected to be present under environmental conditions. In particular, this work showed that, for clarifying structural aspects of complex actinide systems, it is very useful to supplement EXAFS data by accurate results from computational models.

The agreement with experimental data is significantly improved if short-range solvent effects in the first and second actinyl hydration shells are considered in the theoretical models via the inclusion of explicit water molecules. Findings of this work show that it is desirable in future investigations to strive for a systematic and improved description of the near solvation environment of solute molecules. An ambitious, yet

important goal is the accurate evaluation of thermodynamic data and the study of reaction mechanisms, but both require a high computational effort. Such energetic data would allow an accurate determination of speciation distributions in solution.

Besides the detailed study of uranium compounds, analogous investigations of further actinide elements such as thorium, neptunium, or plutonium are necessary for a comprehensive understanding of actinide chemistry under environmental conditions. In this context, the inclusion and evaluation of spin-orbit interaction is another topic of interest that may become crucial, especially for actinide species in lower oxidation states which exhibit an open-shell electronic structure. Thus, a wide field of research on complex issues opens up that can only be mastered by combining experimental and theoretical studies.

Appendix A – Basis Sets

This appendix summarizes all atomic basis sets used in this thesis. The program PARAGAUSS employs products of primitive Gaussian functions of the form $\exp(-\alpha_i r^2)$ and real spherical harmonic functions Y_l^m for the representation of the molecular orbitals. In the following tables the exponents α_i will be listed for the atoms hydrogen, carbon, oxygen, chlorine, uranium, and neptunium. The size of the basis sets and the corresponding size of the contracted basis sets are given in the notation introduced in Section 3.4, i.e. (n_0s, n_1p, n_2d, n_3f) and [N_0s, N_1p, N_2d, N_3f], respectively.

In addition, the size of the auxiliary basis sets to represent the charge density is given by (n_0s, n_1r^2, m_1p, m_2d, m_3f). The exponents of the corresponding *s*- and r^2-type "fitting functions" are generated from the orbital basis (see Section 3.4). The exponents for higher angular momenta *p*, *d*, and *f* are added each as a geometric series with a progression of 2.5, starting with 0.1, 0.2, and 0.3 au, respectively; typically, five "polarization exponents" are used for each angular momentum. The corresponding exponents are given in the following table.

Exponents for polarization fitting functions

	p	**d**	**f**
α_1	0.10000000	0.20000000	0.30000000
α_2	0.25000000	0.50000000	0.75000000
α_3	0.62500000	1.25000000	1.87500000
α_4	1.56250000	3.12500000	4.68750000
α_5	3.90625000	7.81250000	11.71875000

Hydrogen (Z = 1): (6s, 1p) basis set

Ref. 219c,e

Contraction (6s, 1p) → [4s, 1p]

Fitbasis (6s, $1r^2$, 5p)

	s	**p**
α_1	0.08989100	1.00000000
α_2	0.25805300	
α_3	0.79767000	
α_4	2.82385400	
α_5	12.40955800	
α_6	82.63637400	

Carbon (Z = 6): (9s, 5p, 1d) basis set

Ref. 219c,d

Contraction (9s, 5p, 1d) → [5s, 4p, 1d]

Fitbasis (9s, $5r^2$, 5p, 5d)

	s	**p**	**d**
α_1	0.15659000	0.12194000	0.60000000
α_2	0.51190000	0.38554000	
α_3	2.41804900	1.20671000	
α_4	6.17577600	4.15924000	
α_5	16.82356200	18.84180000	
α_6	50.81594200		
α_7	178.35083000		
α_8	782.20479500		
α_9	5240.63525800		

Oxygen (Z = 8): (9s, 5p, 1d) basis set

Ref. 219c,d

Contraction (9s, 5p, 1d) → [5s, 4p, 1d]

Fitbasis (9s, $5r^2$, 5p, 5d)

	s	**p**	**d**
α_1	0.30068600	0.21488200	1.15000000
α_2	1.00427100	0.72316400	
α_3	4.75680300	2.30869000	
α_4	12.28746900	7.84313100	
α_5	33.90580900	34.85646300	
α_6	103.65179300		
α_7	364.72525700		
α_8	1599.70968900		
α_9	10662.28494000		

Chlorine (Z = 17): (12s, 9p, 1d) basis set

Ref. 219ab

Contraction (12s, 9p, 1d) → [6s, 5p, 1d]

Fitbasis (12s, $9r^2$, 5p, 5d)

	s	**p**	**d**
α_1	0.19355800	0.12498600	0.56000000
α_2	0.53839000	0.35827100	
α_3	2.52567000	0.95008300	
α_4	6.46497000	2.71409000	
α_5	20.81380000	6.60076000	
α_6	49.51430000	16.58850000	
α_7	124.49700000	44.79000000	
α_8	339.69100000	139.74500000	
α_9	1030.03000000	587.62200000	
α_{10}	3615.32000000		
α_{11}	15855.30000000		
α_{12}	105747.00000000		

Uranium (Z = 92): (24s, 19p, 16d, 11f) basis set

Ref. 218

Contraction (24s, 19p, 16d, 11f) → [10s, 7p, 7d, 4f]

Fitbasis (24s, $9r^2$, 5p, 5d, 5f)

	s	**p**	**d**	**f**
α_1	0.02058815	0.15790660	0.03447413	0.11032550
α_2	0.04313320	0.40899790	0.08774074	0.30254220
α_3	0.08254175	0.90591220	0.21542030	0.73748150
α_4	0.31243190	2.29137600	0.51211640	1.69235400
α_5	0.65236340	4.64911000	1.20507700	3.75266500
α_6	1.85772200	11.13758000	2.55673600	8.17341700
α_7	3.33603700	22.85757000	5.22965900	17.51736000
α_8	8.81990900	52.73747000	10.89752000	38.22365000
α_9	15.37485000	113.71170000	22.23856000	86.84438000
α_{10}	37.71001000	270.72840000	45.78370000	219.08110000
α_{11}	69.22380000	649.75080000	94.63173000	703.26150000
α_{12}	172.98510000	1673.81000000	205.18560000	
α_{13}	370.13750000	4676.74500000	474.04020000	
α_{24}	849.55400000	14437.84000000	1215.79900000	
α_{15}	1981.83800000	50135.61000000	3707.24200000	
α_{16}	4869.81100000	200185.00000000	16079.47000000	
α_{17}	12511.46000000	948314.40000000		
α_{18}	33651.45000000	5589055.00000000		
α_{19}	95179.62000000	30062560.00000000		
α_{20}	285123.90000000			
α_{21}	912190.10000000			
α_{22}	3147013.00000000			
α_{23}	12113820.00000000			
α_{24}	48171220.00000000			

Neptunium (Z = 93): (24s, 19p, 16d, 11f) basis set

Ref. 218

Contraction (24s, 19p, 16d, 11f) → [10s, 7p, 7d, 4f]

Fitbasis (24s, $9r^2$, 5p, 5d, 5f)

	s	**p**	**d**	**f**
α_1	0.020937410	0.165718100	0.034398650	0.121974000
α_2	0.043471000	0.431333300	0.087542520	0.329353600
α_3	0.082749100	0.961814300	0.215200000	0.792778600
α_4	0.330496200	2.424536000	0.513254100	1.799588000
α_5	0.690906900	4.915218000	1.205769000	3.946944000
α_6	1.992028000	11.691090000	2.559936000	8.496088000
α_7	3.550529000	24.024350000	5.239059000	18.063090000
α_8	9.440492000	55.225330000	10.940750000	39.199340000
α_9	16.552870000	119.456900000	22.274350000	88.734000000
α_{10}	40.235310000	284.361000000	45.848710000	223.337100000
α_{11}	74.075110000	685.276100000	94.758360000	715.691400000
α_{12}	184.141100000	1772.275000000	205.429700000	
α_{13}	397.683700000	4973.800000000	474.839100000	
α_{24}	926.676800000	15421.380000000	1219.480000000	
α_{15}	2143.086000000	53711.960000000	3723.773000000	
α_{16}	5225.524000000	214485.600000000	16176.970000000	
α_{17}	13298.530000000	1012679.000000000		
α_{18}	35522.280000000	5913894.000000000		
α_{19}	99826.910000000	32189820.000000000		
α_{20}	296567.100000000			
α_{21}	937058.000000000			
α_{22}	3190238.000000000			
α_{23}	12204240.000000000			
α_{24}	48165900.000000000			

Appendix B – Computation of Thermodynamics

The total electronic energy obtained from quantum chemical calculations describes a system only at zero temperature and for zero pressure conditions. This appendix summarizes equations how to calculate thermodynamical corrections to close the gap to actual experimental conditions by evaluating reaction enthalpies and Gibbs free energies. The following discussion follows the textbook "*Molecular Thermodynamics*" by McQuarrie and Simon.[259]

One of the most important approximations to be aware of throughout this analysis is that all equations are based on the assumption of non-interacting particles and therefore apply strictly only to the situation of an ideal gas. This will introduce some errors, depending on the extent that the considered systems are non-ideal, i.e. that different molecules of an ensemble interact. Furthermore, for the electronic contributions, it is assumed that the first and higher excited states are entirely inaccessible. This latter approximation is justified for the uranyl(VI) complexes studied in this thesis. It has been suggested that the first exited state of uranyl(VI) compounds is about 20000 cm^{-1} above the ground state.[260] The energy separation between the ground and excited states should not be more than a few hundred cm^{-1} if an excited state is to be significantly populated.[259] Thus at common temperatures the population of excited uranium states is negligible.

The first section introduces the partition function and its connection to the internal thermal energy and to the entropy. The subsequent sections summarize the equations required for calculating the individual contributions to enthalpy and free energy due to translational, electronic, vibrational, and rotational motion.

Partition functions

If the number of available quantum states is much greater than the number of particles (canonical ensemble), the partition function Q of an entire system of independent, indistinguishable atoms or molecules (number of particles N) can be expressed in terms of

the individual atomic or molecular partition function q:

$$Q(N,V,T) = \frac{[q(V,T)]^N}{N!} \tag{B.1}$$

Using the rigid rotator-harmonic oscillator approximation[259] one can write the internal thermal energy U of a polyatomic molecule as the sum of the individual translational E_t, electronic E_e, vibrational E_v, and rotational E_r energy contributions

$$U = E_t + E_e + E_v + E_r \tag{B.2}$$

Eq. (B.2) allows one to express the molecular partition function q as the product of the translational q_t, electronic q_e, vibrational q_v, and rotational q_r partition functions

$$q(V,T) = q_t q_e q_v q_r \tag{B.3}$$

The internal thermal energy can be derived directly from the partition function Q via

$$U = k_b T^2 \left(\frac{\partial \ln Q}{\partial T} \right)_{N,V} \tag{B.4}$$

or in terms of the molecular partition function using Eq. (B.1) and the relationships $N=N_A$ and $N_A k_B = R$ for one mole by

$$U = N k_b T^2 \left(\frac{\partial \ln q}{\partial T} \right)_V = RT^2 \left(\frac{\partial \ln q}{\partial T} \right)_V \tag{B.5}$$

The entropy S can also be obtained from the partition function via

$$S = k_b \ln Q + k_b T \left(\frac{\partial \ln Q}{\partial T} \right)_{N,V} \tag{B.6}$$

or directly from the molecular partition function, applying Eq. (B.1) and Stirling's approximation, $\ln N! = N \ln N - N$:

$$S = N k_B + N k_b \ln \left(\frac{q(V,T)}{N} \right) + N k_b T \left(\frac{\partial \ln q}{\partial T} \right)_V \tag{B.7}$$

Substitution of $q(V,T)$ in Eq. (B.7) via Eq. (B.3) introduces the individual partition functions. If one uses $N=N_A$ and $N_A k_B = R$ for one mole and moves the first term inside the logarithm (as e) one obtains

$$S = R \left(\ln\left(q_t q_e q_v q_r e\right) + T \left(\frac{\partial \ln q}{\partial T} \right)_V \right) \tag{B.8}$$

The total entropy S of a molecule is

$$S = S_t + S_e + S_v + S_r \tag{B.9}$$

Translation

The translational partition function is

$$q_t = \left(\frac{2\pi m k_b T}{h^2} \right)^{3/2} V \tag{B.10}$$

where m is the mass of the molecule. The volume V is not known in general. For an ideal gas, V can be substituted by the pressure P (P = 1atm at standard conditions) via the ideal-gas relationship $pV = NRT$:

$$q_t = \left(\frac{2\pi m k_b T}{h^2} \right)^{3/2} \frac{k_b T}{P} \tag{B.11}$$

The translational partition function is used to calculate the translational contribution to the internal thermal energy by substituting q_t into Eq. (B.5) to yield

$$E_t = RT^2 \left(\frac{3}{2T} \right) = \frac{3}{2} RT \tag{B.12}$$

The translational entropy S_t, which includes a factor e from Stirling's approximation, is obtained in analogous fashion by substituting q_t in Eq. (B.8):

$$S_t = R\left(\ln(q_t e) + T\left(\frac{3}{2T} \right) \right) = R\left(\ln(q_t) + \frac{5}{2} \right) \tag{B.13}$$

Electronic motion

The electronic partition function is given as sum over the state energies

$$q_e = \sum_i g_i \exp(-\varepsilon_i / k_b T) \tag{B.14}$$

where g_i is the degeneracy and ε_i is the energy of the i-th electronic state. For common temperatures first and higher excited states are inaccessible for most atoms.[259] Thus, in general only the first term in the summation of q_e is relevant. Further, the energy of the ground state is set to zero. These assumptions simplify the electronic partition function to

$$q_e = g_0 \tag{B.15}$$

which is the electronic spin multiplicity of the molecule.

As there are no temperature-dependent terms in the partition function q_e, the electronic contribution to the internal thermal energy is zero, based on Eq. (B.5):

$$E_t = RT^2(0) = 0 \tag{B.16}$$

Employing Eq. (B.8) for q_e yields the electronic entropy contribution

$$S_e = R(\ln(q_e) + T \cdot (0)) = R\ln(q_e) = R\ln(g_0) \tag{B.17}$$

Vibrational motion

The contributions from vibrational motion are composed of the individual contributions from each normal (vibrational) mode *K*. Each of the 3*n*–6 modes for non-linear or 3*n*–5 modes for linear molecules (where *n* is the number of atoms in the molecule) has a characteristic vibrational temperature defined by

$$\Theta_{v,K} = \frac{h\nu_K}{k_B} \tag{B.18}$$

where ν_K is the vibrational frequency for the mode *K*.

The zero point vibrational energy for a given mode *K* in terms of the vibrational temperature then is

$$E_{ZPE,K} = \frac{1}{2} R\Theta_{v,K} \tag{B.19}$$

The contribution to the partition function from an individual vibrational mode is given by

$$q_{v,K} = \frac{\exp\left(-\Theta_{v,K}/2T\right)}{1-\exp\left(-\Theta_{v,K}/T\right)} \tag{B.20}$$

and the overall vibrational partition function is obtained from the corresponding product of all individual modes *K* because the normal modes are independent:

$$q_v = \prod_k \frac{\exp\left(-\Theta_{v,K}/2T\right)}{1-\exp\left(-\Theta_{v,K}/T\right)} \tag{B.21}$$

Substitution of q_v into Eq. (B.5) provides the vibrational contribution to the internal thermal energy

$$E_v = R\sum_k \Theta_{v,K}\left(\frac{1}{2} + \frac{1}{\exp\left(\Theta_{v,K}/T\right)-1}\right) \tag{B.22}$$

The first term of this sum reflects the total zero-point vibrational energy, see Eq. (B.19),

$$E_{ZPE} = \frac{1}{2} R\sum_k \Theta_{v,K} \tag{B.23}$$

Substitution of q_v into Eq. (B.8) yields the following contribution to the entropy

$$S_v = R\sum_k \left(\frac{\Theta_{v,K}/T}{\exp\left(\Theta_{v,K}/T\right)-1} - \ln\left[1-\exp\left(-\Theta_{v,K}/T\right)\right]\right) \tag{B.24}$$

Low-frequency modes are included in these equations though some of them can be internal rotations that may have to be treated separately, depending on the temperatures and barriers involved.[259]

Rotational motion

The discussion of molecular rotation can be divided into several classes of systems: single atoms, linear polyatomic molecules, and general non-linear polyatomic molecules. Only the last general case is of interested in the present context. The corresponding rotational partition function is

$$q_r = \frac{\pi^{1/2}}{\sigma_r}\left(\frac{T^{3/2}}{\left(\Theta_{r,x}\Theta_{r,y}\Theta_{r,z}\right)^{1/2}}\right) \tag{B.25}$$

where σ_r is a symmetry index, i.e. the order of the rotational subgroup, and $\Theta_{r,i}$ (i = x, y, z) is the rotational temperature that is related to the moment of inertia I_i via

$$\Theta_{r,i} = \frac{\hbar^2}{2I_i k_B} \tag{B.26}$$

The rotational contribution to the internal thermal energy is derived via Eq. (B.5):

$$E_r = RT^2\left(\frac{3}{2T}\right) = \frac{3}{2}RT \tag{B.27}$$

The corresponding entropy contribution can be determined by applying Eq. (B.8):

$$S_r = R\left(\ln\left(q_r\right) + T\left(\frac{3}{2T}\right)\right) = R\ln\left(q_r + \frac{3}{2}\right) \tag{B.28}$$

Enthalpy and Gibbs free energy

The individual energy contributions discussed have to be added to give the internal thermal energy U according to Eq. (B.2).

The corresponding enthalpy H at a given temperature T (T = 298 K at standard conditions) is then

$$H = U + k_B T \tag{B.29}$$

The Gibbs free energy G can be derived with the help of the total entropy S, Eq. (B.9):

$$G = H - TS \tag{B.30}$$

Bibliography

[1] "radioactivity": *The Columbia Encyclopedia*, 6th ed.; New York: Columbia University Press, 2001–2004. www.bartleby.com/65/ra/radioact.html; 12.01.2006.

[2] Bequerel, H. *C. R. Acad. Sci. Paris* **1896**, *122*, 501.

[3] Choppin, G. R. *Radiochim. Acta* **2004**, *92*, 519.

[4] Street, K.; Seaborg, G. T. *J. Am. Chem. Soc.* **1950**, *72*, 2790.

[5] Thompson, S. G.; Cunningham, B. B.; Seaborg, G. T. *J. Am. Chem. Soc.* **1950**, *72*, 2798.

[6] Nash, K. L.; Cleveland, J. M.; Rees, T. F. *J. Environ. Radioact.* **1988**, *7*, 131.

[7] Choppin, G. R. *Radiochim. Acta* **1988**, *44/45*, 23.

[8] Choppin, G. R. *J. Rad. Nucl. Chem.* **1991**, *147*, 117.

[9] Dozol, M.; Hagemann, R. *Pure. Appl. Chem.* **1993**, *65*, 1081.

[10] Silva, R. J.; Nitsche, H.: *Radiochim. Acta* **1995**, *70/71*, 377.

[11] Lieser, K. H. *Radiochim. Acta* **1995**, *70/71*, 355.

[12] Clark, D. L.; Hobart, D. E.; Neu, M. P. *Chem. Rev.* **1995**, *95*, 25.

[13] Choppin, G. R.; Wong, P. J. *Aqu. Geochem.* **1998**, *4*, 77.

[14] Cotton, F. A.; Wilkinson, G. *Advanced Inorganic Chemistry*, 5th ed.; Wiley: New York, 1988, p. 980-993.

[15] Jacoby, M. *Chem Eng News* **1999**, 44.

[16] Pepper, M.; Bursten, B. E. *Chem. Rev.* **1991**, *91*, 719.

[17] Rösch, N.; Krüger, S.; Mayer, M.; Nasluzov, V. A. in: *Recent Developments and Applications of Modern Density Functional Theory*, Seminario, J., Ed.; Theoretical and Computational Chemistry Series, Vol. 4, Elsevier: Amsterdam, 1996, p. 497-566.

[18] Rösch, N.; Matveev, A. V.; Nasluzov, V. A.; Neyman, K. M.; Moskaleva, L.; Krüger, S. in: *Relativistic Electronic Structure Theory-Applications*, Schwerdtfeger, P., Ed.; Theoretical and Computational Chemistry Series, Vol. 14, Elsevier: Amsterdam, 2004, p. 676-722.

[19] Schreckenbach, G.; Hay, P. J.; Martin, R. L. *J. Comp. Chem.* **1999**, *20*, 70.

[20] Vallet, V.; Wahlgren, U.; Schimmelpfennig, B.; Moll, H.; Szabó, Z.; Grenthe, I. *Inorg. Chem.* **2001**, *40*, 3516.

[21] Privalov, T.; Schimmelpfennig, B.; Wahlgren, U.; Grenthe, I. *J. Phys. Chem. A* **2003**, *107*, 587.

[22] Spencer, S.; Gagliardi, L.; Handy, N. C.; Ioannou, A. G.; Skylaris, C.-K.; Willets, A.; Simper, A. M. *J. Phys. Chem. A* **1999**, *103*, 1831.

[23] Tsushima, S.; Yang, T.; Suzuki, A. *Chem. Phys. Lett.* **2001**, *334*, 365.

[24] Pepper, M.; Bursten, B. E. *J. Am. Chem. Soc.* **1990**, *112*, 7803.

[25] Pyykkö, P. *Chem. Rev.* **1988**, *88*, 563.

[26] Baerends, E. J.; Ellis, D. E.; Ros, P. *Chem. Phys.* **1973**, *2*, 41.

[27] Baerends, E. J.; Ros, P. *Chem. Phys.* **1973**, *2*, 52.

[28] Hay, P. J. *J. Chem. Phys.* **1983**, *79*, 5469.

[29] Hay, P. J.; Wadt, W. R. *J. Chem. Phys.* **1985**, *82*, 270.

[30] Küchle, W.; Dolg, M.; Stoll, H. ; Preuss, H. *J. Chem. Phys.* **1994**, *100*, 7535.

[31] Häberlen, O. D.; Rösch, N. *Chem. Phys. Lett.* **1992**, *199*, 491.

[32] van Lenthe, E.; Baerends, E. J.; Snijders J. G. *J. Chem. Phys.* **1993**, *99*, 4597.

[33] van Lenthe, E.; Baerends, E. J.; Snijders J. G. *J. Chem. Phys.* **1994**, *101*, 9783.

[34] van Lenthe, E.; Ehlers, A.; Baerends, E. J. *J. Chem. Phys.* **1999**, *110*, 8943.

[35] Balasubramanian, K.; Pitzer, K. S. *J. Chem. Phys.* **1983**, *78*, 321.

[36] Visscher, L.; Saue, T.; Nieuwpoort, W. C.; Faegri, K.; Gropen, O. *J. Chem. Phys.* **1993**, *99*, 6704.

[37] Tomasi, J.; Mennucci, B.; Cammi, R. *Chem. Rev.* **2005**, *105*, 2999.

[38] Tsushima, S.; Suzuki, A. *J. Mol. Struct. Theochem* **1999**, *487*, 33.

[39] Hemmingsen, L.; Amara, P.; Ansoborlo, E.; Field, M. J. *J. Phys. Chem. A* **2001**, *104*, 4095.

[40] Farkas, I.; Bányai, I.; Szabó, Z.; Wahlgren, U.; Grenthe, I. *Inorg. Chem.* **2000**, *39*, 799.

[41] Hay, P. J.; Martin, R. L.; Schreckenbach, G. *J. Phys. Chem. A* **2001**, *104*, 6259.

[42] Tsushima, S.; Suzuki, A. *J. Mol. Struct. Theochem* **2000**, *529*, 21.

[43] Fuchs, M. S. K.; Shor, A.; Rösch, N. *Int. J. Quant. Chem.* **2002**, *86*, 487.

[44] Majumdar, D.; Roszak, S.; Balasubramanian, K.; Nitsche, H. *Chem. Phys. Lett.* **2003**, *372*, 232.

[45] Krüger, S.; Schlosser, F.; Rösch, N. in: *Advances in Actinide Science, Proceedings of the Conference Actinides* 2005, Manchester, July 2005; The Royal Society of Chemistry: London, 2006, in press.

[46] Schlosser, F.; Krüger, S.; Rösch, N. *Inorg. Chem.* **2006**, *45*, 1480.

[47] Yang, T.; Tsushima, S.; Suzuki, A. *J. Phys. Chem. A* **2001**, *105*, 10439.

[48] Bühl, M.; Diss, R.; Wipff, G. *J. Am. Chem. Soc.* **2005**, *127*, 13506.

[49] Wadt, W. R.; Hay, P. J. *J. Am. Chem. Soc.* **1979**, *101*, 5198.

[50] Pyykkö, P.; Zhao, Y. *Inorg. Chem.* **1991**, *30*, 3787.

[51] Pyykkö, P.; Li, J.; Runeberg, N. *J. Phys. Chem.* **1994**, *98*, 4809.

[52] Kaldor, U.; Eliav, E.; Landau, A. in: *Reviews of Modern Quantum Chemistry*; Sen, K., Ed.; World Scientific: Singapore, 2002, p. 260-292.

[53] Kaldor, U.; Eliav, E.; Landau, A in: *Recent Advances in Relativistic Molecular Theory*; Hirao, K.; Ishikawa, Y., Eds.; World Scientific: Singapore, 2004, p. 283-327.

[54] Schreckenbach, G.; Hay, P. J.; Martin, R. L. *Inorg. Chem.* **1998**, *37*, 4442.

[55] García-Hernández, M.; Lauterbach, C.; Krüger, S.; Matveev, A.; Rösch, N. *J. Comp. Chem.* **2002**, *23*, 834.

[56] Tatsumi, K.; Hoffmann, R. *Inorg. Chem.* **1980**, *19*, 2656.

[57] Wadt, W. R. *J. Am. Chem. Soc.* **1981**, *103*, 6053.

[58] Pyykkö, P.; Laakkonen, L. J.; Tatsumi, K. *Inorg. Chem.* **1989**, *28*, 1801.

[59] Dyall, K. G. *Mol. Phys.* **1999**, *96*, 511.

[60] Denning, R. G.; Green, J. C.; Hutchings, T. E.; Dallera, C.; Giarda, K.; Brookes, N. B.; Bracovich, L. *J. Chem. Phys.* **2002**, *117*, 8008.

[61] García-Hernández, M.; Willnauer, C.; Krüger, S.; Moskaleva, L. V.; Rösch, N. *Inorg. Chem.* **2006**, *45*, 1356.

[62] Tsushima, S.; Reich, T. *Chem. Phys. Lett.* **2001**, *347*, 127.

[63] Oda, Y.; Aoshima, A. *J. Nucl. Sci. Technol.* **2002**, *39*, 647.

[64] Vázquez, J.; Bo, C.; Poblet, J. M.; de Pablo, J.; Bruno, J. *Inorg Chem.* **2003**, *42*, 6136.

[65] Schlosser, F.; Krüger, S.; Rösch, N. *Eur. J. Inorg. Chem.* **2003**, *17*, 3144.

[66] Schlosser, F.; Krüger, S.; Fuchs-Rohr, M. S. K.; Rösch, N., in preperation.

[67] de Jong, W. A.; Aprà, E.; Windus, T. L.; Nichols, J. A.; Harrison, R. J.; Gutowski, K. E.; Dixon, D. A. *J. Phys. Chem. A* **2005**, *109*, 11568.

[68] Wahlgren, U.; Moll, H.; Grenthe, I.; Schimmelpfennig, B.; Maron, L.; Vallet, V.; Gropen, O. *J. Phys. Chem. A* **1999**, *103*, 8257.

[69] Moskaleva, L.; Krüger, S.; Spörl, A.; Rösch, N. *Inorg. Chem.* **2004**, *43*, 4080.

[70] Bolvin, H.; Wahlgren, U.; Moll, H.; Reich, T.; Geipel, G.; Fanghänel, Th.; Grenthe, I. *J. Phys. Chem. A*, **2001**, *105*, 11441.

[71] Tsushima, S.; Yang, T.; Mochizuki, Y.; Okamoto, Y. *Chem. Phys. Lett.* **2003**, *375*, 204.

[72] Vallet, V.; Moll, H.; Wahlgren, U.; Szabó, Z.; Grenthe, I. *Inorg. Chem.* **2003**, *42*, 1982.

[73] Vallet, V.; Wahlgren, U.; Schimmelpfennig, B.; Szabó, Z.; Grenthe, I. *J. Am. Chem. Soc.*, **2001**, *123*, 11999.

[74] Gibson, J. K.; Haire, R. G.; Santos, M.; Marçalo, J.; de Matos, A. P. *J. Phys. Chem. A* **2005**, *109*, 2768.

[75] Moskaleva, L. V.; Matveev, A. V.; Krüger, S.; Rösch, N. *Chem. Eur. J.* **2006**, 12, 629.

[76] Gagliardi, L.; Roos, B. O. *Inorg. Chem.* **2002**, *41*, 1315.

[77] Chaudhuri, D.; Balasubramanian, K. *Chem. Phys. Lett.* **2004**, *399*, 62.

[78] Choppin, G. R.; Allard, B. in: *Handbook of the Physics and Chemistry of the Actinides*; Vol. 3, A. J. Freeman, C. Keller, Eds.; Elsevier: Amsterdam, 1985, p. 407-429.

[79] Allen, P. G.; Bucher, J. J.; Shuh, D. K.; Edelstein, N. M.; Reich, T. *Inorg. Chem.* **1997**, *36*, 4676.

[80] Åberg, M.; Ferri, D.; Glaser, J.; Grenthe, I. *Inorg. Chem.* **1983**, *22*, 3986.

[81] Thompson, H. A.; Brown Jr., G. E.; Parks, G. A. *Am. Mineral.* **1997**, *82*, 483.

[82] Kim, J. I. in: *Handbook of the Physics and Chemistry of the Actinides*; A. J. Freeman, C. Keller, Eds.; Elsevier: Amsterdam, 1986, Chapter 8.

[83] Maya, L.; Begun, G. M. *J. Inorg. Nucl. Chem.* **1981**, *43*, 2827.

[84] Szabó, Z.; Moll, H.; Grenthe, I. *J. Chem. Soc., Dalton. Trans.* **2000**, *18*, 3158.

[85] Pompe, S.; Schmeide, K.; Bubner, M.; Geipel, G.; Heise, K. H.; Bernhard, G.; Nitsche, H. *Radiochim. Acta* **2000**, *88*, 553.

[86] Stevenson, F. J.: *Humus Chemistry, Genesis, Compositions, Reactions*, 2nd ed.; Wiley: New York, 1994.

[87] Seaborg, G. T., Loveland, W. D.: *The Elements Beyond Uranium*; Wiley: New York, 1990.

[88] Hobart, D. E. *Proc. Robert A. Welch Found. Conf. Chem. Res.* **1990**, *34*, 379.

[89] Katz, J. J.; Seaborg, G. T.; Morss, L. R.: *The Chemistry of the Actinide Elements*, 2nd ed., Vol. 2; Chapman and Hall: New York, 1986, p. 1133-1146.

[90] Hollemann, A. F.; Wiberg, N.: *Lehrbuch der Anorganischen Chemie*, 101. Auflage; de Gruyter, Berlin **1995**, p. 1793-1821.

[91] Fischer, R.; Werner G.-D.; Lehmann, T.; Hoffmann, G.; Weigel, F. *J. Less-Common Met.* **1981**, *80*, 121.

[92] Ehmann, W. D.; Vance, D. E.: *Radiochemistry and Nuclear Methods of Analysis*; Wiley: New York, 1991.

[93] Ross, H.: *Liquid Scintillation Counting and Organic Scintillators*; Lewis Publishers, Chelsea **1991**.

[94] Baes Jr., C. F.; Mesmer, R. E.: *The Hydrolysis of Cations*; Wiley: New York, 1976, p. 174-182.

[95] Keller, C.: *The Chemistry of the Transuranium Elements*; Verlag Chemie Weihnheim, Germany **1971**, p. 94-115.

[96] Katz, J. J.; Seaborg, G. T.; Morss, L. R.: *The Chemistry of the Actinide Elements*, 2nd ed., Vol. 2; Chapman and Hall: New York, 1986, p. 1257-1277.

[97] Quilès, F.; Burneau, A. *Vibr. Spectros.* **1998**, *18*, 61.

[98] Nguyen-Trung, C.; Begun, G. M.; Palmer, D. A. *Inorg. Chem.* **1992**, *31*, 5280.

[99] Den Auwer, C.; Simoni, E.; Conradson, S.; Madic, C. *Eur. J. Inorg. Chem.* **2003**, *21*, 3843.

[100] Reich, T., private communications.

[101] Nitsche, H. *J. All. Comp.* **1995**, *223*, 274.

[102] Lieser, K. H.; Hill, R.; Mühlenweg, U.; Singh, R. N.; Steinkopff, Th. *J. Rad. Nucl. Chem.* **1991**, *147*, 117.

[103] Grenthe, I.; Fuger, J.; Konigs, R. J. M.; Lemire, R. J.; Muller, A. B.; Nguyen-Trung, C.; Wanner, H.: *Chemical Thermodynamics of Uranium*, Vol. 1; Elsevier:: Amsterdam, 1992.

[104] Eliet, V.; Bidoglio, G.; Omenetto, N.; Parma, L.; Grenthe, I. *J. Chem. Soc., Faraday Trans.* **1995**, *91*, 2275.

[105] Palmer, D. A.; Nguyen-Trung, C. *J. Solutution Chem. Soc., Faraday Trans.* **1995**, *91*, 2275.

[106] Clark, D. L.; Conradson, S. D.; Donohoe, R. J.; Keogh, D. W.; Morris, D. E.; Palmer, P. D.; Rogers, R. D.; Tait, C. D. *Inorg. Chem.* **1999**, *38*, 1456.

[107] Yamamura, T.; Kitamura, A.; Fukui, A.; Nishikawa, S.; Yamamoto, T.; Moriyama, H. *Radiochim. Acta* **1998**, *83*, 139.

[108] Sylva, R. N., Davidson, M. R. *J. Chem. Soc., Dalton Trans.* **1979**, *465*, 465.

[109] Åberg, M. *Acta Chem. Scand.* **1969**, *23*, 791.

[110] Åberg, M. *Acta Chem. Scand. A* **1978**, *32*, 101.

[111] Navaza, A.; Villain, F.; Charpin, P. *Polyhedron* **1984**, *3*, 143.

[112] Åberg, M. *Acta Chem. Scand. A* **1976**, *30*, 507.

[113] Åberg, M. *Acta Chem. Scand.* **1970**, *24*, 2901.

[114] Moll, H.; Reich, T.; Szabó, Z. *Radiochim. Acta* **2000**, *88*, 411.

[115] Allen, P. G.; Shuh, D. K.; Bucher, J. J.; Edelstein, N. M.; Reich, T.; Denecke, M. A.; Nitsche, H. *Inorg. Chem.* **1996**, *35*, 784.

[116] Gschneidner, K. A.; Eyring, L.; Choppin, G. R.; Lander, G. H.: *Handbook on the Physics and Chemistry of Rare Earths, Vol. 18 Lanthanides / Actinides: Chemistry*; North-Holland, Amsterdam **1994**, p. 529-558.

[117] Sullivan, J. C.; Hindman, J. C. *J. Phys. Chem.* **1959**, *63*, 1332.

[118] Sullivan, J. C.; Choppin, G. R.; Rao, L. F. *Radiochim. Acta* **1991**, *54*, 17.

[119] Itagaki, H.; Nakayama, S.; Tanka, S.; Yamawaki, M. *Radiochim. Acta* **1992**, *58/59*, 16.

[120] Neck, V.; Kim, J. I.; Kanellakopulos, B. *Radiochim. Acta* **1992**, *56*, 25.

[121] Madic, C.; Begun, G. M.; Hobart, D.´E.; Hahn, R. L. *Inorg. Chem.* **1994**, *23*, 1914.

[122] Cassol, A.; Magon, L.; Tomat, G.; Portanova, R. *Radiochim. Acta* **1972**, *17*, 28.

[123] Blake, C. A.; Coleman, C. F.; Brown, K. B.; Hill, D. G.; Lowrie, R. S.; Schmitt, J. M. *J. Am. Chem. Soc.* **1956**, *78*, 5978.

[124] Ciavatta, L.; Ferri, D.; Grimaldi, M.; Palombari, R.; Salvatore, F. *J. Inorg. Nucl. Chem.* **1979**, *41*, 1175.

[125] Ciavatta, L.; Ferri, D.; Grenthe, I.; Salvatore, F. *Inorg. Chem.* **1981**, *20*, 463.

[126] Strom, E. T.; Woessner, D. E.; Smith, W. B. *J. Am. Chem. Soc.* **1981**, *103*, 1255.

[127] Maya, L. *Inorg. Chem.* **1982**, *21*, 2895.

[128] Åberg, M.; Ferri, D.; Glaser, J.; Grenthe, I. *Inorg. Chem.* **1983**, *22*, 3981.

[129] Allen, P. G.; Bucher, J. J.; Clark, D. L.; Edelstein, N. M.; Ekberg, S. A.; Gohdes, J. W.; Hudson, E. A.; Kaltsoyannis, N.; Lukens, W. W.; Neu, M. P.; Plamer, P. D.; Reich, T.; Shuh, D. K.; Tait, C. D.; Zwick, B. D. *Inorg. Chem.* **1995,** *34*, 4797.

[130] Coda, A.; Della Giusta, A.; Tazzoli, V. *Acta Crystallogr.* **1981**, *B37*, 1496.

[131] Docrat, T. I.; Mosselmans, J. F. W.; Charnock, J. M.; Whiteley, M. W.; Collison, D.; Livens, F. R.; Jones, C.; Edmiston, M. J. *Inorg. Chem.* **1999**, *38*, 1879.

[132] Bernhard, G.; Geipel, G.; Reich, T.; Brendler, V.; Amayri, S.; Nitsche, H. *Radiochim. Acta* **2001**, *89*, 511.

[133] Madic, C.; Hobart, D. E.; Begun, G. M. *Inorg. Chem.* **1983**, *22*, 1494.

[134] Bányai, I.; Glaser, J.; Micskei, K.; Tóth, I.; Zékány, L. *Inorg. Chem.* **1995**, *34*, 3785.

[135] Meinrath, G.; Kimura, T. *J. All. Comp.* **1993**, *202*, 89.

[136] Meinrath, G.; Klenze, R.; Kim, J. I. *Radiochim. Acta* **1996**, *74*, 81.

[137] Kramer-Schnabel, U.; Bischoff, H.; Xi, R. H.; Marx, G. *Radiochim. Acta* **1992**, *56*, 183.

[138] Grenthe, I.; Lagerman, B. *Acta Chem. Scand.* **1991**, *45*, 122.

[139] Ferri, D.; Grenthe, I.; Salvatore, F. *Acta Chem. Scand. A* **1981**, *35*, 165.

[140] Grenthe, I.; Ferri, D.; Salvatore, F.; Riccio, G. *J. Chem. Soc., Dalton Trans.* **1984**, *20*, 2439.

[141] Schmeide, K.; Sachs, S.; Bubner, M.; Reich, T.; Heise, K. H.; Bernhard, G. *Inorg. Chim. Acta* **2003**, *351*, 133.

[142] Sachs, S.; Bubner, M.; Schmeide, K.; Choppin, G. R.; Heise, K. H.; Bernhard, G. *Talanta* **2002**, *57*, 999.

[143] Sachs, S.; Schmeide, K.; Reich, T.; Brendler, V.; Heise, K. H.; Bernhard, G. *Radiochim. Acta* **2005**, *93*,17.

[144] Sachs, S.; Bernhard, G. *Radiochim. Acta* **2005**, *93*, 141.

[145] Halbach, P.; von Borstel, D.; Gundermann, K. D. *Chem. Geol.* **1980**, *29*, 177.

[146] Choppin, G. R.; Kullberg, L. *J. Inorg. Chem.* **1978**, *40*, 651.

[147] Leciejewicz, J.; Alcock, N. W.; Kemp, T. J. *Struct. Bonding* **1996**, *82*, 43.

[148] Templeton, D. H.; Zalkin, A.; Ruben, H.; Templeton, L. L. *Acta Cryst.* **1985**, *C41*, 1439.

[149] Denecke, M. A.; Reich, T.; Pompe, S.; Bubner, M.; Heise, K. H.; Nitsche, H.; Allen, P. G.; Bucher, J. J.; Edelstein, N. M.; Shuh, D. K. *J. Phys. IV 7* **1997**, C2:637.

[150] Denecke, M. A.; Reich, T.; Bubner, M.; Pompe, S.; Heise, K. H.; Nitsche, H.; Allen, P. G.; Bucher, J. J.; Edelstein, N. M.; Shuh, D. K. *J. All. Comp.* **1998**, *271-273*, 123.

[151] Jiang, J.; Rao, L.; Di Bernardo, P.; Zanonato, P. L.; Bismondo, A. *J. Chem. Soc., Dalton Trans.* **2002**, *8*, 1832.

[152] Hudson, E. A.; Allen, P. G.; Terminello, L. J.; Denecke, M. A.; Reich, T. *Phys. Rev. B* **1996**, *54*, 156.

[153] Cousson, A.; Proust, J.; Pagès, M. *Acta Cryst.* **1990**, *C46*, 2316.

[154] Howatson, J.; Grev, D. M.; Morosin, B. *J. Inorg. Nucl. Chem.* **1975**, *37*, 1933.

[155] Moll, H.; Geipel, G.; Reich, T.; Bernhard, G.; Fanghänel, T.; Grenthe, I. *Radiochim. Acta* **2003**, *91*, 11.

[156] Nitsche, H.; Silva, R. J.; Brendler, V.; Geipel, G.; Reich, T.; Teterin, Y. A.; Thieme, M.; Baraniak, L.; Bernhard, G. in: *Actinide Speciation in High Ionic Strength Media*; Reed, D. T.; Clark, S. B.; Rao, L., Eds.; Kluwer Academic/Plenum Publishers: New York, 1999, p. 11-38.

[157] Mentzen, B. F.; Sautereau, H. *Acta Cryst.* **1980**, *B36*, 2051.

[158] Szabó, Z.; Grenthe, I. *Inorg. Chem.* **2000**, *39*, 5036.

[159] Carrell, C. J.; Carrell, H. L.; Erlebacher, J.; Glusker, J. P. *J. Am. Chem. Soc.* **1988**, *110*, 8651.

[160] Denecke, M. A.; Pompe, S.; Reich, T.; Moll, H.; Bubner, M.; Heise, K. H.; Nicolai, R.; Nitsche, H. *Radiochim. Acta* **1997**, *79*, 151.

[161] Denecke, M. A.; Reich, T.; Pompe, S.; Bubner, M.; Heise, K. H.; Nitsche, H.; Allen, P. G.; Bucher, J. J.; Edelstein, N. M.; Shuh, D. K.; Czerwinski, K. R. *Radiochim. Acta* **1998**, *82*, 103.

[162] Skogerboe, R. K.; Wilson, S. A. *Anal. Chem.* **1981**, *53*, 228.

[163] Choppin, G. R. *Radiochim. Acta* **1992**, *58/59*, 113.

[164] Belling, T.; Grauschopf, T.; Krüger, S.; Mayer, M.; Nörtemann, F.; Staufer, M.; Zenger, C.; Rösch N. in: *High Performance Scientific and Engineering Computing*, Bungartz, H.-J.; Durst, F.; Zenger, C., Eds.; Lecture Notes in Computational Science and Engineering, Vol. 8, Springer: Heidelberg, 1999, p. 439-453.

[165] Belling, T.; Grauschopf, T.; Krüger, S.; Nörtemann, F.; Staufer, M.; Mayer, M.; Nasluzov, V. A.; Birkenheuer, U.; Shor, A.; Matveev, A. V.; Hu, A.; Fuchs-Rohr, M. S. K.; Neyman, K. M.; Ganyushin, D. I.; Kerdcharoen, T.; Woiterski, A.; Gordienko, A.; Majumder, S.; Rösch, N. PARAGAUSS Version 3.0, Technische Universität München, 2004. Previous versions of the code have also been used.

[166] Dunlap, B. I.; Rösch, N. *Adv. Quantum Chem.* **1990**, *21*, 317.

[167] Kerdcharoen, T.; Birkenheuer, U.; Krüger, S.; Woiterski, A.; Rösch, N. *Theor. Chem. Acc.* **2003**, *109*, 285.

[168] Nasluzov, V. A.; Rivanenkov, V. V.; Gordienko, A. B.; Neyman, K. M.; Birkenheuer, U.; Rösch, N. *J. Chem. Phys.* **2001**, *115*, 8157.

[169] Nasluzov, V. A.; Ivanova, E. A.; Shor, A. M.; Vayssilov, G. N.; Birkenheuer, U.; Rösch, N. *Phys. Chem. B* **2003**, *107*, 2228.

[170] Matveev, A. V.; Mayer, M.; Rösch, N. *Comp. Phys Commun.* **2004**, *160*, 91.

[171] Batrakov, Y. F.; Krivitsky, A. G.; Pospelov, O. V.; Puchkova, E. V. *Radiochim. Acta* **2004**, *92*, 73.

[172] Koch, W.; Holthausen, M. C.: *A Chemist's Guide to Density Functional Theory*; Wiley: Weinheim, 2000, p. 213-234.

[173] Parr, R. G.; Yang, W.: *Density Functional Theory of Atoms and Molecules*; Oxford University Press, New York **1989**.

[174] Hohenberg, K.; Kohn, W. *Phys. Rev. B* **1964**, *136*, 864.

[175] Kohn, W.; Sham, L. J. *Phys. Rev. A* **1965**, *140*, 1133.

[176] Wolf, A.; Reiher, M.; Hess, B. A. *J. Chem. Phys.* **2002**, *117*, 9215.

[177] Douglas, M.; Kroll, N. M. *Ann. Phys.* **1974**, *82*, 89.

[178] Buenker, R. J.; Chandra, P.; Hess, B. A. *Chem. Phys.* **1984**, *84*, 1.

[179] Matveev, A.; Rösch, N. *J. Chem. Phys.* **2003**, *118*, 3997.

[180] Visscher, L.; van Lenthe, E. *Chem. Phys. Lett.* **1999**, *306*, 357.

[181] Neyman, K. M.; Ganyushin, G. I.; Matveev, A. V.; Nasluzov, V. A. *J. Phys. Chem. A* **2002**, *106*, 5022.

[182] Matveev, A. V.; Majumder, S.; Rösch, N. *J. Chem. Phys.* **2005**, *123*, 164104.

[183] Hess, B. A.; Marian, C. M.; Wahlgren, U.; Gropen, O. *Chem. Phys. Lett.* **1996**, *251*, 365.

[184] Boettger, J. C. *Phys. Rev. B* **2000**, *62*, 7809.

[185] Majumder, S.; Matveev, A. V.; Rösch, N. *Chem. Phys. Lett.* **2003**, *382*, 186.

[186] Vosko, S. H.; Wilk, L.; Nusair, M. *Can. J. Phys.* **1980**, *58*, 1200.

[187] Becke, A. D. *Phys. Rev. A* **1988**, *38*, 3098.

[188] Perdew, J. P. *Phys. Rev. B* **1986**, *33*, 8822; *ibid*. **1986**, *34*, 7406.

[189] Hammer, B.; Hansen, L. B.; Nørskov, J. K. *Phys. Rev. B* **1999**, *59*, 7413.

[190] Ziegler, T. *Chem. Rev.* **1991**, *91*, 651.

[191] Görling, A.; Trickey, S. B.; Gisdakis, P.; Rösch, N. in: *Topics in Organometallic Chemistry*, Vol. 4, Brown, J.; Hoffmann, P., Eds.; Springer: Heidelberg, 1999, p. 109-165.

[192] Krüger, S.; Stener, M.; Rösch, N. *J. Chem. Phys.* **2001**, *114*, 5207.

[193] Schlosser, F., Diplomarbeit, Technische Universität München, **2001**.

[194] Tomasi, J.; Persico, M. *Chem. Rev.* **1994**, *94*, 2027.

[195] Cramer, C. J.; Truhlar, D. G. *Chem. Rev.* **1999**, *99*, 2161.

[196] Gao, J. *Rev. Comp. Chem.* **1995**, *7*, 119.

[197] Kunz, C. F.; Hess, B. A. *J. Chem. Phys.* **2000**, *112*, 1373.

[198] Miertus, S.; Scrocco, E.; Tomasi, J. *J. Chem. Phys.* **1981**, *55*, 117.

[199] Klamt, A.; Schüürmann, G. J. *J. Chem. Soc. Perkin Trans.* **1993**, *2*, 799.

[200] Andzelm, J.; Kölmel, C.; Klamt, A. *J. Chem. Phys.* **1995**, *103*, 9312.

[201] Baldrige, K.; Klamt, A. *J. Chem. Phys.* **1997**, *106*, 6622.

[202] Barone, V.; Cossi, M.; Tomasi, J. *J. Chem. Phys.* **1997**, *107*, 3210.

[203] Bondi, A. *J. Phys. Chem.*, **1964**, 68, 441.

[204] Pasqual-Ahuir, J. L.; Silla, E. *J. Comput. Chem.*, **1990**, 11, 1047.

[205] Silla, E.; Tuñón, I.; Pasqual-Ahuir, J. L. *J. Comput. Chem.*, **1991**, 12, 1077.

[206] Pasqual-Ahuir, J. L.; Silla, E.; Tuñón, I. *J. Comput. Chem.*, **1994**, 15, 1127.

[207] Shor, A; Rösch, N., unpublished results.

[208] Cossi, M.; Mennucci, B.; Cammi, R. *J. Comput. Chem.* **1996**, *17*, 57.

[209] Mennucci, B.; Tomasi, J. *J. Chem. Phys.* **1997**, *106*, 5151.

[210] Chipman, D. M. *J. Chem. Phys.* **1997**, *106*, 10194.

[211] Zhan, C.-G.; Bentley, J.; Chipman, D. M. *J. Chem. Phys.* **1998**, *108*, 177.

[212] Zhan, C.-G.; Chipman, D. M. *J. Chem. Phys.* **1998**, *109*, 10543.

[213] Zhan, C.-G.; Chipman, D. M. *J. Chem. Phys.* **1999**, *110*, 1611.

[214] Chipman, D. M. *J. Chem. Phys.* **1999**, *110*, 8012.

[215] Basile, L. J.; Sullivan, J. C.; Ferraro, J. R.; LaBonville, P. *Appl. Spectrosc.* **1974**, *28*, 142.

[216] Toth, L. M.; Begun, G. M. *J. Phys. Chem.* **1981**, *85*, 547.

[217] Winkler, M.; Krüger, S.; Rösch, N., unpublished results.

[218] Minami, T.; Matsuoka, O. *Theo. Chim. Acta* **1995**, *90*, 27.

[219] [219a] Veillard, A. *Theor. Chim. Acta (Berlin)* **1968**, *12*, 405. [219b] Sakai, Y.; Tatewaki, H.; Huzinaga, S. *J. Comput. Chem.* **1981**, *2*, 108 [Cl: d exponent 0.56]. [219c] Van Duijneveldt, F. B. *IBM Res. Rep.* **1971**, RJ 945. [219d] Huzinaga, S.; Andzelm, J.; Klobukowski, M.; Radzio-Andzelm, E.; Sakai, Y.; Tatewaki, H. *Gaussian Basis Sets for Molecular Calculations*; Elsevier: Amsterdam, 1984 [O: d exponent 1.15; C: d exponent 0.60]. [219e] Frisch, M. J.; Pople, J. A.; Binkley, J. S. *J. Chem. Phys.* **1984**, *80*, 3265 [H: p exponent 1.0].

[220] Nasluzov, V. A.; Rösch, N. *Chem. Phys.* **1996**, *210*, 413.

[221] Becke, A. D. *J. Chem. Phys.* **1988**, *88*, 2547.

[222] Lebedev, V. I. *Zh. Vychisl. Mat. Mat. Fiz.* **1975**, *15*, 48.

[223] Lebedev, V. I. *Zh. Vychisl. Mat. Mat. Fiz.* **1976**, *15*, 293.

[224] Lebedev, V. I. in: *Proc. Conf. Novosibirsk 1978*, Sobolev, S. L., Ed.; Nauka Sibirsk. Otdel.: Novosibirsk, 1980.

[225] Markus, Y. *J. Inorg. Nucl. Chem.* **1975**, *37*, 493.

[226] Cornehl, H. H.; Heinemann, C.; Marçalo, J.; de Matos, A. P.; Schwarz, H. *Angew. Chem. Int. Ed. Engl.* **1996**, *35*, 891.

[227] Jones, L. H.; Penneman, R. A. *J. Chem. Phys.* **1953**, *21*, 542.

[228] Tait, D. C. presented at the Symposium of Heavy Element Complexes: The Convergence of Theory and Experiment, 217th ACS National Meeting, 1999, Anaheim, CA.

[229] Clark, D. L. presented at the Symposium of Heavy Element Complexes: The Convergence of Theory and Experiment, 217th ACS National Meeting, 1999, Anaheim, CA.

[230] Reich, T.; Bernhard, G.; Geipel, G.; Funke, H.; Hennig, C.; Roßberg, A.; Matz, W.; Schell, N.; Nitsche, H. *Radiochim. Acta* **2000**, *88*, 633.

[231] Madic, C.; Begun, G. M.; Hobart, D. E.; Hahn, R. L. *Inorg. Chem.* **1984**, *23*, 1914.

[232] Combes, J.-M.; Chisholm-Brause, C. J.; Brown Jr. , G. E.; Parks, G. A.; Conradosn, S. D.; Eller, P. G.; Triay, I. R. ; Hobart, D. E.; Meijer, A. *Environ. Sci. Technol.* **1992**, *26*, 376.

[233] Martin, R. L., private communications.

[234] Szabo, A.; Ostlund, N.: *Modern Quantum Chemistry*; MacGraw-Hill: New York, 1989.

[235] Jeffrey, G. A.: *An Introduction to Hydrogen Bonding*; Oxford University Press: New York, 1997, p. 12.

[236] Hay, P. J.; Martin, R. L. *J. Chem. Phys.* **1998**, *109*, 3875.

[237] Leung, A. F.; Wong, E. Y. *Phys. Rev.* **1969**, *180*, 380.

[238] Toivonen, J.; Laitinen, R. *Acta Crystallogr.* **1984**, *C40*, 7.

[239] Viossat, P. B.; Dung, N.-H.; Soye, E. C. *Acta Crystallogr.* **1983**, *C39*, 573.

[240] Weast, R. C.: *CRC Handbook of Chemistry and Physics*, 59th ed.; CRC Press: Boca Raton, 1979, p. D-230.

[241] Tsushima, S.; Uchida, Y.; Reich, T. *Chem. Phys. Lett.* **2002**, *357*, 73.

[242] Gagliardi, L.; Grenthe, I.; Roos, B. O. *Inorg. Chem.* **2001**, *40*, 2976.

[243] Clark, D. L.; Conradson, S. D.; Ekberg, S. A.; Hess, N. J.; Neu, M. P.; Palmer, P. D.; Runde, W.; Tait, C. D. *J. Am. Chem. Soc.* **1996**, *118*, 2089.

[244] Schreckenbach, G.: *NMR Chemical Shifts, ESRG-Tensors and Relativity with the ADF program: Applications Across the Entire Periodic Table*; Ryoka Systems Inc.,Tokyo, Japan, **1999**.

[245] Montgomery, J. A.; Frisch, M. J.; Ochterski, J. W.; Petersson, G. A. *J. Chem. Phys.* **1999**, *110*, 2822.

[246] Liptak, M. D.; Shields, G. C. *J. Am. Chem. Soc.* **2001**, *123*, 7314.

[247] Liptak, M. D.; Gross, K. C.; Seybold, P. G.; Feldgus, S.; Shields, G. C. *J. Am. Chem. Soc.* **2002**, *124*, 6421.

[248] Adam, K. R. *J. Phys. Chem. A* **2002**, *106*, 11963.

[249] Gao, D.; Svoronos, P.; Wong, P. K.; Maddalena, D.; Hwang, J.; Walker, H. *J. Phys. Chem. A* **2005**, *109*, 10776.

[250] Bailey, E. H.; Mosselmans, J. F. W.; Schofield, P. F. *Geochim. Cosmochim. Acta* **2004**, *68*, 1711.

[251] [251a] Ferrari, A. M.; Neyman, K. M.; Mayer, M.; Staufer, M.; Gates, B. C.; Rösch, N. *J. Phys. Chem. B* **1999**, *103*, 5311. [251b] Goellner, J. F.; Gates, B. C.; Vayssilov, G. N.;

Rösch, N. *J. Am. Chem. Soc.* **2000**, *122*, 8056. [251c] Vayssilov, G. N.; Gates, B. C.; Rösch, N. *Angew. Chem. Int. Ed.* **2003**, *42*, 1391. [251d] Vayssilov, G. N.; Rösch, N. *J. Phys. Chem. B* **2004**, *108*, 180.

252 Novak, C. F.; Borkowski, M.; Choppin, G. R. *Radiochim. Acta* **1996**, *74*, 111.

253 Pokrovsky, O. S.; Choppin, G. R. *Radiochim. Acta* **1997**, *79*, 167.

254 Den Auwer, C.; Simoni, E.; Conradson, S.; Madic, C. *Eur. J. Inorg. Chem.* **2003**, *21*, 3843.

255 Katz, J. J.; Seaborg, G. T.; Morss, L. R.: *The Chemistry of the Actinide Elements*, 2nd ed., Vol. 2; Chapman and Hall: New York, 1986, p. 1480-1495.

256 Kremleva, A.; Krüger, S.; Rösch, N., unpublished results.

257 Ray, R. S.; Krüger, S.; Rösch, N., unpublished results.

258 Roßberg, A.; Baraniak, L.; Reich, T.; Hennig, C.; Bernhard, G.; Nitsche, H. *Radiochim. Acta* **2000**, *88*, 593.

259 McQuarrie, D. A.; Simon, J. D.: *Molecular Thermodynamcis*; University Science Books: Sausalito, 1999.

260 Denning, R. G. *Struct. Bonding* **1992**, *79*, 215.